



University of Cyprus

School of engineering

Department of civil and environmental engineering

INVESTIGATION OF EARTHQUAKE-INDUCED POUNDINGS OF
SEISMICALLY ISOLATED BUILDINGS

by

Panayiotis C. Polycarpou

Diploma of Civil Engineering, Aristotle University of Thessaloniki, Greece
M.Sc. in Earthquake Resistant Design of Structures, Aristotle University of Thessaloniki, Greece

*Submitted to the Department of Civil and Environmental Engineering of the University of
Cyprus in partial fulfillment of the requirements for the degree of*

Doctor of Philosophy

Nicosia, September 2009

© Panayiotis C. Polycarpou

INVESTIGATION OF EARTHQUAKE-INDUCED POUNDINGS OF
SEISMICALLY ISOLATED BUILDINGS

«ΔΙΕΡΕΥΝΗΣΗ ΣΥΓΚΡΟΥΣΕΩΝ ΣΕΙΣΜΙΚΩΣ ΜΟΝΩΜΕΝΩΝ ΚΤΙΡΙΩΝ
ΛΟΓΩ ΣΕΙΣΜΩΝ»

By

Panayiotis C. Polycarpou

Examination Committee:

Dimos Charmpis, Lecturer (*Chairman*)
Department of Civil and Environmental Engineering, University of Cyprus

Stavros A. Anagnostopoulos, Professor
Department of Civil Engineering, University of Patras, Greece

Marios C. Phocas, Assistant Professor
Department of Civil and Environmental Engineering, University of Cyprus

Nikos D. Lagaros, Lecturer
School of Civil Engineering, National Technical University of Athens, Greece

Petros Komodromos, Lecturer (*Research supervisor*)
Department of Civil and Environmental Engineering, University of Cyprus

Thesis Advisory Committee:

Marios C. Phocas, Assistant Professor
Department of Civil and Environmental Engineering, University of Cyprus

Dimos Charmpis, Lecturer
Department of Civil and Environmental Engineering, University of Cyprus

Petros Komodromos, Lecturer
Department of Civil and Environmental Engineering, University of Cyprus

Thesis Supervisor:

Petros Komodromos, Lecturer
Department of Civil and Environmental Engineering, University of Cyprus



University of Cyprus

School of engineering

Department of civil and environmental engineering

APPROVAL PAGE

Doctor of Philosophy Dissertation

Investigation of earthquake-induced poundings of seismically isolated buildings

by

Panayiotis C. Polycarpou

Research Supervisor:

Petros Komodromos

Committee Member (Chairman)

Dimos Charmpis (Chairman)

Committee Member

Marios C. Phocas

Committee Member

Nikos D. Lagaros

Committee Member

Stavros A. Anagnostopoulos

Panayiotis C. Polycarpou

ABSTRACT

“Investigation of earthquake-induced poundings of seismically isolated buildings”

The current research work investigates, through numerical simulations and parametric studies, the consequences of potential pounding incidences on the seismic response of seismically isolated buildings. Such impact events may occur in cases where the available clearance around a seismically isolated building is limited due to practical constraints, in combination with a very strong seismic excitation that induces larger than expected horizontal displacements. Under such circumstances, the seismically isolated building may hit against the surrounding moat wall at its base or against a structure that is built in close proximity. The superstructures of the buildings are simulated in two dimensions as multi-degree-of-freedom systems with linear elastic shear-type behavior, while for the seismic isolation system's behavior, both linear and bilinear modeling is considered in the performed analyses. For the modeling of impacts, a “penalty method” is used, in which a small interpenetration among two colliding bodies is allowed and used in combination with an impact stiffness coefficient to calculate the elastic impact forces that are applied on the colliding bodies. Several types of such impact models are examined, while two new impact models are proposed to be used for simulating structural pounding.

A relevant software application has been specifically designed and developed in order to effectively and efficiently perform the necessary numerical simulations and parametric studies. The effects of poundings on the performance of a seismically isolated building are demonstrated and discussed using a relevant example. Furthermore, the effect of using different impact models for the calculation of impact forces on the overall seismic response during poundings is also examined.

Subsequently, considering seismically isolated buildings pounding either with the surrounding moat wall or with adjacent fixed-supported buildings, the influence of certain parameters on their dynamic response during strong ground-motions is assessed. Such parameters include the width of the seismic gap, the earthquake characteristics, the impact parameters and the characteristics of the seismic isolation system. Specifically, in the case of poundings with adjacent buildings, an investigation is conducted regarding the type of the adjacent structures and the influence of their characteristics on the response of a seismically isolated building during various earthquake excitations.

Finally, the use of rubber bumpers, which can act as shock-absorbers, is examined as a potential impact mitigation measure to alleviate the detrimental effects of poundings. For the simulation of the rubber bumpers, a new impact model with hysteretic damping is developed and used, based on relevant experiments conducted by other researchers. The proposed non-linear impact model takes into account the finite thickness of the rubber bumper. A series of parametric studies is performed in order to examine the influence of certain parameters, such as the earthquake characteristics, the bumpers' thickness and the number of bumpers that are attached on each side of a seismically isolated building, on the effectiveness of such mitigation measure for poundings.

ΠΕΡΙΛΗΨΗ

«Διερεύνηση συγκρούσεων σεισμικώς μονωμένων κτιρίων λόγω σεισμών»

Στα πλαίσια της παρούσας εργασίας, διερευνώνται, μέσω αριθμητικών προσομοιώσεων και παραμετρικών αναλύσεων, οι επιπτώσεις πιθανών συγκρούσεων κατά τη σεισμική απόκριση σεισμικώς μονωμένων κτιρίων. Συγκρούσεις μπορούν να συμβούν σε περιπτώσεις όπου το διαθέσιμο διάκενο περιμετρικά από ένα σεισμικώς μονωμένο κτίριο, λόγω διαφόρων παραγόντων, είναι περιορισμένο και συγχρόνως μία ισχυρή σεισμική διέγερση υποβάλλει την κατασκευή σε μεγάλες οριζόντιες μετακινήσεις σχετικά με το έδαφος. Κάτω από αυτές τις συνθήκες, το σεισμικώς μονωμένο κτίριο πιθανόν να συγκρουστεί, είτε με τον περιμετρικό τοίχο στη βάση της ανωδομής, είτε και με άλλα γειτονικά κτίρια, τα οποία μπορεί να βρίσκονται σε πολύ κοντινή απόσταση.

Οι ανωδομές των κτιρίων προσομοιώνονται σε δύο διαστάσεις, ως γραμμικά ελαστικά πολυβάθμια συστήματα με διατμητική συμπεριφορά, καθώς για τη προσομοίωση της συμπεριφοράς του συστήματος της σεισμικής μόνωσης χρησιμοποιείται, είτε ισοδύναμο γραμμικό ελαστικό, είτε διγραμμικό ανελαστικό μοντέλο. Η μοντελοποίηση της κρούσης γίνεται με τη χρήση κατάλληλων μοντέλων κρούσης, με τα οποία οι δυνάμεις επαφής υπολογίζονται με βάση την παραδοχή μιας μικρής αλληλοεπικάλυψης μεταξύ των δύο συγκρούμενων σωμάτων που πολλαπλασιάζεται με τη δυσκαμψία ενός υποθετικού ελατηρίου κρούσης, το οποίο προσομοιώνει την τοπική παραμορφωσιμότητα του υλικού στο σημείο επαφής. Χρησιμοποιώντας σχετικά παραδείγματα, εξετάζονται διάφοροι τύποι και παραλλαγές τέτοιων μοντέλων, καθώς και προτείνονται δύο νέα μοντέλα κρούσης που μπορούν να χρησιμοποιηθούν σε προσομοιώσεις συγκρούσεων δομικών κατασκευών.

Ένα εξειδικευμένο λογισμικό έχει σχεδιαστεί και αναπτυχθεί, με χρήση αντικειμενοστραφούς γλώσσας προγραμματισμού, το οποίο παρέχει τη δυνατότητα αποτελεσματικής και αποδοτικής πραγματοποίησης των απαιτούμενων προσομοιώσεων και παραμετρικών αναλύσεων. Οι επιπτώσεις των συγκρούσεων στην απόκριση ενός σεισμικώς μονωμένου κτιρίου μελετώνται και παρουσιάζονται μέσω ενός ενδεικτικού παραδείγματος. Επιπλέον, παρουσιάζονται οι διαφορές στη σεισμική απόκριση της κατασκευής κατά τη διάρκεια συγκρούσεων, λόγω της χρήσης διαφόρων μοντέλων κρούσης για τον υπολογισμό των δυνάμεων κρούσης.

Έπειτα, θεωρώντας ότι σεισμικώς μονωμένα κτίρια μπορεί να συγκρούονται, είτε με τον περιμετρικό τοίχο στη βάση τους, είτε και με γειτονικά συμβατικά κτήρια, πραγματοποιούνται σειρές αναλύσεων, όπου μελετάται η επιρροή διαφόρων παραμέτρων στα μεγέθη απόκρισης των σεισμικώς μονωμένων κτιρίων, κατά τη διάρκεια ισχυρών σεισμικών δράσεων. Στις παραμέτρους αυτές περιλαμβάνονται το πλάτος του περιμετρικού διακένου, τα χαρακτηριστικά της σεισμικής διέγερσης, η δυσκαμψία και η απόσβεση της κρούσης και τα χαρακτηριστικά του συστήματος σεισμικής μόνωσης. Συγκεκριμένα, για την περίπτωση συγκρούσεων ενός σεισμικώς μονωμένου κτιρίου με άλλα γειτονικά κτίρια, μελετήθηκε επίσης η επιρροή των χαρακτηριστικών των γειτονικών κτιρίων, όπως για παράδειγμα ο αριθμός των ορόφων τους.

Τέλος, εξετάζεται η αποτελεσματικότητα της χρήσης παρεμβλημάτων από ελαστομερές υλικό, τα οποία μπορούν να εφαρμοστούν στα πιθανά σημεία συγκρούσεων, ούτως ώστε να λειτουργήσουν σαν ενδεχόμενο μέτρο άμβλυνσης των δυσμενών επιπτώσεων των συγκρούσεων. Για την προσομοίωση της συμπεριφοράς τέτοιων ελαστικών παρεμβλημάτων, αναπτύχθηκε ένα νέο μη-γραμμικό μοντέλο κρούσης με υστερητική απόσβεση, βάσει αποτελεσμάτων από σχετικά πειράματα τα οποία πραγματοποιήθηκαν

στο παρελθόν από άλλους ερευνητές. Με τη χρήση του προτεινόμενου μοντέλου λαμβάνεται υπόψη και το πεπερασμένο πάχος του ελαστικού προσκρουστήρα. Συγκεκριμένα, πραγματοποιούνται σειρές παραμετρικών αναλύσεων όπου εξετάζεται η επιρροή κάποιων παραμέτρων, όπως τα χαρακτηριστικά της σεισμικής δράσης, το πάχος και ο αριθμός των προσκρουστήρων που εφαρμόζονται σε κάθε πλευρά του κτιρίου, στην αποτελεσματικότητα αυτού του μέτρου άμβλυνσης των αρνητικών συνεπειών των συγκρούσεων.

ACKNOWLEDGMENTS

First, I would like to express my deep gratitude to my academic and research advisor, Prof. Petros Komodromos for his guidance, encouragement and unconditional support during my studies at the University of Cyprus. From the first moment of our collaboration, he made me feel comfortable and that I had a lot to learn from him. Indeed, I have learned a lot, including all the knowledge about object-oriented programming and utilization of modern computing technologies. This research work would not have been in any way possible without his zealous devotion and determination towards the success of his students. I really feel lucky to be one of his student and, for now on, luckier to be one of his friends.

My warmest thanks also to my doctoral committee members, Prof. Stavros Anagnostopoulos, Prof. Marios C. Phocas, Prof. Nikos Lagaros and Prof. Demos Charmpis for the valuable advice and their excellent comments towards the improvement of my thesis.

I would like to take this opportunity to thank my professors during my graduate and undergraduate studies at the Aristotle University of Thessaloniki, which they encouraged me with valuable advises for my career and further life. Particularly, I thank Prof. Asimina Athanatopoulou and Prof. Panikos Papadopoulos, who have been my supervisors of my graduate and undergraduate thesis, respectively, as well as Prof. I. N. Doudoumis, Prof. G. Manolis, Prof. A. Kappos and Prof. G. Manos.

Furthermore, I would like to thank my friends and co-workers in the “Archimedes” Laboratory Ernestos Sarris, Eftychia Mavronicola and George Pamboris, who kept me going and supported me during my studies in many different ways. Special thanks to my dearest friend and colleague Loizos Papaloizou, who has been always by my side encouraging and supporting me from the very first day of our studies in Thessaloniki, until this very moment and, hopefully, for many years to come. I also thank my friends Marios Constantinides, Fanos Georgiou and Demetris Fagridas for their love and support during our student-life.

I specifically thank my parents, Charitini and Christodoulos for the true sacrifices that they have been through in order to give their best for me, as well as my brothers Anastasis, Polys and Andreas for their love, encouragement and for helping me in fulfilling my goals.

Last but not least, I would like to express my endless love and gratitude to my wife Theklia, who has been very patient with me, especially during my work on this thesis, as well as our daughter Maria who has been and always will be my inspiration and motivation to accomplish my targets.

Dedicated with all my love to Thekla and Maria
Αφιερωμένο στη Θέκλεια και τη Μαρία με όλη μου την αγάπη

TABLE OF CONTENTS

APPROVAL PAGE	v
ABSTRACT	vii
ΠΕΡΙΛΗΨΗ	viii
ACKNOWLEDGMENTS	x
TABLE OF CONTENTS	xii
LIST OF FIGURES	xv
LIST OF TABLES	xxii
CHAPTER 1 INTRODUCTION	1
1.1 Seismic Isolation.....	1
1.2 Motivation.....	4
1.3 Pounding incidences during past earthquakes	6
1.4 Past research studies on poundings.....	7
1.4.1 Poundings of fixed-supported buildings.....	7
1.4.2 Poundings of bridge segments.....	14
1.4.3 Poundings of seismically isolated buildings.....	16
1.5 General aims	18
1.6 Outline	19
CHAPTER 2 IMPACT MODELING	22
2.1 Overview.....	22
2.2 Major force-based impact models.....	23
2.2.1 Linear model.....	24
2.2.2 Linear viscoelastic impact model	25
2.2.3 Hertz impact model.....	26
2.2.4 Non-linear viscoelastic impact model	27
2.2.5 Hertz impact model with non-linear damping (Hertz damp)	29
2.3 Proposed linear impact model.....	31
2.4 Proposed non-linear impact model with hysteretic damping.....	33
2.5 Estimation of the impact parameters	38
2.5.1 Coefficient of restitution	39
2.5.2 Impact stiffness	39
2.5.3 Finite element analysis	41

CHAPTER 3	MODELING OF SEISMICALLY ISOLATED BUILDINGS CONSIDERING IMPACTS	45
3.1	General.....	45
3.2	Linear elastic model for the isolation system	45
3.3	Bilinear inelastic model for the isolation system.....	46
3.4	Non-classical damping.....	47
	3.4.1 <i>Using a viscous linearized model for the isolation system</i>	47
	3.4.2 <i>Using a bilinear model for the isolation system</i>	48
3.5	Equations of motion.....	49
3.6	Numerical integration	50
3.7	Vertical location of impacts.....	53
	3.7.1 <i>Impacts at the isolation level</i>	53
	3.7.2 <i>Impacts at the isolation and the first floor levels</i>	54
	3.7.3 <i>Impacts at every floor level</i>	55
3.8	Development of the simulation software	56
	3.8.1 <i>Java programming</i>	57
	3.8.2 <i>General description of the program</i>	58
	3.8.3 <i>Analysis procedure</i>	58
	3.8.4 <i>The Graphical User Interface (GUI)</i>	61
	3.8.5 <i>Parametric analysis capabilities</i>	62
CHAPTER 4	ANALYSES CONSIDERING IMPACTS WITH THE SURROUNDING MOAT WALL	64
4.1	General.....	64
4.2	Selected seismic records for the performed analyses	64
4.3	Practical example considering a 4-story building.....	66
	4.3.1 <i>Analyses using the Kobe Earthquake record</i>	66
	4.3.2 <i>Dynamic analyses using five seismic excitations</i>	72
	4.3.3 <i>Differences in using various impact models</i>	73
4.4	Seismically isolated buildings with a basement	78
4.5	Parametric analyses.....	80
	4.5.1 <i>Effect of the flexibility of the Isolation System</i>	80
	4.5.2 <i>Effect of the gap size and the characteristics of earthquake</i>	87
	4.5.3 <i>Effect of the location of the moat wall</i>	95
	4.5.4 <i>Effect of the impact parameters</i>	96

CHAPTER 5	ANALYSES CONSIDERING IMPACTS WITH ADJACENT BUILDINGS.....	99
5.1	Introduction.....	99
5.2	Practical example.....	99
5.3	Parametric analyses.....	104
5.3.1	<i>Effect of the gap size and the ground excitation characteristics.....</i>	<i>104</i>
5.3.2	<i>Effect of the location of the adjacent structure.....</i>	<i>109</i>
5.3.3	<i>Influence of the impact parameters.....</i>	<i>119</i>
CHAPTER 6	MITIGATION MEASURES	122
6.1	Introduction.....	122
6.2	Overview of potential impact mitigation measures	122
6.3	Behavior of rubber bumpers under impact	125
6.4	Proposing an impact model for rubber	127
6.4.1	<i>Verification of the proposed impact model.....</i>	<i>127</i>
6.4.2	<i>Material and bumper stiffness</i>	<i>129</i>
6.4.3	<i>Exceedance of the ultimate compressive strain of rubber.....</i>	<i>130</i>
6.5	Example	134
6.6	Parametric studies.....	140
6.6.1	<i>Effect of the gap size and the earthquake characteristics</i>	<i>140</i>
6.6.2	<i>Effect of the bumper thickness</i>	<i>144</i>
6.6.3	<i>Effect of the maximum compressive capacity of the bumpers</i>	<i>146</i>
6.6.4	<i>Effect of the number of bumpers.....</i>	<i>148</i>
6.6.5	<i>Effect of the wall's stiffness</i>	<i>150</i>
6.6.6	<i>Effect of the impact damping.....</i>	<i>152</i>
CHAPTER 7	CONCLUSIONS	154
7.1	Research contributions.....	154
7.2	Results and discussion	156
7.2.1	<i>Poundings with the moat wall at the isolation level.....</i>	<i>156</i>
7.2.2	<i>Poundings with adjacent fixed-supported buildings</i>	<i>159</i>
7.2.3	<i>Mitigation measures</i>	<i>160</i>
7.3	Future work.....	162
REFERENCES	164

LIST OF FIGURES

Figure 1.1	Avoidance of resonance and minimization of earthquake induced loads using flexible elastomeric bearings.	3
Figure 1.2	Schematic representation of the load-displacement diagrams of the three major types of elastomeric bearings.....	3
Figure 1.3	Two major types of sliding isolation system: (a) the Pure Friction System (PFS) and (b) the Friction Pendulum System (FPS)	4
Figure 2.1	Two free bodies before and after impact.....	24
Figure 2.2	The linear elastic impact model.	24
Figure 2.3	The linear viscoelastic impact model.....	26
Figure 2.4	The Hertzian elastic impact model.....	27
Figure 2.5	The linear viscoelastic impact model [37].....	28
Figure 2.6	The Hertzian impact model with non-linear damping.	30
Figure 2.7	Error estimation for the major force-based impact models.....	31
Figure 2.8	The proposed linear viscoelastic impact model with permanent indentation.....	32
Figure 2.9	The proposed non-linear impact model with hysteretic damping.....	33
Figure 2.10	Graphical User Interface of the software application specially developed for the simulation of two colliding masses, considering the various impact models.....	35
Figure 2.11	The procedure that has been followed in order to derive the formula that provides the impact damping coefficient C_{imp}	37
Figure 2.12	Error estimation for the proposed non-linear model, compared with the corresponding major force-based impact models.....	38
Figure 2.13	The 2D finite element model used in ADINA to simulate the impact of a plate on a wall standing in front of soil.	42
Figure 2.14	Time-history of impact force resulting from FEA compared with analytical results for: (a) 1.0 m wall; and (b) 1.5 m wall, assuming a 1.0 m/sec impact velocity.....	43
Figure 3.1	Linear MDOF system model for the seismically isolated building and the corresponding stiffness matrix.	46
Figure 3.2	Bilinear modeling of the seismic isolation system behavior.....	47

Figure 3.3	Computed maximum impact force in terms of the considered time-step for various values of the impact stiffness, plotted in both decimal and logarithmic scale.....	52
Figure 3.4	Computed maximum impact force in terms of the considered time-step for various values of the impact velocity, plotted in both decimal and logarithmic scale.....	53
Figure 3.5	A seismically isolated structure, with the possibility of poundings at the isolation level.	54
Figure 3.6	Seismically isolated building with basement and potential poundings at both the isolation and the first floor level.	55
Figure 3.7	A seismically isolated building between two fixed-supported buildings.	56
Figure 3.8	A general flow of control of the integration process.....	60
Figure 3.9	The main window in the GUI of the developed software application.	62
Figure 3.10	The parametric analysis dialog of the GUI of the developed software application.....	63
Figure 4.1	Acceleration response spectra of the five selected seismic records, scaled to have a common PGA equal to 1.0 g, considering a viscous damping ratio of 5 %.....	65
Figure 4.2	Relative displacement time-histories at the isolation level of the 4-story seismically isolated building due to the Kobe Earthquake for the two cases of without and with poundings	68
Figure 4.3	Acceleration time-histories at each floor level of the 4-story seismically isolated building, without and with poundings respectively.	69
Figure 4.4	Acceleration time-histories at the top of the seismically isolated building with poundings and without poundings.....	69
Figure 4.5	Comparison of the peak responses of the 4-story seismically isolated building during poundings with the case of unobstructed response without poundings and those of the corresponding fixed-supported building.	70
Figure 4.6	Snapshots of the animated seismically isolated building under the Kobe Earthquake, considering a seismic gap equal to 15 cm.	71
Figure 4.7	Impact force time-history at the base of the 4-story seismically isolated building under the Kobe Earthquake, considering a gap width equal to 15 cm and the modified linear viscoelastic impact model to simulate poundings.....	72

Figure 4.8	Amplification of the maximum responses of the seismically isolated building when the width of the available gap around the seismically isolated building is 10 % smaller than the maximum induced relative displacement at the isolation level, for each seismic record.	73
Figure 4.9	Impact force time-histories at the base of the 4-story seismically isolated building, considering the six different impact models.....	76
Figure 4.10	Plots of the impact force in terms of indentation for the 4-story seismically isolated building under the Kobe Earthquake, with a seismic gap equal to 15 cm, considering the six different impact models.	77
Figure 4.11	Peak responses of the 4-story seismically isolated building for both cases of with and without a basement.	79
Figure 4.12	The six eigenmodes of the 5-story seismically isolated building with an equivalent effective stiffness for the isolation stiffness equal to 35 MN.	81
Figure 4.13	Amplifications of the peak floor responses of the 5-story seismically isolated building due to poundings with the moat wall, in terms of the flexibility of the equivalent linear elastic isolation system, considering two seismic gap widths and the Kobe Earthquake record.....	83
Figure 4.14	Displacement and velocity spectra of the five seismic records, considering 15% damping.....	84
Figure 4.15	Maximum amplifications of the response of the 5-story seismically isolated building due to poundings with the moat wall for the selected earthquakes, in terms of the flexibility of the equivalent linear isolation system, considering seismic a gap width equal to 20 cm and 25 cm.	85
Figure 4.16	Maximum impact velocity in terms of the flexibility of the seismic isolation system.	86
Figure 4.17	Number of impact incidences at each side of the 5-story seismically isolated building, in terms of the flexibility of the equivalent linear elastic isolation system.....	87
Figure 4.18	Maximum responses of the 4-story seismically isolated building during poundings, under the Kobe Earthquake, in terms of the width of the seismic gap.....	89
Figure 4.19	Maximum responses of the 4-story seismically isolated building during poundings, under the Northridge Earthquake, in terms of the width of the seismic gap.....	89
Figure 4.20	Maximum responses of the seismically isolated building in terms of the width of the seismic gap, for the five selected earthquakes.	90

Figure 4.21	Maximum and mean curves over the various seismic records (unscaled).....	91
Figure 4.22	Maximum responses of the seismically isolated building in terms of the width of the seismic gap, for the various earthquakes, scaled to have a PGA equal to 1 g.....	92
Figure 4.23	Maximum responses of the seismically isolated building in terms of the width of the seismic gap, for the various earthquakes, scaled to have a PGA equal to 0.6 g.....	93
Figure 4.24	Maximum impact velocities of the seismically isolated building in terms of the width of the seismic gap, for the five selected earthquakes.	94
Figure 4.25	Number of impacts incidences in terms of the width of the seismic gap.	95
Figure 4.26	Maximum floor accelerations and interstory deflections considering the moat wall on the left, on both sides, or on the right side of the 4-story seismically isolated building.....	96
Figure 4.27	Influence of the coefficient of restitution (COR) and the impact stiffness (k_{imp}) on the peak floor accelerations and interstory deflections, under the Kobe Earthquake.	98
Figure 5.1	The first two eigenmodes and eigenperiods of the 3-, 4-, 5- and 6-story fixed supported buildings, which are assumed to be adjacent to the seismically isolated building.....	100
Figure 5.2	Amplification of the maximum floor accelerations of the seismically isolated building due to poundings with adjacent structures, when the available seismic gap size is 10 % smaller than the maximum induced relative displacement at the isolation level.	102
Figure 5.3	Amplification of the maximum interstory deflections of the seismically isolated building due to poundings with adjacent structures, when the available seismic gap size is 10 % smaller than the maximum induced relative displacement at the isolation level.	103
Figure 5.4	Peak responses of the seismically isolated building in terms of the width of the seismic gap. The vertical lines indicate the SRSS of the peak displacements of the neighboring buildings for each earthquake excitation, plotted with the corresponding color and line-type.....	105
Figure 5.5	Peak responses at each floor of the seismically isolated building in terms of the width of the seismic gap for the Kobe and the San Fernando earthquakes.....	108
Figure 5.6	Peak responses of the seismically isolated building under the Kobe Earthquake during poundings with the adjacent 4-story building that is	

	considered either on the left, on the right or on both sides of the seismically isolated building.....	109
Figure 5.7	Envelopes of the peak absolute floor accelerations and interstory deflections of the seismically isolated building, for the two cases of having the adjacent structure on the one side or on its both sides, considering the Kobe Earthquake.	111
Figure 5.8	Envelopes of the peak absolute floor accelerations and interstory deflections of the seismically isolated building, for the two cases of having the adjacent structure on the one side or on its both sides, considering the Northridge Converter Station record.	112
Figure 5.9	Envelopes of the peak absolute floor accelerations and interstory deflections of the seismically isolated building, for the two cases of having the adjacent structure on the one side or on its both sides, considering the Northridge Olive View Station record.....	113
Figure 5.10	Envelopes of the peak absolute floor accelerations and interstory deflections of the seismically isolated building, for the two cases of having the adjacent structure on the one side or on its both sides, considering the Kocaeli Earthquake record.	114
Figure 5.11	Envelopes of the peak absolute floor accelerations and interstory deflections of the seismically isolated building, for the two cases of having the adjacent structure on the one side or on its both sides, considering the San Fernando Earthquake record.....	115
Figure 5.12	The case of a separation distance between the adjacent buildings larger than the gap size.....	116
Figure 5.13	Envelopes of the peak responses of the seismically isolated building, considering the distance between the adjacent superstructures equal or larger from the corresponding seismic gap width at the base.	118
Figure 5.14	Variation of the response of the seismically isolated building during poundings with adjacent fixed-supported structures, in terms of the <i>COR</i> and the impact stiffness for a 25 cm gap width.....	120
Figure 5.15	Variation of the response of the seismically isolated building during poundings with adjacent fixed-supported structures, in terms of the <i>COR</i> and the impact stiffness for a 15 cm gap width.....	121
Figure 6.1	Pieces of rubber can be attached at potential impact locations around the seismically isolated building, as an impact mitigation measure.	124
Figure 6.2	Load-strain curves obtained from static compressive loading of rubber shock-absorbers of 6, 8 and 10 mm thick (Kajita et al [43]).....	125
Figure 6.3	Test apparatus for small-scale experiments with rubber shock-absorbers, conducted by Kajita et al [43]......	125

Figure 6.4	Force-displacement curves obtained from impact tests, involving a 10 mm thick rubber shock-absorber [43].	126
Figure 6.5	Force-displacement curves for the case of incorporating a rubber shock-absorber of 10mm thickness between two steel rods of 300 Kg mass each.	129
Figure 6.6	Modeling of the impact response of a rubber bumper with an ultimate compression displacement equal to δ_u , considering three different values for the coefficient of restitution.	132
Figure 6.7	Error estimation of the non-linear impact model with hysteretic damping, considering the case where the indentation exceeds the maximum compressive capacity of the rubber bumper.	133
Figure 6.8	Locations of rubber shock-absorbers in a plan view of the building.	134
Figure 6.9	Geometrical characteristics of a rubber shock-absorber.	135
Figure 6.10	Effect of the attachment of 5 cm thick rubber shock-absorbers on the total acceleration time-history response at the isolation level, during the Kobe Earthquake.	135
Figure 6.11	Effect of the attachment of 5 cm thick rubber shock-absorbers on the total acceleration time-history response at the isolation level, during the San Fernando Earthquake.	136
Figure 6.12	Impact force time-histories for the two cases of without and with rubber bumpers attached at the base of the seismically isolated building, considering the Kobe Earthquake.	137
Figure 6.13	Impact force time-histories for the two cases of without and with rubber bumpers attached at the base of the seismically isolated building, considering the San Fernando Earthquake.	137
Figure 6.14	Impact force in terms of the resulting indentation for the two cases of without and with bumpers.	138
Figure 6.15	Differences on the maximum responses of the seismically isolated building, under the Kobe Earthquake, due to the attachment of 5 cm thick rubber shock-absorbers at the potential impact locations.	139
Figure 6.16	Differences on the maximum responses of the seismically isolated building, under the San Fernando Earthquake, due to the attachment of 5 cm thick rubber shock-absorbers at potential impact locations.	140
Figure 6.17	Amplification of the peak floor accelerations, due to the usage of rubber shock-absorbers, in terms of the width of the seismic gap.	142
Figure 6.18	Amplification of the peak interstory deflections, due to the usage of rubber shock-absorbers, in terms of the width of the seismic gap.	142

Figure 6.19	Amplification of the maximum responses of the 4-story seismically isolated building due to the usage of rubber shock-absorbers, in terms of the peak ground acceleration of the excitation.	144
Figure 6.20	Peak responses of the seismically isolated building in terms of the seismic gap width, assuming different thicknesses of the incorporated bumpers.	146
Figure 6.21	Attachment of a rubber shock-absorber in a cavity on the wall.	147
Figure 6.22	Peak responses of the seismically isolated building in terms of the seismic gap width, assuming different values for the maximum compressive strain of the incorporated bumpers.	148
Figure 6.23	Peak responses of the seismically isolated building in terms of the seismic gap width, for various numbers of rubber shock-absorbers.	149
Figure 6.24	Maximum indentation in terms of the seismic gap size, for the various excitations and four cases regarding the number of rubber shock-absorbers.	150
Figure 6.25	Peak responses of the seismically isolated building in terms of the seismic gap width, assuming three different values for the stiffness of the moat wall.	151
Figure 6.26	Peak responses of the seismically isolated buildings under Northridge Converter Station seismic record, assuming a seismic gap 23.5 cm wide and 5 cm thick rubber bumpers.	153

LIST OF TABLES

Table 2.1	Values of the impact stiffness in terms of depth resulting from FEA, for the two impact models under investigation.	43
Table 2.2	Approximate values of the impact stiffness, for the linear and non-linear models, used to simulate poundings of a seismically isolated building with a moat wall.	44
Table 4.1	Earthquake records that were used in the simulations	65
Table 4.2	Structural characteristics of the buildings that have been used in the simulations.	67
Table 4.3	Peak responses of the 4-story structure with a seismic gap = 15 cm, under the Kobe Earthquake, for the six different impact models.	74
Table 4.4	The considered seismic records with the corresponding scale factors.	88
Table 5.1	Maximum relative displacements (cm) of the seismically isolated building (base and top) and the fixed-supported buildings, under five earthquake excitations.	101
Table 5.2	The difference $\Delta d = d_{SRSS} - d_{Req}$ (cm), where the negative sign denotes insufficiency.	107

CHAPTER 1 INTRODUCTION

1.1 Seismic Isolation

Although methods of conventional earthquake-resistant design have substantially improved in the last few decades, strong earthquakes still cause undesirable damage even in cases of buildings designed according to the most rigorous seismic codes. The latter ensure the required strength and ductility to withstand cycles of inelastic deformations during severe seismic loads avoiding structural collapse and casualties, but allowing significant structural and non-structural damage as well as damage of sensitive contents of a building. In high seismicity areas, this compromise is necessary, as it is almost impossible to build a conventionally fixed-supported low-to-medium-rise building of reasonable cost and acceptable architectural design to withstand severe seismic loads without inelastic deformations. This is due to the fact that the fundamental frequencies of such buildings, unfortunately, fall within the predominant frequencies range of common earthquakes, resulting in unavoidable amplifications of ground accelerations, due to resonance, and large interstory deflections. However, this design approach tolerates significant structural and non-structural damage as well as damage of the contents of a building during strong earthquakes, which, in some cases, may not be acceptable.

In recent years, there has been an increasing demand to avoid, or at least minimize, structural and non-structural damage, prevent functionality disruption and protect sensitive equipment in buildings even under extreme earthquake excitations, which is very difficult to be achieved with conventional earthquake-resistant design. This is particularly the case for special buildings, such as hospitals, telecommunication centers and museums. Even in cases of seismic excitations of moderate intensity, where structural damages may not occur, the relatively high acceleration response can be harmful for sensitive equipment that may be housed in the building. Furthermore, in some cases, the retrofitting of existing structures may be very difficult to be achieved with conventional earthquake-resistant design due to many practical constraints. For example, many historical buildings with unique architecture need to increase their ability to resist strong earthquakes, while it is often

prohibited to significantly alter their architecture. In some other cases, any potential interruption of the operation of a building, which may house important services and activities, such as hospitals, telecommunications centers and schools, is undesirable, complicating significantly the retrofitting phase.

Today, seismic isolation ([73], [46], [62], [49]) is more widely used, aiming to mitigate the detrimental effects of strong earthquake ground motions on structures. The utilization of seismic isolation results to significantly lower lateral seismic loads acting on the superstructure by the incorporation of either flexible isolators or sliding systems at the base of the building, which shift its fundamental period outside of the dangerous for resonance range of periods (Figure 1.1). Both floor accelerations and interstory deflections can be significantly reduced. Large deformations can be confined at the isolators, which are specifically designed to accommodate cycles of such inelastic deformations. This innovative earthquake-resistant design technology aims not only to the prevention of collapse and life safety but also to the protection of the structure and its contents, as well as the continuation of the operation of the accommodated equipment, even after a very strong earthquake.

The two major categories of seismic isolators (or “seismic bearings”) are the *elastomeric bearings* and the *sliding systems*. The elastomeric bearings are usually manufactured by *laminated* elastomeric material, consisting of alternating individual layers of elastomer and non-elastic laminates, usually thin steel plates. In this way, they provide the necessary flexibility in the horizontal direction and a restoring force due to the elasticity of the elastomer, while they ensure rigidity in the vertical direction. The three most widely used types of elastomeric bearings are: (a) the Natural Rubber Bearings (NRB), which are made of natural rubber, (b) the High Damping Rubber Bearings (HDRB), which are made of special dissipative rubber compounds, providing significant energy dissipation during cyclic loading and (c) the Lead Rubber Bearings, whereas one or more lead cores are incorporated in the bearing in order to provide additional damping through its yielding during cyclic loading. The typical behavior of the three different types of elastomeric isolators under cyclic loading is shown in Figure 1.2.

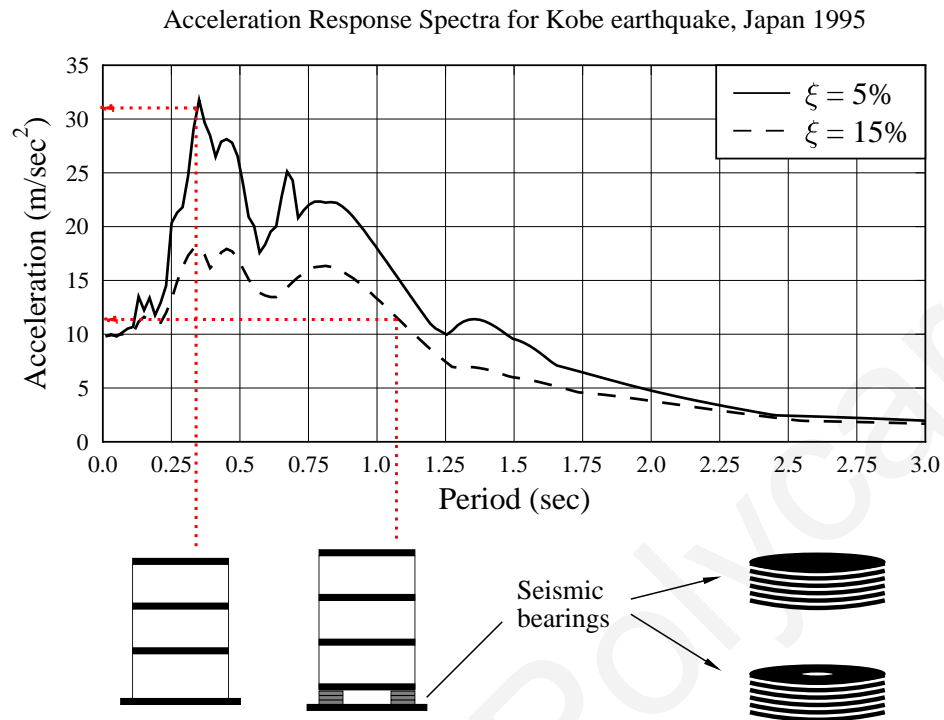


Figure 1.1 Avoidance of resonance and minimization of earthquake induced loads using flexible elastomeric bearings.

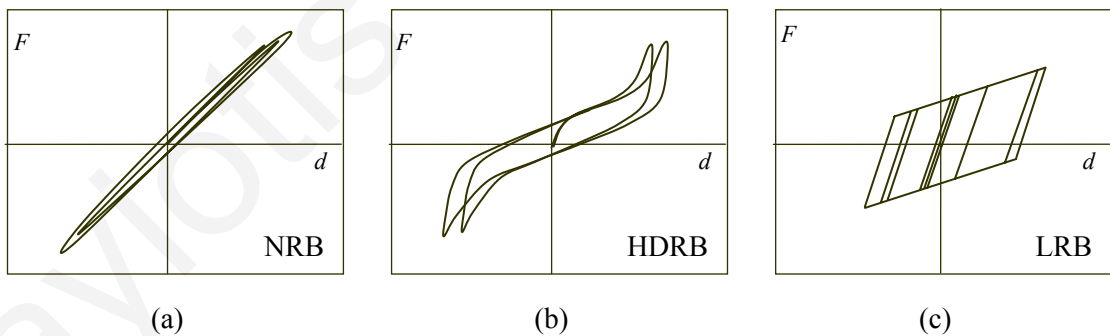


Figure 1.2 Schematic representation of the load-displacement diagrams of the three major types of elastomeric bearings.

The sliding isolation systems are based on the limitation of the shear-force that can be transferred through the bearings to the superstructure. In particular, the value of the friction coefficient of the isolators influences the maximum base shear-force that can be transferred to the superstructure during a strong ground motion. The two main types of sliding systems

are (a) the Pure-Friction System (PFS), which consists of a flat sliding surface and does not have any inherent restoring force, and (b) the Friction Pendulum System (FPS), which consists of a friction slider moving on a concave surface, providing both restoring force and dissipation of energy through the friction mechanism.

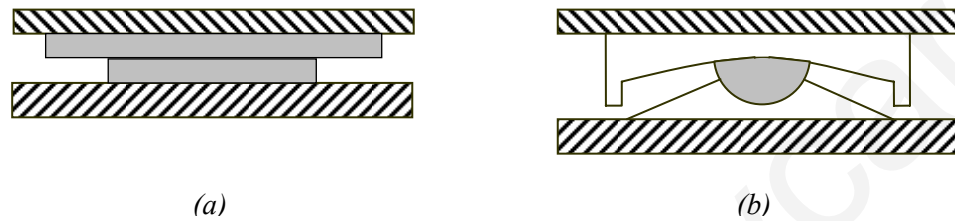


Figure 1.3 Two major types of sliding isolation system: (a) the Pure Friction System (PFS) and (b) the Friction Pendulum System (FPS)

In contrast to the classical techniques of retrofitting, seismic isolation can be implemented without significant modifications on the structure's architecture, since the induced seismic loads are significantly reduced. In addition, an existing building can be seismically isolated without the interruption of its operation, since the intervention is limited at the isolation level. For these reasons, seismic isolation is increasingly implemented in high seismicity areas as one of the most promising anti-seismic technology, in particular for the retrofitting and seismic upgrading of existing valuable buildings or buildings that host critical services or sensitive equipment.

1.2 Motivation

Seismically isolated buildings are expected to experience large relative displacements during strong earthquake excitations, especially when the latter contain long-period impulses ([75], [36], [56], [33]). In order to accommodate such large relative displacements, a sufficiently wide clearance, which is known as "seismic gap", must be provided around the building. In modern anti-seismic codes, including the Eurocode 8 [28], the minimum size of the seismic gap around a seismically isolated building is not provided explicitly for obvious reasons, letting the engineer to estimate a sufficiently wide seismic gap, considering all the relevant factors. Most codes indicate only that the size of the gap must be "sufficient" without further information. A common practice is to take the width

of the seismic gap to be equal to the ultimate permitted lateral displacement of the isolation system [75]. Obviously, it cannot be less than the expected maximum design displacement of the seismically isolated building, but it also cannot be too large due to economic and practical reasons, especially in some cases of retrofitting existing structures or when the buildings are situated in densely built locations. In addition, for an extreme case of having a displacement larger than the ultimate capacity of the isolation system, the failure of the seismic isolators would render the superstructure unstable with destructive consequences. Beyond the fact that the width of the seismic gap is limited, there are uncertainties regarding the characteristics of the design earthquake and especially the expected maximum relative displacement of the seismically isolated building, which is the determinant factor for the estimation of the seismic gap.

Therefore a potential risk is the possibility of the seismically isolated building pounding against an adjacent structure during a larger than expected earthquake. Adjacent structures may be either the surrounding moat wall or a neighboring fixed-supported building, constructed in close proximity with the seismically isolated building. For the prevention of poundings of seismically isolated buildings, the codes do not take into account the existence of adjacent deformable buildings. In such cases, due to the deformations of the superstructures of the neighboring buildings, poundings may happen before the collision of the seismically isolated building to the surrounding moat wall, at the isolation level.

Taking all these aspects into account, it is essential to thoroughly investigate the possibility of poundings of seismically isolated buildings and the consequences that they may have on the effectiveness of seismic isolation. In particular, there is a scientific interest and a practical necessity to investigate the complex research problem of earthquake induced poundings of seismically isolated buildings, since there is an increasing number of seismic isolation applications in earthquake-prone areas, while there is a lack of knowledge and understanding of the consequences of such structural impacts during strong earthquakes. For the achievement of this investigation, a large number of simulations needs to be conducted, in order to examine the effects of poundings on the dynamic response of seismically isolated structures, as well as the various parameters that affect their responses.

Such investigation will contribute to the understanding of how potential poundings may affect the performance of seismically isolated buildings and whether relevant impact mitigation measures may be useful.

1.3 Pounding incidences during past earthquakes

Although the seismic isolation technology began to be implemented in structures only during the last few decades, a case of pounding occurrences, during a strong earthquake, can be found in the literature [63]. In particular, the base-isolated Fire Command and Control (FCC) building in Los Angeles experienced impacts at its base during the 1994 Northridge Earthquake, as it was observed in the recorded strong motion data. The building is a two-story steel frame structure with an isolation system consisting of high damping elastomeric bearings. According to the reconnaissance report, one-sided impact occurred against the concrete entry bridge in the northeast corner of the building. The accelerometers that were attached on each floor of the building, recorded an amplification of the acceleration response at the isolation level, in the direction of pounding, from 0.22 g that was the peak ground acceleration, to 0.35 g, while at the other direction the ground accelerations were reduced due to the seismic isolation from 0.18 to 0.07 g.

Poundings of fixed-supported buildings have been more frequently observed around the world, especially during very strong earthquakes, ranging from light local to heavier damage that might even have initiated collapse ([3], [10], [20], [23], [25]). After the 1985 Mexico Earthquake, great attention was given to structural poundings, since they had been considered as a leading cause of building collapses, based on an exaggeration concerning the actual damage due to poundings ([4], [6]). Although the number of buildings that were severely damaged due to poundings was initially overestimated [70], after reconsideration, a few years later, it was reported that only in 4 % of the severely damaged or collapsed buildings, during the Mexico City Earthquake, poundings could have played a significant factor ([3], [4], [6]). Furthermore, it has been observed that the most severe damage due to poundings occurred in cases of unequal heights, different structural systems and different configurations of the adjacent buildings [10].

Moreover, pounding incidences have also been observed in bridges during the 1994 Northridge Earthquake [21], the 1995 Kobe Earthquake in Japan [22], the 1999 Chi-Chi

Earthquake in Taiwan [24], the 1999 Kocaeli Earthquake in Turkey [23], the 2001 Nisqually Earthquake in Washington [25] and the 2001 Bhuj Earthquake in Gujarat, India [26]. In general, the damage, as identified in the reconnaissance reports, was mainly localized at girder-ends and abutments in most of the cases, while only in few cases pounding was identified as potential contributor to the collapse of bridge decks [22].

1.4 Past research studies on poundings

Numerous research studies have been conducted in order to examine the effects of earthquake induced poundings on the seismic response of structures. The following paragraphs outline the results from relevant numerical and experimental research works that are provided in the scientific literature.

1.4.1 Poundings of fixed-supported buildings

Anagnostopoulos [2] investigated numerically the case of typical fixed-supported buildings, standing next to each other in close distance, undergoing strong seismic excitations. This work is one of the most cited research studies regarding the problem of structural seismic poundings, since it was one of the first research works where numerical simulations had been conducted to investigate this problem, which was given great attention after the Mexico City Earthquake in 1985 [10]. The buildings were simulated in series using single-degree-of-freedom (SDOF) systems with non-linear behavior and a forced-based impact model, which will be described in detail in the next chapter, to calculate the impact forces acting on the colliding masses. Several determinant factors were examined parametrically, such as the number of buildings in a row, the gap size, the strength of the SDOF systems, the relative size of system masses and the impact parameters. The results concerned the amplification of the displacement response due to poundings. It was found that the detrimental effects of poundings were more pronounced for the first and the last buildings in the row. On the contrary, for the “interior” buildings, sometimes poundings were found to be beneficial. This remark coincides with reconnaissance reports from past earthquakes, where “corner” buildings seemed to have more severe damages due to poundings than the “interior” buildings. In addition, it was concluded that, when there are substantial differences in the masses of the adjacent

buildings, the effects of poundings are more pronounced for the structure with the smaller mass. Finally, the increment of the gap size was found to reduce the effects of poundings.

Later, as an extension of the previous work, Anagnostopoulos and Spiliopoulos [7] examined parametrically the case of poundings of buildings in series, simulated as multi-degree-of-freedom (MDOF) systems. They concluded that poundings affect considerably the response when the adjacent buildings have significant differences in height, flexibility or mass. Specifically, in the case of unequal heights, if the lower building is relatively stiff, then the taller building exhibits a “whiplash” type behavior, leading to excessive interstory deflections and ductility demands for the upper stories. The ductility demand in such cases could reach the value of 5, for the considered simulations. The case of a relatively flexible building pounding against a much stiffer structure at lower floors is very similar to the case of a seismically isolated building that hits on the surrounding moat wall due to an inadequate seismic gap.

The specific case of a tall flexible building pounding with an adjacent lower building that is much stiffer, has been investigated by Maison and Kasai [54]. In particular, they examined the case of an actual 15-story building, simulated as a MDOF system with shear-beam behavior, pounding against an adjacent 8-story building, which was considered as completely rigid. Poundings were assumed to happen only at a single floor of the building of interest. The results indicated that for the floors above the pounding level, the story drifts, shear forces and overturning moments are amplified due to impacts. The amplification of the story drifts of the last story in some cases may reach 290 %. The base shear force becomes larger when impacts occur in higher floors, due to the fact that the impact velocities, and consequently the collision forces, are higher in that case, which are reflected to the building’s base. As an extension of that research, in a latter work, the same researchers [55], examined the same case, simulating both buildings as MDOF systems.

Papadrakakis et al [67] simulated building interaction during earthquake excitations using a Lagrange multiplier approach, satisfying the geometric compatibility and utilizing the impulse-momentum relationship and energy dissipation conditions to calculate the velocities after impact. More details about their methodology concerning the structure-to-structure interactions are provided in the following chapter, which refers to the specific

subject of impact modeling. For the implementation of their methodology, they simulated two adjacent buildings as MDOF systems, considering both cases of aligned and unaligned floor levels. They used rotational and translational springs to simulate the deformability of the ground and considered only harmonic motions, as ground excitations. They observed greater amplification of the response due to poundings for the less excited structures, while the effect of poundings was found to be beneficial for buildings vibrating near resonance.

Stavroulakis and Abdalla [74] studied the pounding problem, providing a methodology for estimating the order of magnitude and the distribution of the contact forces between two adjacent buildings when using the pseudo-static method to represent the earthquake-induced forces. They concluded that for equal-in-height buildings, the contact forces are reduced with the increment of the gap size, while for the case of unequal heights the maximum contact force arises at the top of the shorter building.

Davis [16] used a SDOF system impacting against a rigid barrier in order to produce impact velocity spectra for a range of the model parameters. The Hertz non-linear contact law was employed in the simulations. A peak on the impact velocity spectrum was observed for an excitation period near the half of the corresponding eigenperiod of the non-impacting oscillator. In addition, for cases of a finite gap size, there is a lower cut-off period on the impact velocity spectrum, where usually the maximum impact velocity is observed, while below that period no-poundings occur.

Athanasiadou et al [8] performed an extended parametric investigation regarding poundings between structures in series, using SDOF systems with an elastoplastic behavior, taking also into account the phase difference of the traveling waves of the seismic excitation. For the simulation of impact, they followed the stereomechanical approach, where the contact is instantaneous and the velocities after impact are calculated based on the conservation of momentum, taking also into account an amount of dissipated energy represented by the coefficient of restitution. They also found that the effects of poundings are more pronounced for buildings at the end of the row as well as for the stiffer buildings in the row. In addition, they observed that poundings become more critical for the response of the structures in series when the phase difference of the traveling wave of the excitation increases.

As an extension of the previous work on poundings [67], Papadrakakis et al [65] simulated the problem in three dimensions, using MDOF systems and the Lagrange multiplier approach to simulate contacts. A relatively stiff two-story building was considered adjacent to two more flexible buildings of the same height, in orthogonal directions in plan. The effect of stiffness irregularities in plan was also investigated. The numerical analyses revealed that the strain-energy loading, which the stiff structure experienced during poundings with the adjacent flexible structures, could increase up to 68 times compared to the corresponding response without poundings. In addition, the amplification of the response reached up to 40 % in the case of the three-building orthogonal scheme with stiffness irregularities, due to the torsional response, compared to the case of the two-building pounding.

Pantelides and Ma [64], considering a SDOF structural system with either elastic or elastoplastic behavior pounding against a rigid barrier, investigated through numerical simulations certain parameters that affect pounding among concrete structures. For the estimation of the impact forces, they used the Hertz contact law and found that the response of the structures is not sensitive to the value of the impact stiffness. The parametric studies showed that the damping capacity of the structure affects the response during poundings more significantly for flexible systems rather than for relatively stiff systems with a natural period lower than 0.3 sec. Furthermore, the response during poundings of the inelastic structure is lower than in the case of the corresponding elastic structure, except from the displacement response, where the opposite was observed. In addition, the Uniform Building Code provisions for the estimation of the minimum required separation distance to prevent poundings were found to be quite conservative for the four cases of earthquake excitations that had been examined.

Liolios [52] focused on the simulation of the interaction between adjacent buildings, taking also into account the friction and treating this case as a hemivariational inequality problem of the mathematical theory of elasticity. Specifically, he examined the effect of the non-linear elastoplastic behavior of contact material on the overall response of the structure during poundings. Two single-story buildings were examined, different in plan, with the one being symmetric in the direction of the excitation and the other with

asymmetric plan, resulting to torsional vibrations. Substantial torsional response was observed for the first building due to the interaction with its adjacent building during the ground excitation.

Chau and Wei [12] examined analytically the case of impacts between two SDOF oscillators under harmonic excitations, based on the previous work of Davis [16]. They also used the impact velocity as a qualitative data for the pounding effects. They observed that when the difference in the natural periods between the two oscillators increases, the impact velocity also increases drastically. Additionally, the impact velocity spectrum was found to be relatively insensitive to the separation distance between the two oscillators.

A similar approach was followed by Jankowski [39], in order to derive a pounding force response spectrum under earthquake excitation. In particular, two adjacent structures were simulated using SDOF systems and a non-linear impact model with viscous damping to compute the impact force. Both elastic and elastoplastic behavior was considered for the structures that were analyzed under various seismic records. It was concluded that the structural parameters, such as the gap size, the natural vibration periods of the structures, damping, mass and ductility as well as the time-lag of input ground motion records, may substantially affect the peak pounding force value.

Dimitrakopoulos et al [18], using dimensional analysis, investigated the case of poundings among two or three SDOF oscillators, under various pulse-type ground excitations, in an effort to identify distinct physical similarities. The response was presented in dimensionless terms of the maximum displacement of the oscillator normalized to the persistency of the excitation pulse. The interaction between the adjacent structures was treated as a mathematical inequality problem, simplified though to be frictionless and centric. They observed that when the response is presented in the dimensionless Π -terms, regardless of the acceleration level and duration of the pulse, all response spectra become self-similar and follow a single master curve. They also conclude that due to pounding, the response of the most flexible among a pair of two oscillators is amplified in the low range of the frequency spectrum, while the response of the stiffest oscillator is amplified in the upper range of the frequency spectrum.

Anagnostopoulos and Karamaneas [6] proposed the use of collision shear walls to minimize seismic separation and to protect adjacent buildings from collapse due to earthquake-induced pounding. They used non-linear dynamic analyses to simulate poundings between two real buildings of unequal heights, a case where slab-to-column impacts occurred. The results showed that the presence of the collision shear walls can mitigate the detrimental effects of poundings on the response of both adjacent buildings through the minimization of the gap size. Local repairable damage may occur at the impact locations on the collision walls, while away from those locations no significant threat seems to be posed to the rest of the structural members due to poundings.

Jankowski [40] performed three-dimensional non-linear dynamic analyses and parametric studies to investigate the case of earthquake-induced poundings between equal height buildings with substantially different dynamic properties. Two 3-story structures, the one relatively stiff and heavy and the other more flexible and lighter, were simulated as MDOF systems with elastoplastic behavior and lumped masses. Using the El Centro Earthquake record as ground excitation, it was found that poundings lead to substantial amplification of the response of the flexible building and considerable permanent deformation due to yielding. The stiffer and heavier building, though, seemed to be almost unaffected from poundings. In addition, from the parametric studies it was found that only the maximum induced displacement of the flexible building is affected by the structural characteristics, such as the gap size, mass, story stiffness and strength, during poundings.

Beside the analytical and numerical studies on structural poundings, some researchers tried to investigate the problem through small-scale experiments. Filiatrault et al [29] conducted an experimental study of poundings between two steel-frame structures of eight and three stories, respectively, subjected to shake-table tests in a single direction. They observed very limited effects of poundings on the horizontal displacements, except for the case of a zero gap size, where the lateral displacements of the 3-story building were reduced substantially. On the contrary, floor accelerations were drastically increased due to pounding especially at the pounding floors, where the peak absolute acceleration could reach up to 20 – 30 g. They compared the experimental results with the predictions resulting from two pounding analysis software applications and found good correlation

regarding the displacements and impact forces, but the amplitude of short acceleration impulses due to impact could not be accurately predicted.

Papadrakakis and Mouzakis [66] performed shake-table experiments for a pair of two-story buildings, made of reinforced concrete, with equal story heights but different stiffness. The test structures were subjected to harmonic excitations considering zero initial gap size. The tests showed that the stiffer structure suffers more from poundings when the excitation frequency is near the eigenfrequency of the adjacent flexible structure and its input energy in that case is larger than the corresponding energy during its resonance. They recorded a dramatic increase of the acceleration response during poundings, especially for the stiffer structure and its top floor level. Nevertheless, these acceleration impulses, due to their short duration, are resisted by the inertia of the slabs and do not directly affect the deformations of the structure. The researchers also observed local damage at the area of impact, which was recorded as interpenetration, leading to an increase of the gap size that affected negatively the response. Finally, the experimental results were compared to analytical predictions, with which they were found to be in good agreement.

Chau et al [13] also conducted shake-table experiments involving two SDOF steel towers with different natural frequencies, damping ratios and separation distances, subjected to both sinusoidal waves of various magnitudes and frequencies, as well as a real earthquake acceleration record. They observed that under harmonic excitations, the maximum impact velocity occurs when the excitation frequency value is between the eigenfrequencies of the two structures. The tests revealed that poundings between the two structures may occur periodically or not periodically. Nevertheless, it was observed that a group of non-periodic poundings may repeat periodically. The researchers used the experimental results to validate the analytical solutions presented in a previous work [12] and found that the analytical scheme is reliable to predict the region of frequencies that poundings can occur, considering a given gap size. In addition, the results obtained during the shake-table test, using the earthquake excitation, were found to be in a good agreement with the corresponding results from theory.

Chau et al [14] conducted shake table tests, considering the steel models of two real asymmetric tall buildings in Hong Kong with irregularities in plan that cause torsional

vibrations under earthquake excitations. Torsional poundings were observed between the two models at the top and mid-levels due to the higher mode responses of the structures. It was also observed that energy may be transferred from the more massive building to the lighter building through impacts, causing abnormally large vibrational response of the lighter building compared to the case without any poundings.

1.4.2 Poundings of bridge segments

Significant research studies have also been conducted to investigate poundings in bridges. Although the structural system of bridges is quite different from that of multistory buildings, some of the effects of poundings are the same or very similar for both types of structures. Therefore, it is useful to consider some representative results obtained from studies on poundings of bridges, as presented below.

Jankowski et al [41] simulated the segments of the superstructure of an elevated seismically isolated bridge as SDOF systems in series with non-linear behavior, interacting both in longitudinal and transverse directions. The results indicate that the largest impact forces and induced shear forces occur for the widest gaps between segments where impacts still occur.

DesRoches and Muthukumar [17] examine the parameters that affect the overall response of a multiple-frame bridge due to pounding of adjacent frames. It was found that the most important parameters are the ratio of the fundamental periods of the simulated frames and the characteristic period of the ground motion. The amplification in the frame's response due to one-sided pounding was found to be more severe for cases with highly out-of-phase frames, in particular for the stiffer structures.

Zhu et al [83] developed a new three-dimensional (3D) contact model to simulate impacts, taking also into account sliding phenomena among bridge girders during impacts. Small-scale experiments were conducted to verify the accuracy of the proposed model, which was found to be appropriate for the 3D simulation of poundings of bridge segments. Numerical simulations of a three-span elevated bridge under seismic excitations revealed a significant increase of the girder's rotating angle due to poundings.

Kim and Shinozuka [48] used two-dimensional (2D) non-linear finite element analysis to model a bridge and investigate the effects of earthquake-induced pounding at expansion joints. The numerical results indicated that impact affects significantly the acceleration and velocity responses, but only slightly the displacement response. The researchers argued that, due to the fact that usually there are no substantial differences in natural periods of the adjacent segments of a bridge, the amplification of the response due to poundings is relatively low and no considerable threat is posed for the safety of such structures due to impacts.

Ruangrassamee and Kawashima [71] suggested the use of semi-active control and variable dampers to mitigate the effects of poundings in bridge segments. An investigation was conducted numerically and was found that poundings can be minimized due to the reduction of the relative displacement among adjacent decks with the use of variable dampers.

Watanabe and Kawashima [79] numerically simulated two adjacent bridge decks as elastic rods that collide along their longitudinal direction, considering a linear impact spring to calculate the impact forces. They compared the derived results with the exact solutions based on wave propagation theory. It was found that the simulation of poundings with an impact spring provides a good estimate to obtain an overall behavior of the colliding structures, except for the acceleration response.

Recently, Guo et al [32] conducted experimental and analytical investigation for the use of magnetorheological (MR) dampers to mitigate poundings in highway bridges. During the large-scale shake-table experiments, the acceleration response due to poundings during the El Centro Earthquake excitation, before the implementation of the dampers, was found to be increased up to 250 %, appearing in time-histories in the form of sharp spikes. After the implementation of the MR dampers, a significant reduction on the amplification of the response was observed.

In the above overview, on previous research work on structural poundings, one may notice that some observations regarding the results from various numerical and experimental investigations are contradictory. In the conclusions section, Kim and

Shinozuka [48] made an interesting remark about the actual effects of earthquake induced poundings on structures. They argued that poundings may be beneficial or detrimental for a structure depending on certain parameters and conditions and no general conclusions can be safely derived from all conducted research on the topic. A common conclusion is that the effect of pounding on the response of the structure is a very complex one, depending on various parameters describing the structures and the characteristics of the ground motion.

1.4.3 Poundings of seismically isolated buildings

Compared to the extensive research work on poundings of conventional buildings and bridges, very limited research studies have been carried out for poundings of seismically isolated buildings, which exhibit quite different dynamic characteristics from fixed-supported buildings. In particular, as mentioned in the beginning of the chapter, poundings of seismically isolated buildings occur primarily as a result of the large relative displacements at the isolation level, while in the case of fixed-supported buildings poundings occur due to the deformations of the superstructures. Furthermore, it is more likely to have more rigorous performance requirements and higher expectations for buildings that utilize an innovative earthquake-resistant design, such as the seismic isolation technology, than for conventionally fixed-supported buildings. The conclusions derived from previous studies on poundings of seismically isolated structures are summarized below.

Tsai H.C. [76] was the first who analytically investigated the possibility of a seismically isolated building pounding against the surrounding moat wall. Specifically, he simulated the superstructure of an isolated building either as a viscoelastic or elastoplastic shear-beam, with the isolation system modeled as either linearly elastic or bilinearly elastoplastic. The surrounding moat wall was simplified as a spring and a dashpot in parallel, separated by a finite seismic gap from the seismically isolated shear-beam. The analysis was based on wave propagation theory, while the Newmark's implicit integration method was used. The results indicated that the sudden change of the stiffness at the base of the structure creates impact waves that travel along its height and induce an extremely high acceleration response in the shear-beam, especially if the latter remains elastic. If the shear beam yields during the excitation, the impact waves cannot propagate through the shear-beam and only

the base is subjected to high accelerations. In addition, it was found that the viscous damping of the moat wall did not seem to affect the beam acceleration during poundings, while acceleration the response is reduced when a non-linear (exponential) behavior of the wall is implemented. The high acceleration response was also found to be minimized when a relatively low strength was provided for the wall due to the dissipation of the energy through its elastoplastic behavior. Nevertheless, in that case, larger displacements occurred.

Malhotra [57] also used wave propagation theory, simulating the superstructure as a uniform shear-beam, in order to investigate the response of a seismically isolated building pounding against the surrounding retaining wall, which was represented by an elastic spring. The structure was let to hit against the barrier at its base with a constant velocity. He considered the base-isolated shear-beam vibrating in three different stages, before, during and after impact, avoiding the use of impact elements. The numerical calculations revealed that that the base shear-force of the seismically isolated beam increased with the stiffness of the structure or with the stiffness of the retaining wall. In addition, the results indicated that the base shear-force may sometimes become higher than the total weight of the building, depending also on the impact velocity.

Quite similar work with the above two studies has been done by Dimova, S.L. [19], who examined the response of a sliding system during earthquake induced poundings, emphasizing the minimization of numerical errors due to the sudden change of the sign of the velocity. In particular, considering a rigid block sliding with an initial velocity against a rigid barrier, and using the stereomechanical method to model impact, a solution scheme is proposed for choosing an appropriate time-step size, in order to avoid numerical errors.

Matsagar and Jangid [58] parametrically examined poundings of seismically isolated buildings, simulating their superstructure as a shear-type MDOF system and considering various types of seismic isolation system behavior. Impacts were assumed to happen only at the base of the building with the surrounding moat wall, which was simulated with a linear spring and a dashpot. Certain parameters were varied in order to examine their effects on the response of the seismically isolated buildings during poundings. The variation of the top-floor accelerations and the base relative displacements due to poundings were examined, under different earthquake excitations. The analysis results

showed that, in general, the accelerations of the building increase, while the relative displacements at the base of the seismically isolated building are reduced due to poundings. Furthermore, it was also observed that the superstructure's accelerations increase with the width of the seismic gap up to a certain value and, then, the accelerations decrease with further increase of the gap. Finally, they concluded that poundings affect more the response of seismically isolated buildings when the latter have a flexible superstructure, an increased number of stories or relatively stiff adjacent structures.

Agarwal et al [1] examine the case of poundings between two-story buildings that were taken to be either fixed-supported or seismically isolated. In the case of seismically isolated buildings, a sliding isolation system with varying friction was considered. The case of poundings between a seismically isolated building and a fixed-supported building was not taken into account. Four different seismic records were used in the analyses in order to examine the behavior of these structures under seismic loadings, taking into account potential impact phenomena. In the case of two adjacent seismically isolated buildings, the results showed that pounding occurred only at very small initial seismic gaps, because both buildings tended to slide in the same direction, keeping the gap between them approximately constant. Furthermore, it was found that friction varying base isolation is able to reduce the number of impacts for some earthquakes, while that is increased for others.

Although the previous research on earthquake-induced poundings of seismically isolated buildings that has been described above provides some basic information about the effects of impacts on the response, still there is a need for further investigation of the problem, using more effective modeling approaches and taking into account more influencing parameters.

1.5 General aims

The limited research studies that have been conducted regarding poundings of seismically isolated buildings, in combination with the reports of such events during strong earthquakes, lead to the need for investigation of this problem and consideration of appropriate measures for confronting its consequences. The general aim of this research study is the numerical investigation of poundings of seismically isolated buildings using

software applications that are specially designed and developed, utilizing modern computing technologies and object-oriented design and programming. Specifically, the methodology is based on the development of specialized software tools that provide the ability of conducting two-dimensional dynamic analyses of buildings, simulated as multi-degree-of-freedom systems, with the possibility of poundings between adjacent structures. Poundings of a seismically isolated building may occur either with the surrounding moat wall or with other adjacent buildings. Emphasis is also given on the simulation of poundings using various impact models, in order to assess their suitability to sufficiently well simulate the problem under consideration. The investigation of the effects of earthquake-induced poundings on the effectiveness of seismic isolation through parametric analyses will reveal the parameters that have the greater impact on the dynamic response of a seismically isolated building. Subsequently, the effectiveness of proposed practical measures on mitigating the effects of poundings for cases of relatively narrow seismic gaps is also investigated, by performing relevant numerical simulations and parametric studies.

This research work aims to provide useful knowledge about the consequences of poundings on the seismic performance of seismically isolated buildings. Since seismic isolation is one of the most innovative and promising anti-seismic technologies, which is widely used in earthquake-prone areas, it is important to understand all risks and limitations that are involved in its utilization and assess the effectiveness of potential impact mitigation measures. Finally, an important aspect of this work is the promotion of the utilization of modern software design and computer-aided methods, such as object-oriented programming, in engineering research.

1.6 Outline

Some general information about the earthquake-resistance technology of seismic isolation and the problem of earthquake-induced poundings that is addressed in the current thesis has been presented in this first chapter, along with the basic remarks and conclusions from previous relevant studies. In addition, the major objectives of this research work have been outlined in the above paragraph.

Chapter 2 refers to the modeling of impacts in cases of numerical simulation of structural poundings, while the major force-based impact models from the relevant

scientific literature are presented. Furthermore, a modification of the linear viscoelastic impact model is proposed in order to improve its accuracy, while a new non-linear impact model with hysteretic damping is developed. A finite-element analysis is performed, simulating the collision of a concrete plate on a wall, in order to estimate an appropriate value for the impact stiffness parameter to be used in the simulations of structural poundings.

The methodology that has been followed to address the problem and the related assumptions are presented in Chapter 3. The various configurations of the seismically isolated building, regarding the type, characteristics and location of the adjacent structures, are also described in this chapter. Finally, a brief description of the specially designed and developed software application that is used for the necessary numerical simulations and parametric studies is made.

In Chapter 4, a series of simulations and parametric studies is described, considering a seismically isolated building pounding at its base with the surrounding moat wall due to an inadequate seismic gap width. First, a single analysis of a typical seismically isolated building is performed in order to provide a general aspect of the effects of earthquake-induced poundings on its dynamic response. Then, the results of a series of parametric analyses are presented, demonstrating the effect of certain parameters on the response of seismically isolated buildings during poundings. Such parameters include the flexibility of the isolation system, the available seismic gap size, the ground motion characteristics and the impact parameters. Also, the case of using different impact models for simulating poundings of a seismically isolated building is considered in this chapter.

The case of a seismically isolated building pounding against other fixed-supported buildings that are in close proximity is investigated in Chapter 5. In particular, parametric analyses are performed in order to examine, among other parameters, the influence of the type, the characteristics and the location of the adjacent fixed-supported buildings on the response of a seismically isolated building considering poundings.

In Chapter 6, the possibility of attaching layers of rubber at the impact locations (i.e. at the isolation level) to act as collision bumpers aiming at the mitigation of the detrimental

effects of impacts on the structural response and, consequently, the equipment that may be housed in the building, are examined. For the modeling of the behavior of rubber bumpers under dynamic compressive loadings, a proposed non-linear hysteretic impact model is used that takes into account the finite thickness of the bumpers, after it is validated based on experimental results from the literature. A parametric investigation is performed in order to examine whether the use of rubber shock-absorbers is beneficial, considering that with their implementation the available clearance around a seismically isolated building is reduced.

Finally, the contributions of the current study are presented, in Chapter 7, while the general conclusions regarding the results of this research are discussed. In addition, some plans and suggestions for future work in this specific research area are also included in this chapter.

CHAPTER 2 IMPACT MODELING

2.1 Overview

The numerical modeling of impact and the estimation of the impact forces acting on the colliding bodies is an essential topic, not only for the cases of structural poundings, but also for other research purposes involving numerical simulation of contact and impact problems. In most cases, impacts involve local plastic deformations, friction, thermal, acoustic and other complex phenomena that render their detailed modeling very difficult, if not impossible. However, in the case of structural poundings, a simple impact model that can be used to estimate with sufficient accuracy the impact forces acting on the colliding structures is only needed.

Structural impact is usually considered in the literature using methods that are based either on *stereomechanical* or *forced-based* approaches [31]. The stereomechanical, also known as impulse-based, approach assume that the duration of an impact is zero and compute instantaneous changes of the velocities based on the preservation of momentum, taking also into account the *coefficient of restitution*. The latter is defined as the ratio of the relative velocity between the colliding bodies after and before impact:

$$0 \leq COR = \frac{\Delta V_{,after}}{\Delta V_{,before}} \leq 1 \quad (2.1)$$

A value of the coefficient of restitution equal to 0 corresponds to perfectly plastic impact, while a value equal to 1 corresponds to the case of no energy dissipation during impact, which means that the impact is perfectly elastic. The velocities of the colliding masses at the instant of impact are calculated as:

$$v'_1 = v_1 - (1 + COR) \cdot \frac{m_2 \cdot (v_1 - v_2)}{m_1 + m_2} \quad (2.2)$$

$$v'_2 = v_2 + (1 + COR) \cdot \frac{m_1 \cdot (v_1 - v_2)}{m_1 + m_2} \quad (2.3)$$

Force-based, also known as *penalty*, methods seem to be more suitable for numerical simulations of multiple deformable bodies. These methods allow interpenetration between the colliding structures, which is justified by their deformability at the vicinity of the contact. Contact springs are automatically formed when an impact is detected, kept as long as the bodies remain in contact and removed as soon as the structures detach from each other. The interpenetration depth is used together with the stiffness of the contact spring to estimate, according to the impact model, the contact forces that are applied to the structures, pushing them apart. Usually, in simulations involving structural pounding, the impacts are considered to be central, i.e. without friction developed in the tangential direction. In a real case of poundings between adjacent buildings, friction phenomena occur during an impact, which in the case of a 3D analysis may significantly affect the torsional vibration of the buildings [52]. Nevertheless, when 2D analysis is considered, it can be assumed that any friction forces in the tangential direction do not affect the computed response and therefore are omitted.

Many researchers have used the stereomechanical method to simulate structural poundings due to its advantage of avoiding the estimation of proper values for the impact stiffness [8], [17], [65]. However, this method of impact modeling has the disadvantage that only one impact incident can be considered at each time step. Therefore, in cases where the buildings are in series with very small or no gap size, there is a question about the appropriateness of using such a method. On the other hand, force-based impact models allow the efficient simulation of more than one impacts occurring on the structure at the same time, due to the fact that the computed impact forces are superimposed in the corresponding equation of motion.

Since in most numerical studies on structural poundings, force-based impact models are used, it is useful to make a brief description of some of the most popular force-based impact models, as well as some of their implementations.

2.2 Major force-based impact models

Usually the description of an impact model refers to the general case of two free bodies, each one with a mass m_i and a velocity v_i that collide to each other with a small indentation (Figure 2.1).

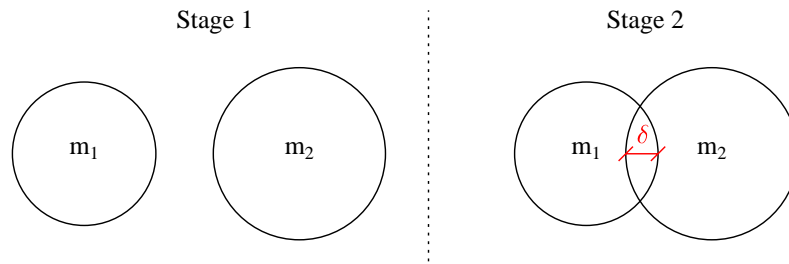


Figure 2.1 Two free bodies before and after impact

2.2.1 Linear model

The simplest force-based impact model is based on a linear impact spring, which provides an elastic impact force that is activated whenever the bodies come into contact and equals:

$$F_{imp}(t) = k_{imp} \cdot \delta(t) \quad (2.4)$$

where k_{imp} is the stiffness of the linear impact spring and $\delta(t)$ is the interpenetration depth of the colliding bodies that overlap each other at time t . Figure 2.2 presents plots of the impact force in terms of time and displacement of a moving body that hits against another stationary structure. The duration of the impact as well as the interpenetration depth depend on the stiffness of the impact spring, which is difficult to be accurately determined, as will be shown in the next sections. Many researchers have used the linear elastic impact model in relevant studies, mainly due to its simplicity ([29], [54], [71], [76], [79]).

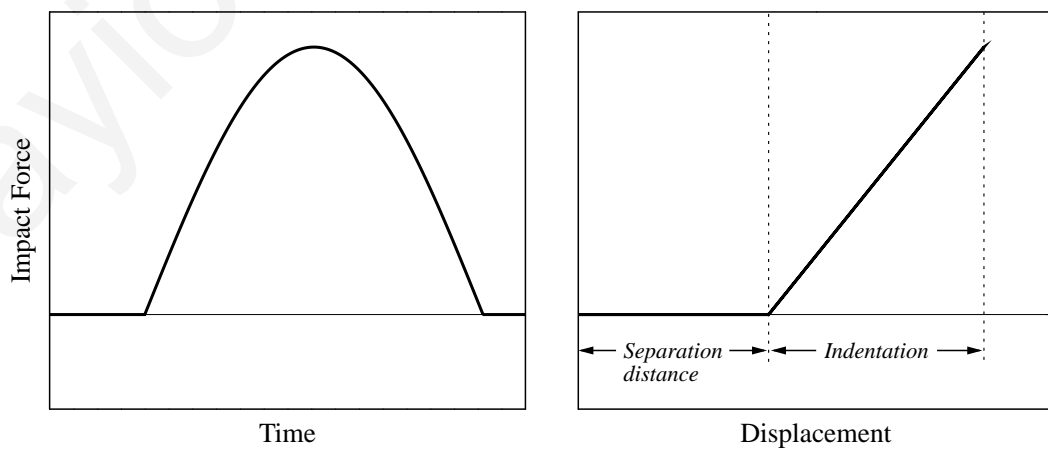


Figure 2.2 The linear elastic impact model.

2.2.2 Linear viscoelastic impact model

In addition to the impact spring, a viscous impact dashpot may be incorporated in parallel, in order to capture the energy loss during impact. This impact model is also known as Kelvin-Voigt model. Whenever there is impact, the impact force at time t is provided by the expression:

$$F_{imp}(t) = k_{imp} \cdot \delta(t) + c_{imp} \cdot \dot{\delta}(t) \quad (2.5)$$

where c_{imp} is the impact viscous damping coefficient and $\dot{\delta}(t)$ is the relative velocity between the structures in contact at time t .

Anagnostopoulos [2] has provided the following analytical expressions that associate the impact viscous damping coefficient with the coefficient of restitution (COR) and the masses, m_1 and m_2 , of the colliding bodies:

$$c_{imp} = 2 \cdot \xi_{imp} \sqrt{k_{imp} \frac{m_1 \cdot m_2}{m_1 + m_2}} \quad (2.6)$$

$$\xi_{imp} = -\frac{\ln(COR)}{\sqrt{\pi^2 + (\ln(COR))^2}} \quad (2.7)$$

In the above equations, ξ_{imp} is the impact viscous damping ratio ($0 < \xi_{imp} < 1$). The derivation of the above formulas was based on the assumption of an equivalent SDOF system that represents the two bodies in contact and the conservation of energy before and after impact [5].

A characteristic, which may be considered as a weakness, of this impact model is the effect of the damping term on the values of the impact force at the two extreme time instances of the impact duration. Specifically, due to the damping term, the impact force values upon impact exhibit an initial jump, while during the detaching phase, the damping term causes negative impact forces, i.e. tensile forces, that pull the colliding bodies together, instead of pushing them apart (Figure 2.3). Nevertheless, this simple impact model has been found to provide sufficiently accurate results for the overall structural response, given that proper values are used for the impact parameters ([32]).

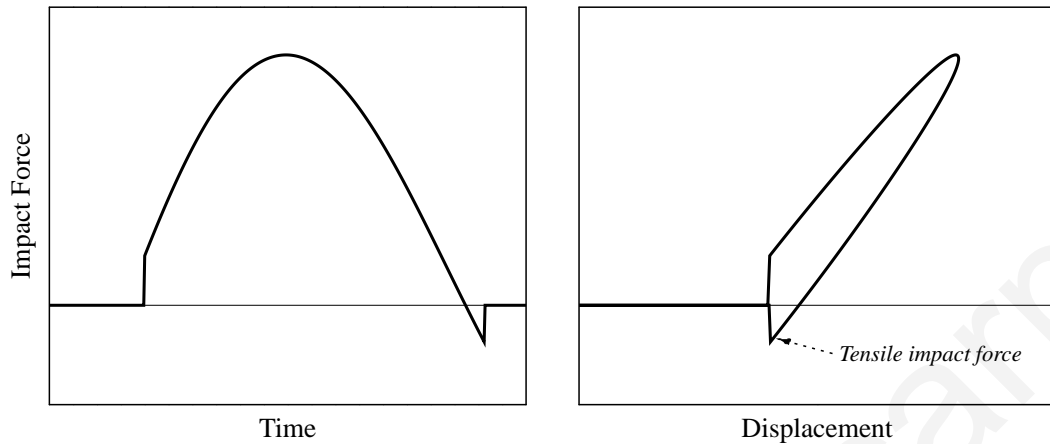


Figure 2.3 The linear viscoelastic impact model.

Due to its simplicity, the linear viscoelastic impact model, as proposed by Anagnostopoulos [2], has been systematically used in numerical simulations involving structural pounding ([1], [6], [7], [32], [41]). However, some other researchers used a linear viscoelastic impact model without using the above formulas, following a different approach to calculate the impact damping coefficient ([55], [58], [63], [80]).

2.2.3 *Hertz impact model*

According to the Hertz contact law, the impact force acting on a sphere colliding against a rigid half-space increases exponentially with the interpenetration, usually with an exponent of 1.5 ([31]). Based on this idea, several researchers used, instead of a linear, a non linear impact spring in an effort to represent more realistically structural impacts. In such cases the impact force equals:

$$F_{imp}(t) = k_{imp} \cdot \delta(t)^{1.5} \quad (2.8)$$

The Hertzian elastic impact model has been used in several numerical studies on structural poundings ([16], [12], [13], [64], [76]).

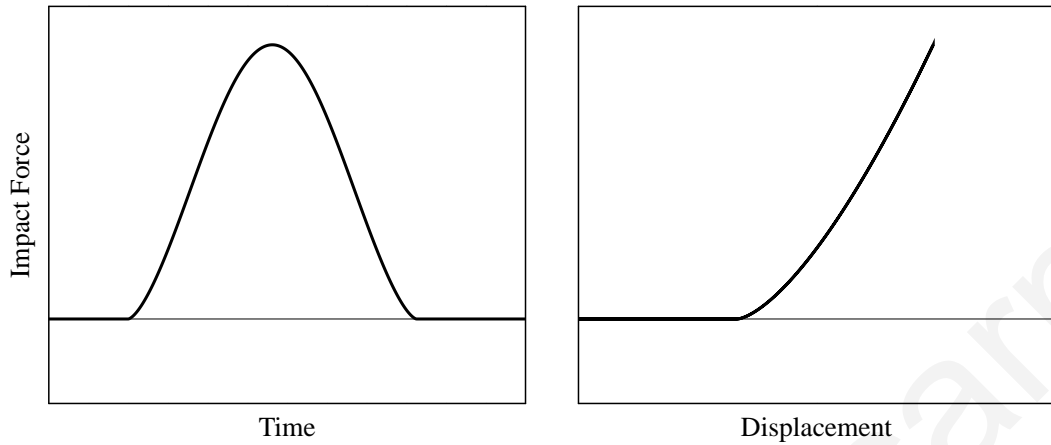


Figure 2.4 The Hertzian elastic impact model.

2.2.4 Non-linear viscoelastic impact model

In order to improve the Hertzian elastic impact model, Jankowski [37] incorporated a non-linear damper parallel to the non-linear spring in order to include an energy dissipation mechanism. He assumed that the larger amount of the kinetic energy is dissipated during the approach phase, while during the restitution phase the dissipation of energy is negligible. Therefore, the non-linear dashpot is activated only during the approach phase:

$$F_{imp}(t) = k_{imp} \cdot \delta(t)^{1.5} + c_{imp}(t) \cdot \dot{\delta}(t) \quad \text{for } \dot{\delta}(t) > 0 \quad (2.9)$$

During the restitution phase, the energy dissipation is omitted and the impact force equals:

$$F_{imp}(t) = k_{imp} \cdot \delta(t)^{1.5} \quad \text{for } \dot{\delta}(t) < 0 \quad (2.10)$$

Using a similar methodology with Anagnostopoulos [5], Jankowski [38] proposed the following formulas for the estimation of the impact damping coefficient $c_{imp}(t)$, which is expressed in terms of the impact viscous damping ratio ξ_{imp} and the interpenetration depth:

$$c_{imp}(t) = 2 \cdot \xi_{imp} \sqrt{k_{imp} \cdot \sqrt{\delta(t)} \cdot \frac{m_1 \cdot m_2}{m_1 + m_2}} \quad (2.11)$$

$$\xi_{imp} = \frac{9\sqrt{5}}{2} \cdot \frac{1 - COR^2}{COR(COR(9\pi - 16) + 16)} \quad (2.12)$$

Due to the fact that the equivalent SDOF system used for the derivation of the above formulas is non-linear, the methodology that was followed by Jankowski [38] encompasses assumptions and uncertainties that did not take place in the corresponding methodology taken by Anagnostopoulos [5] for the estimation of the impact damping for the linear viscoelastic impact model. Though, during the validation of the impact model, good correlation was obtained compared to analytical results ([38]).

By incorporating the indentation term in Equation 2.11, which provides the impact damping coefficient, the discontinuity at the beginning of the approach phase, which is a characteristic of linear viscoelastic impact model, is theoretically eliminated. Nevertheless, the impact force still increases in a relatively sudden manner during the approach phase, as it can be seen in Figure 2.5. The tensile forces during the restitution phase are avoided, anyway, due to the fact that during the restitution phase damping is omitted. Another worth-mentioned remark is that the damping ratio, provided for the non-linear viscoelastic impact model according to Equation 2.12, may take values greater than 1 and specifically approaches infinity for $COR = 0$ (perfectly plastic impact), in contrary to the damping ratio of the linear viscoelastic impact model, provided by Equation 2.7, which takes values between 0 and 1.

The linear viscoelastic impact model, as proposed by Jankowski, has been used in several studies to numerically investigate poundings of structures ([32], [39], [40]).

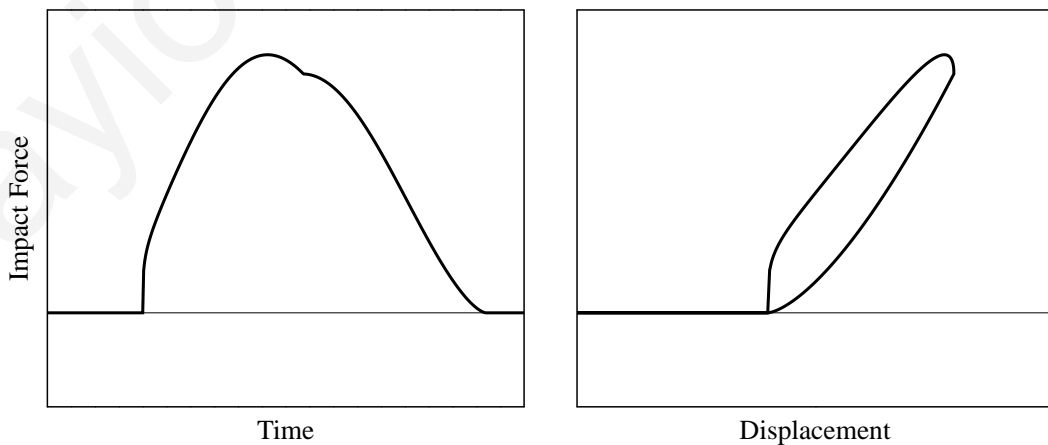


Figure 2.5 The linear viscoelastic impact model [37].

Guo et al [32] used both the linear viscoelastic and the non-linear viscoelastic impact models to simulate poundings among bridge decks and compared the results with corresponding shake-table test results. The results showed that both the linear and the non-linear impact models can predict the experimental results well if the parameters of the impact models are properly selected. Based on reported results, the researchers considered the linear viscoelastic model as a better choice for the pounding prediction of highway bridges, because it is a simpler model than the non-linear viscoelastic model.

2.2.5 Hertz impact model with non-linear damping (Hertzdamp)

A similar with the above approach was taken by Muthukumar and DesRoches [61], as they have used a Hertz impact spring together with a non-linear damper during the whole duration of the impact. This impact model was initially used for other applications [51] concerning impacts of laminates. According to this impact model, the impact force is increasing with an exponent n , which may be equal to or different from 1.5:

$$F_{imp}(t) = k_{imp} \cdot \delta(t)^n + c_{imp}(t) \cdot \dot{\delta}(t) \quad (2.13)$$

The impact damping coefficient, c_{imp} , is determined by the formula:

$$c_{imp}(t) = \frac{3 \cdot k_{imp} \cdot (1 - COR^2)}{4 \cdot v_{imp}} \cdot \delta(t)^n \quad (2.14)$$

where, v_{imp} is the impact velocity, i.e. the relative velocity of the colliding bodies at the time of impact. The above formula suggests that impact damping also depends on the approaching velocity of the two colliding bodies.

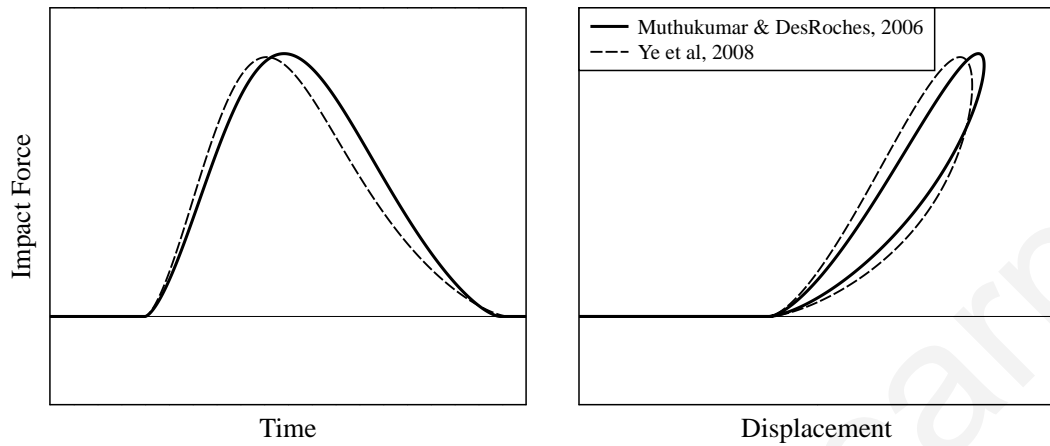


Figure 2.6 The Hertzian impact model with non-linear damping.

Mahmoud et al [53] examined the effectiveness of the non-linear viscoelastic and the Hertzdamp impact models by comparing them with experimental results involving steel-to-steel and concrete-to-concrete impacts. They concluded that both models have advantages and disadvantages and that their accuracy depends on the type of the simulation analysis conducted.

Ye et al [81] noticed that the formulas for the estimation of impact damping for the Hertzdamp impact model produce incorrect calculation of the response. Specifically, the computed coefficient of restitution does not always coincide with the one that is predefined (Figure 2.7). Therefore, following a more accurate mathematical approximation, they proposed a new formula for the impact damping ratio in order to minimize this error:

$$\xi_{imp} = \frac{8}{5} \cdot \frac{k_{imp} \cdot (1 - COR)}{COR \cdot v_{imp}} \quad (2.15)$$

A typical test is conducted in order to demonstrate the accuracy of the pre-described inelastic impact models. Particularly, the computed coefficient of restitution is compared with the one provided in the corresponding formula that is used to estimate the impact damping term. The results for the three aforementioned major impact models are presented in Figure 2.7. It is observed that in some cases, especially for the Hertzdamp model as mentioned before, there is a significant error in the provided response.

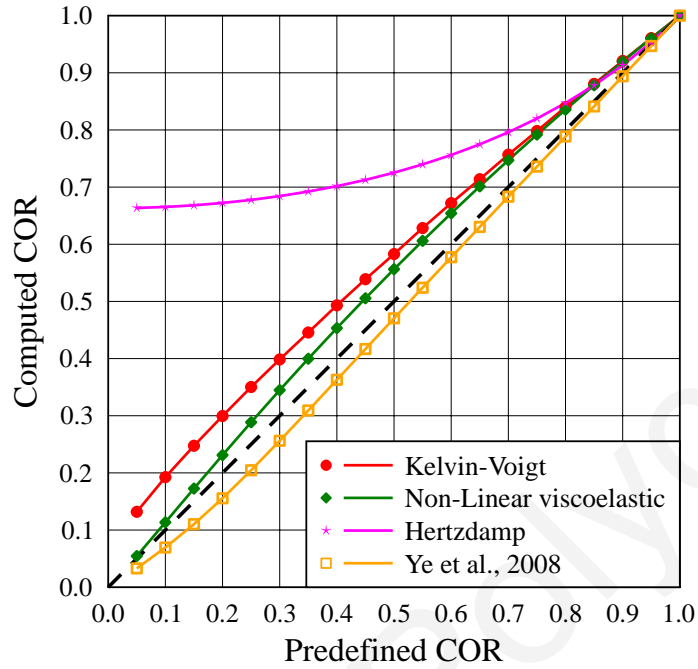


Figure 2.7 Error estimation for the major force-based impact models.

2.3 Proposed linear impact model

In an effort to improve the performance of the linear viscoelastic impact model, a minor adjustment is proposed, in order to avoid the tensile impact forces that arise between the colliding structures at the end of the restitution period, due to the damping term. In particular, when the impact force is about to change sign, the impact spring and dashpot are removed, considering that the two bodies are detached from each other, avoiding the abnormal tensile forces. Thus, a remaining plastic deformation is assumed at each body, which increases the corresponding available gap between them (Figure 2.8). Therefore, based on Equation 2.5, the formula that provides the impact force for the new linear viscoelastic impact model can be written as follows:

$$F_{imp}(t + \Delta t) = \begin{cases} k_{imp} \cdot \delta(t) + c_{imp} \cdot \dot{\delta}(t) & \text{when } F_{imp}(t) \geq 0 \\ 0 & \text{when } F_{imp}(t) < 0 \end{cases} \quad (2.16)$$

Meaning that at every time-step, during the integration procedure, the value of the impact force computed at the previous step must be checked according to the above formula and then calculate the impact force for the current time-step.

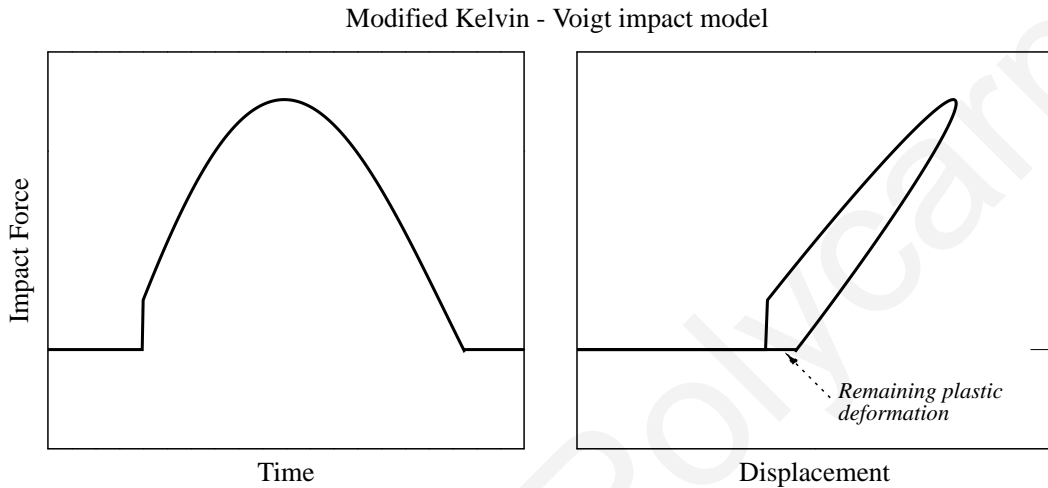


Figure 2.8 The proposed linear viscoelastic impact model with permanent indentation.

With the above minor adjustment on the linear viscoelastic impact model, a small amount of the dissipated energy, which corresponds to the small area below the horizontal axis in the force-displacement diagram, is omitted, raising a question about its effect on the accuracy of the model. Nevertheless, an analytical investigation that was conducted in the field of applied impact mechanics from Butcher and Segalman [11] showed that the elimination of the impact force discontinuity at release, results in a minimal decrease in equivalent damping. In addition, the same researchers mentioned that the results using the modified linear viscoelastic impact model are very close to the corresponding results obtained using the typical Kelvin-Voigt model for relatively low damping ratios, while the variation between the two models increases as the damping increases.

In the following sections, the effect of this modification will be demonstrated using a typical example of a seismically isolated building pounding against the surrounding moat wall, considering different impact models.

2.4 Proposed non-linear impact model with hysteretic damping

The use of viscous damping for a linear impact model does not involve any substantial difficulties for the estimation of the impact damping coefficient. In contrary, for the case of using a non-linear impact spring, the derivation of the appropriate formula to estimate the impact damping involves numerous assumptions and uncertainties ([38], [81]). Nevertheless, if we make the assumption that the impact energy is dissipated through hysteretic instead of viscous damping, this obstacle can be avoided. In this section, a new impact model is presented that considers only hysteretic dissipation of the kinetic energy during impact. A simple methodology that has been followed to derive the necessary formulas that describe the proposed non-linear impact model is presented below.

Firstly, it is assumed that the impact force is exponentially increased with the indentation. Figure 2.9 displays the shape of the force-displacement graph of the proposed impact model. Impact is separated in two stages: the approach phase and the restitution phase. The enclosed area A_h is the area of the *hysteresis loop* and expresses the dissipated energy during impact. No impact dashpots are assumed. The impact force, during the approach phase, can be easily expressed by the formula ($n > 1$):

$$F_{imp}^A = k_{imp} \cdot \delta^n \quad \text{for} \quad \dot{\delta} > 0 \quad (2.17)$$

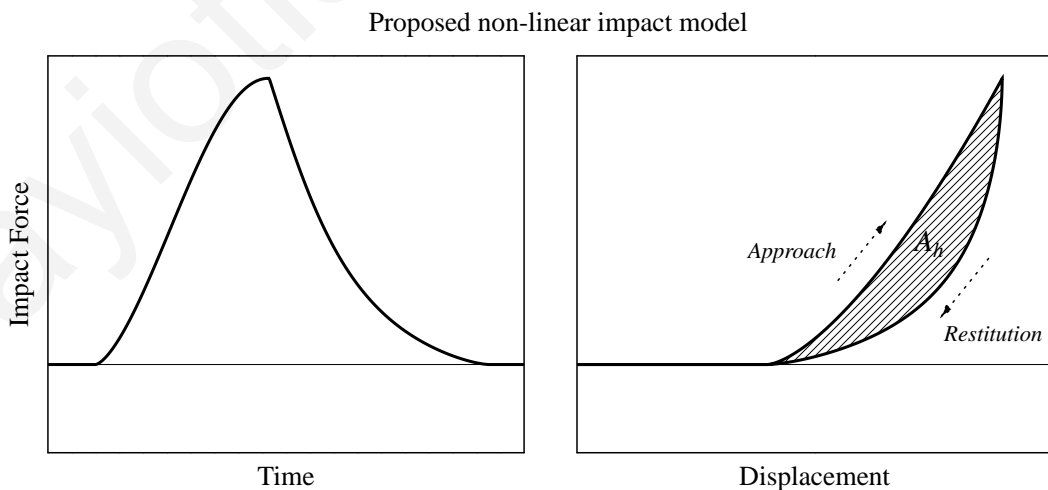


Figure 2.9 The proposed non-linear impact model with hysteretic damping.

For the determination of the trend of the curve during the restitution phase, the corresponding equation must fulfill the equilibrium of the kinetic energy loss with the dissipated energy due to impact, which is represented by the area A_h of the hysteresis loop. When two rigid bodies collide, the kinetic energy loss due to impact is described by the following expression ([31]):

$$\Delta E = \frac{1}{2} \cdot \frac{m_1 \cdot m_2}{m_1 + m_2} \cdot (1 - COR^2) \cdot v_{imp}^2 \quad (2.18)$$

where v_{imp} is the impact velocity, that is the relative velocity of the two bodies just before impact. During the restitution phase, the impact force can be described by the following expression, which is similar to the one providing the impact force in the case of using the Hertzdamp model ([51], [61]):

$$F_{imp}^R = k_{imp} \cdot \delta^n + k_{imp} \cdot \delta^n \cdot C_{imp} \cdot \dot{\delta} \quad \text{for } \dot{\delta} < 0 \quad (2.19)$$

which can also be expressed as:

$$F_{imp}^R = k_{imp} \cdot \delta^n \cdot (1 + C_{imp} \cdot \dot{\delta}) \quad \text{for } \dot{\delta} < 0 \quad (2.20)$$

Since the relative velocity during the restitution phase is always negative, the second part of the equation expresses the reduction of the impact force due to damping, forming in this way the hysteresis loop. The only remaining unknown parameter is the term C_{imp} that can be called as the “impact damping coefficient”. It is assumed that the impact damping coefficient depends on the same parameters that determine the kinetic energy loss (Equation 2.18):

$$C_{imp} = f \left(COR, m_{eff} = \frac{m_1 \cdot m_2}{m_1 + m_2}, v_{imp} \right) \quad (2.21)$$

For the derivation of the formula, a single condition that must be fulfilled is taken into account. In particular, for a coefficient of restitution equal to 1, no energy must be dissipated during impact, which corresponds to perfectly elastic impact, meaning that the impact damping coefficient must be equal to zero. Therefore, the solution may have the following simple form:

$$C_{imp} = a_1 \cdot (1 - COR^2) \quad (2.22)$$

where a_1 is a constant that, for a given system and a coefficient of restitution, should have such value so that the kinetic energy loss (Equation 2.18) is equal to the area A_h of the hysteresis loop. In order to achieve that, an iterative procedure is followed, solving numerically the equations of motion for a given problem and varying each time the constant a_1 explicitly, until the aforementioned equilibrium is fulfilled.

For this purpose, a simple software application has been developed that simulates the impact of two rigid bodies, solving numerically the equation of motion using the Central Difference Method. In particular, the two bodies are simulated as two single masses that are let freely to collide with an initial velocity, which is provided for the one of the two masses. A very small time step is used for the analysis (2×10^{-4}) in order to minimize errors due to excessive overlapping (see Section 2.5.2). The duration of each analysis is less than two seconds. The Graphical User Interface (GUI) of the developed software (Figure 2.10) provides the ability to visually control the computed results through animation and plots of the responses.

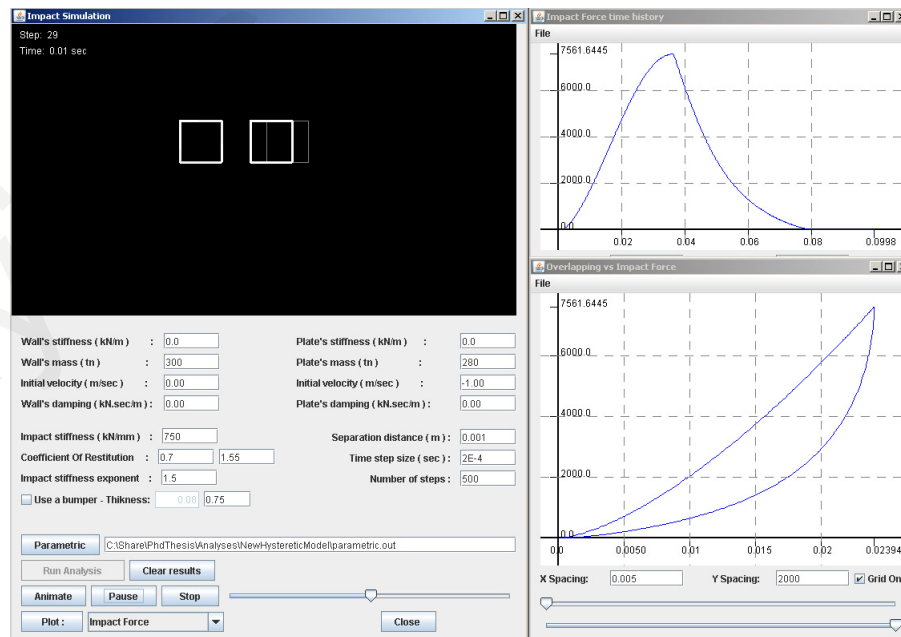


Figure 2.10 Graphical User Interface of the software application specially developed for the simulation of two colliding masses, considering the various impact models.

A specific case of two masses of 280 and 300 tons, pounding at each other with an impact velocity equal to 1.0 m/sec has been considered for the necessary analyses. The procedure that has been followed for the derivation of the impact stiffness coefficient, using the above software tool, is demonstrated in the flowchart of Figure 2.11. Beginning from Equation 2.22, an initial value is selected for the coefficient a_1 and the coefficient of restitution COR . After each simulation, the kinetic energy loss is checked whether it equals the area of the hysteresis loop obtained from the analysis and, if not, the constant a_1 is modified and a new analysis is performed. This iterative procedure is repeated until a proper value is obtained for a_1 corresponding to the selected value of COR . Then, another value for the COR is selected and, finally, through this process, a plot is constructed providing the relationship between the COR and a_1 . Using a “curve-fitting” technique, the coefficient a_1 is expressed in terms of the coefficient of restitution and is substituted in Equation 2.22, providing a new expression for the impact damping coefficient.

Similarly, two more coefficients, a_2 and a_3 , are expressed in terms of the impact velocity, v_{imp} , and the effective mass, m_{eff} , following the same iterative procedure. The impact velocity has been varied between the values of 0.5 and 2.5 m/sec, while the one of the two masses has been varied between the values of 100 and 1000 tons.

Consequently, the final formula for the estimation of impact damping coefficient can be obtained, in terms of the coefficient of restitution, the impact velocity and the masses of the colliding structures:

$$C_{imp} = 1.55 \cdot \frac{1 - COR^2}{COR^{0.7076} \cdot \left(\frac{m_1 \cdot m_2}{m_1 + m_2} \right)^{0.0025} \cdot v_{imp}^{0.9755}} \quad (2.23)$$

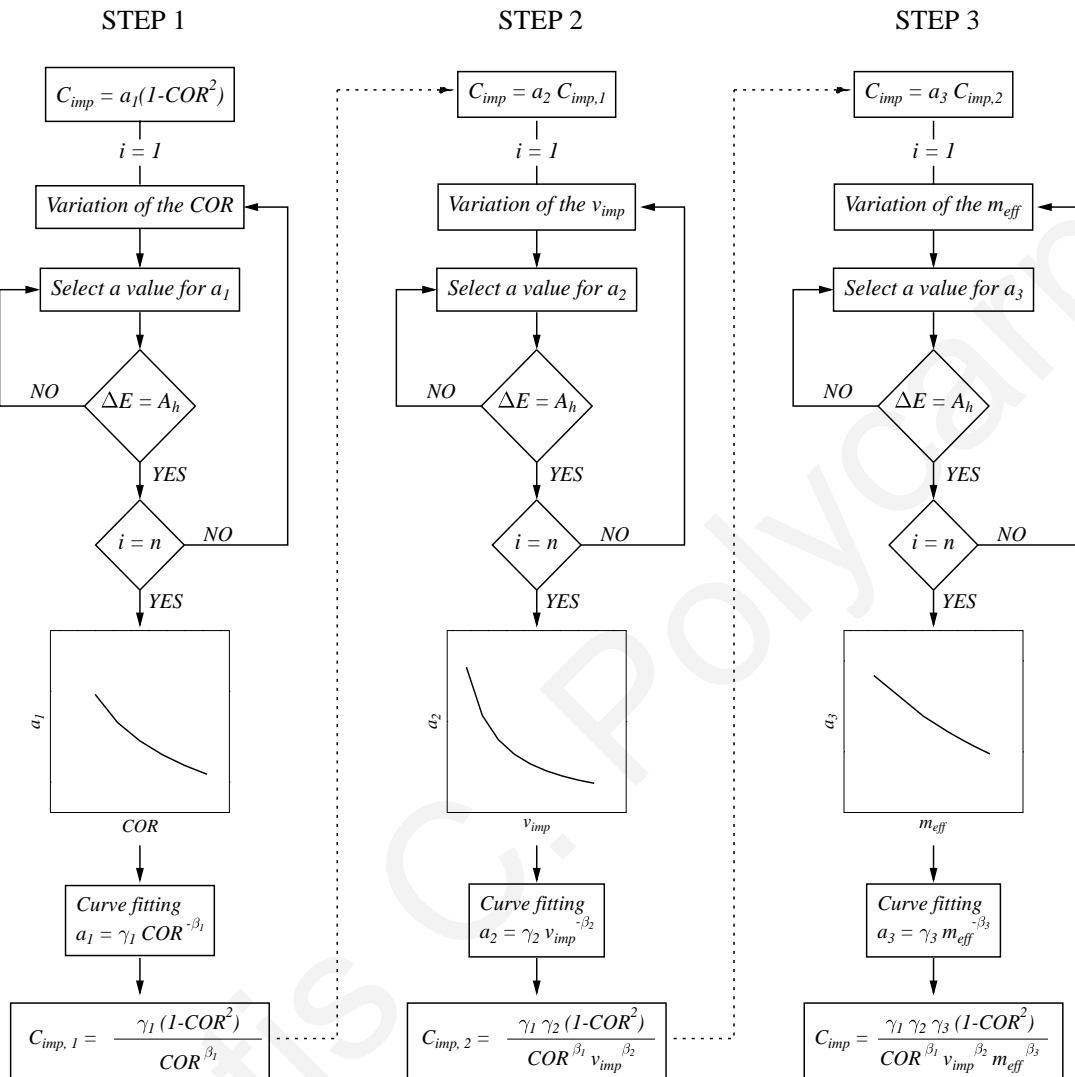


Figure 2.11 The procedure that has been followed in order to derive the formula that provides the impact damping coefficient C_{imp} .

The above formula is an approximation of the impact damping term. An analytical expression can be probably derived following a more rigorous regression analysis approach, something that is included in the future extensions of this study. Nevertheless, for the purposes of the current study, Equation 2.23 is used for the calculation of the impact damping coefficient that determines the hysteresis loop for the proposed non-linear hysteretic impact model.

In order to check the accuracy of the proposed non-linear impact model regarding the calculation of the velocities after impact, the relationship between the provided COR with the one obtained from the numerical analysis is plotted in Figure 2.12, along with the corresponding curves of the previously described impact models. It is observed that the proposed non-linear hysteretic model demonstrates the best behavior among the rest of the impact models, providing good accuracy for the velocities after impact.

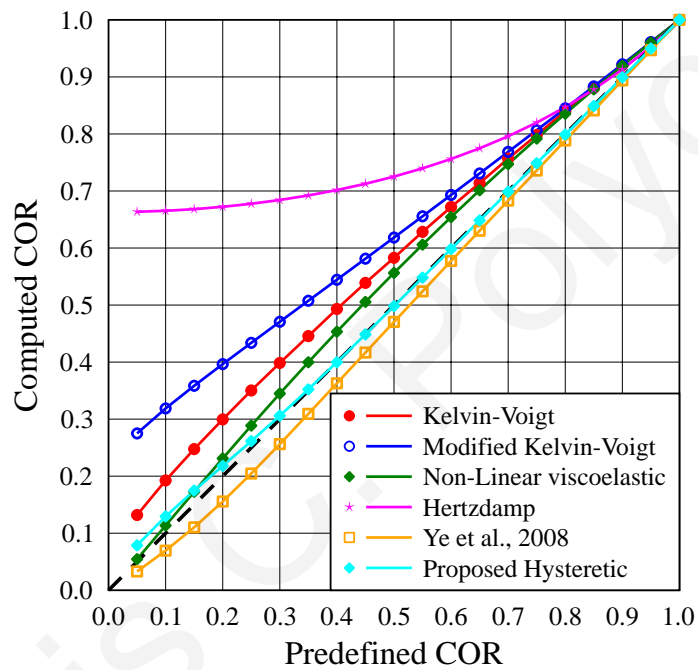


Figure 2.12 Error estimation for the proposed non-linear model, compared with the corresponding major force-based impact models

2.5 Estimation of the impact parameters

When using the force-based impact models, it is very important to appropriately determine the value for the impact parameters, i.e. the impact stiffness and the coefficient of restitution, which is usually used for the estimation of the impact damping coefficient. A wide range of diverse values of these parameters has been used in the literature for different kinds of impact problems, since their exact value is practically unknown. A brief overview of the basic approaches that several researchers have followed for the estimation of these parameters is provided below.

2.5.1 Coefficient of restitution

Anagnostopoulos [2] used a value of the coefficient of restitution equal to 0.65, which was an educated guess, based on experimental data obtained from experiments with spheres and plates [31]. In the same research study, the effect of choosing different values for the coefficient of restitution was examined and found that this parameter has negligible effect on the displacement response of buildings during poundings, except for the case of perfectly elastic impact ($COR = 1.0$), where the amplification of the response is higher. Furthermore, he argues that it is more favorable to choose a relatively high, rather than a low value for this impact parameter because it leads to more conservative results.

Athanasiadou et al [8] simulated poundings of structures in series using the stereomechanical approach taking also into account an amount of dissipated energy represented by the coefficient of restitution, for which a value of 0.5 was considered in the performed analyses. Through a parametric investigation, they also observed that the value of the coefficient of restitution did not significantly affect the computed response of the structures during poundings. DesRoches and Muthukumar [17], using the same approach for the impact modeling, assumed a value for the coefficient of restitution equal to 0.8.

Recently, Guo et al [32] performed an experimental study, involving impact of two steel plates with additional mass of 2.5 tons each to simulate poundings of bridge decks. It was found that the coefficient of restitution ranged from 0.62 to 0.75. Generally, the coefficient of restitution of strong impacts was smaller than that of slight impacts, which means that the strong impacts dissipate more energy during the poundings.

2.5.2 Impact stiffness

The value of the impact stiffness depends on the mechanical properties of the material and the geometry of the contact surface of the colliding bodies. According to Goldsmith [31], the impact stiffness for the case of two colliding spheres, each with radius R_i , can be estimated from the following formula:

$$k_h = \frac{4}{3 \cdot \pi \cdot (h_1 + h_2)} \cdot \left[\frac{R_1 \cdot R_2}{R_1 + R_2} \right]^{1/2} \quad (2.24)$$

where:

$$h_i = \frac{1 - \nu_i}{\pi \cdot E_i} \quad (2.25)$$

For the case of structural poundings, an approximation of the colliding structures with equivalent spheres can be made using the following formula [31]:

$$R_i = \sqrt[3]{\frac{3 \cdot m_i}{4 \cdot \pi \cdot \rho}} \quad (2.26)$$

where ν_i is the Poisson's ratio, E_i is the Young's modulus, m_i is the mass and ρ is the density for each one of the two spheres.

Furthermore, a wide range of diverse values has been used in the literature for different kinds of impact problems, since its exact value is practically unknown. Anagnostopoulos [2] assumed an impact stiffness value for the linear viscoelastic impact model equal to twenty times the stiffness of the stiffer structure considered in the analysis. He also examined the effect of choosing different values for the impact parameters on the response during poundings. It was found that a ten-fold decrease of the impact stiffness does not cause any substantial differences in the displacement response of the pounding buildings. Nevertheless, for a 100 times reduction of the impact stiffness, the amplification of the response due to poundings was significantly reduced. Furthermore, it was noted that despite the insensitivity of the displacement response to the impact stiffness value, the acceleration response is highly affected by this parameter.

Van Mier et al [77], who experimentally examined the case of impact between concrete bodies, concluded that the impact stiffness, considering a non-linear impact spring, should vary from 40 to 80 kN/mm^{1.5} in order to match experimental results. Guo et al [32], also based on experiments, used an impact stiffness of 3.67×10^7 N/m for the linear model and a value of 1.45×10^9 N/m^{3/2} for the non-linear viscoelastic impact model in order to fit the experimental results. However, those values concerned the specific specimens of relatively small dimensions and masses and may not represent properly the impact forces that are applied during poundings of a real building against a wall or another structure.

Maison and Kasai [55] considered that the impact linear spring stiffness was equal to the in-plane stiffness of the slab. They varied the impact stiffness from 50000 kip/in (8756 kN/mm) to 500 kip/in (87.6 kN/mm), assuming different widths of the building's plan, and argued that no significant effect was observed on the response during poundings. However, it was observed that for the small values, the effect of the impact stiffness on the response was increased. Davis [16] and Chau and Wei [12] simulated poundings using the Hertz contact law and found, from parametric investigation, that the impact velocity is insensitive to the variation of the impact stiffness. Ruangrassamee and Kawashima [71] as well as Watanabe and Kawashima [79] simulated bridge decks as elastic rods and assumed that the impact spring stiffness is equal to the in-plane stiffness of the deck, multiplied by the number of discrete elements used to simulate the deck.

2.5.3 Finite element analysis

Searching for proper values for the impact parameters to be used in the current study, a detail finite element analysis (FEA) has been performed, using the ADINA software, which is capable of solving contact problems. In particular, a two dimensional model with a concrete slab of a certain mass, representing the structure's base slab, is driven with a certain velocity on a cantilever-wall which stood in front of soil (Figure 2.13). The results of this analysis are also to evaluate the effectiveness of the various impact models to accurately simulate poundings that are expected to occur by a seismically isolated building during a very strong earthquake.

The thickness of the concrete slab is assumed to be 20 cm, the wall has a width of 25 cm and the backfill soil has dimensions of 2.0 m \times 2.0 m. The FEA is performed for different heights of the moat wall, in order to examine its effect on the value of the impact stiffness. The impact velocity is assumed to be 1 m/sec. Non-linear inelastic materials are used for both concrete and soil.

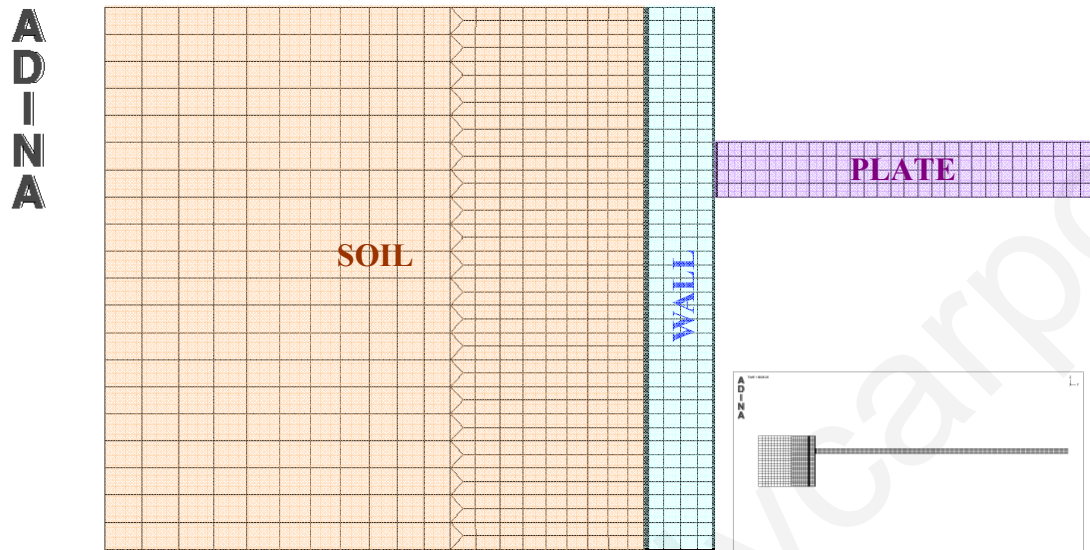


Figure 2.13 The 2D finite element model used in ADINA to simulate the impact of a plate on a wall standing in front of soil.

Using the linear and the non-linear viscoelastic impact models, the same problem is solved numerically. The time-histories of contact force and plate's displacement resulting from FEA are compared with the relevant results of the selected impact models. As Figure 2.14 shows, both linear and non-linear impact models match sufficiently well the results from the FEA using appropriate values for the impact stiffness. For both impact models, a coefficient of restitution equal to 0.7 is used to fit the results obtained from FEA.

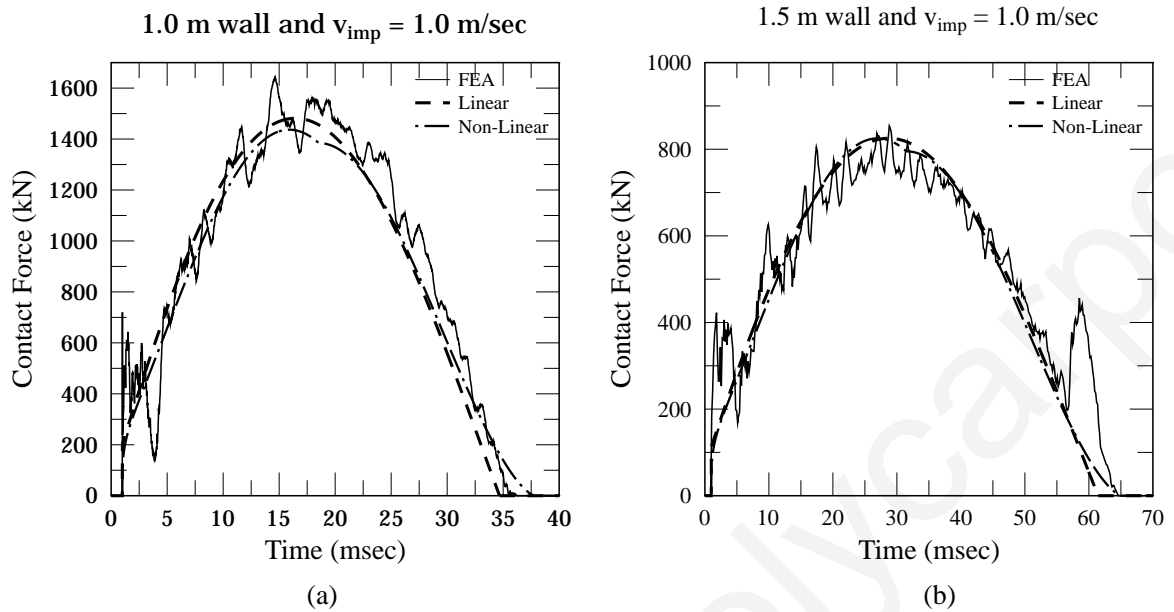


Figure 2.14 Time-history of impact force resulting from FEA compared with analytical results for: (a) 1.0 m wall; and (b) 1.5 m wall, assuming a 1.0 m/sec impact velocity.

Since the model that is used is two dimensional, the units of the impact stiffness obtained from the analysis are expressed in terms of depth (Table 2.1), while for the determination of the impact surface the third dimension is needed. Assuming that the problem is a plain-strain problem and that the width of the building at the pounding side is approximate 28 m, the values of Table 2.2 are proposed for the linear and non-linear impact stiffness respectively.

Table 2.1 Values of the impact stiffness in terms of depth resulting from FEA, for the two impact models under investigation.

Wall height (m)	Kelvin-Voigt (Anagnostopoulos 1988) kN/mm/m	Non-Linear viscoelastic (Jankowski 2004) kN/mm ^{1.5} /m
1.00	150	50
1.25	90	27
1.50	45	10
2.00	25	5

Table 2.2 Approximate values of the impact stiffness, for the linear and non-linear models, used to simulate poundings of a seismically isolated building with a moat wall.

Wall height (m)	Kelvin-Voigt kN/mm	Non-Linear viscoelastic kN/mm^{1.5}
1.00	4166.67	1388.89
1.25	2500	750
1.50	1250	277.77
2.00	694.44	138.89

CHAPTER 3 MODELING OF SEISMICALLY ISOLATED BUILDINGS CONSIDERING IMPACTS

3.1 General

In this chapter, the basic assumptions and methodology that have been considered in the simulations and parametric studies of the present research work are described. The modeling of the structures is performed in two dimensions (2D) in the current study. Although a 2D analysis is much simpler than the modeling in three dimensions (3D), the latter involves more complex responses of the seismically isolated building during poundings, such as torsional effects, which cannot be considered in the former case.

In many cases, simulations of seismically isolated buildings using equivalent single degree-of-freedom (SDOF) systems represent very satisfactorily the structural response due to the increased participation of the fundamental mode. However, when poundings occur, the contribution of higher eigenmodes, which are excited, can no longer be neglected as insignificant for the analysis. Therefore, in the current research work, the superstructure is modeled as a multi-degree of freedom (MDOF) system, with shear-beam behavior and the masses lumped at the floor levels, assuming that the superstructure remains elastic during earthquake excitations.

3.2 Linear elastic model for the isolation system

Many modern anti-seismic codes allow the use of linear models as a simple way to simulate the behavior of the isolation system under dynamic loadings. Although linear elastic models have significant difficulties in capturing satisfactorily the behavior of a seismic isolation system [60], it is useful to examine the simple case of having an equivalent linear elastic isolation system to examine certain aspect of the problem. For the linearized model of the isolation system, an effective stiffness and an effective damping coefficient are defined and used. Therefore, if the superstructure consists of n number of stories, the MDOF system that corresponds to the seismically isolated building would have $n+1$ degrees-of-freedom (Figure 3.1). For the construction of the damping matrix non-

classical damping is used, for which a detailed description is provided in a following paragraph.

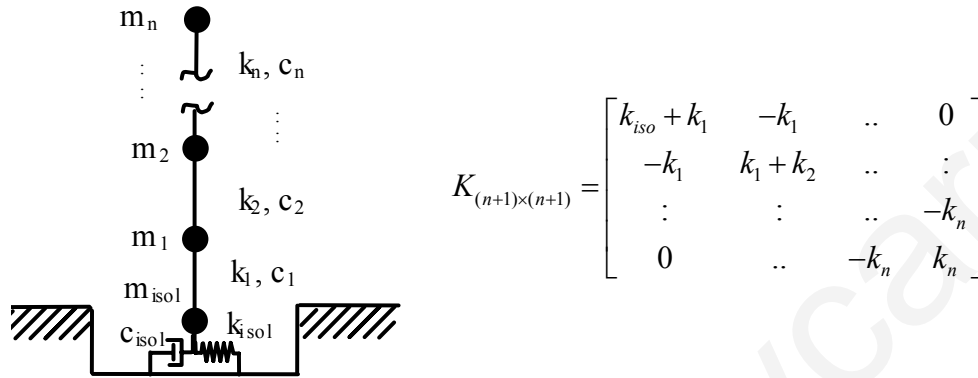


Figure 3.1 Linear MDOF system model for the seismically isolated building and the corresponding stiffness matrix.

3.3 Bilinear inelastic model for the isolation system

A more representative and appropriate model for simulating the dynamic response of the isolation system is the bilinear inelastic model (Figure 3.2), which represents satisfactorily the response under cyclic loading of the most commonly used seismic isolation systems [62], such as the Lead Rubber Bearings (LRB) and the Friction Pendulum Systems (FPS). In the case of LRB, the bilinear behavior is justified by the yielding of the lead core after the exceedance of a certain shear force (f_y). In particular, prior to the yielding of the lead core, the isolation system has an initial stiffness K_1 , which is much higher (approximately 10 times) than the post-yield stiffness K_2 , which corresponds solely to the stiffness of the rubber. Similarly, in the case of the FPS, instead of the yielding of the lead core, the reduction in stiffness corresponds to the beginning of sliding. Therefore, considering the behavior of a FPS under dynamic loading, the bilinear inelastic model is found to be suitable for its simulation, as well.

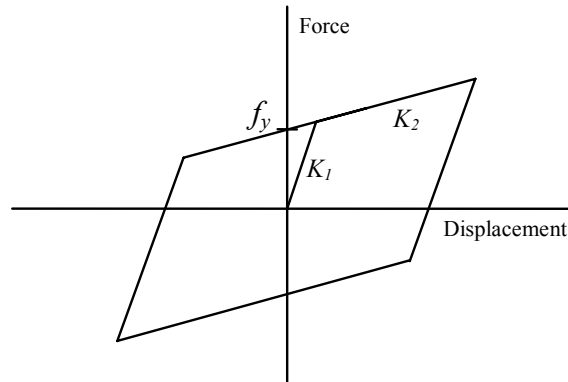


Figure 3.2 Bilinear modeling of the seismic isolation system behavior.

3.4 Non-classical damping

In the case of seismically isolated buildings undergoing earthquake excitations, the energy dissipation mechanisms of the corresponding MDOF system are not uniformly distributed, as they differ significantly between the isolation system and the superstructure. In particular, most of the excitation's energy is dissipated through the seismic isolation system's devices rather than through the vibration of the superstructure. In such cases, the usage of classical Rayleigh damping for the construction of the damping matrix may not be appropriate [15]. Therefore, in the current study a different approach is made in order to take into account the dissipation of energy in a more appropriate, yet simple, manner.

3.4.1 Using a viscous linearized model for the isolation system

For the numerical simulations using a linear elastic seismic isolation system, non-classical damping is used by applying a simple technique to take into account the excess in damping that is provided by the seismic isolation system. At first, assuming a uniformly distributed energy dissipation mechanism along the height of the superstructure, a primary damping matrix \underline{C}_p is constructed, according to the Rayleigh damping method [15], assuming a viscous damping ratio for the two extreme eigenmodes of the MDOF system to represent the viscous energy dissipation due to the deformation of the superstructure.

$$\underline{C}_p = \alpha \cdot \underline{M} + \beta \cdot \underline{K} \quad (3.1)$$

where \underline{M} and \underline{K} are the mass and the stiffness matrices, respectively, while:

$$\begin{bmatrix} \alpha \\ \beta \end{bmatrix} = \begin{bmatrix} 1/(2 \cdot \omega_i) & \omega_i/2 \\ 1/(2 \cdot \omega_j) & \omega_j/2 \end{bmatrix}^{-1} \cdot \begin{bmatrix} \zeta_i \\ \zeta_j \end{bmatrix} \quad (3.2)$$

where ω_i is the eigenfrequency and ζ_i is the viscous damping ratio for the i^{th} eigenmodes, while the indexes i and j correspond to the first and last eigenmodes of the MDOF system.

Then, considering an almost “rigid body” behavior for the superstructure of the seismically isolated building, an equivalent SDOF system is formed using the total mass of the building (m_{tot}) and the effective stiffness (k_{iso}) of the isolation system. For this SDOF system, the equivalent viscous damping coefficient is calculated to correspond to the excess in damping that is provided by the isolation system, beyond the uniform viscous damping that is assumed for the entire MDOF system:

$$c_{iso} = 2 \cdot (\zeta_{iso} - \zeta_{sstr}) \cdot \sqrt{m_{tot} \cdot k_{iso}} \quad (3.3)$$

where ζ_{iso} and ζ_{sstr} are the selected damping ratios for the seismic isolation and the superstructure, respectively. The viscous damping ratio that corresponds to the superstructure is subtracted from the corresponding seismic isolation damping ratio, since it has already been taken into account during the construction of the primary viscous damping matrix, using the Rayleigh damping assumption. The final damping matrix \underline{C} is assembled by superposing the primary damping matrix to the equivalent viscous damping coefficient c_{iso} that corresponds to the excess in damping provided by the seismic isolation system. In particular, the value of c_{iso} is added to the first element (first row and first column) of the primary damping matrix \underline{C}_p , since the seismic isolation system is located at the base of the building.

3.4.2 Using a bilinear model for the isolation system

When a bilinear model is used for the seismic isolation system, which is more appropriate, the energy during the ground excitation is mainly dissipated hysteretically. Although some

additional viscous damping must be considered, in order to take into account the energy absorbed through other dissipating mechanisms of the isolators, such as friction, heat and sound. This, relatively small amount of dissipated energy, compared to the corresponding hysteretic damping, is taken into account again assuming non-classical damping and a relatively low viscous damping ratio for the seismic isolation system. The primary damping matrix is constructed in the same way as in the case of a linear elastic isolation model, but in this case the initial stiffness K_I is used (Figure 3.2) instead of the effective stiffness k_{iso} .

3.5 Equations of motion

The differential equations of motion for a seismically isolated building, which is modeled as a MDOF system, are expressed in the following matrix form:

$$\underline{F}^I(t) + \underline{F}^D(t) + \underline{F}^E(t) = \underline{\emptyset} \quad (3.4)$$

where \underline{F}^I , \underline{F}^D and \underline{F}^E are the inertia, damping and elastic forces, respectively, acting on the structure at time t . In the case of a ground excitation with an acceleration time-history $\ddot{U}_g(t)$, the inertia forces are expressed as:

$$\underline{F}^I(t) = \underline{M} \cdot \ddot{\underline{U}}(t) + \underline{M} \cdot \underline{l} \cdot \ddot{U}_g(t) \quad (3.5)$$

where $\underline{l} = [l_1 \ l_2 \ \dots \ l_n]^T$. The damping forces are expressed in terms of the floor velocities and the damping matrix of the MDOF system, taking into account the impact damping forces in the case of poundings:

$$\underline{F}^D(t) = \begin{cases} \underline{C} \cdot \dot{\underline{U}}(t) & \text{no impact} \\ \underline{C} \cdot \dot{\underline{U}}(t) + \underline{e} \cdot F_{imp}^D(t) & \text{during impact} \end{cases} \quad (3.6)$$

Each of the terms e_i of vector \underline{e} , which has a dimension equal to the number of the degrees of freedom, is equal to zero when no contact is detected in DOF i , while it takes

the value of 1 when an impact occurs in the corresponding floor. When a linear elastic model is used for simulating the seismic isolation system, the elastic forces are formed based on the floor relative displacements and the stiffness matrix, taking also into account the impact forces in the case of poundings:

$$\underline{F}^E(t) = \begin{cases} \underline{K} \cdot \underline{U}(t) & \text{no impact} \\ \underline{K} \cdot \underline{U}(t) + \underline{e} \cdot F_{imp}^E(t) & \text{during impact} \end{cases} \quad (3.7)$$

When considering the bilinear behavior of the isolation system, the elastic forces (\underline{f}_s) of the superstructure are computed based on the stiffness matrix and the corresponding displacements at time t , while for the isolation system the elastic forces are calculated according to the bilinear model considering the displacement time-history $u(t)$ and the velocity sign at the isolation level at time t :

$$\underline{F}^E(t) = \begin{cases} \underline{f}_s(u(t), \dot{u}(t)) & \text{no impact} \\ \underline{f}_s(u(t), \dot{u}(t)) + \underline{e} \cdot F_{imp}^E(t) & \text{during impact} \end{cases} \quad (3.8)$$

$F_{imp}^E(t)$ and $F_{imp}^D(t)$ are the elastic and damping contact forces during impact, respectively, which are calculated according to the corresponding impact model. The impact forces are non-zero only whenever the relative displacements at the corresponding level exceed the available clearance, leading to poundings with the adjacent structure.

3.6 Numerical integration

The equations of motion are directly integrated using the Central Difference Method (CDM), computing the displacements at time $(t + \Delta t)$ from Equation 3.9 [9]:

$$\underline{U}(t + \Delta t) = \hat{\underline{M}}^{-1}(t) \cdot \hat{\underline{R}}(t) \quad (3.9)$$

The terms $\hat{\underline{M}}$ and $\hat{\underline{R}}$ are given by Equations 3.10 and 3.11, respectively, for both cases of without and with impact:

$$\hat{M}(t) = \frac{I}{\Delta t^2} \cdot \underline{M} + \frac{I}{2 \cdot \Delta t} \cdot \underline{C} \quad (3.10)$$

$$\hat{R}(t) = \begin{cases} \begin{aligned} & -\underline{M} \cdot \underline{t} \cdot \ddot{u}_g(t) - \underline{f}_s(u(t), \dot{u}(t)) + \frac{2}{\Delta t^2} \cdot \underline{M} \cdot u(t) - \\ & \left(\frac{I}{\Delta t^2} \cdot \underline{M} - \frac{I}{2 \cdot \Delta t} \cdot \underline{C} \right) \cdot u(t - \Delta t) \end{aligned} & \text{no impact} \\ \\ \begin{aligned} & -\underline{M} \cdot \underline{t} \cdot \ddot{u}_g(t) - \underline{f}_s(u(t), \dot{u}(t)) + \frac{2}{\Delta t^2} \cdot \underline{M} \cdot u(t) - \\ & \left(\frac{I}{\Delta t^2} \cdot \underline{M} - \frac{I}{2 \cdot \Delta t} \cdot \underline{C} \right) \cdot u(t - \Delta t) - \\ & \left(F_{imp}^E(t) + F_{imp}^D(t) \right) \cdot \underline{e} \end{aligned} & \text{during impact} \end{cases} \quad (3.11)$$

In order to ensure the stability and the accuracy of the CDM, a sufficiently small time-step must be used for the time-integration, according to the following formula:

$$\Delta t < \Delta t_{cr} \frac{2}{\omega_{max}} = \frac{T_{min}}{\pi} \quad (3.12)$$

where ω_{max} is the maximum eigenfrequency of the system. However, during impacts, ω_{max} should be the equivalent eigenfrequency of the force-based impact model, which is:

$$\omega_{imp} = \sqrt{\frac{k_{imp}}{m_{eff}}} \quad (3.13)$$

For example, for a $k_{imp} = 2500$ kN/mm and two colliding masses of 250 tons each, the equivalent eigenfrequency of the impact model is equal to 141.42 rad/sec. Therefore, according to the stability criterion of the CDM (Eq. 3.12), the critical time-step is about 1.4×10^{-2} sec. In the current study, the time-step is taken to be between the values of 2×10^{-4} and 2×10^{-5} sec, which are much smaller than the aforementioned critical time-step.

The selection of a small time-step is also important for the accuracy of the computed impact force when simulating poundings using a “penalty method”. This effect is presented

in Figure 3.3 and Figure 3.4, considering two colliding rigid bodies, each with a mass equal to 300 tons, and the linear elastic impact model to compute the impact forces. In particular, the computed impact force is plotted in terms of the size of the time-step in both decimal and logarithmic scale. It is observed that as the time-step size increases, the dispersion in the impact force values increases. In addition, for higher values of the impact stiffness or the impact velocity, a smaller time-step is needed to avoid errors in the computed responses. According to the plots, a value of the time-step size smaller than 2×10^{-3} sec may provide sufficient accuracy, for the particular case. As mentioned previously, the selected values of the time-step size that is used in the conducted analyses in the context of this study are much lower than that limit, avoiding this kind of numerical errors and instabilities in the computed responses. Such small time-steps can be easily used in numerical simulations and parametric studies, considering the significant increase of the computational speed of the latest computing resources.

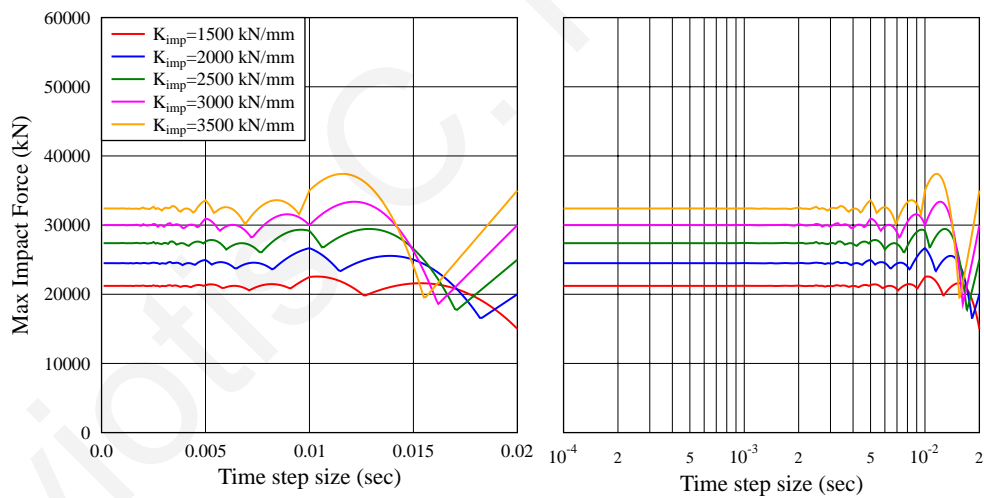


Figure 3.3 Computed maximum impact force in terms of the considered time-step for various values of the impact stiffness, plotted in both decimal and logarithmic scale.

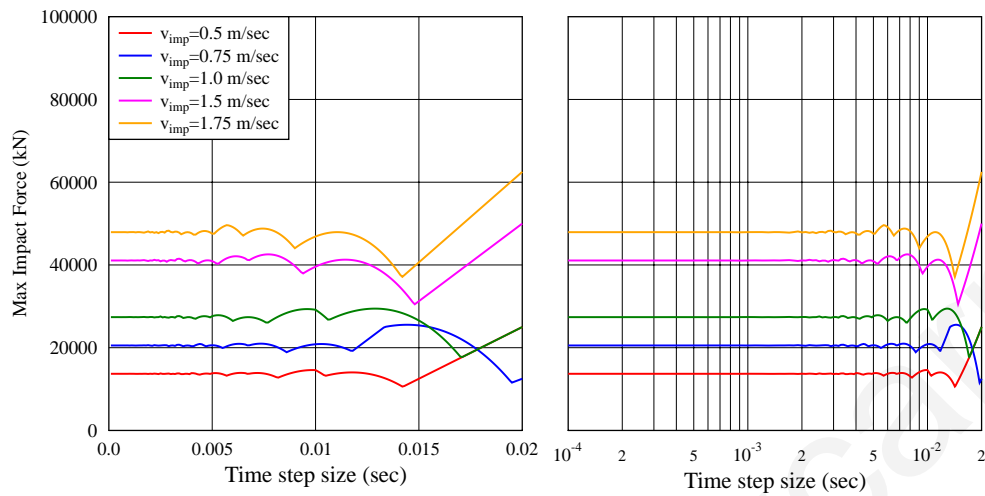


Figure 3.4 Computed maximum impact force in terms of the considered time-step for various values of the impact velocity, plotted in both decimal and logarithmic scale.

3.7 Vertical location of impacts

As already mentioned, two general cases can be distinguished, regarding the locations of potential impacts of seismically isolated buildings. In particular, poundings may occur either with the surrounding moat wall or with other adjacent buildings. The configurations that are considered in the current study, regarding poundings of a seismically isolated building with adjacent structures, are described in the following paragraphs. These cases are based on a two-dimensional simplification of the real problem that involves three dimensional vibrations of the seismically isolated building and its adjacent structures. However, in order to model such problems in three dimensions, three-dimensional analysis of the structures is needed along with a 3D impact model.

3.7.1 *Impacts at the isolation level*

The most common case of structural impact for a seismically isolated building is when poundings occur between the moat wall and the slab at the isolation level (Figure 3.5). In particular, this is the case when the available seismic gap is limited due to practical reasons or when a larger than the expected maximum relative displacement occurs at the isolation level during a very strong earthquake, without any other adjacent buildings to be constructed at a very close distance.

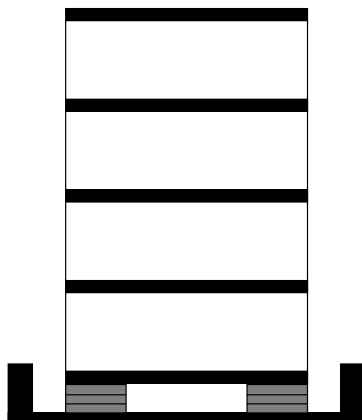


Figure 3.5 A seismically isolated structure, with the possibility of poundings at the isolation level.

Under a very strong earthquake excitation, there is a possibility that the isolation system reaches its ultimate horizontal deformation, leading to an unstable condition for the seismically isolated building. This is another extreme case for the seismically isolated building, which is not investigated in this study.

In particular, it is assumed that the size of the available seismic gap, in all cases under examination, is smaller than the ultimate displacement capacity of the isolation system. This is usually the most common practice in the design of a seismically isolated building, i.e. the width of the seismic gap to be such as to prevent instability due to the failure of the isolation system in the extreme case of a larger than expected horizontal relative displacement at the isolation level.

3.7.2 Impacts at the isolation and the first floor levels

According to another common configuration, the seismic isolation system can be installed at the bottom of a basement, as shown in Figure 3.6, with sufficient clearance from adjacent buildings. In such a case, poundings may occur at both the basement and the ground-floor levels, whenever the respective clearance with the moat wall is exceeded.

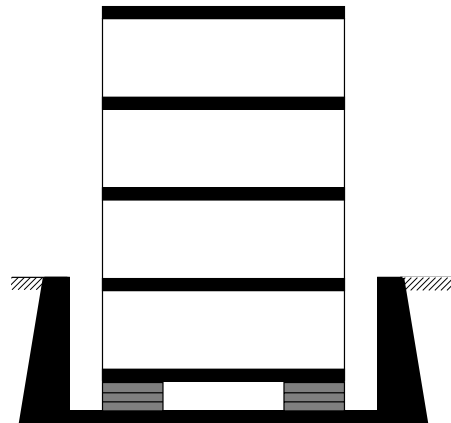


Figure 3.6 Seismically isolated building with basement and potential poundings at both the isolation and the first floor level.

Although in cases of having a basement seismic isolation is usually implemented at the top of the basement's columns, the above configuration represents a possible scenario that should be examined. The simulation of a seismically isolated building with the isolation level being at the top of the basement's columns is a problem that requires the extension of the previously described methodology and is included in the future extensions of this research work.

3.7.3 Impacts at every floor level

The last configuration refers to the case of a seismically isolated building, pounding with adjacent fixed-supported buildings that are in very close distance, due to the deformations of their superstructures (Figure 3.7). There are often cases where adjacent buildings are constructed very close to each other especially, in densely-resided areas. Thus, it is possible to have one of those buildings seismically isolated, during either a new construction or a retrofitting of an existing building.

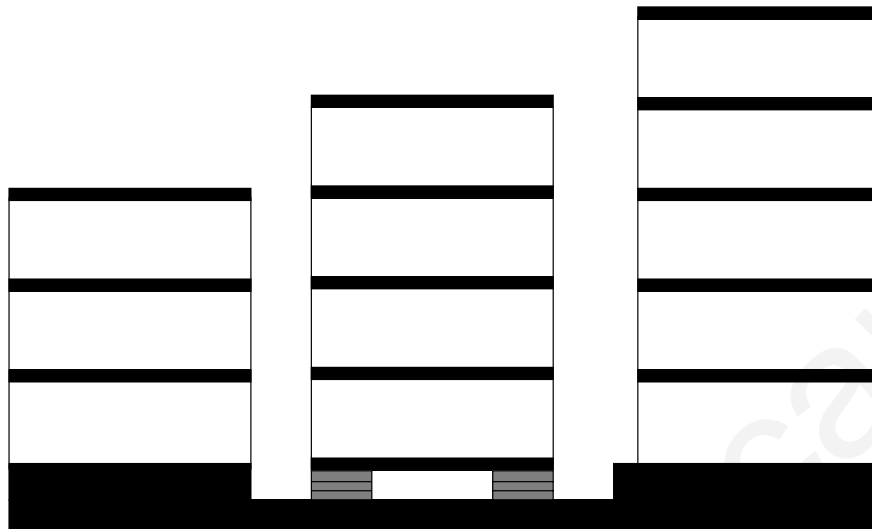


Figure 3.7 A seismically isolated building between two fixed-supported buildings.

The separation distance between the superstructure and the adjacent buildings may be equal or greater than the width of the seismic gap at the isolation level. In addition, a seismically isolated building may be adjacent to one or two fixed-supported buildings, in each direction, experiencing one-sided or two-sided impacts, respectively.

In the current study the slabs of neighboring buildings are assumed to be at the same level. The case of impacts occurring between the slabs, i.e. at the structure's columns, which is the worst case scenario, and must be always avoided, is not considered in the framework of this study.

Moreover, for all considered configurations of the seismically isolated building, the seismic gap size can be either equal (symmetrical) or unequal (asymmetrical) on both sides of the building.

3.8 Development of the simulation software

For the purposes of the present research work, a specialized software tool, able to efficiently perform dynamic analyses of multi-degree-of-freedom systems, considering possible impact phenomena, is necessary. In addition, the option of using different impact models is essential, as well as the ability of investigating parametrically the effects of

certain factors by conducting efficiently large numbers of numerical simulations with varying parameters.

Taking into account these specific needs, it is obvious that none of the available general-purpose commercial software applications could provide these capabilities. Therefore, the development of a specialized software application in order to enable the effective and efficient performance of the necessary simulations, aiming to a more meticulous investigation, has been a primary aim of the current study. Object-oriented programming and Java technologies have been employed in the development of the software application, taking into account the significant advantages that these technologies offer. In particular, the Java programming language is used for the computational part, while the Java Swing is employed for the Graphical User Interface (GUI) and the computer graphics.

3.8.1 Java programming

The Java programming language is a pure object-oriented programming (OOP) language that combines the best ideas, concepts and mechanisms of other OOP languages, such as inheritance, virtual functions and polymorphism, garbage collection and exception handling, while offers modularity, robustness, reusability, portability, superior memory management and multithreading capabilities. In addition, the various Java Application Programming Interfaces (APIs) allow efficient development of applications with computer graphics, database connectivity and graphical user interfaces without a need to use any other programming language or library. In particular, the Swing API [30] provides several components that can be used for the development of graphical user interfaces (GUI), while the Java2D API can be used to develop high quality two-dimensional (2D) graphics.

The use of the Java programming language in engineering applications sometimes raises concerns about the performance limitations and scalability of Java. The expected performance difference between Java and other high-level programming languages, such as C/C++, is due to the fact that, while the latter are compiled into executable machine instructions for the underlying architecture and operating system, Java code is compiled into byte-code, which is translated into machine instructions during execution by the Java

Virtual Machine (JVM). Although this two-phase compilation-interpretation has some operating cost on the computational performance, it provides portability and architectural neutrality to the Java software applications. Furthermore, the latest JVM allows just-in-time compilation that improves further the performance, by using run-time optimization through profiling and recompilation during execution of the program, by taking advantage of the specific hardware conditions that are available. Komodromos and Williams [50] conducted a detail analysis and comparison of the performance of Java vs. C/C++ software implementations, using common algorithms. The results revealed that although the Java implementations are relatively slower than those developed using C/C++, the difference, which is less than 50 % of the computing time, is not that significant compared to the advantages that are offered by the Java programming language.

3.8.2 General description of the program

A primary aim of this research work was the development of a specialized software tool to efficiently and effectively conduct the necessary numerical simulations and parametric studies of seismically isolated structures with automatic impact detection and handling capabilities. In particular, a software application has been developed, which is capable of performing efficiently two dimensional (2D) simulations of MDOF systems with shear-beam behavior under dynamic loading.

The developed software allows the consideration of poundings of a seismically isolated building, either with the surrounding moat wall, which is assumed to move with the ground, or with one or more adjacent buildings. Moreover, the software allows both linear and bilinear models to be used for the simulation of the seismic isolation system. The ability to automatically perform large numbers of numerical simulations is also provided, in order to parametrically investigate the effects of certain parameters, such as the structural characteristics, the size of the separation gap and the earthquake characteristics.

3.8.3 Analysis procedure

In the developed software, there are two different iteration schemes regarding the number of buildings considered in the analyses and the possibility of pounding with each other or

with the surrounding moat wall. In particular, the first solution scheme concerns the cases where the buildings are to be analyzed independently, without considering any contacts with other buildings. The case of a building pounding with the surrounding moat wall also falls within this category. The equations of motion are solved separately for each structure, taking only into account contacts, if there are any, with the surrounding moat wall.

The second iteration scheme refers to the case of two or more buildings that undergo the same ground excitation and interact with each other through impacts due to insufficient separation distances between them. In this case, the equations of motion are coupled and therefore, all systems are analyzed simultaneously. At each time-step, after computing the displacements for each MDOF system, each floor level of the superstructure is checked for contacts with its adjacent floor of the building that is on its right side. If an impact is detected, the impact force is calculated, based on the selected impact model and applied to both impacting floors with different signs. In the case of a seismically isolated building, the isolation level is checked for impacts with the moat wall on both sides. Then, the equations of motions are formulated for each system, including any computed impact forces and proceed to the next time step. A general flow-chart of the analysis procedure is illustrated in Figure 3.8.

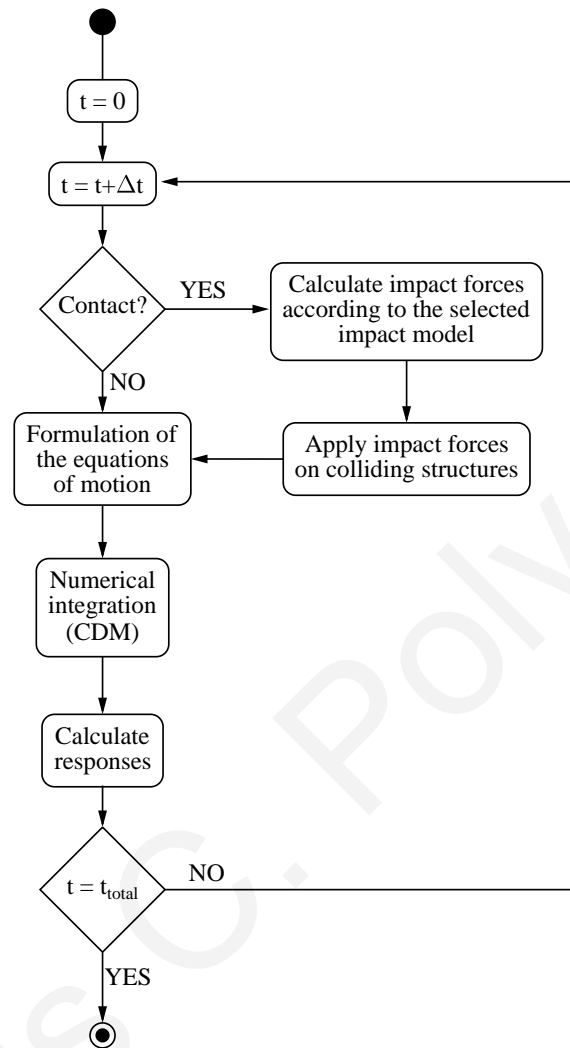


Figure 3.8 A general flow of control of the integration process

A typical non-linear (bilinear behavior of the isolation system) dynamic analysis of a 4-story seismically isolated building, which is subjected to an earthquake excitation with a duration of 30 sec, considering also poundings with the adjacent moat wall, needs about 6 to 8 sec to be performed with a common personal computer (PC). The short duration of such analysis allows to efficiently perform large number of simulations in order to investigate parametrically the problem of poundings in seismically isolated buildings.

3.8.4 The Graphical User Interface (GUI)

The ability of controlling and handling the computed results is an essential need for this research study. Specifically, experience from other commercial analysis-software applications reveals the effectiveness of several abilities of GUI, such as the fast and easy input of data, the animation option for dynamic analyses and the fast generation of graphs. Therefore, a GUI with numerous capabilities has been designed for the developed software, enabling the easy performance of simulations and parametric analyses (Figure 3.9). As mentioned before, the Java Swing and Java 2D have been employed for the development of the GUI of this specialized software application.

The basic capabilities of the GUI include the following features:

- Input data regarding the structural characteristics can be either imported from a text file or defined using the GUI. The same data can be also exported from the GUI to text files.
- Any kind of ground excitation can be imported from a data file in the form of time-acceleration pairs of values.
- The time-step to be used for the analysis and the output step size are also defined through the GUI.
- After the analysis, it is possible to export the computed results in text files.
- Selected results can be used to generate plots, which can be saved in vector form (.eps files).
- Animation of deformed shapes of the buildings can be produced with a specified speed, with the option of “pausing” and “restarting”. In addition, vector drawing files (.eps) can be produced at any time of the animated response.

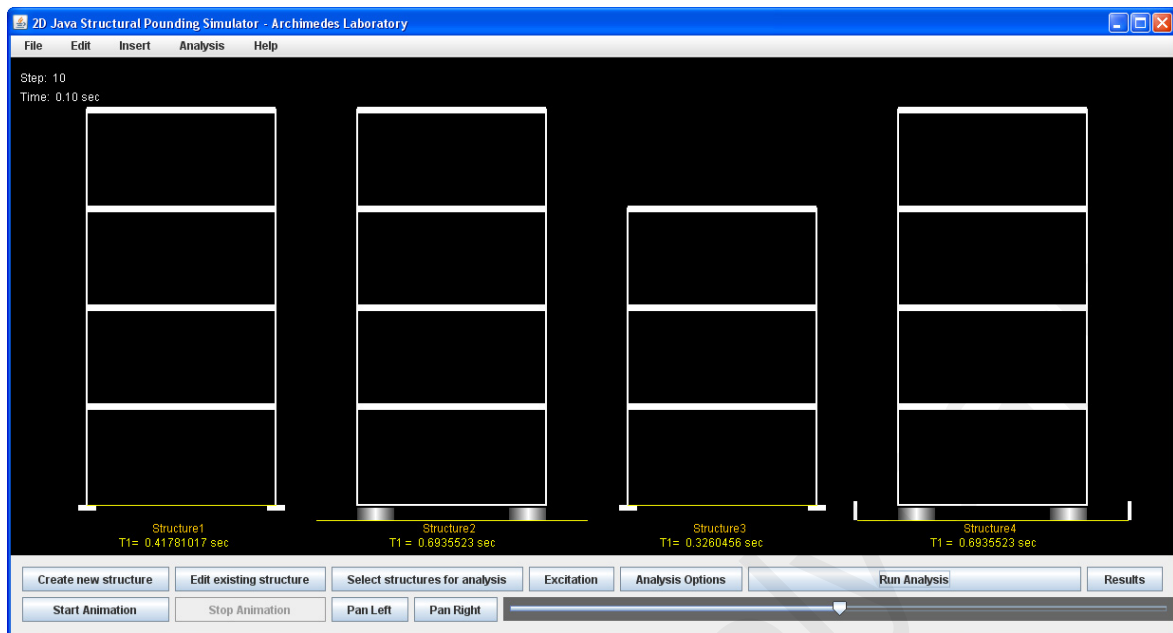


Figure 3.9 The main window in the GUI of the developed software application.

3.8.5 *Parametric analysis capabilities*

Furthermore, the developed software enables the performance of parametric studies, by executing automatically large number of simulations, while varying a certain parameter in order to assess its effectiveness on the computed response. One or more buildings may be considered to be analyzed, either in parallel or in series. A certain parameter is selected to be investigated, such as the size of the seismic gap, the impact stiffness, the coefficient of restitution and the seismic isolation effective stiffness (when a linearized isolation system is assumed). The value of each parameter changes automatically after each simulation, regarding its pre-defined minimum and maximum values and the number of simulations to be performed. A list of such parametric analyses may be constructed by the user and then conducted by the program, which stores the necessary results in corresponding output text files that can be easily elaborated. The GUI of the parametric analysis tool is displayed in Figure 3.10.

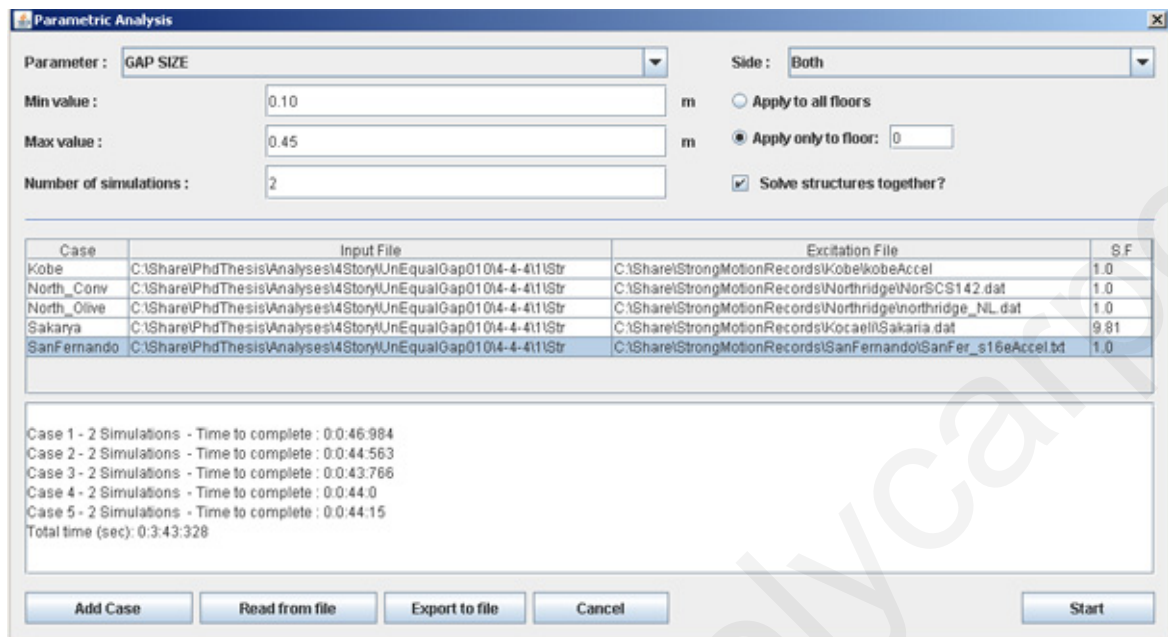


Figure 3.10 The parametric analysis dialog of the GUI of the developed software application.

CHAPTER 4 ANALYSES CONSIDERING IMPACTS WITH THE SURROUNDING MOAT WALL

4.1 General

The results presented in this chapter are based on the assumption that there are no adjacent buildings at close distance and, therefore, impacts may occur only at the seismic isolation level when the base isolated building exceeds the available seismic gap and hits against the surrounding moat wall under a strong earthquake excitation. At first, some detailed results of a single analysis are presented in order to provide a general aspect of the effects of seismic poundings on the dynamic response of a typical seismically isolated building. Particularly, the effects of poundings are exhibited mainly in terms of absolute floor accelerations and interstory deflections, which are considered to be the most important response quantities for a seismically isolated building, subjected to an earthquake excitation, especially concerning damage that may be caused. Then, the results of the parametric studies, regarding the effect of certain factors on these response quantities of the seismically isolated building, during poundings with the surrounding moat wall, are presented.

4.2 Selected seismic records for the performed analyses

Five different seismic records (Table 4.1) are used in the simulations of the current study in order to examine the effects of the characteristics of the excitation on the seismic response of the seismically isolated building during poundings. The accelerograms of the specific earthquakes have been taken from the Pacific Earthquake Engineering Research (PEER) strong motion database [69]. All selected earthquakes are characterized by low-frequency content, in order to induce large displacements to the seismically isolated building, since this is one of the most decisive factors for the occurrence of poundings in such structures. The acceleration response spectra of the selected seismic records, scaled to have a peak ground acceleration (PGA) equal to 1 g, are plotted together in Figure 4.1, in order to demonstrate their differences.

Table 4.1 Earthquake records that were used in the simulations

Earthquake	Mw	Station	PGA (g)	Duration (sec)
Kobe, Japan 1995	6.9	0 KJMA	0.821	48.00
Northridge, USA 1994	6.7	74 Sylmar – Converter Station	0.897	40.00
Northridge, USA 1994	6.7	24514 Sylmar – Olive View Med FF	0.604	30.00
Kocaeli, Turkey 1999	7.4	Sakarya	0.628	20.00
San Fernando, USA 1971	6.6	Pacoima Dam, S16	1.170	71.12

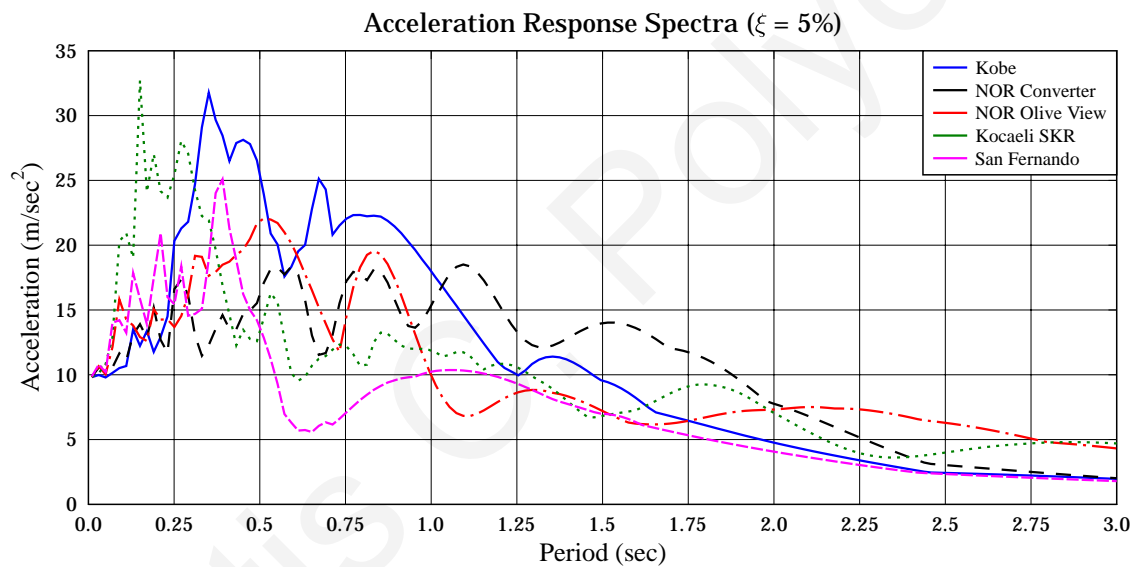


Figure 4.1 Acceleration response spectra of the five selected seismic records, scaled to have a common PGA equal to 1.0 g, considering a viscous damping ratio of 5 %.

In order to avoid redundancy, in cases where no more than a single seismic excitation is needed to demonstrate the effect of certain parameters, besides the earthquake characteristics, on the computed response, the 1995 Kobe Earthquake acceleration record (KJMA Station) is used in the performed analyses. There is no specific reason for selecting this particular earthquake, besides the fact that it is very popular, due its catastrophic consequences on structures, as well as on human lives, and that has been widely used in many relevant research studies.

4.3 Practical example considering a 4-story building

A typical 4-story building is considered under the following three different circumstances as: (a) fixed-supported, (b) seismically isolated without the possibility of poundings, and (c) seismically isolated with a finite seismic gap on either of its sides, to illustrate the pounding effects on its structural response.

The superstructure is assumed to have 4 floors, each with a lumped mass of 320 tons, except of the top floor, where a mass of 250 tons is considered. Each story has a horizontal stiffness of 600 MN/m. In the case of the seismically isolated building, an additional mass of 320 tons is assumed to be lumped at the isolation level, while the isolation system's behavior is simulated using the bilinear inelastic model. The fundamental period of the fixed-supported 4-story building is equal to $T_{fixed} = 0.398$ sec. Additional to the hysteretic damping of the seismic isolation system, a 5 % viscous damping ratio has also been considered using non-classical damping according to the methodology described in Chapter 3. All structural characteristics of the selected buildings are provided in Table 4.2. For the case of poundings, the modified linear viscoelastic impact model is used with an impact spring stiffness equal to 2500 kN/mm and a COR equal to 0.7. The effective mass of the moat wall, which is used for the estimation of the impact forces, has been considered to be 500 tons.

4.3.1 *Analyses using the Kobe Earthquake record*

In order to observe the effects of poundings on the response time-history of the seismically isolated building, dynamic analysis of the building, for each of the cases described above, is performed, using the Kobe Earthquake record as the ground excitation. For the case of poundings, the size of the seismic gap is taken to be equal to 15 cm, which is 10 % smaller than the maximum relative displacement (16.74 cm) at the isolation level of the seismically isolated building under the same excitation (Figure 4.2). This assumption is based on the uncertainties concerning the characteristics of the design-earthquake and the estimation of the maximum design displacement for the seismically isolated building.

Table 4.2 Structural characteristics of the buildings that have been used in the simulations.

Parameter	Value
<u>- Superstructure's characteristics:</u>	
Story stiffness (k_i)	600 MN/m
Story mass (m_i)	320 tons
Top-story mass (m_n)	250 tons
Superstructure's damping ratio (ζ_{sup})	2 %
<u>- Fixed-supported building:</u>	
Story stiffness (k_i)	600 MN/m
Story mass (m_i)	320 tons
Top-story mass (m_n)	250 tons
Damping ratio (ζ)	5 %
<u>- Seismic isolation system:</u>	
Mass at the seismic isolation level (m_{iso})	320 tons
Viscous damping ratio (ζ_{iso})	5 %
<u>- Bilinear characteristics of the seismic isolation system:</u>	
Initial stiffness (K_1)	200 MN/m
Post yield stiffness (K_2)	25 MN/m
Characteristic strength (f_y)	$0.1 \times W_{tot}^*$

* W_{tot} = total weight of the building

Figure 4.2 presents the displacement time-histories at the base of the seismically isolated building under the Kobe Earthquake for both the case without poundings and the case of a seismic gap equal to 15 cm, where the base mat unavoidably hits against the surrounding moat wall, specifically at two time instances. It is observed that the differences in the two plots are very difficult to be identified, since only a slight reduction of the peak values due to impact can be detected.

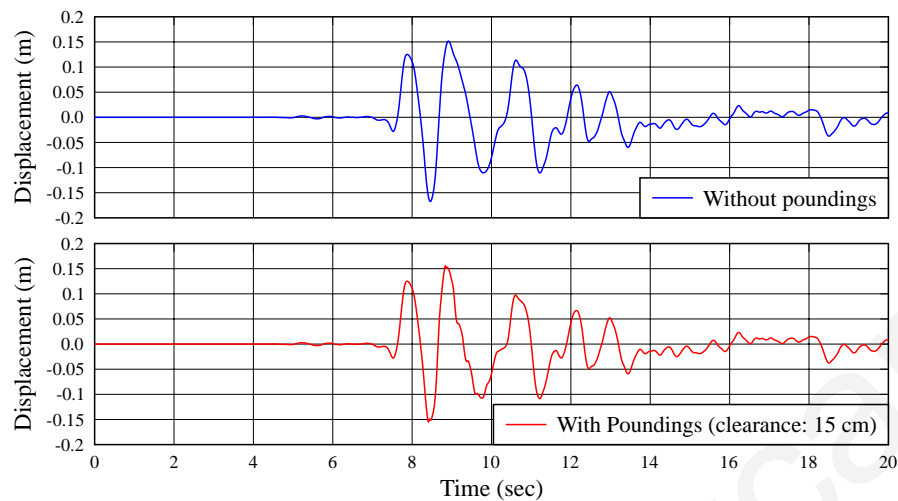


Figure 4.2 Relative displacement time-histories at the isolation level of the 4-story seismically isolated building due to the Kobe Earthquake for the two cases of without and with poundings

In contrast to the relative displacements responses, floor accelerations, as expected, are found to be more sensitive to impact occurrences. Although the width of the clearance is less than 2 cm smaller than the maximum unobstructed relative displacement at that level, the effects of pounding are very apparent, especially on the acceleration response at the isolation level where impacts occur. Figure 4.3 presents the acceleration time-histories of the seismically isolated building during poundings, compared to the corresponding time-histories for the case without poundings. Very high accelerations are observed at the time of impact. In particular, the high spikes in the acceleration response reach up to 5 times the corresponding peak floor accelerations without poundings, in which case the response, as shown by the plot, is much smoother. Nevertheless, due to damping, short time after the impact occurrences, the response tends to become identical to the corresponding response without poundings. The latter observation can be seen more clearly in Figure 4.4, in which the accelerations of the top-floor for the two cases are plotted together, with different line colors and widths.

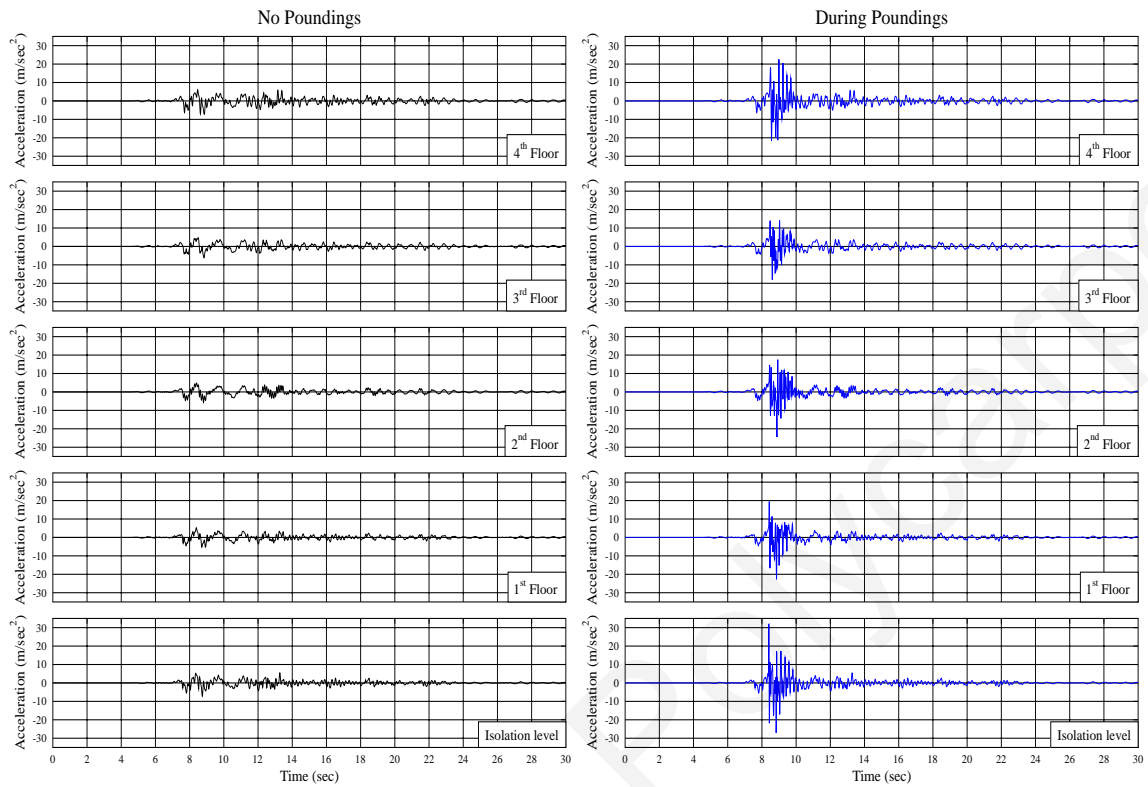


Figure 4.3 Acceleration time-histories at each floor level of the 4-story seismically isolated building, without and with poundings respectively.

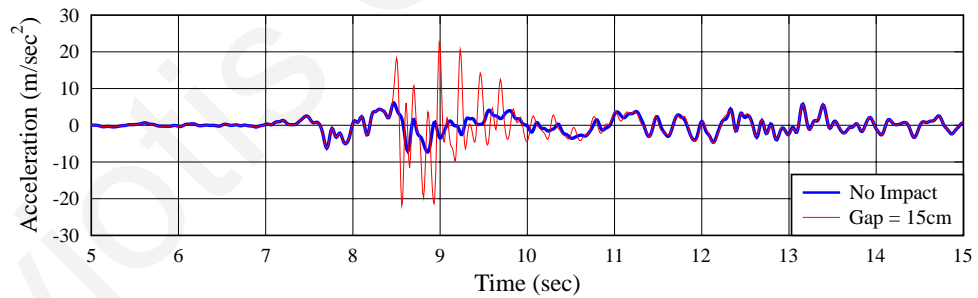


Figure 4.4 Acceleration time-histories at the top of the seismically isolated building with poundings and without poundings.

The peak values of the interstory deflections and absolute floor accelerations of the seismically isolated building during impact are plotted in Figure 4.5 and compared with the corresponding values of the fixed-supported level and base-isolated building without impacts. It is observed that, during poundings, interstory deflections at the upper floors, reach the peak values of the deflections of the fixed-supported building. Consequently, almost the same

shear forces that act on the corresponding fixed-supported building with the same characteristics, act on the particular stories of the superstructure. If not sufficient strength is provided to the structural elements, taking into account these effects of potential poundings during the design of the superstructure of the seismically isolated building, there is a great possibility of causing considerable damage in such cases.

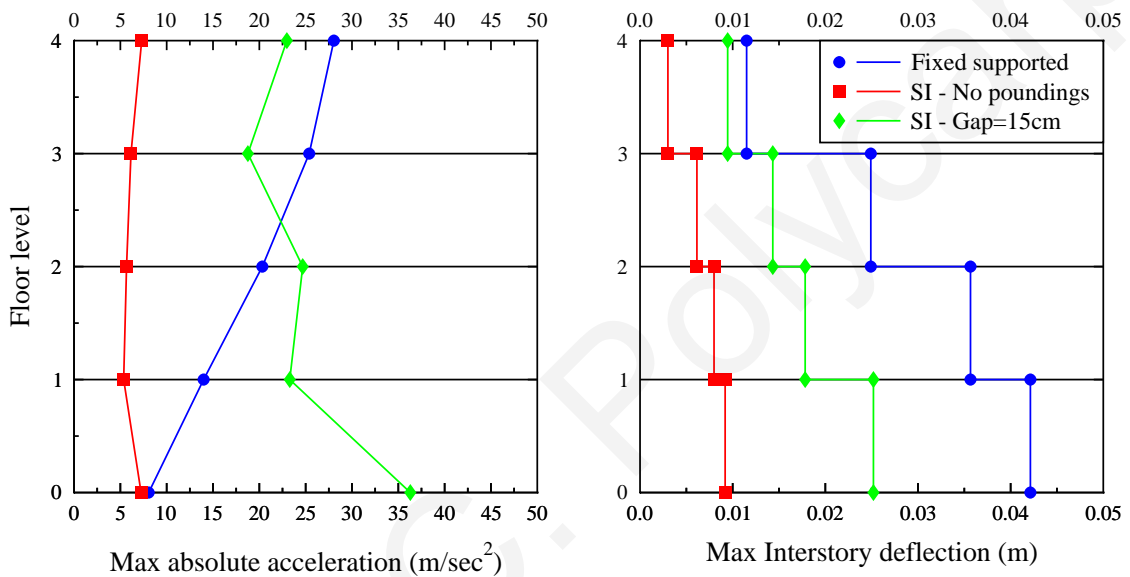


Figure 4.5 Comparison of the peak responses of the 4-story seismically isolated building during poundings with the case of unobstructed response without poundings and those of the corresponding fixed-supported building.

Comparing the computed peak absolute floor accelerations of the building, the influence of poundings in the response is much more pronounced at the lower floors, where the peak floor accelerations become much higher than those for the corresponding fixed-supported building. Due to poundings with the moat wall, the seismically isolated building may experience maximum floor accelerations at the isolation level, where impacts occur, instead of the top-floor, which is the most common case for a MDOF system. It is well known from previous studies ([31],[2],[54],[29],[76]) that the acceleration response is highly affected by impacts. These high values of floor accelerations that are caused by poundings can damage sensitive equipment that may be accommodated in the building.

As mentioned in the previous chapter, the specially developed software tool provides the ability of animating the structures that are analyzed under the selected ground excitations. Through the animation option, a representative overview of the response of the structure during poundings is provided below. In particular, Figure 4.6 presents some snapshots that have been generated using the developed software, for the case of the aforementioned 4-story seismically isolated building, considering a seismic gap that is 15 cm wide. It is observed that poundings excite higher modes of deformation of the seismically isolated building, instead of moving, according to its fundamental mode, with the superstructure behaving as an almost rigid-body. However, in some cases, more detailed examination of the results is needed to ensure the information given through the animation. For example, in this case, two impact events are observed in the animation. In particular, the first impact happens on the left side of the seismically isolated building at time 8.4 sec and the second happens on the right side at time 8.8 sec (Figure 4.6).

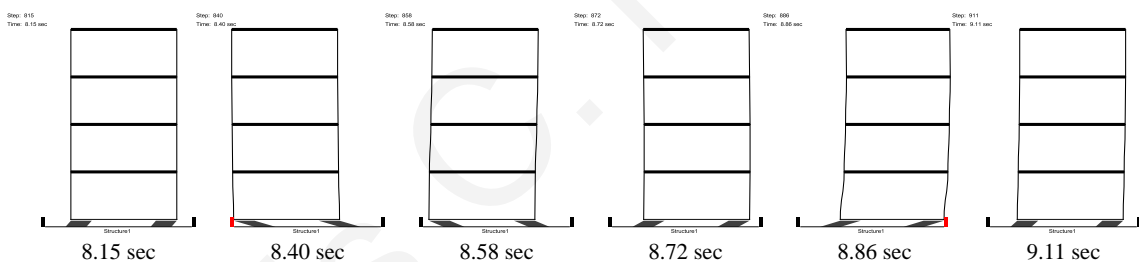


Figure 4.6 Snapshots of the animated seismically isolated building under the Kobe Earthquake, considering a seismic gap equal to 15 cm.

Nevertheless, in Figure 4.7 the time-history of the impact force indicates that there are three impact events. Specifically, the first pounding event on the left side is followed in very short time by a second, much smaller impact due to the effect of the deformation of the superstructure and the inertia forces, acting at the upper stories in the opposite direction from the impact force. While the impact forces push the base-mat away from the moat wall, the inertia forces of the superstructure are driving the building against the wall. Consequently, the base mat rebounds on the moat wall.

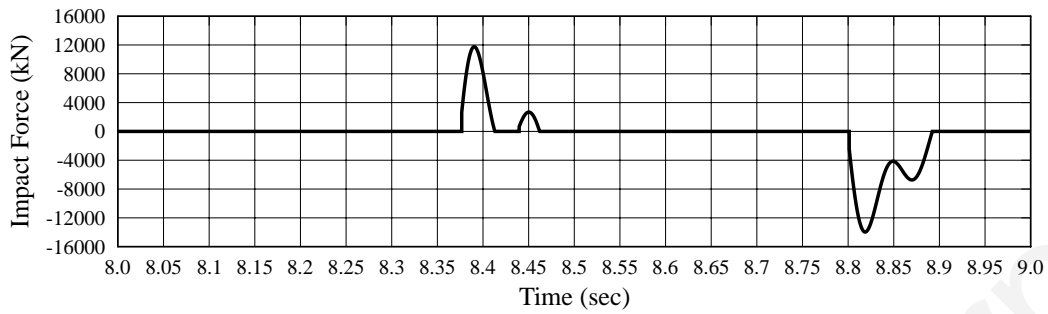


Figure 4.7 Impact force time-history at the base of the 4-story seismically isolated building under the Kobe Earthquake, considering a gap width equal to 15 cm and the modified linear viscoelastic impact model to simulate poundings.

4.3.2 *Dynamic analyses using five seismic excitations*

The same model of the seismically isolated building, which is examined above, is simulated under the five aforementioned seismic records in order to provide a more general view of the effects of poundings on the computed response. Figure 4.8 presents the amplification factors of the peak floor accelerations and interstory deflections of the 4-story seismically isolated building during poundings with the adjacent moat wall. The amplification factor is defined as the ratio of the maximum response when poundings occur divided by the corresponding maximum response value without poundings:

$$Ampl = \frac{R_{Pounding}}{R_{NoImp}} \quad (5.1)$$

According to the simulation results, the total accelerations as well as the interstory deflections and, therefore, the story shear forces of the seismically isolated building increase significantly due to poundings. This occurs when the width of the available seismic gap is slightly exceeded. In these cases, the available clearance is only 10 % less than the one that is needed to avoid impact and, nevertheless, the responses are amplified from 2 to 6 times, compared to the corresponding responses of the seismically isolated building without poundings. In addition, it is observed that the amplification of the peak floor accelerations is, in general, greater than the amplification of the peak interstory deflections, since the former are much more sensitive to impact loadings, as described above. The higher amplification of the interstory deflections at the upper stories indicate

that poundings may change the mode of deformation of a seismically isolated building, exciting higher modes of the building, instead of moving, according to its fundamental mode as an almost rigid-body. The same observation can be easily made from the corresponding animations that are generated during the simulation.

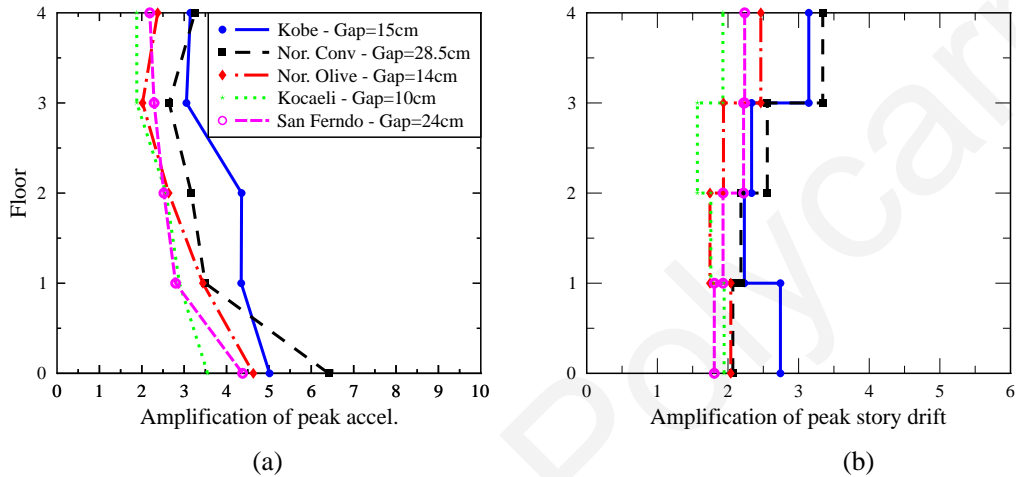


Figure 4.8 Amplification of the maximum responses of the seismically isolated building when the width of the available gap around the seismically isolated building is 10 % smaller than the maximum induced relative displacement at the isolation level, for each seismic record.

4.3.3 Differences in using various impact models

This example is also used to compare the selected following impact models: the linear model, the linear viscoelastic impact model [2], the non-linear viscoelastic impact model [37], the Hertz damp impact model [61] the modified linear viscoelastic impact model and the proposed non-linear impact model with hysteretic damping.

In particular, the aforementioned impact models are used, to consider potential poundings of the 4-story seismically isolated building with the surrounding moat wall, under the Kobe Earthquake. The impact stiffness for both linear viscoelastic impact models is taken to be equal to 2500 kN/mm, while for the non-linear impact models a value of the impact stiffness equal to 750 kN/mm^{1.5} is used. These values for the impact stiffness have been selected from Table 2.2, assuming a wall height equal to 1.25 m, providing the same maximum impact force when using the two different types of impact models. The

coefficient of restitution is assumed to be equal to 0.7 for all cases, while the mass of the surrounding moat wall is taken to be equal to 500 tons.

Table 4.3 presents the peak responses of the seismically isolated structure, subjected to the Kobe Earthquake, with the separation gap equal to 15 cm, considering the six different impact models. In general, the differences are very small, as concerns the computed response.

Table 4.3 Peak responses of the 4-story structure with a seismic gap = 15 cm, under the Kobe Earthquake, for the six different impact models.

Peak Response	1	2	3	4	5	6
Base floor displacement [cm]	15.615	15.462	15.555	15.614	15.688	15.750
Top floor displacement [cm]	19.368	18.832	19.424	19.309	19.225	19.201
Interstory Deflection [cm]	2.631	1.899	2.519	2.361	2.358	2.291
Acceleration (top floor) [m/sec ²]	25.736	21.258	22.972	21.421	22.418	21.665
Acceleration (base floor) [m/sec ²]	39.169	36.297	36.297	30.321	35.457	36.287
Remaining Plastic deformation [cm]	----	----	0.687	----	----	----

1: Linear elastic; 2: Kelvin-Voigt; 3: Modified Kelvin-Voigt; 4: Non-linear viscoelastic; 5: Hertz damp; 6: Non-Linear Hysteretic

It would be expected that the two linear viscoelastic impact models would lead to almost identical responses, due to the fact that their only difference is the tensile forces during detachment. However, there is a considerable variation of the maximum interstory deflection and the top-floor displacement that are computed considering the classic Kelvin-Voigt model from the corresponding results of the rest five cases. This variation can be explained by the information provided in Figure 4.9. Specifically, Figure 4.9 presents the time-histories of the impact force at the base of the isolated building for the six different impact models. The impact velocities during the first impact on the left side and the second impact on the right side, respectively, are also provided in the figure. It is observed that during the first impact, on the left side, which corresponds to positive values, the value of

the maximum impact force is almost the same for all impact models, about 12 MN. The impact velocity during the first impact, as expected, is exactly the same for all cases. However, the maximum impact force during the second impact (on the other side of the building), for the case of using the linear viscoelastic impact model (classic Kelvin-Voigt model), is significantly lower than the corresponding maximum values for the rest five cases. As it is well known, the maximum impact force depends on the impact velocity, which explains why in the case of the Kelvin-Voigt model is much lower than in the rest of the cases. This reduction of the impact velocity is due to the tensile forces that arise during the detaching phase of the first impact. This remark is justified by the fact that for the case of using the proposed modified linear viscoelastic impact model, which results in a small permanent indentation, this problem is eliminated.

Conclusively, the following remark can be made for the case of using the linear viscoelastic impact model for simulating structural poundings, where impacts may occur consecutively: Even though by omitting the tensile forces during the restitution phase an amount of dissipated energy is omitted, eventually, more accurate results are obtained, since these tensile forces affect the detaching velocity and, consequently, the response during successive impacts. Therefore, the small variation that is proposed for the linear viscoelastic model seems to be beneficial for the accuracy of this impact model when it is used in cases of multiple impact incidences in a row. Figure 4.10 provides the impact force-indentation diagrams for each one of the aforementioned six cases.

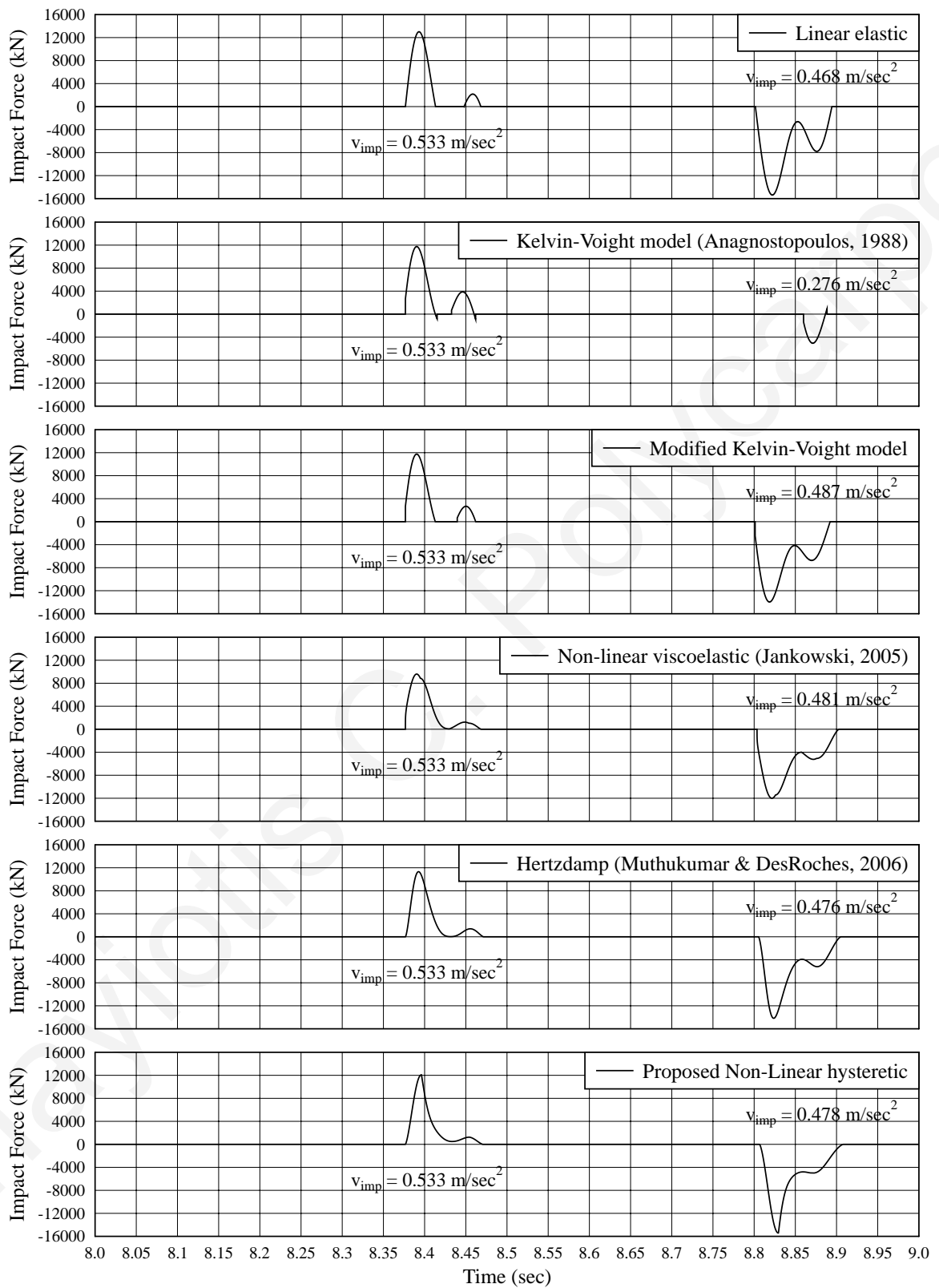


Figure 4.9 Impact force time-histories at the base of the 4-story seismically isolated building, considering the six different impact models.

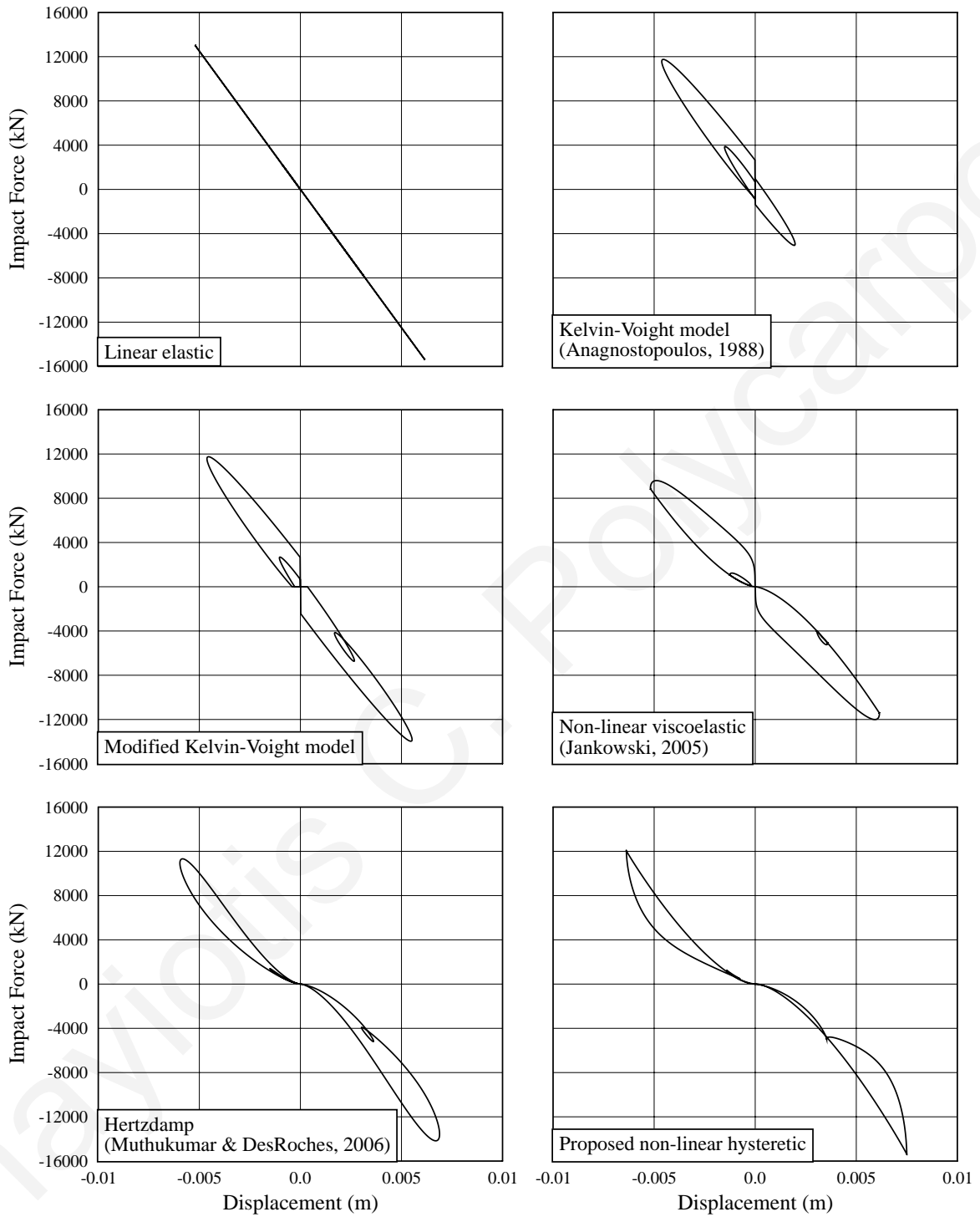


Figure 4.10 Plots of the impact force in terms of indentation for the 4-story seismically isolated building under the Kobe Earthquake, with a seismic gap equal to 15 cm, considering the six different impact models.

4.4 Seismically isolated buildings with a basement

As already mentioned, another possible configuration of a seismically isolated building, regarding poundings with the surrounding moat wall, is the case of having the isolation system installed at the bottom of a basement. In that case pounding may occur at both the basement and the ground-floor levels, whenever the respective clearance is exceeded. In order to investigate that case, a set of analyses has been conducted, considering the moat wall reaching up to the first floor (Figure 3.6).

For the performed numerical simulations, the 4-story seismically isolated building that has been used in the previous analyses is considered with a seismic gap that is 10 % smaller than the maximum induced relative displacement from each one of the five earthquakes. The results are compared with the corresponding responses that have been obtained considering the moat wall only around the isolation level.

The comparative curves of the peak floor accelerations and peak interstory deflections are plotted in Figure 4.11 for the five selected seismic excitations. It is observed that in all cases, the peak absolute floor accelerations become greater in the case of having a basement, where impacts may occur at each of the two first floors. In particular, in almost all of the cases, the larger amplification of the peak floor acceleration is observed at the ground level (1st floor).

This trend may be justified by the fact that the velocity of the floor that pounds on the wall is reduced in a shorter time duration when a second impact occurs, at the same time, on the same side of the building. The reduced duration of impact may explain the higher peak floor accelerations acting on the pounding floors, which may lead to undesirable damage of the structure or the equipment that may be housed in the building.

The amplification of the peak interstory deflection at the first story is always reduced when impact occurs at both the basement and the ground-floor levels, compared to the case of impacts only at the isolation level. On the other hand, the interstory deflections of upper stories of the seismically isolated building with basement are amplified more than the corresponding deflections when there is no basement.

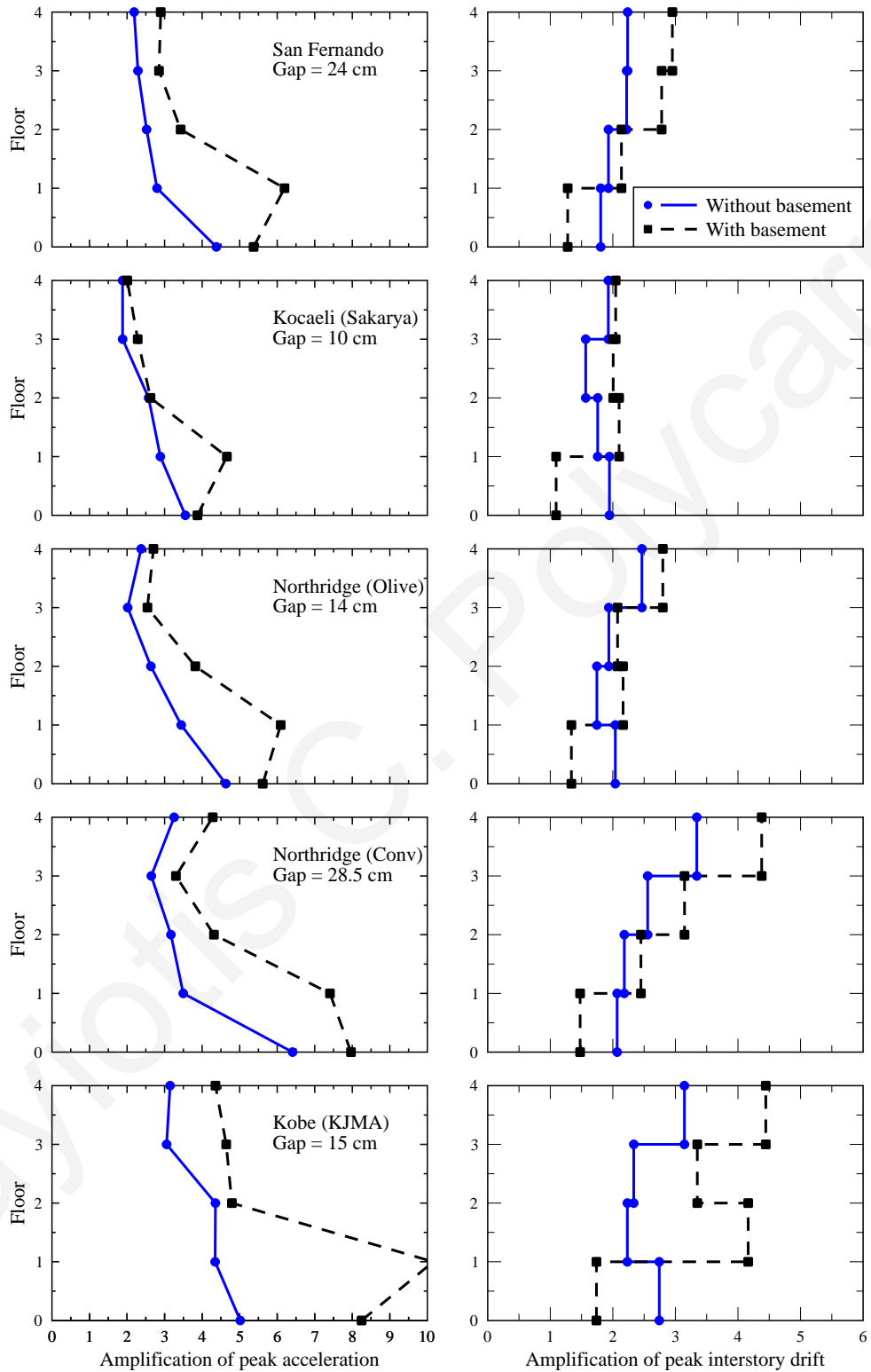


Figure 4.11 Peak responses of the 4-story seismically isolated building for both cases of with and without a basement.

4.5 Parametric analyses

This section refers to the results of a parametric investigation regarding the effects of certain parameters, such as the flexibility of the isolation system, the size of the seismic gap, the earthquake characteristics, the number of stories and the values of the impact parameters, on the response of a typical seismically isolated building during poundings with the surrounding moat wall.

In the parametric studies, a 3-story, a 4-story and a 5-story typical seismically isolated building are considered. The buildings have the characteristics provided in Table 4.2. Certain influencing design parameters are purposely varied in order to assess how they may affect the effectiveness of seismic isolation during poundings. In case of poundings, the modified linear viscoelastic model with plastic deformations is employed, assuming a coefficient of restitution equal to 0.7 and, unless differently stated, a value of impact stiffness equal to 2500 kN/mm. The mass of the surrounding moat wall, which is used for the calculation of the impact damping according to the corresponding impact model, is taken to be equal to 500 tons on both sides of the seismically isolated building.

4.5.1 *Effect of the flexibility of the Isolation System*

In order to investigate the effect of the flexibility of the seismic isolation system, an equivalent linear elastic model is used for the seismic isolation system of the 5-story building with an effective stiffness that varies from 15 MN/m to 75 MN/m. The ratio of the fundamental period of the seismically isolated building to that of the corresponding fixed-supported superstructure $T_{iso}/T_{superstr}$ ranges between the values of 2.25 and 4.5, according to the variation of the effective stiffness of the seismic isolation system. According to the rule of thumb, usually this ratio for a seismically isolated building must be around 3.0, considering an equivalent linear model for the isolation system [49], in order to ensure that its fundamental period falls outside the dangerous for resonance range of periods of the excitation. Furthermore the fundamental mode of deformation of the building should demonstrate an almost rigid-body-motion of the superstructure. The eigenmodes and eigenperiods of the 5-story seismically isolated building, assuming an isolation stiffness

value equal to 35 MN, are provided in Figure 4.12. The characteristics of the superstructure are kept the same as those provided in Table 4.2.

The equivalent viscous damping ratio for the seismic isolation system is taken to be equal to 15 %, considering non-classical damping (see Chapter 3). Each of these MDOF systems is analyzed for the various seismic excitations, considering two different gap sizes, 20 and 25 cm, and assuming equal gaps on both sides of the buildings.

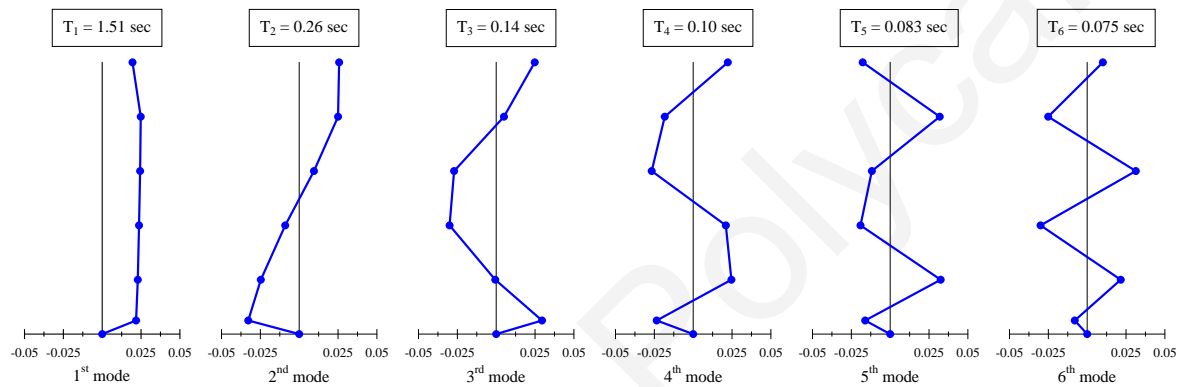


Figure 4.12 The six eigenmodes of the 5-story seismically isolated building with an equivalent effective stiffness for the isolation stiffness equal to 35 MN.

The amplifications of the peak absolute floor accelerations and interstory drifts of the 5-story seismically isolated building, with a fundamental period of 1.10 to 2.20 seconds, are presented in Figure 4.13, for the Kobe Earthquake excitation. It is observed that the shapes of the amplification curves have similar trends with the corresponding displacement response spectrum (Figure 4.14) in the same range of periods. This is justified by the fact that, since the seismically isolated building moves mainly according to its fundamental mode, it tends to have almost the same maximum displacement at the isolation level as the one provided by the corresponding response spectrum. Therefore, the amplification of the response due to impact seems to depend on the difference between the available gap size and the maximum response displacement of the corresponding SDOF system, resulting to the observed similarities.

It is also observed that the amplifications of the peak floor accelerations are always higher at the base of the building, where poundings occur with the moat wall. This is due

to the sensitivity of the acceleration response to local impact, as mentioned previously. On the other hand, the amplifications of the peak interstory deflections are much more considerable for the upper floors, indicating an excitation of the higher modes of the seismically isolated building due to poundings. The plots indicate that the excitation of higher modes of deformation is more pronounced for buildings with more flexible seismic isolation systems.

The interstory deflections of the seismically isolated building when poundings occur, in some cases, become over 10 times larger than the corresponding deflections without impact incidences. This means that a high ductility factor is needed for the superstructure to avoid collapse in such extreme cases. This observation indicates that by increasing the flexibility of the isolation system, in order to maximize its effectiveness, the structure may become vulnerable to poundings, especially if the earthquake contains large rapid ground displacements, due to near source effects.

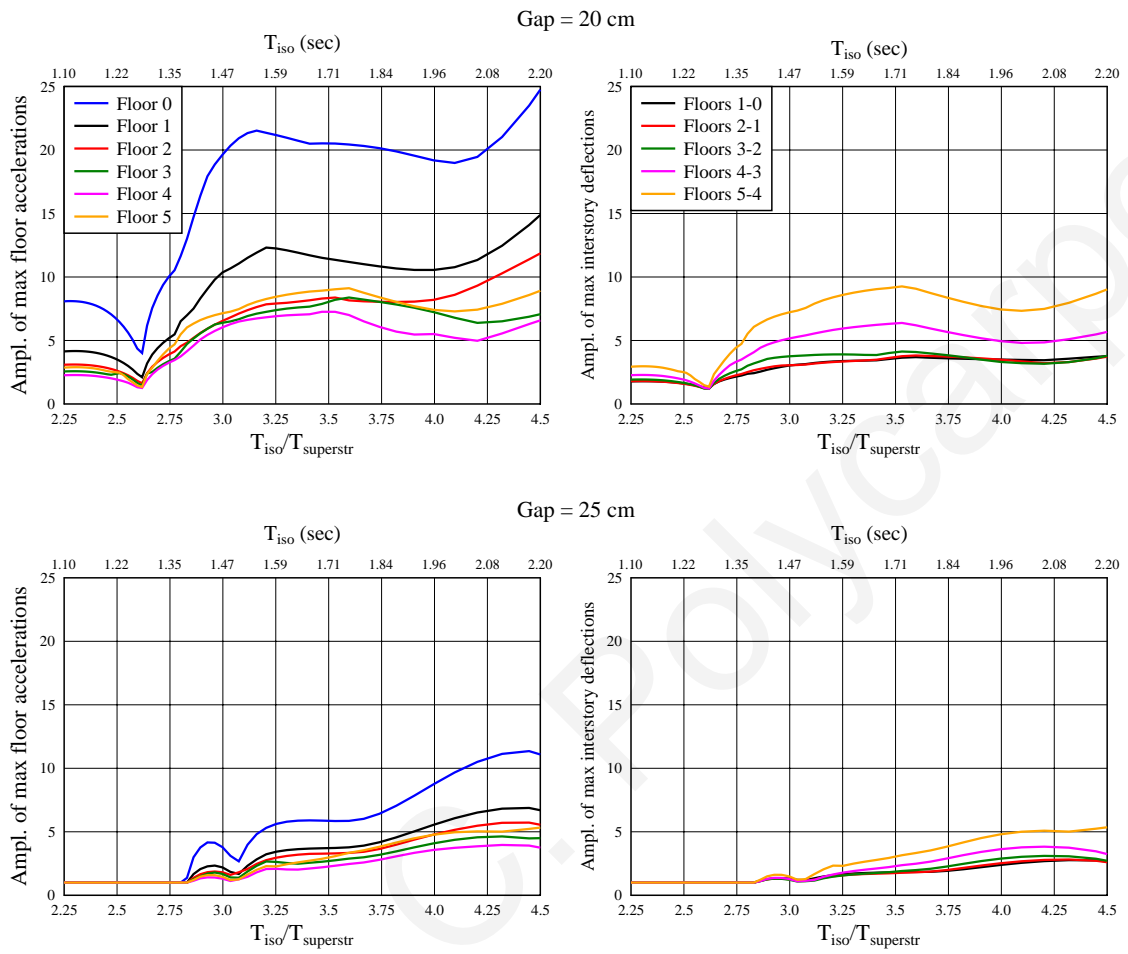


Figure 4.13 Amplifications of the peak floor responses of the 5-story seismically isolated building due to poundings with the moat wall, in terms of the flexibility of the equivalent linear elastic isolation system, considering two seismic gap widths and the Kobe Earthquake record.

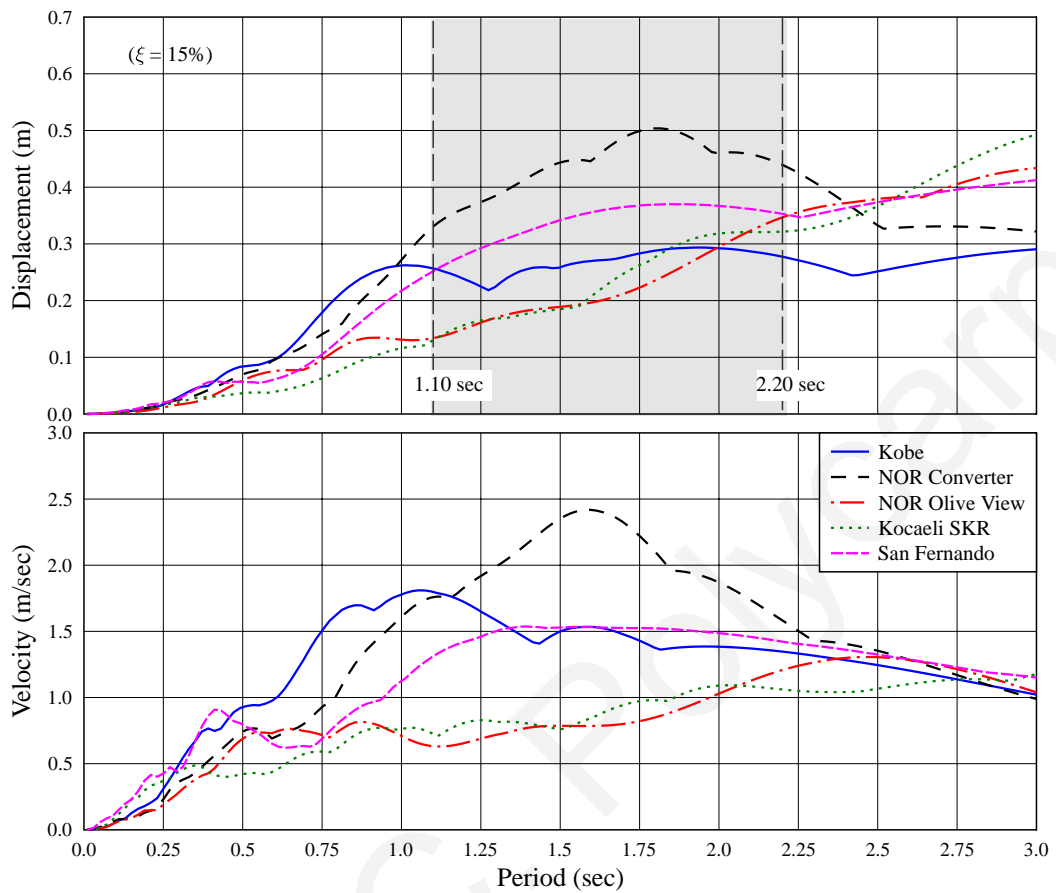


Figure 4.14 Displacement and velocity spectra of the five seismic records, considering 15% damping.

The same parametric analysis has been conducted using all selected seismic records, as presented in Table 4.1, in order to ensure that the above observations are valid for all excitations. Indeed, the plots of Figure 4.15 show that the effect of poundings is, in general, more significant for flexible seismically isolated buildings, following a similar trend with the displacement response spectrum. However, it is observed that there are some differences regarding the effect of the width of the seismic gap. While for the Kobe and the Northridge Olive View earthquake records the response is reduced in the case of a 25 cm gap, compared to the corresponding response for a 20 cm gap, for the rest of the earthquakes the response reduces slightly or in some cases increases. This indicates that besides the difference between the available gap size and the maximum response

displacement of the corresponding SDOF system, there are other factors that determine the magnitude of the response-amplification due to poundings.

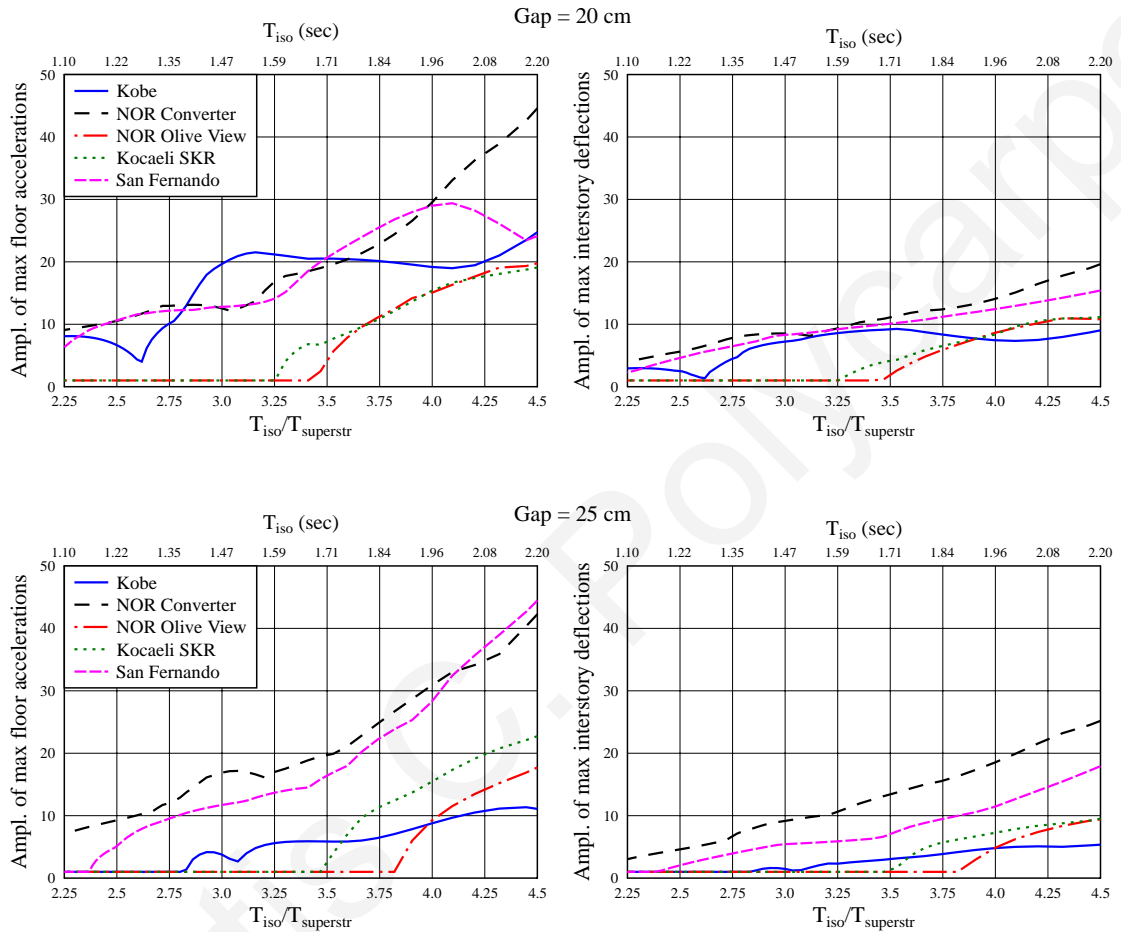


Figure 4.15 Maximum amplifications of the response of the 5-story seismically isolated building due to poundings with the moat wall for the selected earthquakes, in terms of the flexibility of the equivalent linear isolation system, considering seismic a gap width equal to 20 cm and 25 cm.

Figure 4.16 presents the maximum impact velocities in terms of the flexibility of the seismic isolation system, for the various earthquakes and for both cases of the seismic gap width. In general, impact velocity seems to increase with the flexibility of the isolation system. Nevertheless, there are some cases for the narrow gap width (20 cm) whereas, for very flexible systems, the impact velocity reduces.

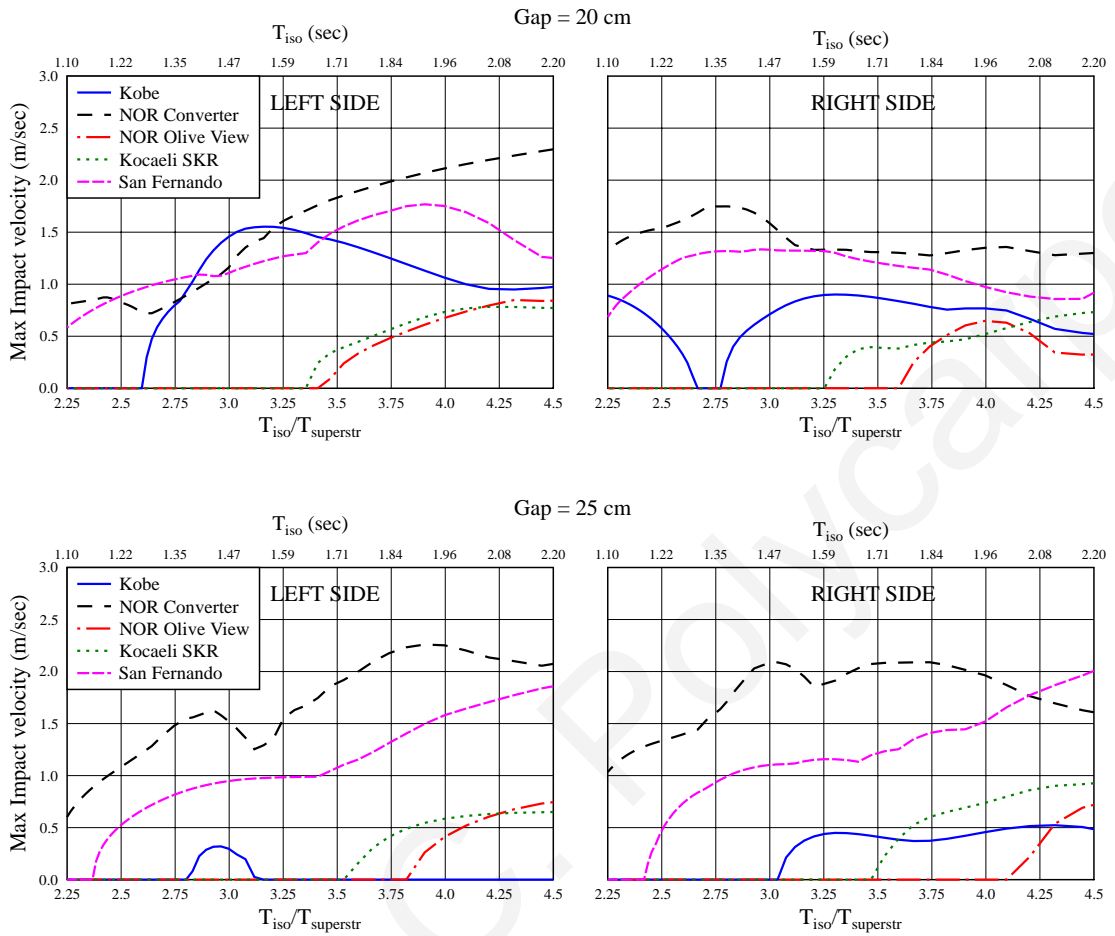


Figure 4.16 Maximum impact velocity in terms of the flexibility of the seismic isolation system.

Figure 4.17 presents the number of impact incidences that occur during the various earthquakes, in terms of the flexibility of the seismic isolation system. It is observed that, similarly to the impact velocity trends, the number of impact incidences increases with the flexibility of the isolation system. However, some variation of the curves is observed, due to the characteristics of each earthquake and, specifically, due to the shapes of the corresponding displacement and velocity response spectra in the particular range of periods.

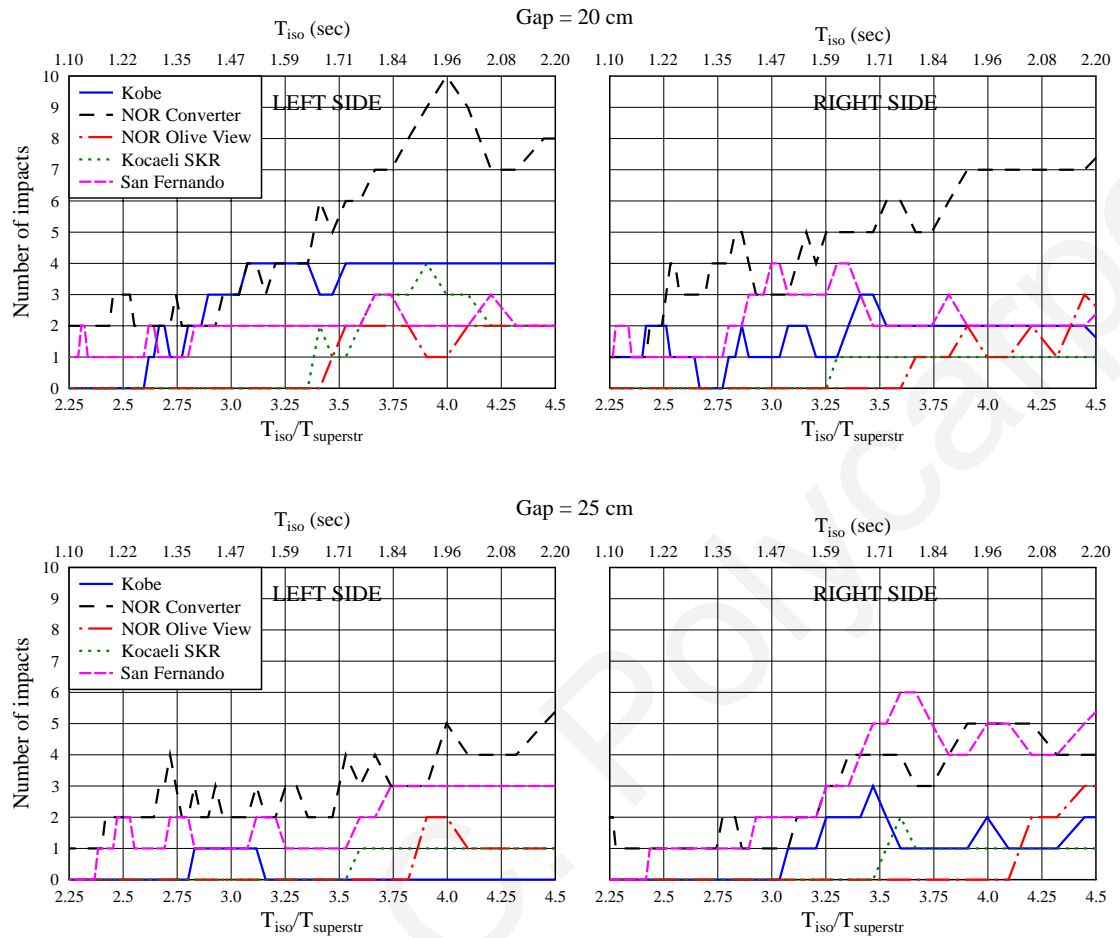


Figure 4.17 Number of impact incidences at each side of the 5-story seismically isolated building, in terms of the flexibility of the equivalent linear elastic isolation system.

4.5.2 *Effect of the gap size and the characteristics of earthquake*

In order to examine the effect of the seismic gap size on the response of the seismically isolated building during poundings with the moat wall, the three aforementioned seismically isolated buildings are considered, using the bilinear inelastic model to simulate the behavior of the seismic isolation system. The structural characteristics of the three seismically isolated buildings are those presented in Table 4.2. Moreover, the five seismic records that have been previously presented are used either scaled to have a PGA equal to 0.6 and 1.0 g (Table 4.4), or without any scaling. The width of the seismic gap is varied from 10 to 45 cm with a step of 0.5 cm, considering equal gap sizes on both sides of the building.

Table 4.4 The considered seismic records with the corresponding scale factors

Earthquake	Mw	Station	PGA (g)	Scale Factor	
				PGA = 1 g	PGA = 0.6 g
Kobe, 1995	6.9	0 KJMA	0.821	1.218	0.731
Northridge, 1994	6.7	Olive View	0.604	1.655	0.993
Northridge, 1994	6.7	Converter Station	0.897	1.115	0.669
Kocaeli, 1999	7.4	Sakarya	0.628	1.592	0.955
San Fernando 1971	6.6	Pacoima Dam, S16	1.170	0.854	0.513

The plots in Figure 4.18 present the peak floor accelerations and peak interstory deflections of the 4-story seismically isolated building under the Kobe Earthquake record (PGA = 0.82 g), in terms of the width of the seismic gap. The simulation results indicate that, as the seismic gap increases, both floor accelerations and interstory deflections of the superstructure decrease. However, for the Northridge Converter Station record (PGA = 0.9 g) the response is quite different (Figure 4.19). In particular, for relatively narrow gap sizes the response increases with the width of the available clearance and, after a certain value, the response of the seismically isolated building begins to decrease, as the seismic gap increases. The difference between the two cases of seismic excitations is that the value of the maximum induced relative displacement of the seismically isolated building during the Northridge excitation is almost two times larger than in the case of the Kobe Earthquake. Therefore, the trend of these plots depends on the characteristics of the earthquake excitation and, more specifically, on the predominant frequencies, in combination with the structural characteristics of the seismically isolated building.

The variation of the response due to the characteristics of the excitation is shown in Figure 4.20, where the maximum responses are plotted for all considered seismic records and for the three seismically isolated buildings under investigation. It is observed that, in general and for a range of values of the width of the seismic gap around the maximum induced displacement, the response decreases with the increment of the seismic gap size. Additionally, some small differences are observed between the responses of the three

buildings, mainly regarding the shape of the curves. Nevertheless, the behavior of the three buildings during poundings is in general very similar.

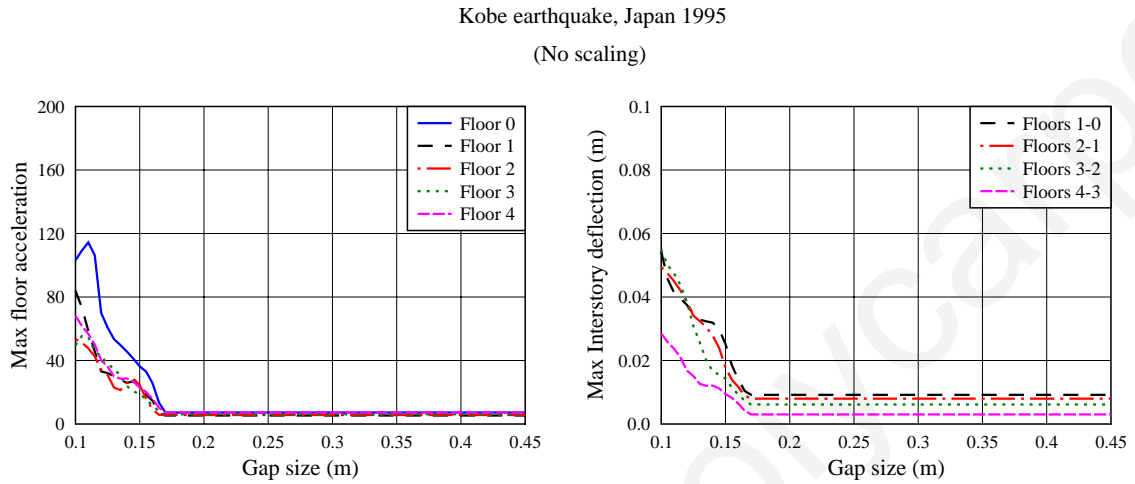


Figure 4.18 Maximum responses of the 4-story seismically isolated building during poundings, under the Kobe Earthquake, in terms of the width of the seismic gap.

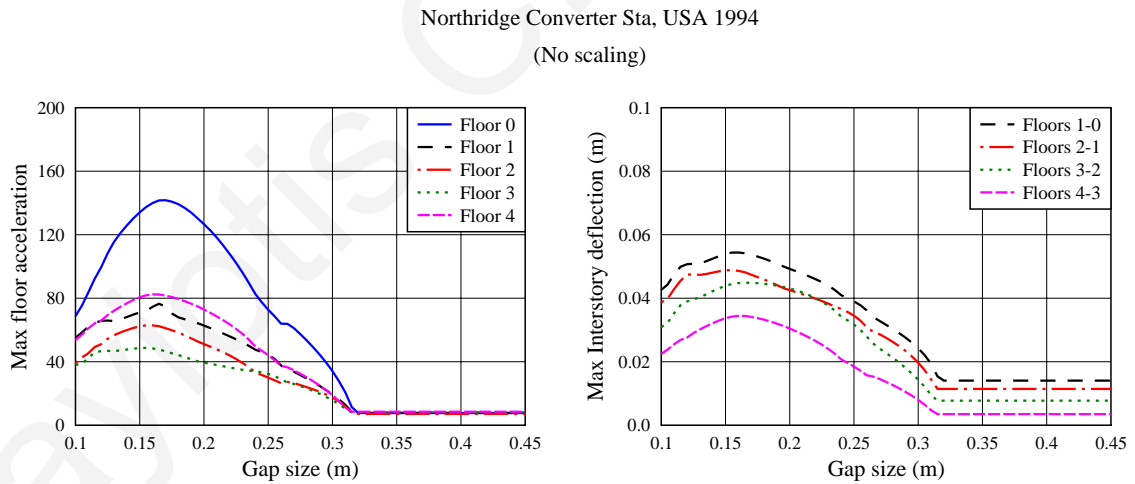


Figure 4.19 Maximum responses of the 4-story seismically isolated building during poundings, under the Northridge Earthquake, in terms of the width of the seismic gap.

In the particular case of the Northridge Converter Station record, it seems that providing a seismic gap equal to 10 cm, rather than an 18 cm gap, would be less detrimental for the 4-story seismically isolated building. However, for another excitation, such as the Kobe

record, this would be the worst case scenario, leading to substantial amplification of the response. Therefore, in order to provide a more general relationship between the peak responses and the width of the seismic gap, the maximum and mean response quantities over the five unscaled seismic excitations are plotted in Figure 4.21.

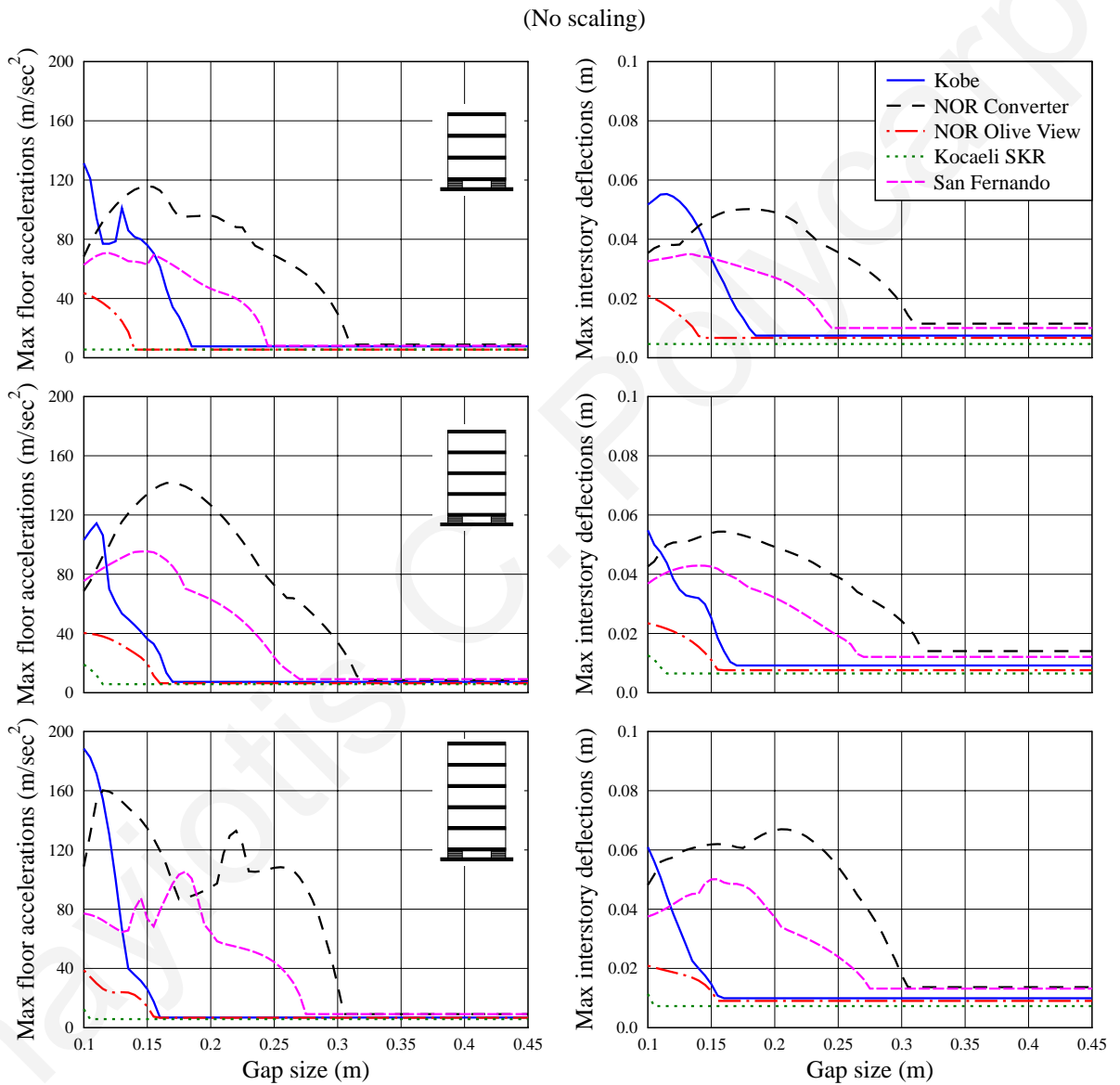


Figure 4.20 Maximum responses of the seismically isolated building in terms of the width of the seismic gap, for the five selected earthquakes.

The “mean values” curves clearly indicate that the response is reduced with the increment of the seismic gap size. Plots of the ratios of the maximum to the mean values of

the peak responses are also provided in Figure 4.21, showing that the variability due to the excitation is more prominent for wider seismic gaps, where impacts occur only under certain excitations, while the rest do not cause any poundings.

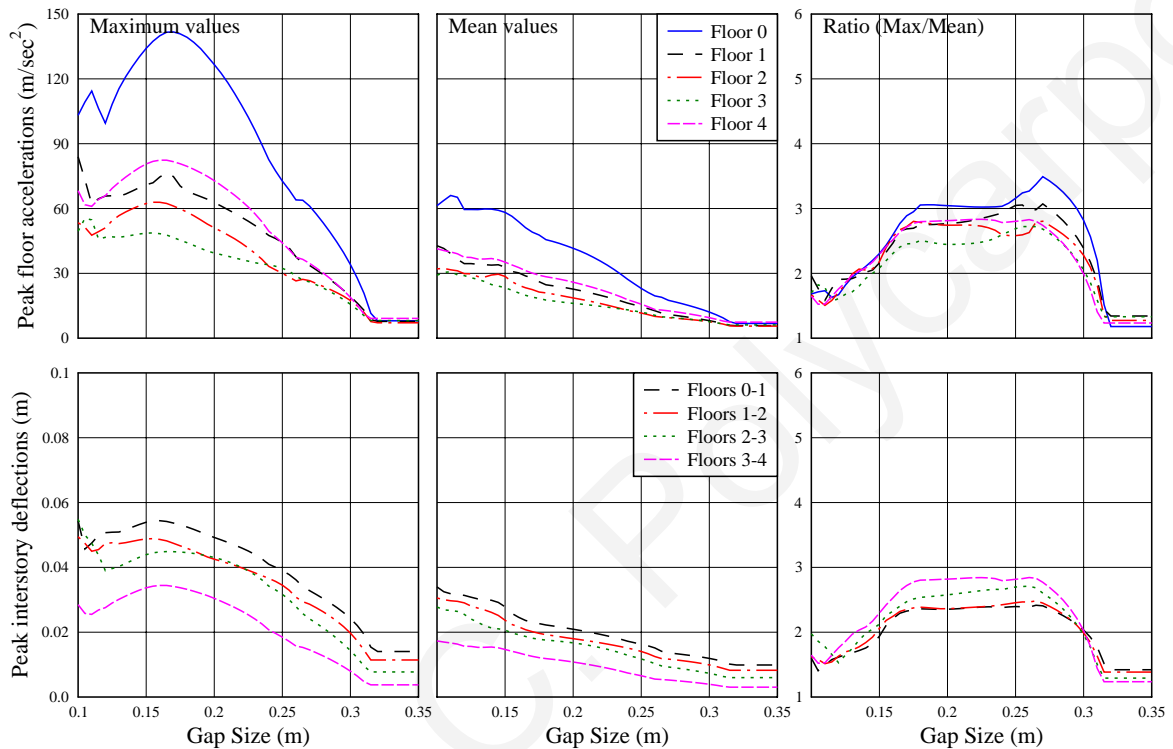


Figure 4.21 Maximum and mean curves over the various seismic records (unscaled).

In order to examine how the value of the peak ground acceleration affects the response during poundings, all seismic excitations are scaled to have either a PGA equal to 1.0 or 0.6 g. The maximum responses of the three seismically isolated buildings for these two cases are provided in Figure 4.22 and Figure 4.23, respectively. In the case of a PGA equal to 1.0 g (Figure 4.22), which is a very strong ground excitation, it is observed that, despite the fact that all excitations have the same PGAs, the differences between the curves for each earthquake are still large. This indicates that the most important characteristic of the earthquake, regarding its effects on the response during poundings, is the range of the predominant frequencies and not the peak ground acceleration of the excitation. In particular, ground motion recordings that contain long period impulses induce large horizontal displacements for relatively flexible structures, such as seismically isolated

buildings, increasing the possibility of poundings to occur when an inadequate seismic gap is provided around the building.

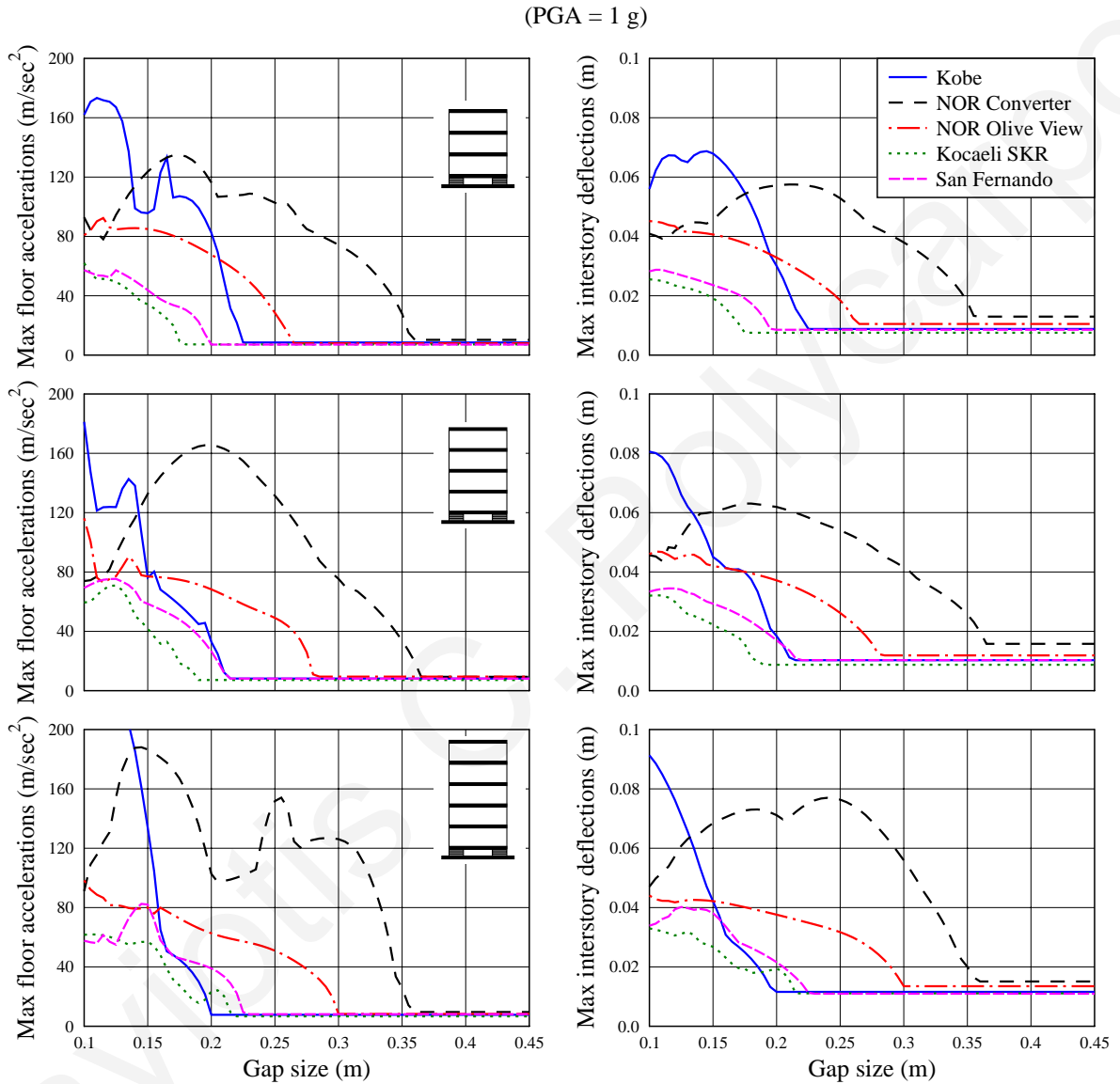


Figure 4.22 Maximum responses of the seismically isolated building in terms of the width of the seismic gap, for the various earthquakes, scaled to have a PGA equal to 1 g.

On the other hand, when the same seismic excitations are scaled to 0.6 g (Figure 4.23), which is also a relatively strong intensity, poundings occur for some of the earthquakes and only for relatively narrow seismic gap sizes. This fact indicates that the problem of

poundings in seismically isolated buildings is an extreme situation, which is more likely to take place in cases of very to extremely strong earthquakes.

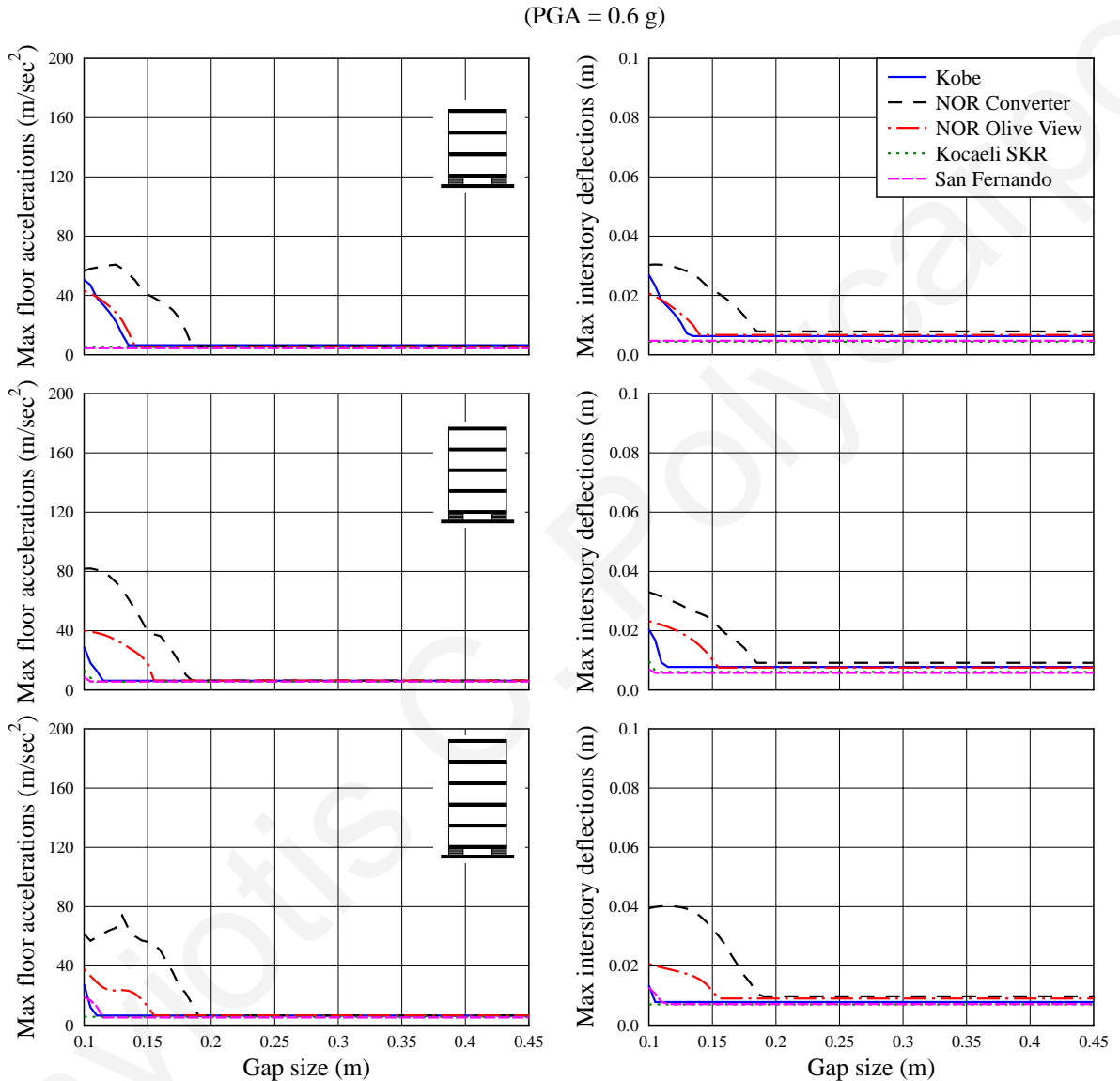


Figure 4.23 Maximum responses of the seismically isolated building in terms of the width of the seismic gap, for the various earthquakes, scaled to have a PGA equal to 0.6 g.

Figure 4.24 and Figure 4.25 present the maximum impact velocities and number of impact incidences, respectively, on the left and right side of the seismically isolated building for the various seismic excitations, in terms of the seismic gap width. It is observed that the trends of the maximum impact velocity are very similar to the

corresponding maximum responses of the seismically isolated building during poundings, indicating that the amplification of the response due to impact is proportional to the impact velocity. It is also observed that the number of impacts by itself is not a determinant factor for the amplification of the response during poundings. In particular, there are cases when a single impact, in combination with a high impact velocity, induces larger amplification of the response rather than two or three impact incidences with lower impact velocities. In general, it is observed that the number of impacts is larger for narrow gap sizes.

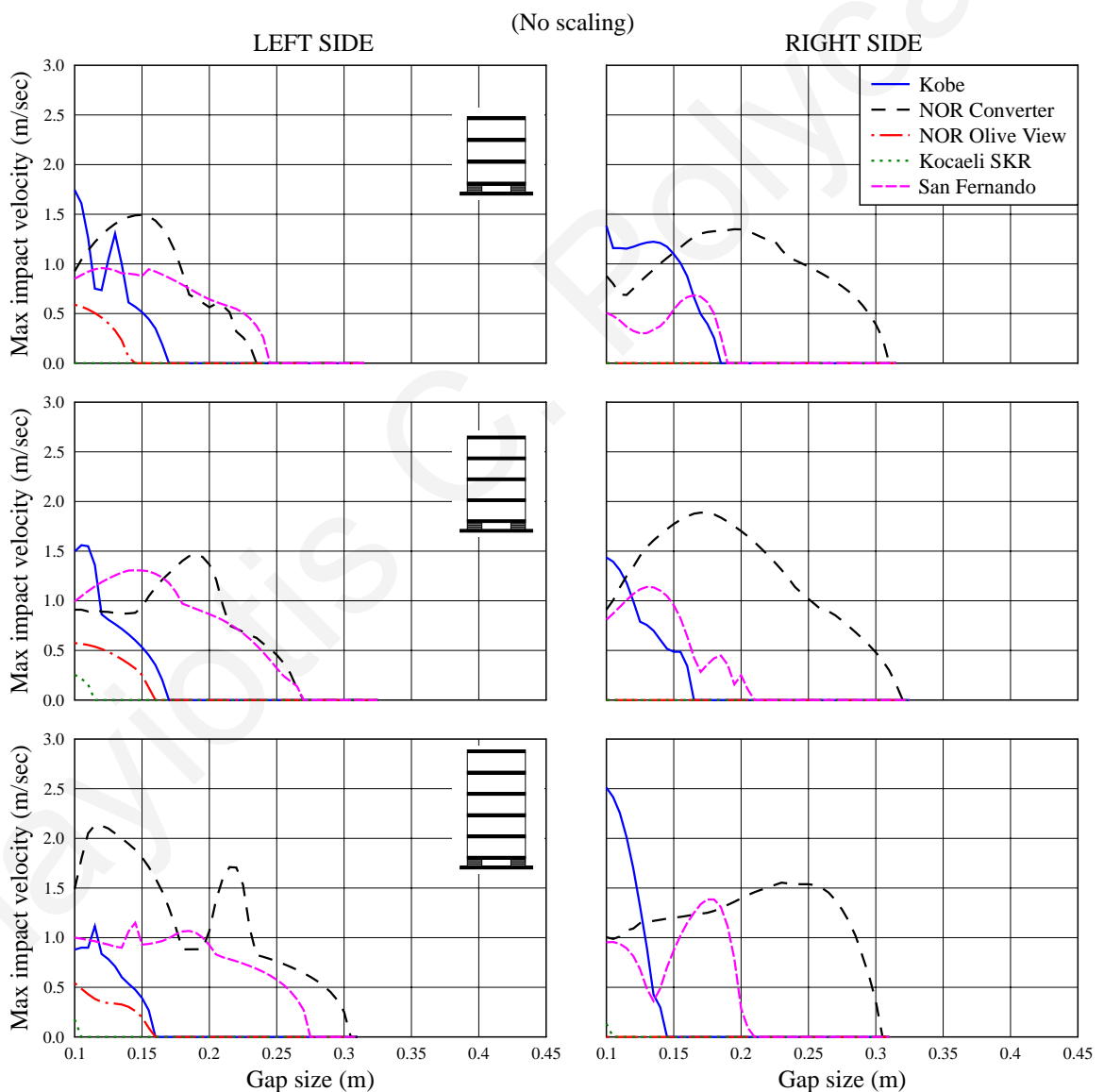


Figure 4.24 Maximum impact velocities of the seismically isolated building in terms of the width of the seismic gap, for the five selected earthquakes.

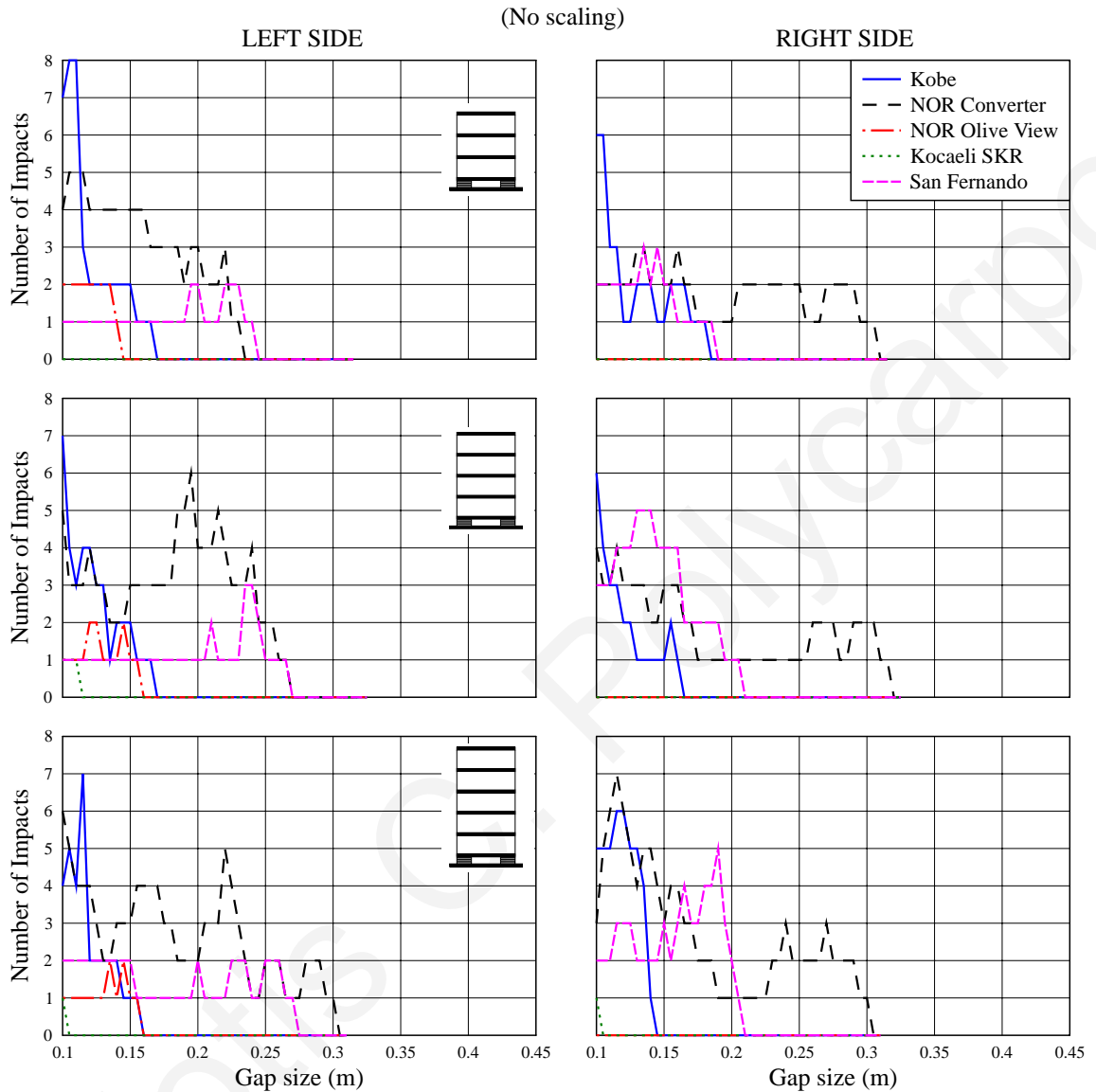


Figure 4.25 Number of impacts incidences in terms of the width of the seismic gap.

4.5.3 Effect of the location of the moat wall

In another set of simulations, the moat wall is presumed to be present only on the left side or only on the right side of the 4-story seismically isolated building in order to compare the results with the corresponding responses with the moat wall considered on both sides of the building. Figure 4.11 shows comparative maximum response results, under the various earthquakes, considering a finite width of the seismic gap on the left side, on both sides, or on the right side of the 4-story seismically isolated building. It is observed that for two

excitations the building hits only on the left moat wall. In the cases of two-sided poundings, the maximum response covers, almost always, the corresponding responses from one-sided poundings. However, in the case of poundings only on the one side of the building, the amplification of the response can be of the same magnitude as in the case of two-sided poundings. The simulation results also indicate that in the case of very narrow seismic gaps, the response may be increased due to the presence of the moat wall on both sides of the seismically isolated building. For wider seismic gaps, the curves of the maximum responses during poundings on both sides of the building coincide with those of one-sided poundings, which may be on the left or on the right side of the building.

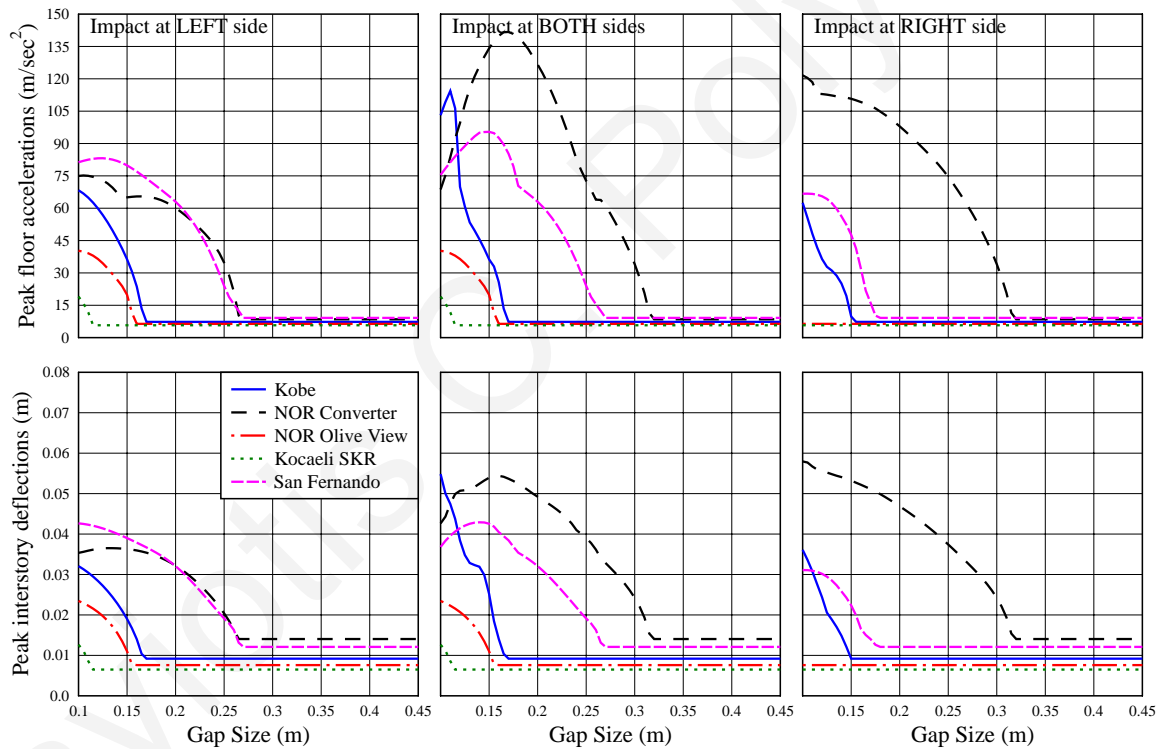


Figure 4.26 Maximum floor accelerations and interstory deflections considering the moat wall on the left, on both sides, or on the right side of the 4-story seismically isolated building.

4.5.4 *Effect of the impact parameters*

In order to examine the effect of the impact stiffness and the coefficient of restitution on the peak response of a seismically isolated building during poundings, another series of

parametric studies is performed. In this investigation the 4-story seismically isolated building is simulated under the Kobe Earthquake, assuming a seismic gap equal to 15 cm, which is 10 % smaller than the maximum induced displacement in order to cause poundings. The impact stiffness k_{imp} of the linear impact spring is varied in the range of 500 to 5000 kN/mm, while the coefficient of restitution is varied in the range of 0.1 to 1.0.

The variation of the amplification of peak floor accelerations and peak interstory deflections of the 4-story seismically isolated building in terms of the two impact parameters are presented in Figure 4.27. It is observed that the effect of impact parameters is localized, since the only response quantity that seems to be substantially affected by the variation of these two parameters is the peak floor acceleration at the seismic isolation level, where impacts occur. In particular, the peak floor acceleration at that level increase very rapidly in contrary to the peak floor accelerations of the upper floors, which are slightly affected by the impact stiffness after a certain value of k_{imp} . It is evident that the floors that are away from the impact level are more insensitive to the impact stiffness. Similar observations as regards the effects of the impact stiffness value on the response involving poundings have been made by other researchers ([31],[2],[54],[29],[76]).

Furthermore, the results show that, for values of the coefficient of restitution lower than 0.4, the peak floor acceleration at the isolation level increases and reaches its maximum value when the impact becomes highly overdamped. The rest of the response remains insensitive to the variation of the coefficient of restitution, i.e. the impact damping.

The amplification of both accelerations and interstory deflections due to poundings of the seismically isolated building with the moat wall seems to be slightly reduced for very low values of the impact stiffness. In particular, this occurs when the latter ranges below the value of ~ 1200 kN/mm ($=1.2$ GN/m), which corresponds to two times the superstructure's story stiffness. For higher values of the impact stiffness, the acceleration at the isolation level continues to increase, while the rest of the responses remain almost insensitive to this parameter. Anagnostopoulos [2], based on this observation, proposed the incorporation of a soft material between the pounding structures in order to mitigate the

detrimental effect of poundings. Such a possibility is examined in a following chapter of this work, as a potential impact mitigation measure.

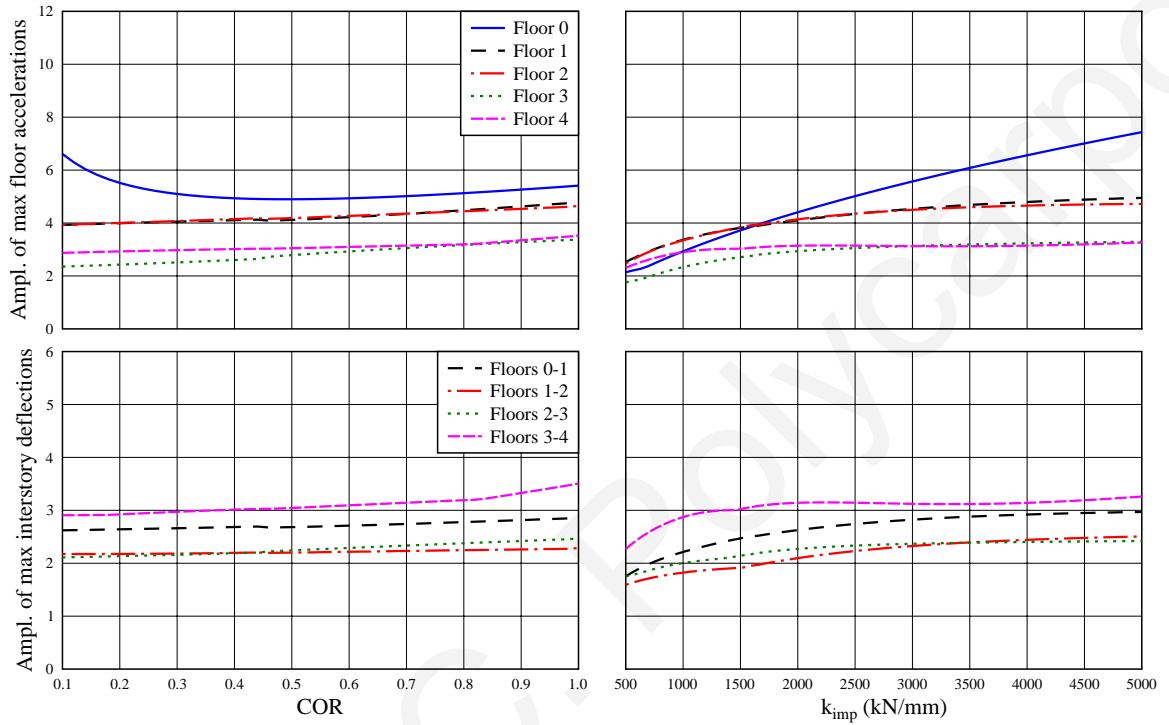


Figure 4.27 Influence of the coefficient of restitution (COR) and the impact stiffness (k_{imp}) on the peak floor accelerations and interstory deflections, under the Kobe Earthquake.

CHAPTER 5 ANALYSES CONSIDERING IMPACTS WITH ADJACENT BUILDINGS

5.1 Introduction

In this chapter, the case of a seismically isolated building pounding with adjacent fixed-supported buildings at upper floors is examined. Although very rare, this scenario may happen in cases of retrofitting an existing building, which is in relatively close distance to other fixed-supported buildings, by using seismic isolation. Moreover, the consideration of this scenario in simulations of the current study renders the latter more comprehensive regarding the investigation of poundings of seismically isolated buildings.

In the performed simulations, a 4-story seismically isolated building is considered to be adjacent to other conventionally fixed-supported buildings, with the possibility of poundings occurring not only at its base with the moat wall, but also at the upper floors of the buildings due to the deformation of their superstructures. The same structural characteristics that have been used in the previous chapter, which are provided in Table 4.2, are considered for the buildings under investigation. One or two fixed-supported multistory buildings are considered to be located next to a seismically isolated building in the same or in larger distance as the surrounding moat wall. Therefore, poundings may occur either with the moat wall at the base of the seismically isolated building or with the adjacent buildings at the levels of the upper floors of their superstructures. For simplicity, it is assumed that the slabs of the neighboring buildings are located at the same levels. Therefore, the impact forces act directly on the concentrated masses of the MDOF systems, as shown in Figure 3.7, without considering any local structural damage.

5.2 Practical example

The seismically isolated building is considered in six different configurations as regards the type and the characteristics of the adjacent structures. In the first case, the adjacent structure is only the surrounding moat wall, as simulated in the previous chapter, while in the remaining five cases two same multistory buildings, with two, three, four, five and six

stories in each case, respectively, are placed on both sides of the seismically isolated building. The separation distance, unless differently indicated, is considered to be the same on both sides of the building. The first two eigenmodes of the fixed-supported buildings are provided in Figure 5.1.

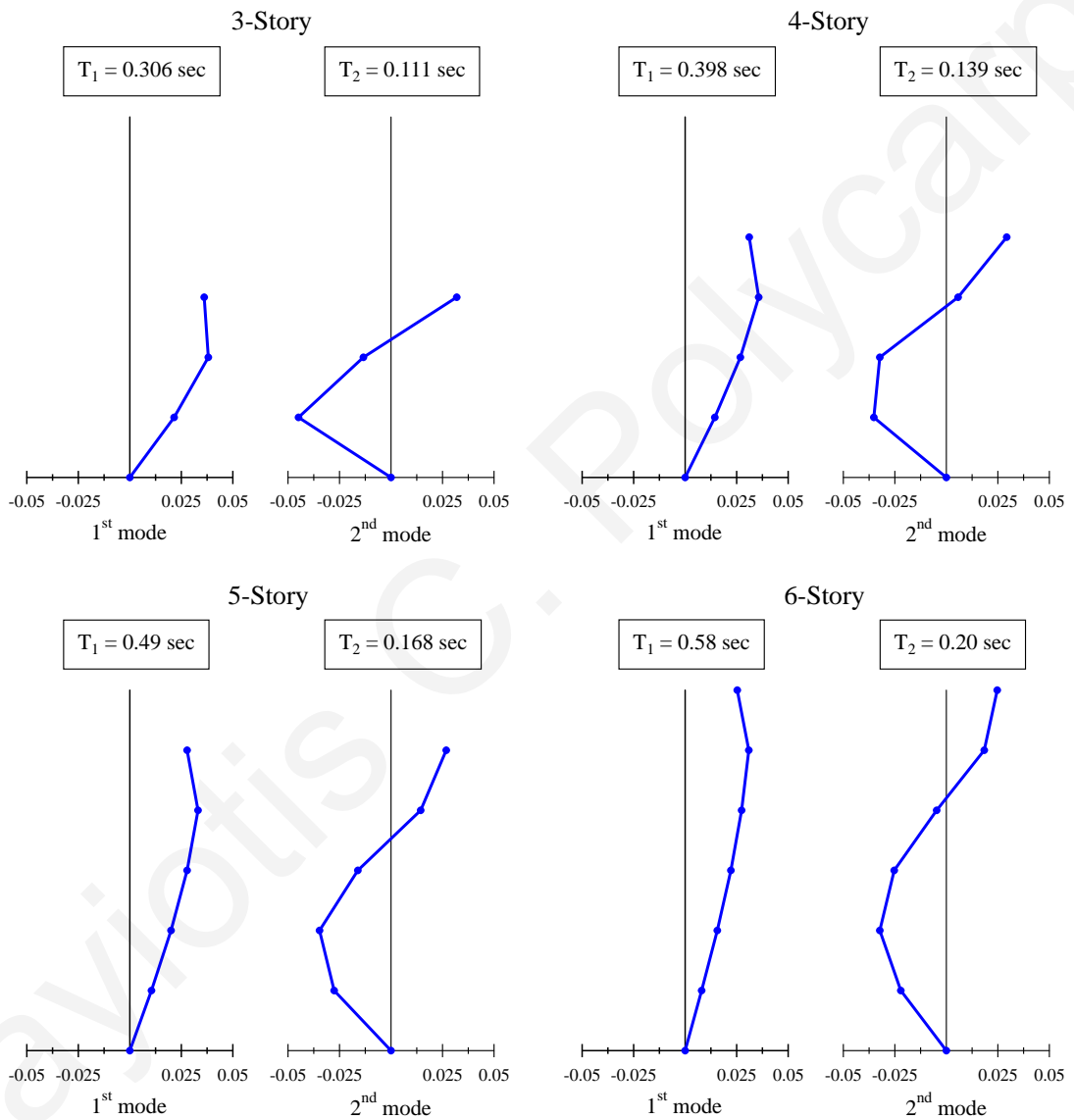


Figure 5.1 The first two eigenmodes and eigenperiods of the 3-, 4-, 5- and 6-story fixed supported buildings, which are assumed to be adjacent to the seismically isolated building.

The size of the seismic gap is considered to be different for each earthquake record. In particular for each seismic record, the width of the seismic gap is taken to be 10 % smaller

than the maximum relative displacement at the isolation level of the seismically isolated building under the specific excitation. The maximum induced relative displacements at the base and the top of the isolated building, as well as the displacements at the top of the fixed-supported buildings, for each seismic record, are provided in Table 5.1.

Table 5.1 Maximum relative displacements (cm) of the seismically isolated building (base and top) and the fixed-supported buildings, under five earthquake excitations.


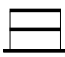

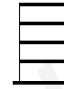

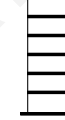
Earthquake excitation	(Base - Top)					
						
Kobe	16.74 - 18.85	1.49	5.57	11.40	16.88	15.22
Northridge Conv.	31.71 - 35.25	1.49	3.41	6.43	10.50	17.70
Northridge Olive	15.63 - 17.07	1.18	3.28	5.60	9.75	13.54
Sakarya	11.40 - 12.51	2.12	4.50	5.23	6.30	7.51
San Fernando	26.78 - 29.52	3.47	5.67	14.61	13.40	8.66

Figure 5.2 and Figure 5.3 present the amplification factors of the peak floor accelerations and interstory deflections, respectively, of the 4-story seismically isolated building during poundings with the adjacent structures. The amplification factor is defined as the ratio of the maximum response when poundings occur divided by the corresponding maximum response value without poundings, as also mentioned in the previous chapter. It is observed that the amplification of the peak floor accelerations is, in general, much higher than the amplification of the peak interstory deflections, since the former are much more sensitive to local impact. In addition, the maximum amplification of the acceleration response is usually located (i) at the isolation level (for the case of poundings occurring only with the moat wall), (ii) at the floor of the same level as the roof of the adjacent fixed-supported buildings or (iii) at the top floor of the seismically isolated building, when that is shorter than the neighboring fixed-supported buildings. It is also observed that in the cases of the 2-story and 3-story fixed-supported buildings, the interstory deflections of the 3rd and 4th story of the seismically isolated building are significantly amplified, due to a “whiplash” behavior [7] of the latter during poundings.

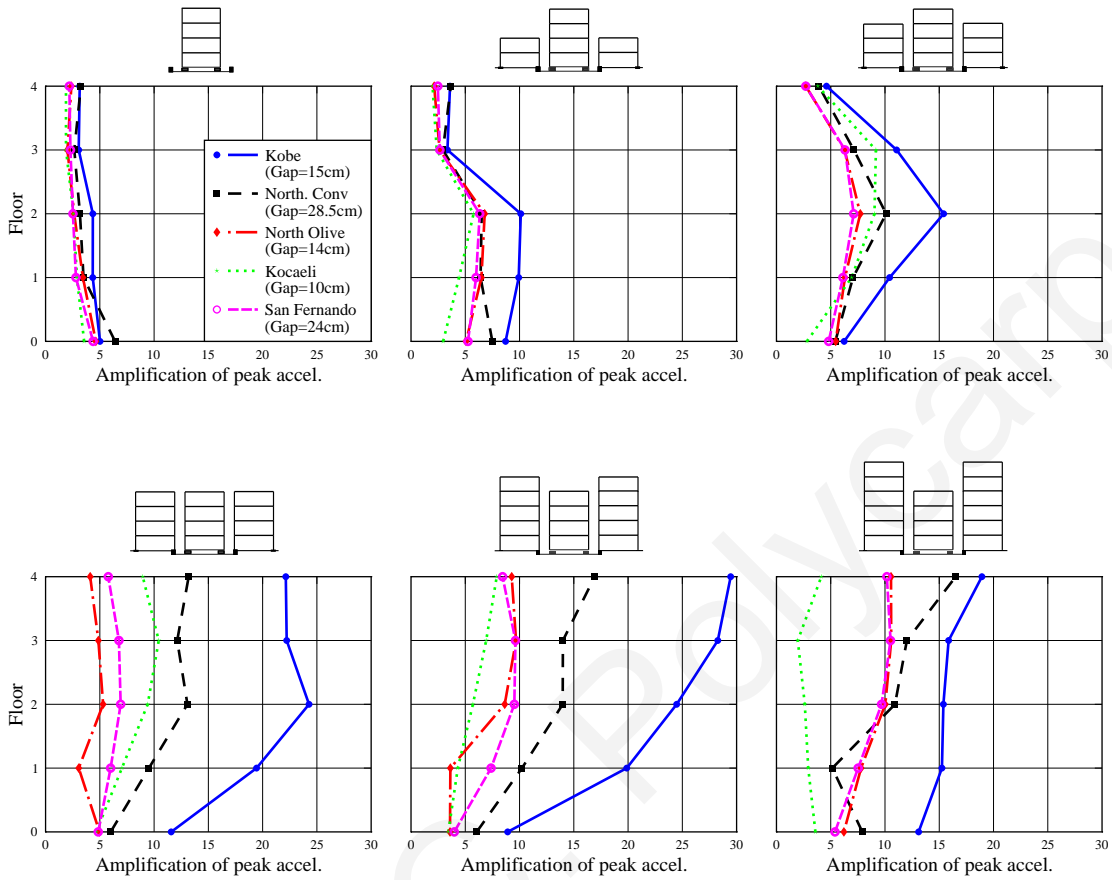


Figure 5.2 Amplification of the maximum floor accelerations of the seismically isolated building due to poundings with adjacent structures, when the available seismic gap size is 10 % smaller than the maximum induced relative displacement at the isolation level.

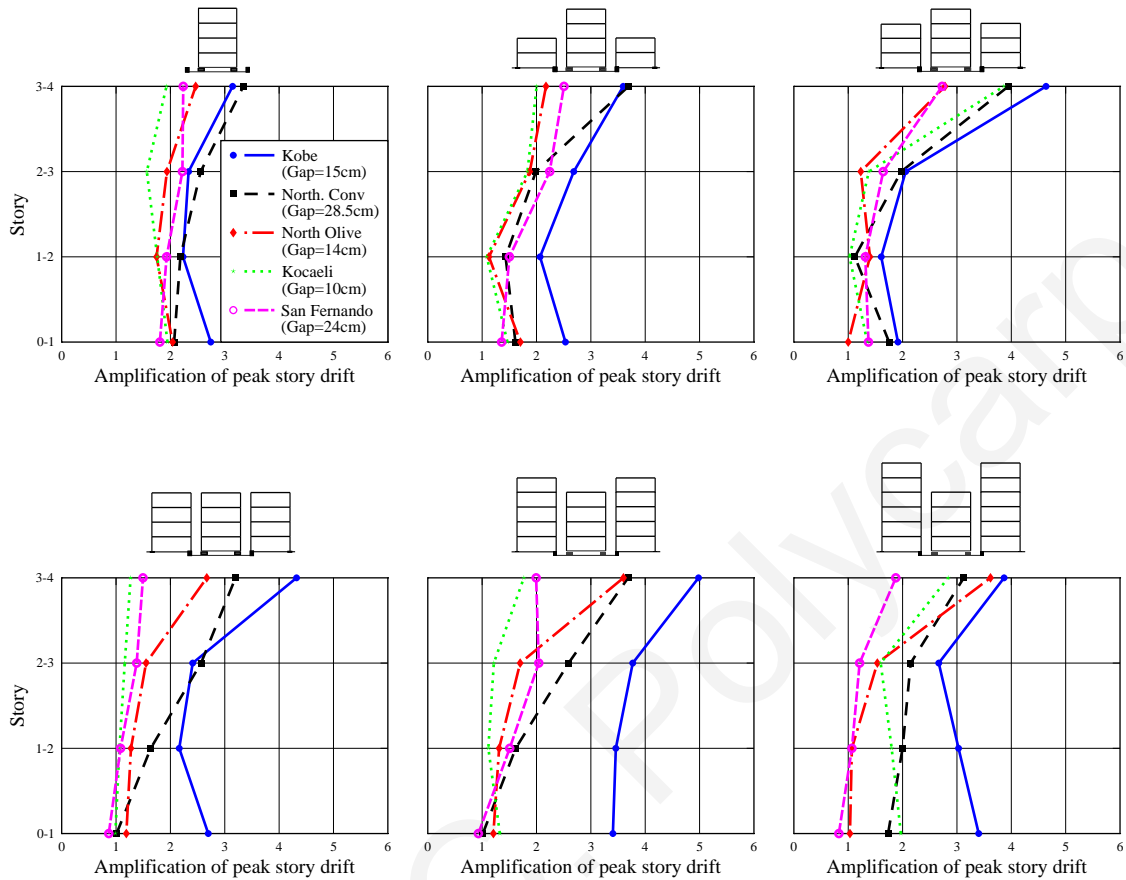


Figure 5.3 Amplification of the maximum interstory deflections of the seismically isolated building due to poundings with adjacent structures, when the available seismic gap size is 10 % smaller than the maximum induced relative displacement at the isolation level.

Moreover, the amplifications of the response of the seismically isolated building during poundings seem to depend on the earthquake characteristics in combination with the number of stories and, consequently, the flexibility of the adjacent buildings. The amplification of the response due to poundings, occurring only at the base of the building is more or less the same for all seismic excitations. However, in the case where the seismically isolated building is between other multistory buildings, which have different dynamic responses under each earthquake, the amplification curves for each seismic record have significant dispersions. The worst-case scenario for the seismically isolated building is when the adjacent fixed-supported buildings have fundamental eigenfrequencies in resonance with the dominant frequencies of the earthquake excitation.

5.3 Parametric analyses

A series of simulations is conducted in order to investigate how the presence and oscillations of fixed-supported buildings in proximity to a seismically isolated building affects the dynamic response of the latter during earthquakes with the possibility of poundings. In particular, considering the 4-story seismically isolated building, the effects of various factors on its response during poundings with its adjacent fixed-supported buildings are examined. Such factors are the seismic gap size, the earthquake characteristics, the number of stories of the adjacent fixed-supported buildings, the location of the adjacent structures and the impact parameters.

5.3.1 *Effect of the gap size and the ground excitation characteristics*

A set of parametric analyses is performed in order to examine how the width of the seismic gap affects the response of the seismically isolated building in the six different cases regarding the type of the adjacent structures. In particular, the width of the gap between the seismically isolated building and the adjacent structures is varied between 10 and 45 cm, with a step of 0.5 cm, simultaneously on both sides of the building. This means that 70 simulations are needed for only one configuration case and one earthquake excitation. Figure 5.4 presents the maximum responses of the seismically isolated building in terms of the size of the available clearance for the six configuration cases and for the five earthquake excitations. Plots in Figure 5.5 display the maximum responses at each floor, only for the case of having two 4-story buildings adjacent to the seismically isolated building, compared to the case of the seismically isolated building surrounded only by the moat wall, for the Kobe and the San Fernando earthquakes.

It is observed that the response in general decreases with the increase of the available clearance around the seismically isolated building. However, the variations of some curves indicate that this is not always true, especially for relatively narrow seismic gap sizes in combination with the earthquake characteristics. Specifically, very small widths of the seismic gap, in combination with a strong ground excitation, don't allow the structure to develop high impact velocities as in the case of wider seismic gaps, leading to relatively milder consequences from potential pounding.

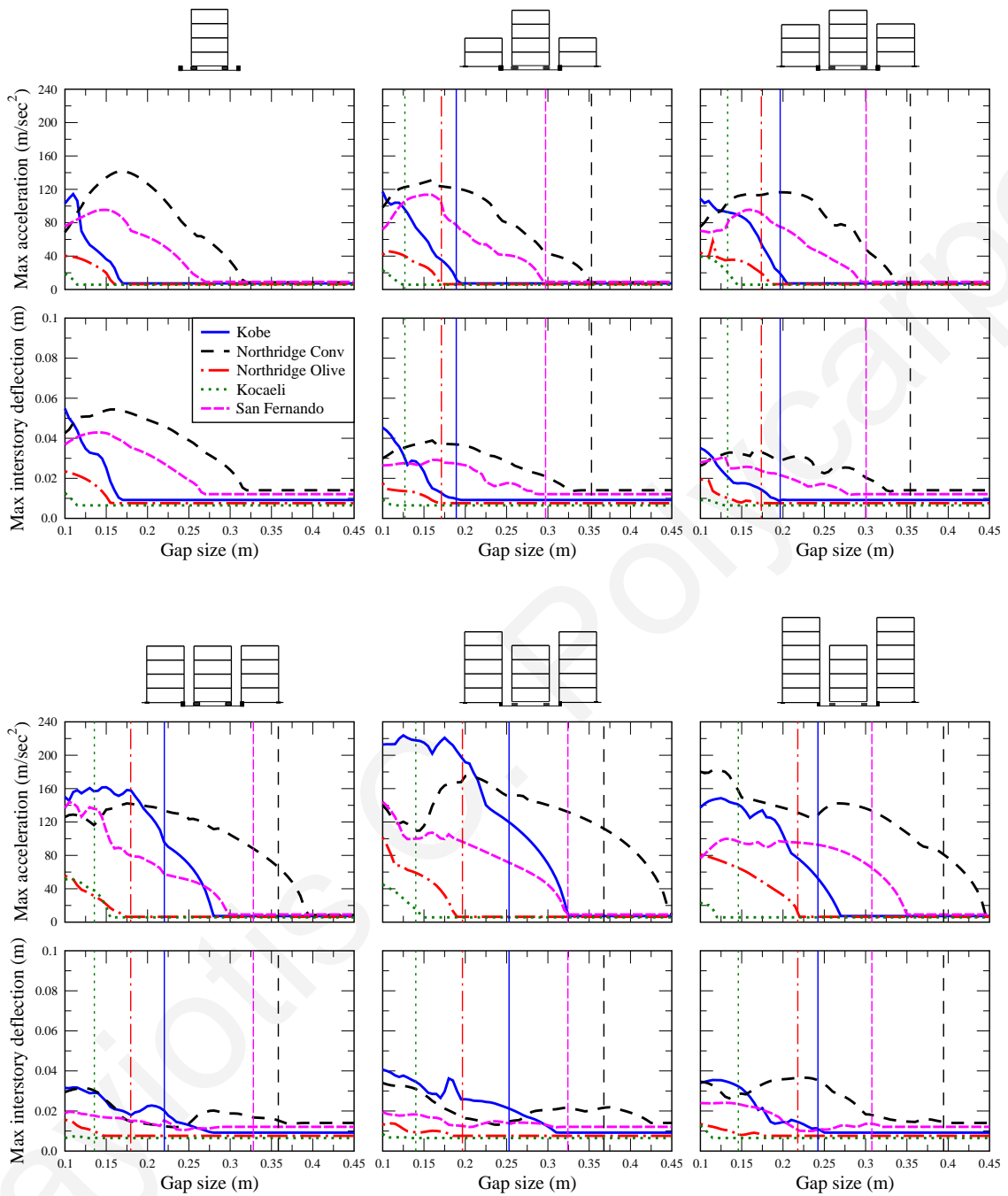


Figure 5.4 Peak responses of the seismically isolated building in terms of the width of the seismic gap. The vertical lines indicate the SRSS of the peak displacements of the neighboring buildings for each earthquake excitation, plotted with the corresponding color and line-type.

Considering the type of the adjacent structure, the results indicate that the presence of fixed-supported buildings in close distance to a seismically isolated building affects

significantly the response of the latter during poundings. In general, the plots indicate that the amplification of the peak floor accelerations due to impact is, in general, increasing with the number of stories of the adjacent building. An important observation is that, in such a case, poundings may occur for much wider widths of the seismic gap compared to the case of impacts occurring only at the base with the moat wall. This is justified by the fact that the adjacent multistory buildings have some horizontal flexibility in contrast to the surrounding moat wall, which remains un-deformed relatively to the ground during the excitation. Therefore, the seismically isolated building may pound against the neighboring buildings at the upper stories, due to the deformation of the superstructures of the buildings in series, before hitting the surrounding moat wall.

The earthquake characteristics and particular the range of predominant periods, in combination with the fundamental periods of the adjacent structures seem to play a significant role to the severity of the structural impact. In particular, the detrimental effects of poundings are more pronounced when the fundamental period of the adjacent fixed-supported buildings fall within the predominant periods of the seismic ground motion. A representative example is the case of having the 5-story fixed supported buildings adjacent to the seismically isolated building, under the Kobe Earthquake record.

Some modern anti-seismic codes suggest the use of the SRSS (Square Root of the Sum of Squares) approach for the determination of the minimum required seismic gap between two adjacent buildings in order to avoid structural poundings during strong earthquakes ([27], [28], [34]). Relevant research on the investigation of poundings of fixed-supported buildings showed that the SRSS of the maximum displacements of two adjacent buildings can be sufficient [2], while in fewer times it may be insufficient, but with minor impact effects ([7], [55]). In almost half of the cases that have been analyzed in the current study, a seismic gap, equal to the SRSS of the design peak relative displacements of the adjacent structures, is insufficient under the specific earthquake excitations. Table 5.2 displays the difference $\Delta d = d_{SRSS} - d_{Req}$ for each one of the cases of the configurations of the adjacent buildings and for all five seismic records, where $d_{SRSS} = \sqrt{(\max d_{iso})^2 + (\max d_{fixed})^2}$ and d_{Req} is the minimum required seismic gap in order to avoid poundings according to the

simulations. Therefore, the negative sign of the difference Δd denotes that a seismic gap width equal to d_{SRSS} is insufficient. The computed d_{SRSS} is also plotted in the graphs of Figure 5.4 with vertical lines.

Table 5.2 The difference $\Delta d = d_{SRSS} - d_{Req}$ (cm), where the negative sign denotes insufficiency.






Earthquake excitation					
Kobe	-0.09	-0.34	-5.47	-6.70	-1.77
Northridge Conv.	0.78	1.91	-3.17	-7.72	-5.06
Northridge Olive	0.61	-0.62	2.46	1.66	0.29
Sakarya	0.69	-0.70	-1.44	0.01	3.59
San Fernando	0.72	1.06	3.31	0.42	-3.74

Figure 5.5 suggests that, while for the case without adjacent buildings the highest value of the peak floor acceleration during poundings corresponds to the isolation level, for the cases with adjacent buildings, the highest value corresponds mainly to the top floor. This is due to the location of impacts, since the floor acceleration response is highly affected by local impacts and the corresponding impact velocity, which is obviously higher at the top floors of the building.

Furthermore, the peak interstory deflections during poundings for the case of buildings in series are most of the times smaller than those when impacts occur only with the moat wall, especially for relatively narrow seismic gaps. This indicates that in these cases, the adjacent buildings act as constrainers, preventing the large horizontal displacements that may take place when the seismically isolated building hits only against the moat wall at the isolation level.

It can be seen from Figure 5.5 that in the case of poundings occurring only at the isolation level, the peak interstory deflection decreases, in most of the times, when moving along the height of the building, from the ground-floor to the top story, while for the case of three buildings in series, this does not happen. This observation indicates that the

excitation of higher modes of deformation is much more pronounced for the case of having poundings of buildings in series.

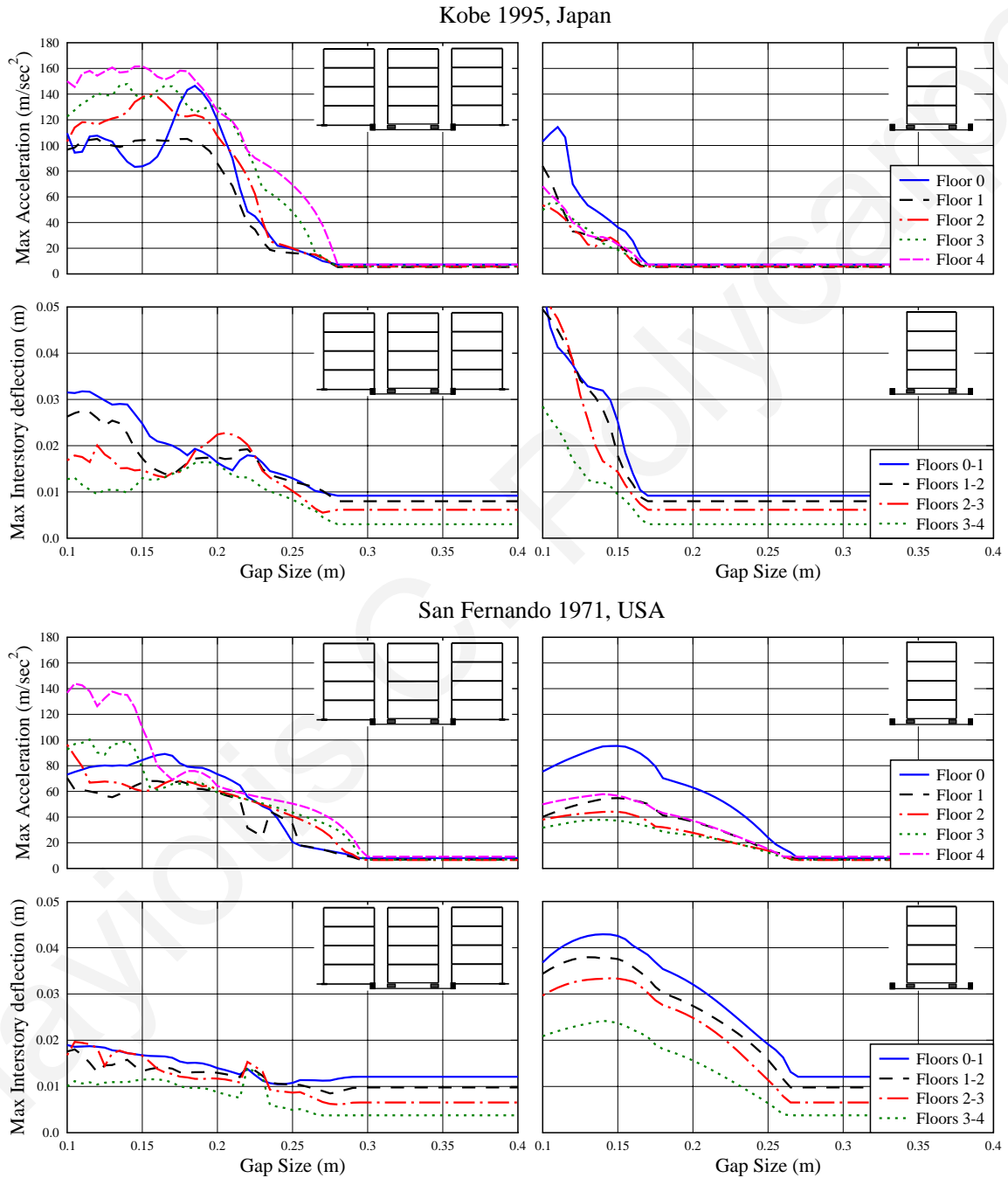


Figure 5.5 Peak responses at each floor of the seismically isolated building in terms of the width of the seismic gap for the Kobe and the San Fernando earthquakes.

5.3.2 *Effect of the location of the adjacent structure*

In order to identify the role of the side where the adjacent fixed-supported building is located relative to the seismically isolated building, a further set of simulations is conducted. In Figure 5.6, the responses of the 4-story seismically isolated building, during the Kobe Earthquake, are compared under three different configurations regarding the location of the adjacent 4-story, fixed-supported buildings. As anticipated, the location of the adjacent building, in combination with the excitation characteristics affect the response of the seismically isolated building during impact. For example, when the adjacent building is on the left side of the seismically isolated building, poundings occur for a seismic gap that is up to approximately 28 cm, while when it is on the right side, impacts do not occur for seismic gap widths larger than about 22 cm.

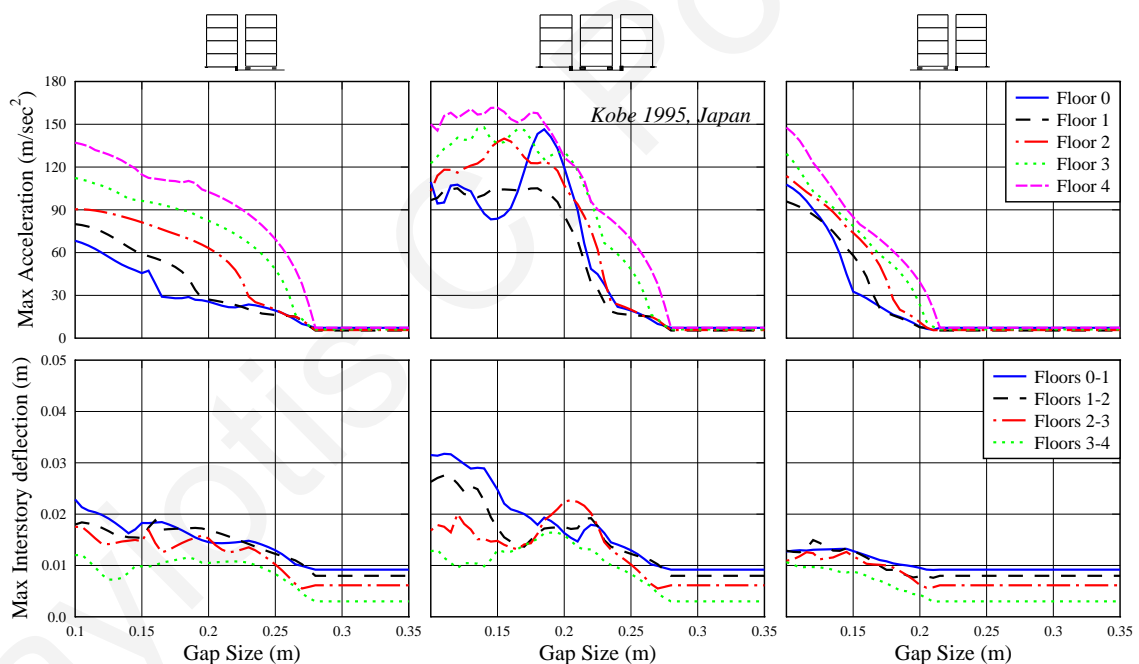


Figure 5.6 Peak responses of the seismically isolated building under the Kobe Earthquake during poundings with the adjacent 4-story building that is considered either on the left, on the right or on both sides of the seismically isolated building.

The plots of Figure 5.7 to Figure 5.11 present the envelopes of the peak floor accelerations and peak interstory deflections, for all six configurations of the seismically

isolated building and for the five earthquakes. With the continuous blue line are plotted the envelopes of the maximum responses considering one-sided impacts (with the adjacent structure either on the left or on the right) of the seismically isolated building and with the dashed line are plotted the corresponding maximum responses considering poundings on both sides of the seismically isolated building. It is observed that the response in the case of having the fixed-supported buildings on both sides of the seismically isolated building, in most of the cases, differentiates only for relatively narrow gap sizes. Specifically, for a seismic gap width larger than a certain value, the presence of two fixed-supported buildings on both sides of the seismically isolated building makes no difference to the response during poundings. Furthermore, this seems to depend also on the earthquake excitation's characteristics. For example, in the cases of relatively weak seismic excitations, such as the Northridge Olive View record and the Kocaeli Earthquake record, the differences between the two curves are negligible.

The differentiation of the two curves in the range of very narrow gap sizes is due to the fact that in those cases the buildings experience larger number of impact incidences, repeatedly, especially when the adjacent structures are on both sides. In such cases the excitation of higher modes of deformation of the seismically isolated building are more pronounced. For wider seismic gaps, a single impact on one side of the seismically isolated building may determine the maximum response and therefore, in such case, the two curves overlap.

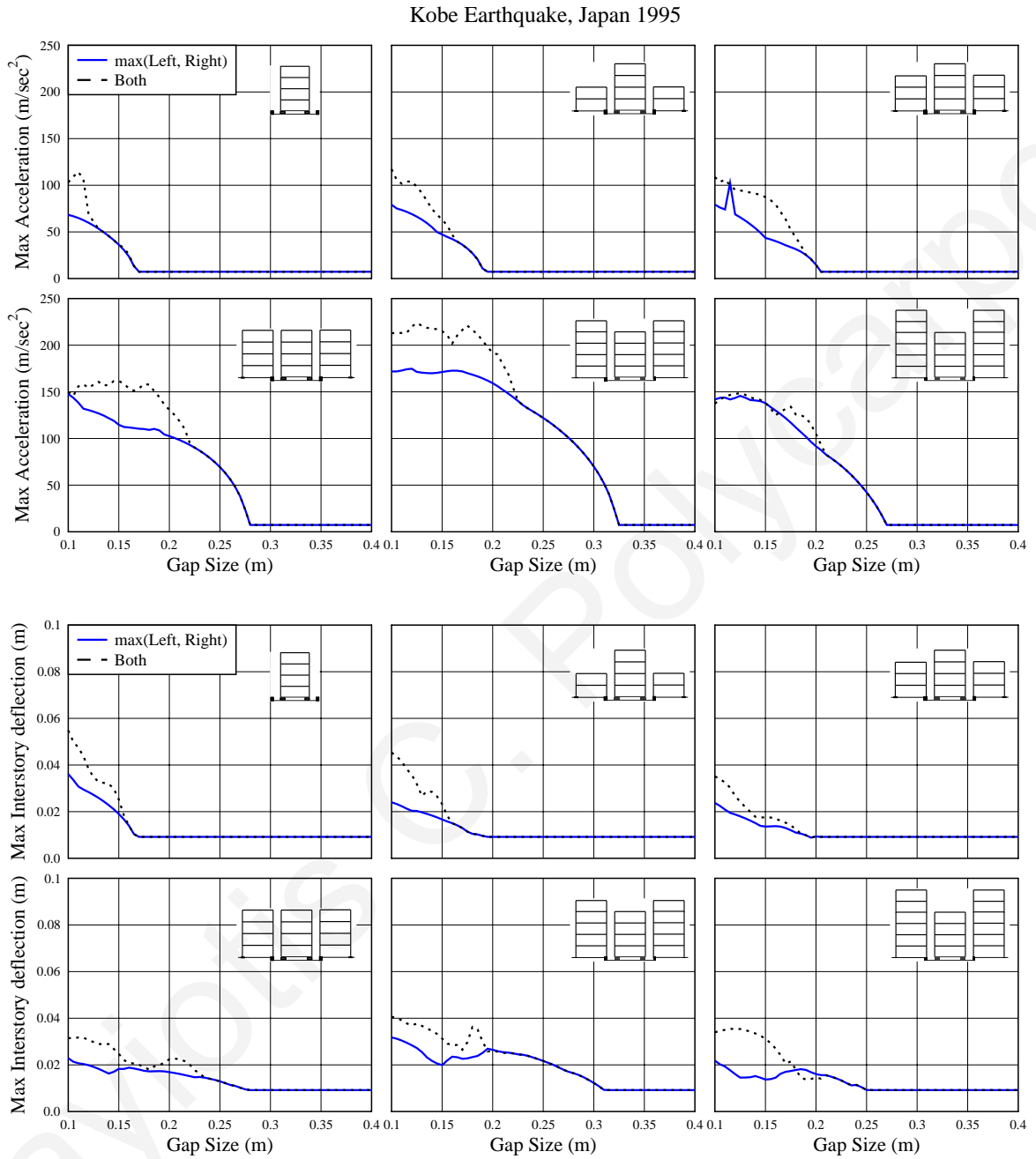


Figure 5.7 Envelopes of the peak absolute floor accelerations and interstory deflections of the seismically isolated building, for the two cases of having the adjacent structure on the one side or on its both sides, considering the Kobe Earthquake.

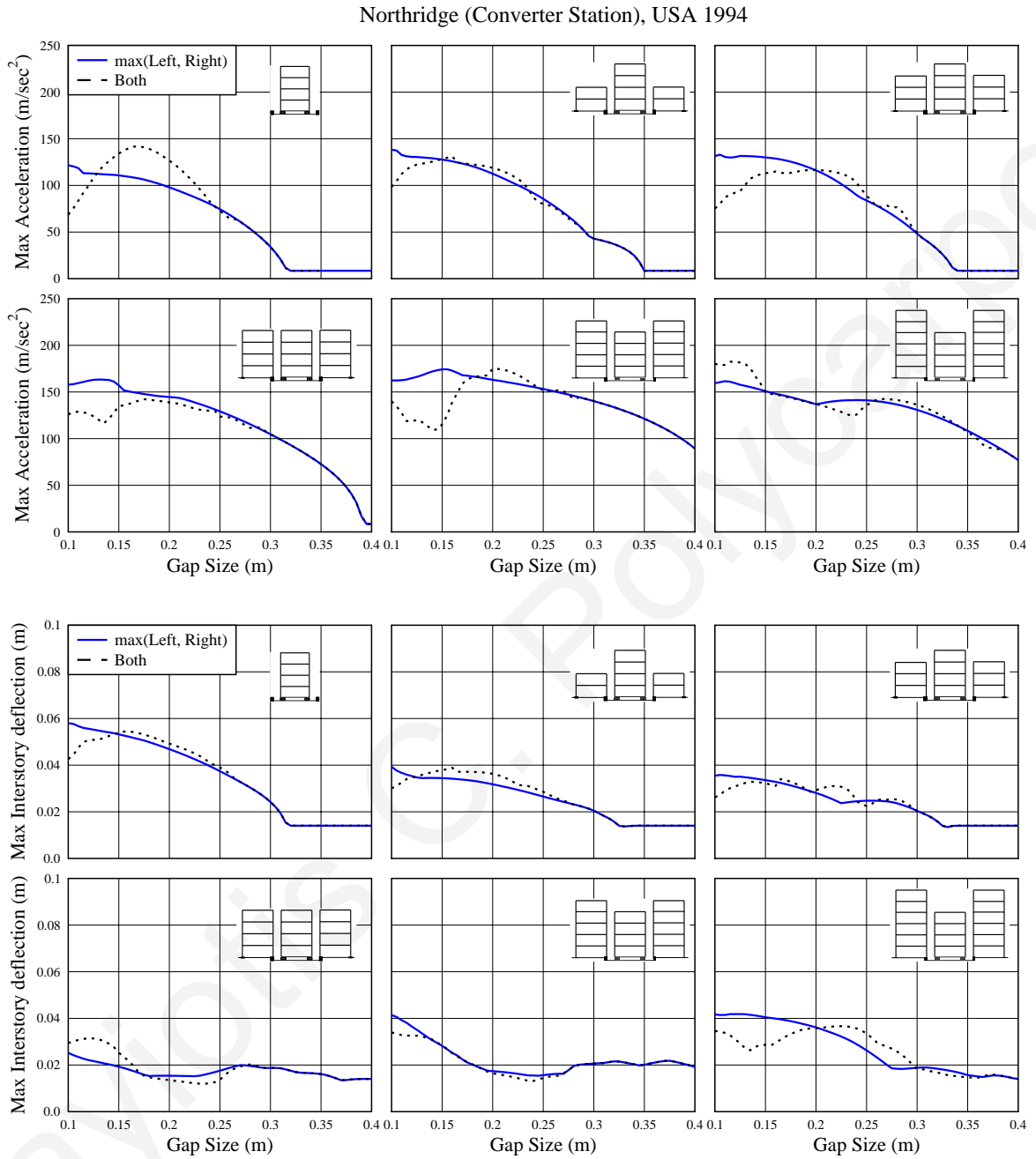


Figure 5.8 Envelopes of the peak absolute floor accelerations and interstory deflections of the seismically isolated building, for the two cases of having the adjacent structure on the one side or on its both sides, considering the Northridge Converter Station record.

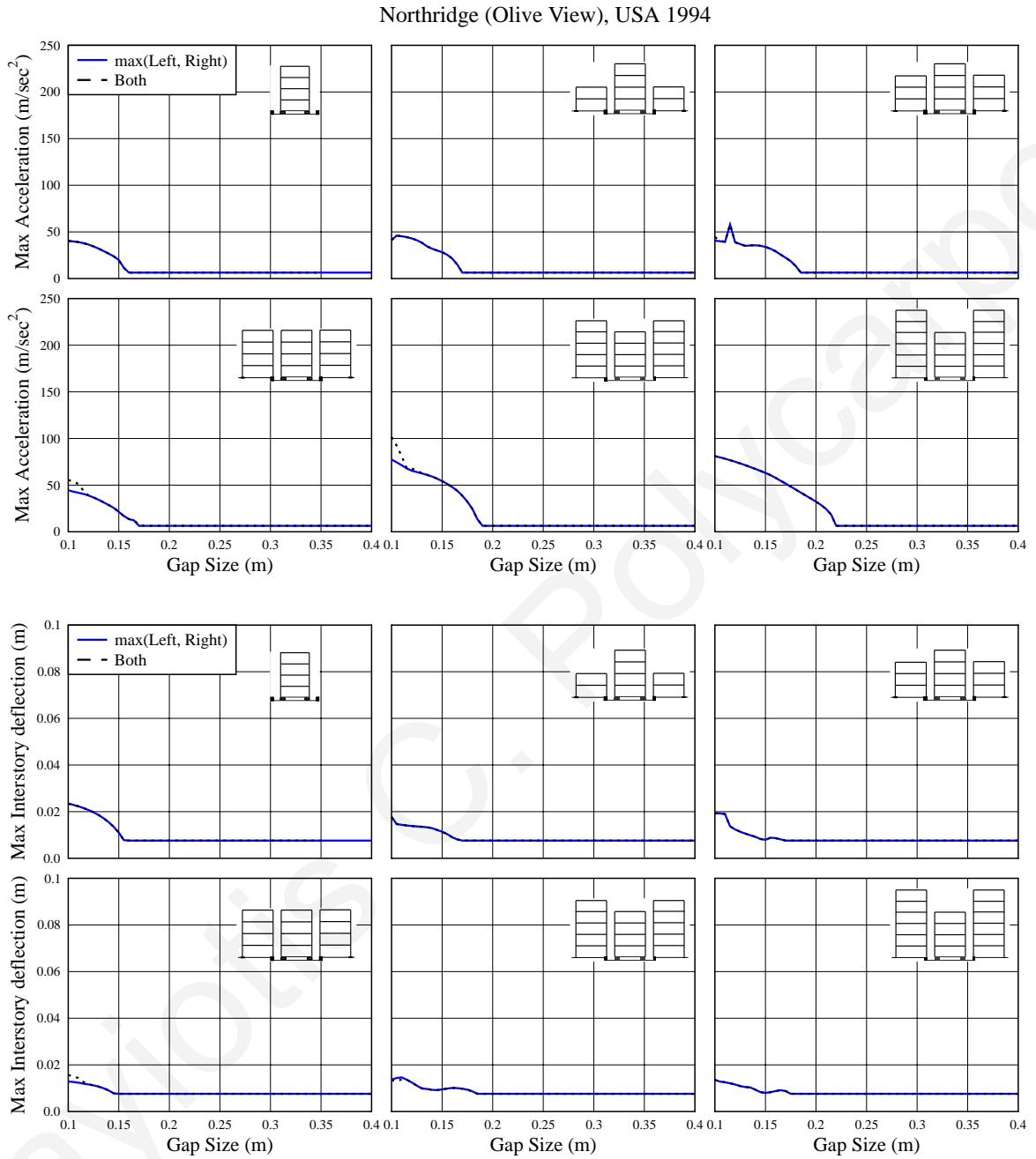


Figure 5.9 Envelopes of the peak absolute floor accelerations and interstory deflections of the seismically isolated building, for the two cases of having the adjacent structure on the one side or on its both sides, considering the Northridge Olive View Station record.

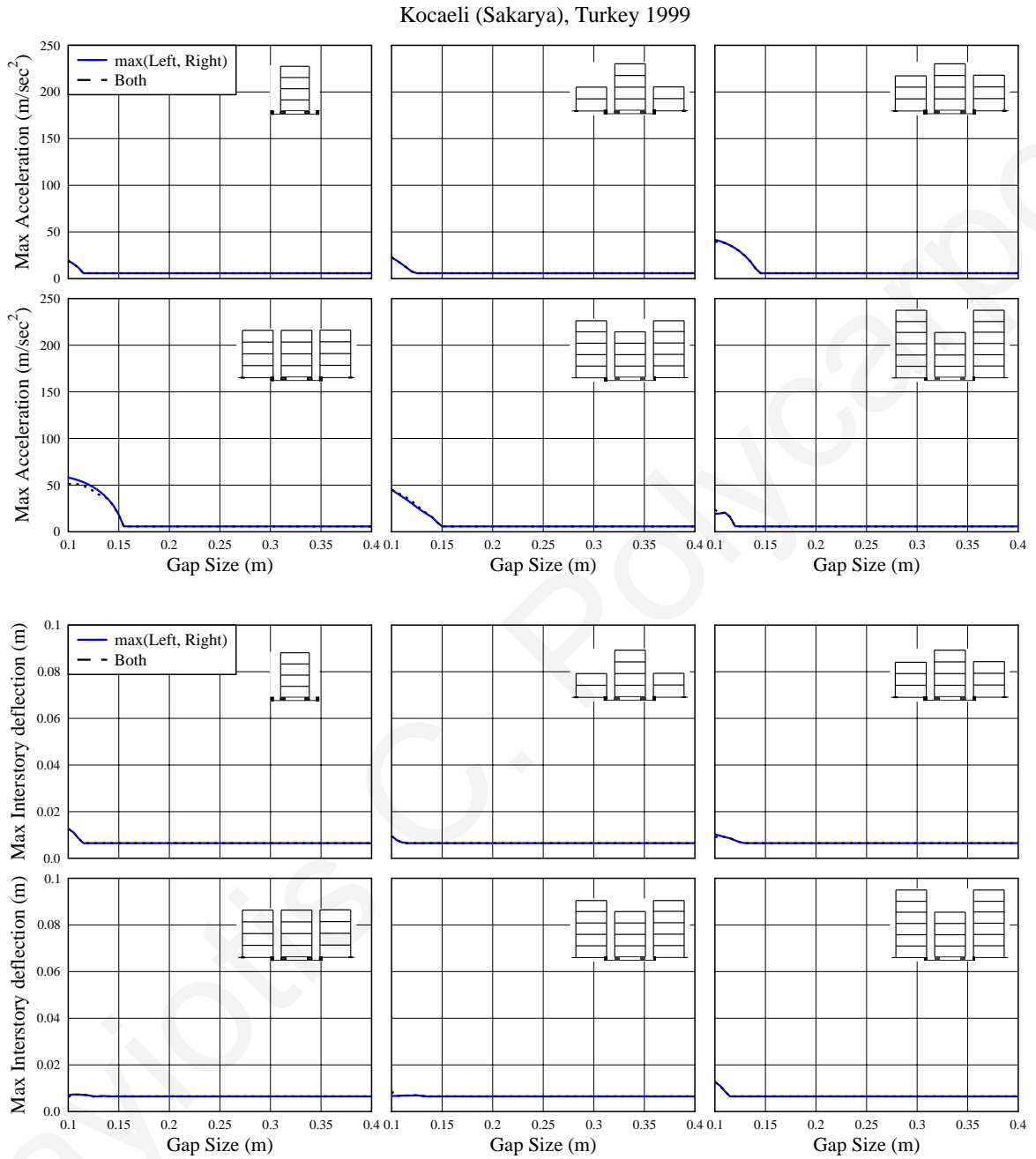


Figure 5.10 Envelopes of the peak absolute floor accelerations and interstory deflections of the seismically isolated building, for the two cases of having the adjacent structure on the one side or on its both sides, considering the Kocaeli Earthquake record.

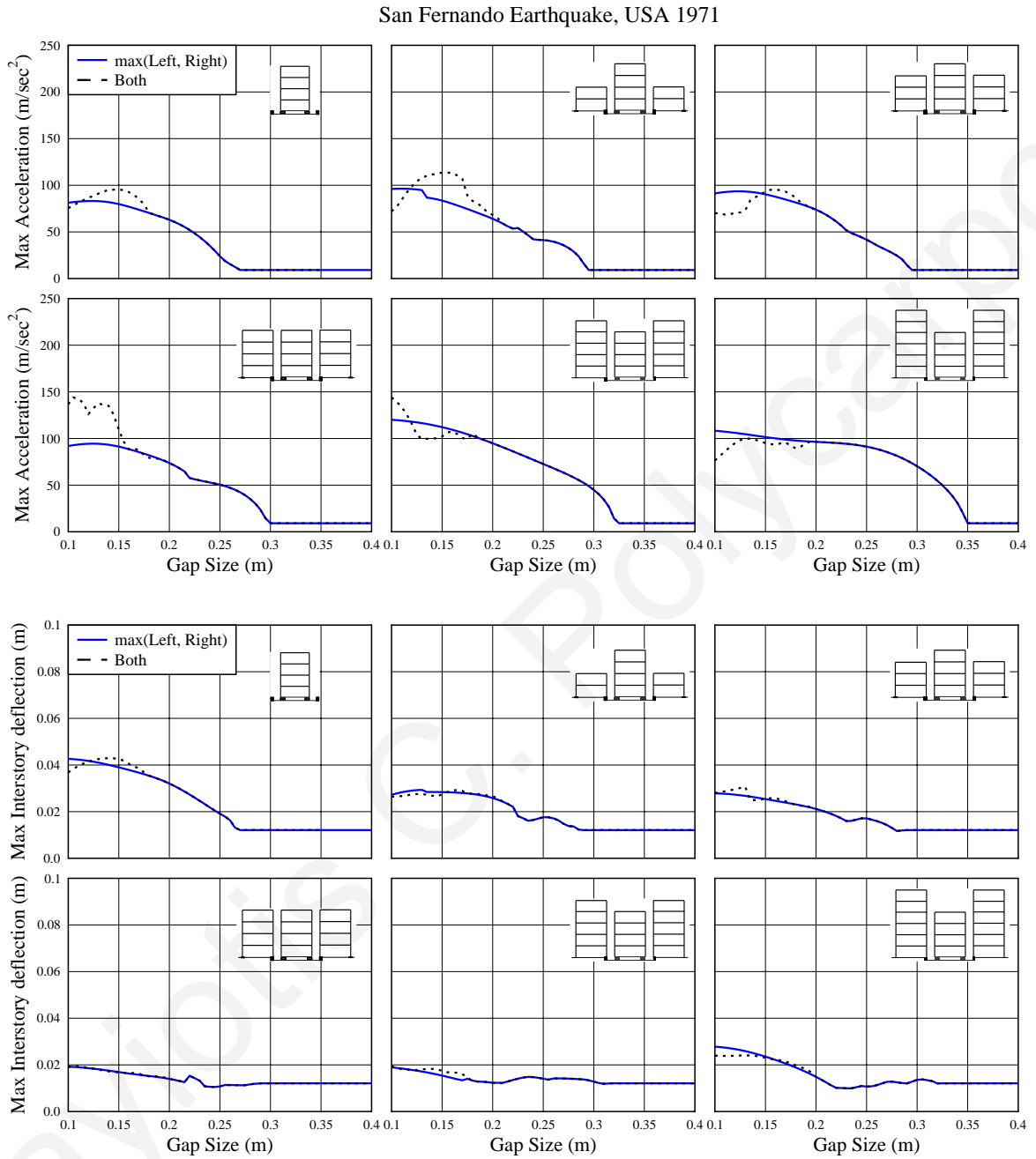


Figure 5.11 Envelopes of the peak absolute floor accelerations and interstory deflections of the seismically isolated building, for the two cases of having the adjacent structure on the one side or on its both sides, considering the San Fernando Earthquake record.

Moreover, the case of having a separation distance between the adjacent superstructures larger than the available seismic gap size at the base of the seismically isolated building is examined. Figure 5.12 describes the considered configuration of the seismically isolated building regarding the location of the adjacent structures. In particular, in the simulations the separation distance d is between the fixed-supported buildings and the superstructure of the seismically isolated building is assumed to be either 5 or 10 cm larger than the gap size. The configuration is considered to be symmetric. The 4-story seismically isolated building and its adjacent 4-story fixed-supported buildings are simulated under three seismic records, with the seismic gap size at the base varied from 10 to 45 cm.

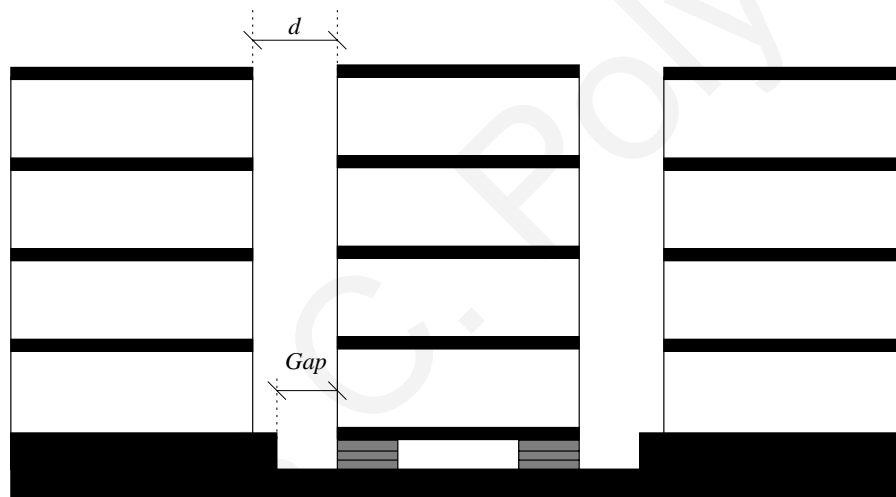


Figure 5.12 The case of a separation distance between the adjacent buildings larger than the gap size.

The plots in Figure 5.13 present the envelopes of the peak responses of the seismically isolated building under each seismic excitation, considering the adjacent 4-story fixed-supported buildings either at a distance of 5 cm or 10 cm larger than the base gap size. The case of the adjacent buildings being aligned with the moat wall ($d = gap$) and the case of poundings of the seismically isolated building only with the moat wall ($d = \infty$) are also presented in these plots.

It is observed that for three of the five earthquakes, the curves representing the case of having a larger separation distance between the buildings than the seismic gap width at the

base coincide with the corresponding curves for poundings only at the base. This indicates that, in those cases, no poundings occur between the adjacent fixed-supported buildings and the superstructure of the seismically isolated building.

Only during the Kobe and the Northridge Converter Station records the upper stories of the seismically isolated building hit against the adjacent buildings. The results for those two cases indicate that, as the distance between the buildings increases, the seismic gap that is needed at the base of the seismically isolated building, in order to avoid poundings, is reduced. The peak floor accelerations are, in general, reduced compared to the case of a building separation distance equal to the seismic gap. However, there are some values of narrow seismic gap where the opposite happens. In addition, it is observed that, while the peak floor accelerations are reduced with the increment of the separation distance between the adjacent structures and the moat wall, the peak interstory deflections are amplified. As mentioned previously, this is the characteristic difference between the case of poundings only with the moat wall at the isolation level and the case of poundings with adjacent buildings.

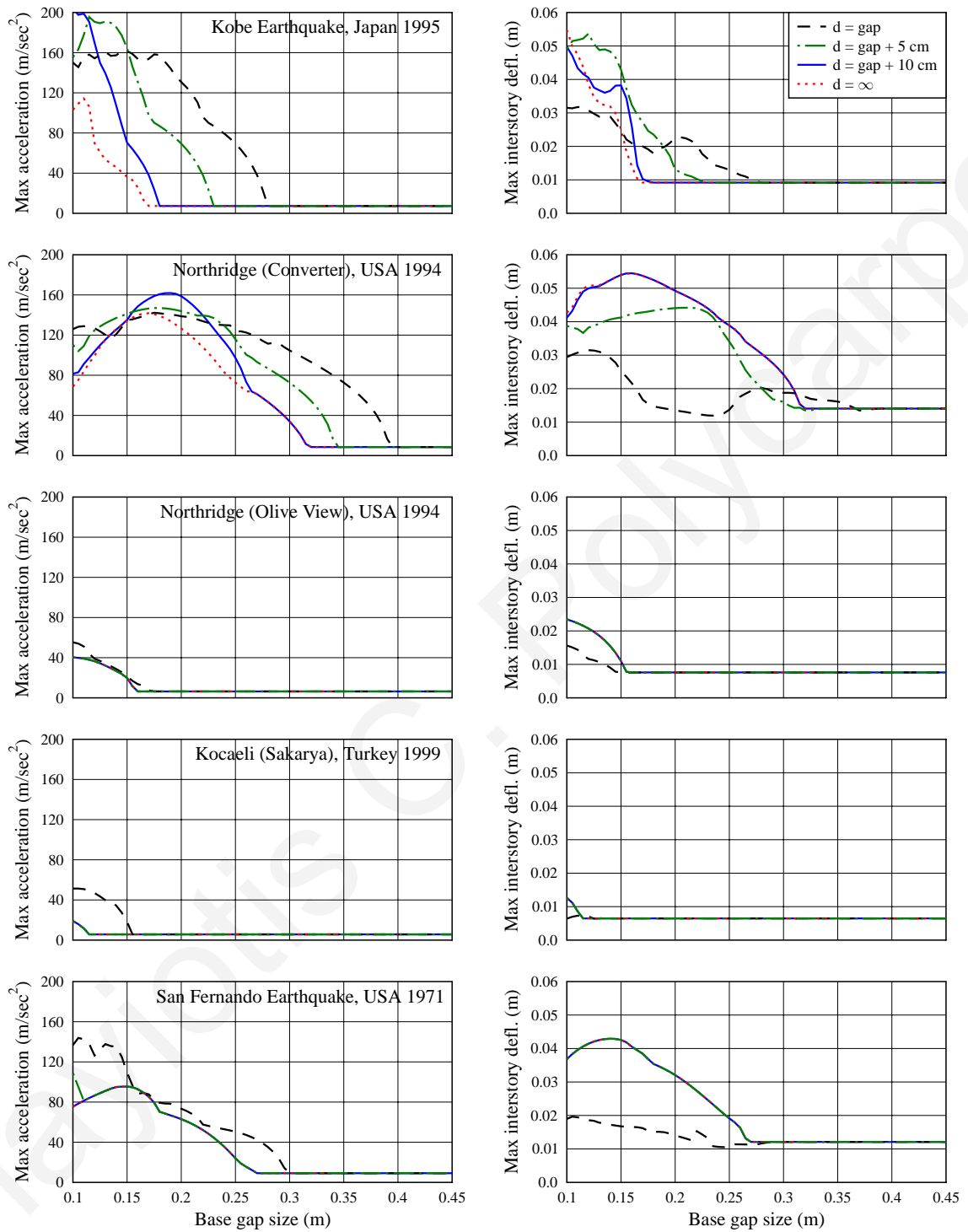


Figure 5.13 Envelopes of the peak responses of the seismically isolated building, considering the distance between the adjacent superstructures equal or larger from the corresponding seismic gap width at the base.

5.3.3 Influence of the impact parameters

Another series of parametric analyses has been performed, in order to examine the influence of selecting different values for the impact parameters, when using the corresponding linear viscoelastic impact model and considering poundings at the upper floors of the seismically isolated building. Considering the case where the 4-story seismically isolated building is placed between two same 4-story fixed-supported buildings, the impact stiffness and the coefficient of restitution vary in the ranges of 500–5000 kN/mm and 0.1–1.0, respectively. Two cases of seismic gap size are examined and the Kobe Earthquake record is selected as the imposed seismic excitation. In the first case (Figure 5.14), the width of the seismic gap equals 25 cm and poundings occur only at the two top floor levels of the seismically isolated building, while in the second case, where the separation distance equals to 15 cm (Figure 5.15), poundings occur at all floor levels.

Plots in Figure 5.14 indicate that the influence of the value of the impact parameters on the interstory deflections is negligible, while a small variation is observed for the acceleration response at the two floors, where impacts occur. Specifically, for values of the coefficient of restitution lower than 0.5, the acceleration increases and reaches its maximum value when the impact becomes highly overdamped. For values greater than 0.5, the acceleration response is almost insensitive to the variation of the *COR*.

On the other hand, an increase of the impact stiffness amplifies the peak floor acceleration at the impacting floor, while at the rest of the floor levels the acceleration remains almost constant with the variation of the k_{imp} . An interesting observation is that the peak floor accelerations at the top floor are more sensitive to the variation of the impact stiffness than that at the third floor, indicating that the rate, with which the accelerations increase, depends on the impact velocity. This is also shown in Figure 5.15, where the rate of the increase of the peak floor accelerations is higher, since the width of the seismic gap is smaller and it causes more severe impacts. In addition, in the case of relatively narrow seismic gaps, the interstory deflections are not as insensitive to the variation of the impact parameters as in the first case. Conclusively, the influence of the values of the impact parameters on the overall response during poundings is higher in cases of high impact velocities. The values of the coefficient of restitution and the impact stiffness that have

been used in the simulations are shown with dotted lines in both figures, indicating the relatively limited influence of their selected values.

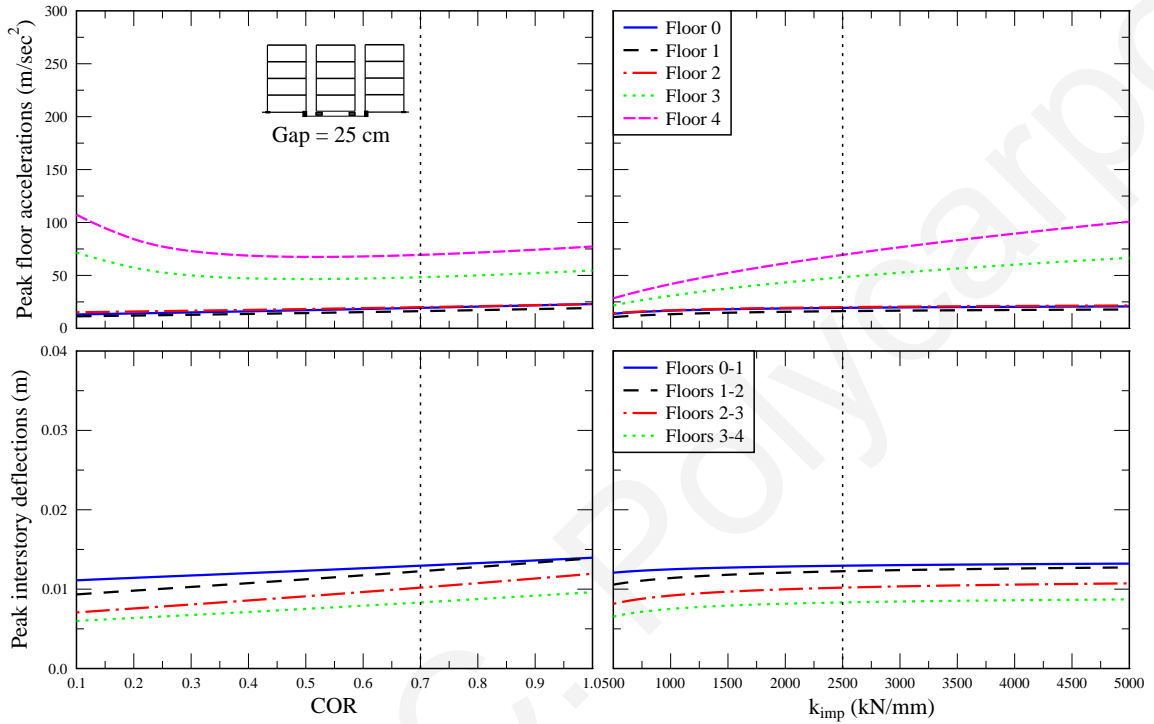


Figure 5.14 Variation of the response of the seismically isolated building during poundings with adjacent fixed-supported structures, in terms of the *COR* and the impact stiffness for a 25 cm gap width.

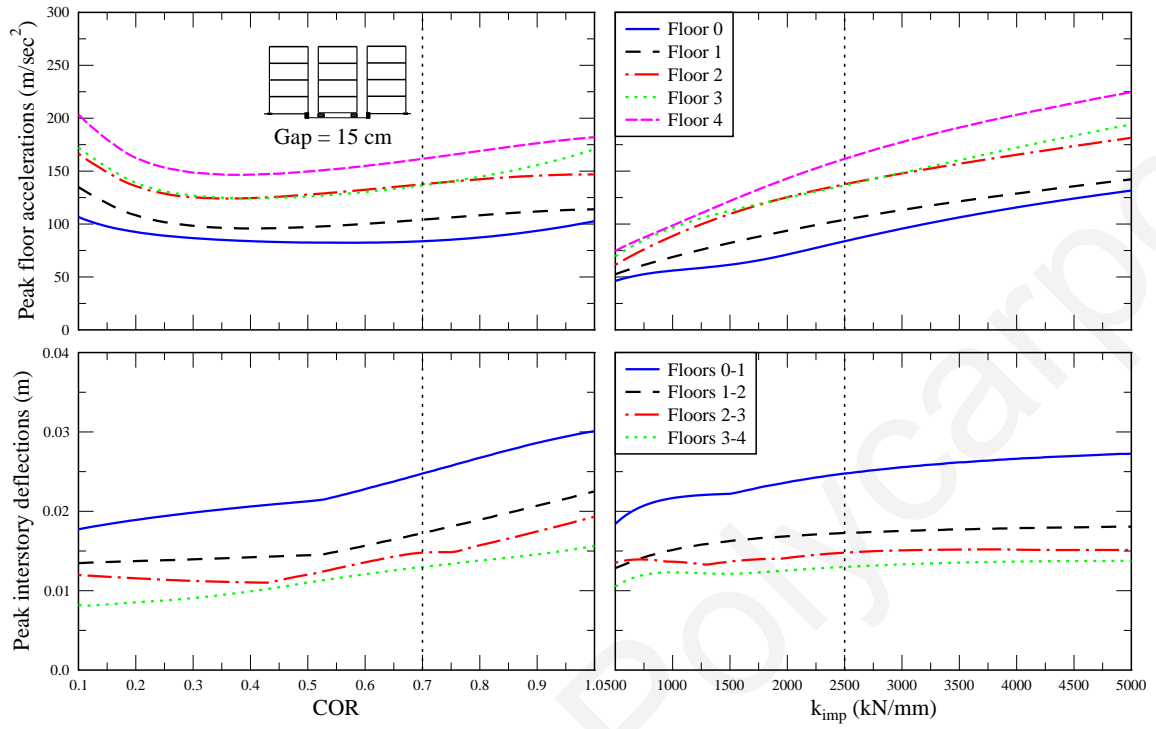


Figure 5.15 Variation of the response of the seismically isolated building during poundings with adjacent fixed-supported structures, in terms of the *COR* and the impact stiffness for a 15 cm gap width.

CHAPTER 6 MITIGATION MEASURES

6.1 Introduction

The results from numerical simulations and parametric studies presented in previous chapters demonstrate the detrimental effects of potential poundings on the effectiveness of seismic isolation. In particular, both floor accelerations and interstory deflections of the seismically isolated building increase due to impact incidences, either with the surrounding moat wall or with an adjacent building. At the pounding floors, short-period impulses of high amplitude are observed in the acceleration response and their amplitude is highly affected by the impact stiffness. The presence of high spikes in acceleration response due to poundings is a very critical issue, especially for buildings that may accommodate sensitive equipment. Certain mitigation techniques can be applied in order to avoid poundings or reduce their detrimental effects on structural response. However, the great majority of these measures refer to the case of pounding among adjacent fixed-supported buildings or among bridge decks [78].

6.2 Overview of potential impact mitigation measures

Undoubtedly, the best mitigation measure for earthquake-induced poundings of buildings, in general, is to provide a sufficiently wide seismic gap between the structures in order to avoid any impact incidences. Due to practical constraints, the size of the separation distances between buildings in series cannot be unlimited, especially in metropolitan areas, where neighboring buildings are often constructed with very small or without any gap. Therefore, several methods have been proposed by researchers for the estimation of the optimum separation distance between fixed-supported buildings for the avoidance of structural poundings. A common practice, which has been adopted by Eurocode 8 [28] and applies to buildings, or structurally independent units, belonging to the same property, is to provide a seismic gap width at least equal to the Square Root of the Sum of the Squares (SRSS) of the maximum horizontal displacements of the individual buildings, assuming that the latter do not occur at the same time during the excitation. Furthermore, the Uniform Building Code (UBC) [34], taking into account that the structural characteristics

of one of the two buildings is most of the times unknown, requires a minimum separation distance equal to $0.375 \times R_w$ times the maximum horizontal displacement of the building under consideration, where R_w is the behavior factor. Pantelides and Ma [64] argued that the UBC requirements for the seismic separation distance may be conservative. Anagnostopoulos and Spiliopoulos [7] found that, for the cases examined, the provisions of Eurocode 8 were more conservative than those of the UBC. They observed that in some cases of using the UBC provisions some pounding occurred, but with negligible effects. Finally, Penzien [68] proposed a formula for the evaluation of the minimum safe distance between two adjacent fixed-supported buildings to avoid impact, using an analytical procedure and the CQC method.

Although providing an adequate width of the seismic gap is the most preferable solution to preclude poundings, sometimes this is not feasible, like for example in cases of existing buildings in densely populated areas. Moreover, even for new construction, seismic separation requirements may not be easy to apply, as there is often strong opposition by property owners, developers and engineers for a number of economic, technical and legal reasons ([2],[6],[7]). Therefore, for such cases, other solutions can be applied as mitigation measures against poundings. For example, Anagnostopoulos and Karamaneas [6], based on the observation that for very small or no seismic gap the effect of impacts are reduced, proposed the use of collision shear walls to minimize seismic separation and to protect adjacent fixed-supported buildings from collapse due to earthquake-induced pounding.

Some other researchers proposed the linkage between two adjacent buildings with the incorporation of viscoelastic dampers ([59], [82]). Although this method seems to be quite effective and promising for mitigating poundings, it still has a number of disadvantages, including possible high forces in the links, the fact that the dynamic characteristics and the design failure mechanisms change, and the uncertainties inherent when the two structures of different characteristics must become one [78]. Mainly due to the last reason, Eurocode 8 does not allow any linkage between buildings that are not designed as coupled, from the design stage. Such linkage cannot be applied on a seismically isolated building, as it will restrain the relative displacements, disabling, essentially, the operation of the seismic isolation.

Another proposed measure for reducing the effects of pounding is the attachment of layers of soft material, such as rubber, on certain locations, where impact is likely to happen, in order to act as shock-absorbers. Anagnostopoulos [2] examined the case of filling the seismic gap with a soft material to act as shock-absorber by simply considering a decreased impact stiffness value for the linear viscoelastic impact model that he used for the simulation of poundings of buildings in series. He concluded that the use of bumpers may reduce, in some cases, the response due to poundings. Nevertheless, the maximum response values remain higher than the corresponding values without poundings. Jankowski et al [42] numerically simulated the use of several devices to mitigate structural pounding among bridge segments during earthquakes. They examined the case of using dampers and stiffeners as connectors of the segments in series or rubber bumpers to absorb impact energy between girders. The rubber bumpers in that case were simulated using a linear spring-dashpot element and the results showed that the incorporation of such devices may substantially reduce the overall response due to poundings.

In the case of seismically isolated buildings, the incorporation of a layer of flexible material, such as a soft elastomeric compound, between the building and the adjacent structures that acts as a collision bumper (Figure 6.1) can be an effective measure to minimize the detrimental effects of impacts. Nevertheless, there is a need for a thorough investigation of this approach, since the introduction of such material, with a certain thickness, reduces the width of the available seismic gap. In addition, there is a question about the modeling of the behavior of the rubber bumper under impact loadings.

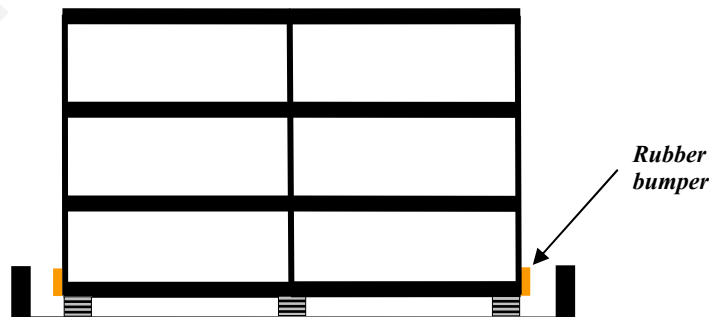


Figure 6.1 Pieces of rubber can be attached at potential impact locations around the seismically isolated building, as an impact mitigation measure.

6.3 Behavior of rubber bumpers under impact

Relevant experimental studies reveal that such layers of rubber under static and dynamic compressive loading exhibit a non-linear behavior ([43], [44], [45], [72]). In particular, it has been observed that the compressive stress-strain curve, obtained from experiments, such as those conducted by Kajita et al [43], has an exponential-type trend (see Figure 6.2).

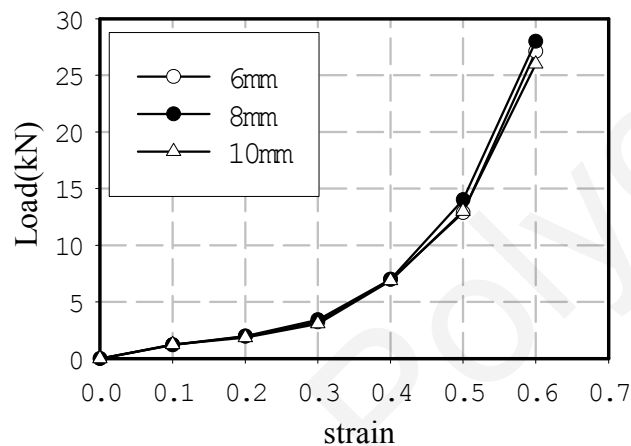


Figure 6.2 Load-strain curves obtained from static compressive loading of rubber shock-absorbers of 6, 8 and 10 mm thick (Kajita et al [43]).

Beside static tests, Kajita et al [43] also conducted impact tests between two steel rods of about 300 Kg each that were forced to collide with each other at a certain speed. At the contact area, layers of rubber were attached, with dimensions 40 mm × 40 mm and with varying thicknesses.

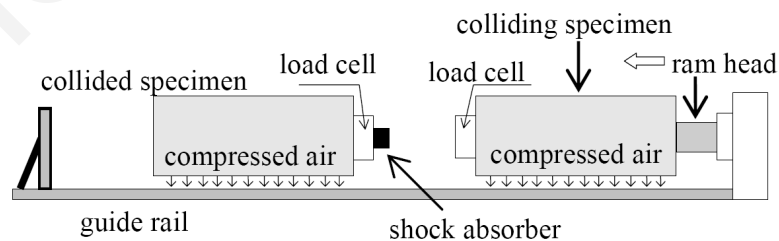


Figure 6.3 Test apparatus for small-scale experiments with rubber shock-absorbers, conducted by Kajita et al [43].

Figure 6.4 presents the corresponding experimental results, concerning the case of using a rubber bumper with a thickness of 10 mm. The force-displacement curve obtained from the corresponding static test is also included in the graph. It is observed that the curves obtained from impact tests do not follow the same path with the corresponding static test. Specifically, during dynamic loading, higher values of the impact force are developed for a certain deformation, compared to the corresponding values obtained from static test. Similar behavior was observed in other relevant experimental studies, whereas dynamic tests showed that the behavior of rubber under static and dynamic loading differs significantly. Shim et al [72] found, through experiments, that the behavior of rubber under compression and tension is rate-dependent. Also, Ishikawa et al [35] observed that the values of the impact loading curve were about 2.5 times larger than the load values of the corresponding static loading test.

Moreover, the experimental results demonstrate an immediate drop of the impact force at the beginning of the restitution phase, which returns to zero also with an exponential trend, indicating an inelastic behavior of the bumper. Test measurements also showed that the residual strain in specimens after unloading was negligible [72].

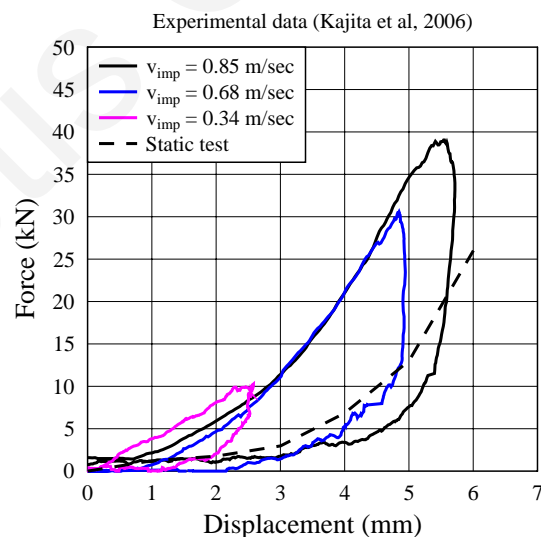


Figure 6.4 Force-displacement curves obtained from impact tests, involving a 10 mm thick rubber shock-absorber [43].

6.4 Proposing an impact model for rubber

A simple and efficient method is required for the modeling of the behavior of rubber shock-absorbers, in order to be properly considered in a numerical simulation involving poundings of structures, such as seismically isolated buildings. Considering the above observations and, specifically, the trends of the stress-strain curves obtained from experiments, the use of linear impact models for simulating the response of rubber during impact loading does not seem to be the most suitable approach. On the contrary, the use of a non-linear impact model would be much more appropriate for the simulation of the incorporated rubber bumpers, according to the available experimental data.

The most common non-linear impact models, which are presented in Section 2.2 of the thesis, do not seem to be able to represent sufficiently well the non-linear behavior of the rubber shock-absorbers that has been observed during experiments. In particular, the Hertzian elastic model cannot represent the inelastic behavior of rubber, while the non-linear viscoelastic impact model is characterized by a quite different force-displacement curve than those of the rubber bumpers. In addition, the formulas that provide the impact damping coefficient refer only to the case of using an exponent of 1.5, which is relatively low to represent the non-linear behavior of rubber. The Hertzdamp model, besides its considerably large inaccuracy for low values of the coefficient of restitution (Figure 2.7), is unable to describe sufficiently well the exact behavior of rubber shock-absorbers. On the contrary, the new non-linear impact model with hysteretic damping that has been proposed herein (Section 2.4) has the same basic characteristics of the pre-described experimental data.

6.4.1 *Verification of the proposed impact model*

In order to validate the accuracy of the proposed non-linear hysteretic impact model, the load-displacement curves obtained from the collision tests, conducted by Kajita et al [43], are compared with the corresponding results from numerical analyses, using the developed software that simulates the impact of two free bodies (Figure 2.10) and considering the proposed impact model.

The evaluation of the unknown values of impact stiffness and exponent are based on the static test curve (Figure 6.5(a)). In particular, the static test curve can be approximated with an exponent equal to 2.65 and an exponential static stiffness of $0.2 \text{ kN/mm}^{2.65}$. The impact stiffness, for the dynamic response, is taken to be equal to $0.45 \text{ kN/mm}^{2.65}$, much higher than the static stiffness, while the exponent is kept the same. According to Kajita et al [44] the energy loss during impact was found to be around 40 % to 50 % when using the rubber shock-absorbers. Accordingly, the coefficient of restitution is assumed to be equal to 0.45 for the simulations. Nevertheless, the value of the coefficient of restitution, in the proposed impact model, does not affect the value of the maximum impact force, but only the trend of the restitution phase, determining the hysteretic energy loss.

Plots in Figure 6.5(b-d) present the force-displacement curves obtained from analyses, together with the corresponding experimental curves of Kajita et al [43]. The numerical results considering the Hertz damp impact model [61], using the same values for the impact parameters, are also plotted for comparison. It is observed that, in general, the trends of the numerical analysis, using the proposed hysteretic impact model, are very similar to the experimental ones with a small variation on the maximum value of the impact force, for two of the three cases. Furthermore, the most important advantage of this model is that the trend during the approach phase, which determines the acceleration response during impact, is roughly the same with the trend that was revealed from the experiments. In addition, the shape and size of the hysteresis loop of the proposed impact model is very close to the corresponding experimental results. On the contrary, the dynamic behavior obtained from the use of the Hertz damp model differ significantly from the impact tests results, especially regarding the area of the hysteresis loop that indicates the dissipation of energy by the shock-absorber.

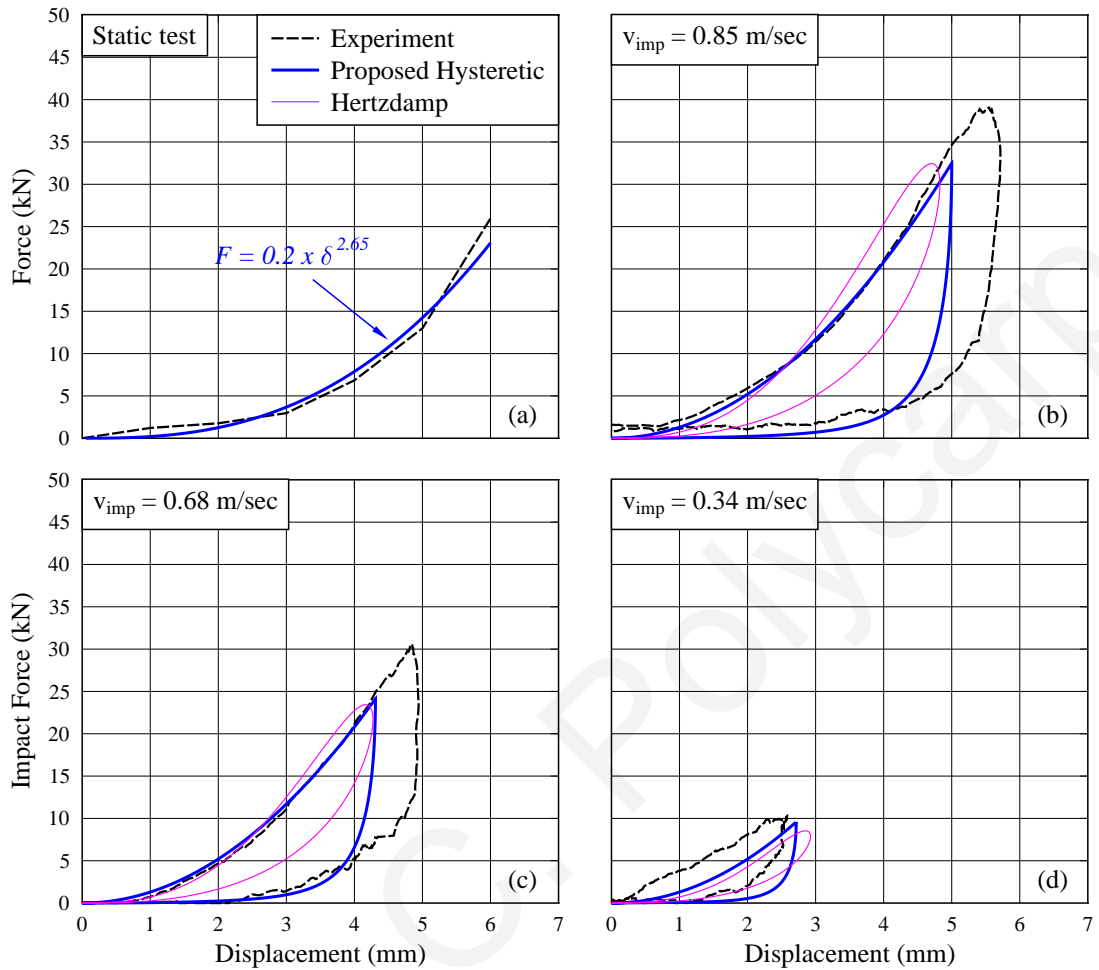


Figure 6.5 Force-displacement curves for the case of incorporating a rubber shock-absorber of 10mm thickness between two steel rods of 300 Kg mass each.

6.4.2 *Material and bumper stiffness*

The impact stiffness value that has been used in the above numerical simulations corresponds to the dimensions and material of the specific bumper that had been used in the experiments [43]. It is observed that there is a relation between the static exponential stiffness and the corresponding impact stiffness of the bumper. In particular, the impact stiffness in the cases studied in Reference [43], was found to be approximately 2.25 times higher than the corresponding static stiffness. Similar ratios between the static and dynamic stiffness have been observed from other researchers, as mentioned above.

Therefore, if the static stiffness is known, then the corresponding impact stiffness can be easily estimated, based on the above observations. Jankowski et al [42] used a linear spring to simulate rubber bumpers between bridge segments, with a stiffness value equal to:

$$k_{st} = \frac{A \cdot E_r}{t} \quad (6.1)$$

where A is the contact area, E_r is the Young's Modulus for rubber and t is the thickness of the bumper. However, as seen from experimental results, a linear model is not appropriate for simulating the behavior of rubber under compressive loadings. In order to take a non-linear behavior into account, it is assumed that the static stiffness of a bumper of constant thickness t is expressed as:

$$k_{st} = \frac{A \cdot K_r}{t^n} \quad (6.2)$$

where K_r expresses the material stiffness and n is the exponent that characterizes the non-linear behavior. Consequently, in the case of a value of k_{st} equal to $0.2 \text{ kN/mm}^{2.65}$ and the dimensions of the shock-absorber used in the experiments described above, the term K_r is found to be equal to 55835 kN/m^2 . This value of K_r can be used in Equation 6.2 to evaluate the static stiffness, and then the impact stiffness (Equation 6.3) of a rubber bumper with the same material and different dimensions.

$$k_{imp} = 2.25 \cdot k_{st} = 2.25 \cdot \frac{A \cdot K_r}{t^n} \quad (6.3)$$

For example, the impact stiffness for a bumper made of the same material, with dimensions of $150 \text{ mm} \times 150 \text{ mm}$ and a thickness of 50 mm can be computed as:

$$k_{imp} = 2.25 \cdot \frac{0.15 \cdot 0.15 \cdot 55835}{50^{2.65}} = 0.089 \text{ kN/mm}^{2.65}$$

6.4.3 Exceedance of the ultimate compressive strain of rubber

Since a rubber shock-absorber has a certain finite thickness, there is a possibility to reach its ultimate compressive strain during severe impacts, whereas the impact stiffness should be that of the colliding wall and not, anymore, that of the rubber bumper. In order to take

into account this case, the following assumption has been implemented in the simulations involving poundings of seismically isolated buildings with the surrounding moat wall, considering the incorporation of rubber bumpers at the impact points. In particular, during the approach phase, it is assumed that after a certain indentation δ_u , which corresponds to the compressive strain capacity of the rubber bumper, the exponential trend alters to a linear trend with a linear post-yield stiffness k_w :

$$F_{imp} = \left\{ \begin{array}{ll} k_{imp} \cdot \delta^n & \text{for } \delta < \delta_u \\ k_{imp} \cdot \delta_u^n + k_w \cdot (\delta - \delta_u) & \text{for } \delta > \delta_u \end{array} \right\} \text{ when } \dot{\delta} > 0 \quad (6.4)$$

The maximum indentation δ_u is expressed as a percentage of the bumper's thickness and a typical value is around 75 % – 80 % of the thickness, t , of the rubber bumper. It can be assumed that the linear impact stiffness k_w expresses the static stiffness of the moat wall. The effect of choosing different values for this parameter is examined in the following paragraphs.

During the restitution period, the impact force is provided by Equation 2.20, i.e. the damping is the same in both linear and non-linear sections of the impact model. Figure 6.6 presents the impact force time-histories and the force-displacement diagrams of the non-linear impact model with hysteretic damping, considering the case of exceeding the maximum compressive strain of the rubber shock-absorber, for three different values of the coefficient of restitution. It is observed that for the case of using relatively low values for the coefficient of restitution, the trend during the restitution period tends to drop below zero. Thus, in order to avoid any tensile forces, in such cases the computed impact force is automatically set equal to zero. However, no permanent indentation is considered in that case, since it is assumed that the rubber, essentially, returns to its initial position.

Following this assumption, for the case of exceeding the maximum strain of rubber bumper, the question arises whether the equilibrium of the kinetic energy loss with the area of the hysteresis loop is still fulfilled for the non-linear hysteretic impact model. In order to examine the effect of the above assumptions on the accuracy of the proposed model

regarding the calculation of the post-impact velocities, a small parametric study is performed.

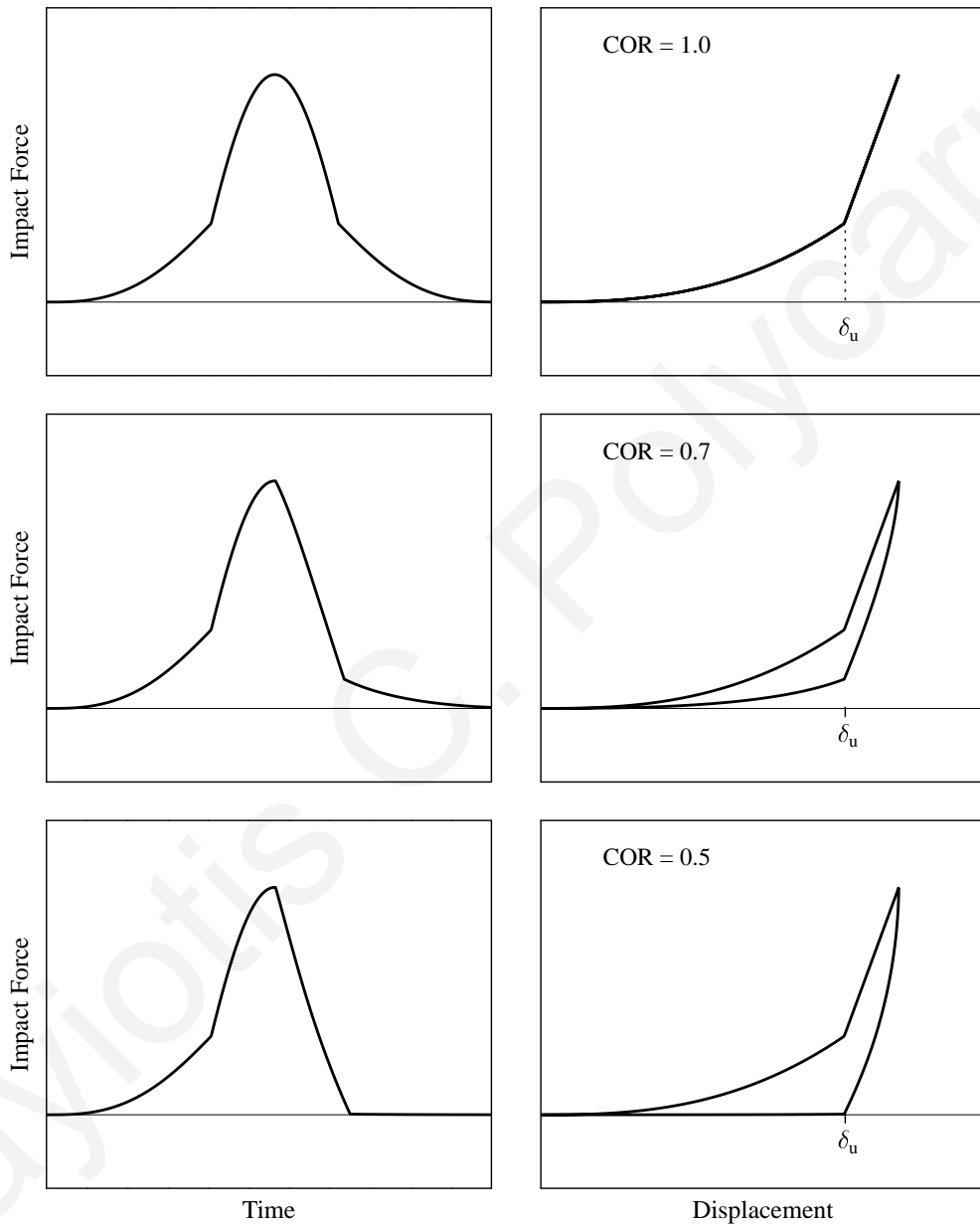


Figure 6.6 Modeling of the impact response of a rubber bumper with an ultimate compression displacement equal to δ_u , considering three different values for the coefficient of restitution.

In particular, the computed coefficient of restitution is plotted in the graphs of Figure 6.7 in terms of the one provided in the corresponding formula describing the non-linear

impact model. For the derivation of these plots, a free body is considered with a mass of 500 tons, impacting against a rigid wall of the same mass, with an impact velocity equal to 1.0 m/sec. Four rubber bumpers with dimensions 150 mm \times 150 mm and a thickness of 50 mm are considered in parallel, with a maximum strain equal to 0.75. The exponent is taken equal to 2.65 and the exponential stiffness equal to 0.36 kN/mm^{2.65}.

Figure 6.7(a) provides the computed error, for three different values of the post-yield linear stiffness k_w , while Figure 6.7(b) displays the same plots with varying impact velocity. It is observed that the post-yield linear stiffness slightly affects the computed error, which is maintained at very low levels. On the other hand, impact velocity affects more the computed error, which is increased in the cases of high values of the former. In particular, the results indicate that the computed damping corresponds to less dissipated energy than the one defined by the theory, based on the provided COR. This is because of the linear part of the impact model that corresponds to the exceedance of compressive capacity of the bumper, which becomes greater for higher impact velocities. In addition, a larger error is observed for medium values of the coefficient of restitution, specifically around 0.5.

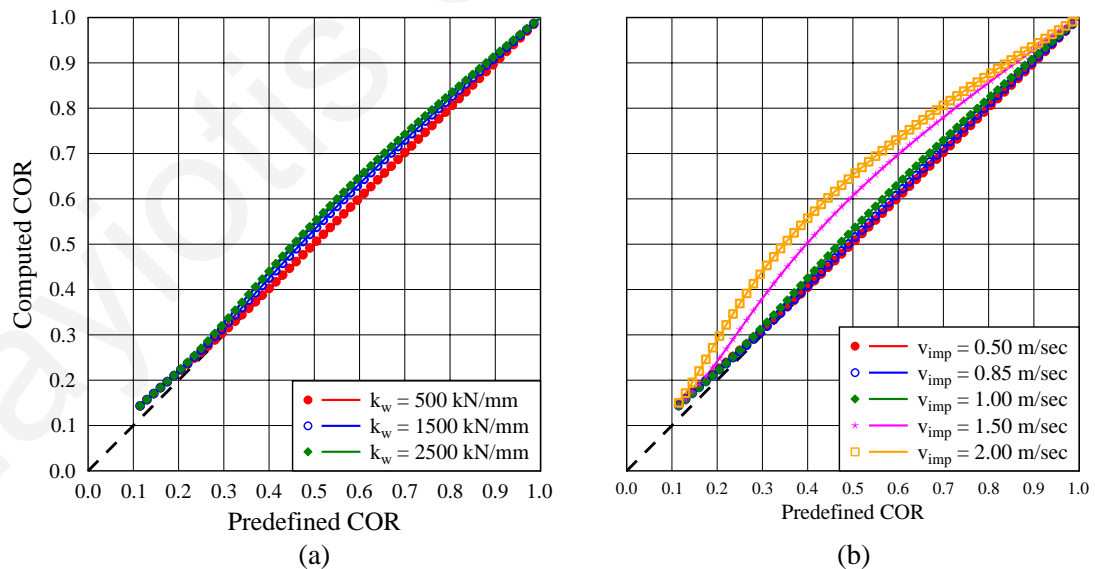


Figure 6.7 Error estimation of the non-linear impact model with hysteretic damping, considering the case where the indentation exceeds the maximum compressive capacity of the rubber bumper.

6.5 Example

A practical example is presented in order to demonstrate the effect of implementing a rubber shock-absorber as an impact mitigation measure for cases of narrow seismic gaps around a seismically isolated building. For the numerical simulations, the 4-story seismically isolated building that has been described in Section 4.3 is considered, under the Kobe and the San Fernando earthquake records. The initial seismic gap around the building is considered to be equal to 15 and 24 cm, respectively, which is equal to 10 % smaller than the maximum unconstrained displacement at the isolation level, under the corresponding excitation. These two representative seismic records are selected in order to demonstrate the effect of the earthquake characteristics on the effectiveness of the rubber bumpers as impact mitigation measure. In the next section, series of parametric analyses are performed including more earthquake records.

The same building is considered under a second configuration, where four 5 cm thick rubber shock-absorbers are attached at each side of the seismically isolated building at the isolation level (Figure 6.8), with the clearance being reduced to 19 cm. The bumpers are assumed to have a square section with dimensions 150 mm \times 150 mm (Figure 6.9). The same material stiffness and impact exponent that have been derived from the experiments are used for the calculation of the impact stiffness, which is found to be 0.36 kN/mm^{2.65}. The post-yield linear impact stiffness is taken to be equal to 1500 kN/mm.

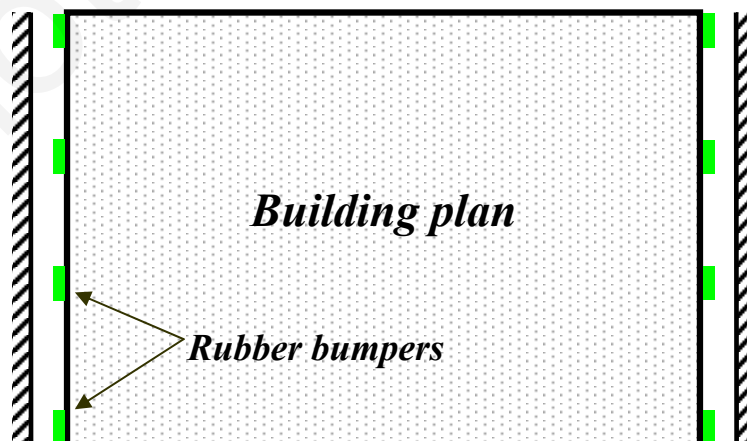


Figure 6.8 Locations of rubber shock-absorbers in a plan view of the building.

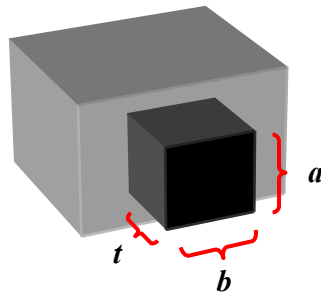


Figure 6.9 Geometrical characteristics of a rubber shock-absorber.

Figure 6.10 presents the total acceleration time-histories at the base of the seismically isolated building, where poundings occur, for both cases, without and with bumpers, as well as for the case where no poundings occur, for the Kobe Earthquake record. It is observed that, in general, the value of the peak floor acceleration remains almost the same after the implementation of the rubber shock-absorber and, therefore, potential use of such measure in the particular case does not seem to be beneficial for the seismically isolated building, under the specific earthquake excitation.

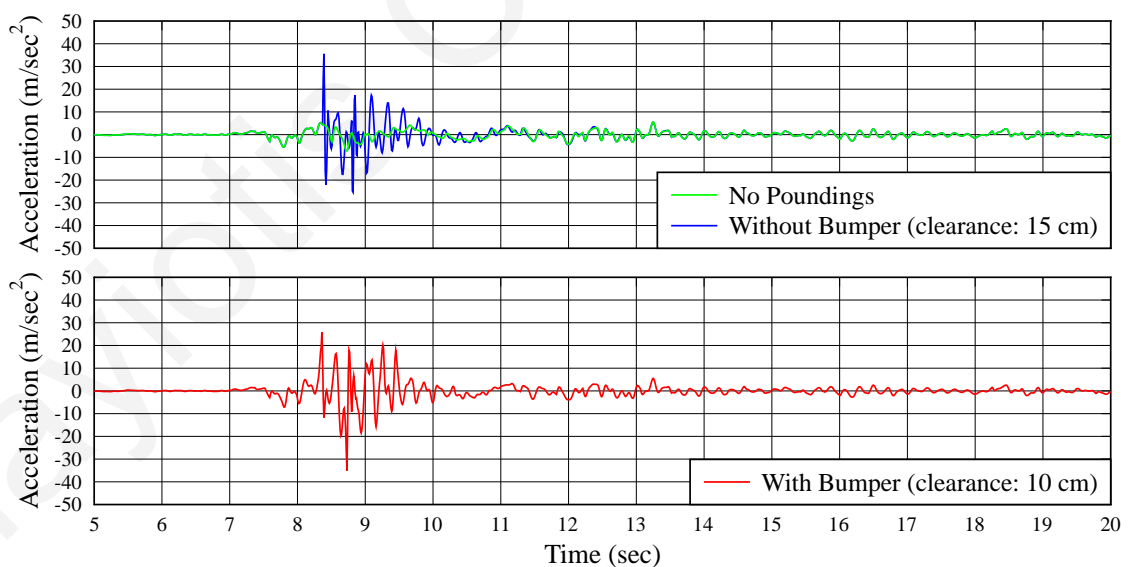


Figure 6.10 Effect of the attachment of 5 cm thick rubber shock-absorbers on the total acceleration time-history response at the isolation level, during the Kobe Earthquake.

On the contrary, when considering the San Fernando Earthquake record, the use of rubber bumpers seems to be quite effective. According to Figure 6.11, although that when having bumpers the available clearance is reduced from 24 cm to 19 cm, the maximum acceleration response is lower than the corresponding peak acceleration without bumpers. In particular, the high spikes in the acceleration response are eliminated due to the implementation of the rubber shock-absorbers. However, the peak acceleration values are still higher than the corresponding response of the seismically isolated building without poundings.

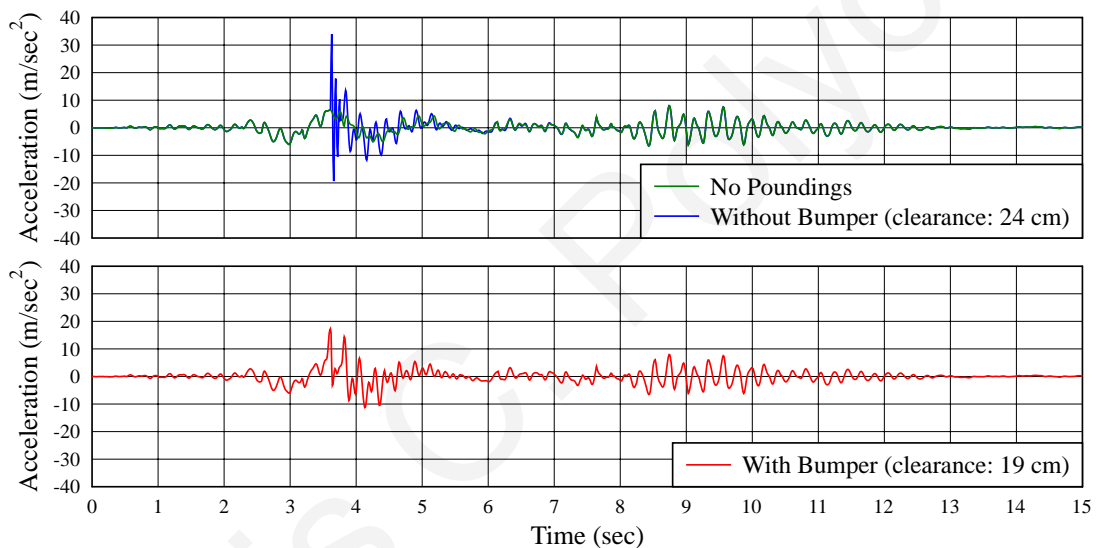


Figure 6.11 Effect of the attachment of 5 cm thick rubber shock-absorbers on the total acceleration time-history response at the isolation level, during the San Fernando Earthquake.

The different effect, from using rubber bumpers, on the computed floor accelerations for the two different seismic excitations can be explained from the corresponding time-histories of the impact forces at the particular floor level. Figure 6.12 and Figure 6.13 provide the impact force time-histories for the two cases of without and with bumpers of 5 cm thick, for the Kobe and San Fernando earthquakes, respectively. It is observed that, under the Kobe Earthquake, the values of the maximum impact forces, when using rubber shock-absorbers, are almost the same with the corresponding values in the case of without the usage of any bumpers, where the seismic gap width is larger. On the other hand, under the San Fernando Earthquake, the maximum impact forces are reduced after implementing

the rubber bumpers (Figure 6.13). In general, it is observed that in the cases with rubber bumpers, the duration of the impact elongates, while the first impacts occur in shorter time due to the reduced seismic gap width after the employment of the bumpers.

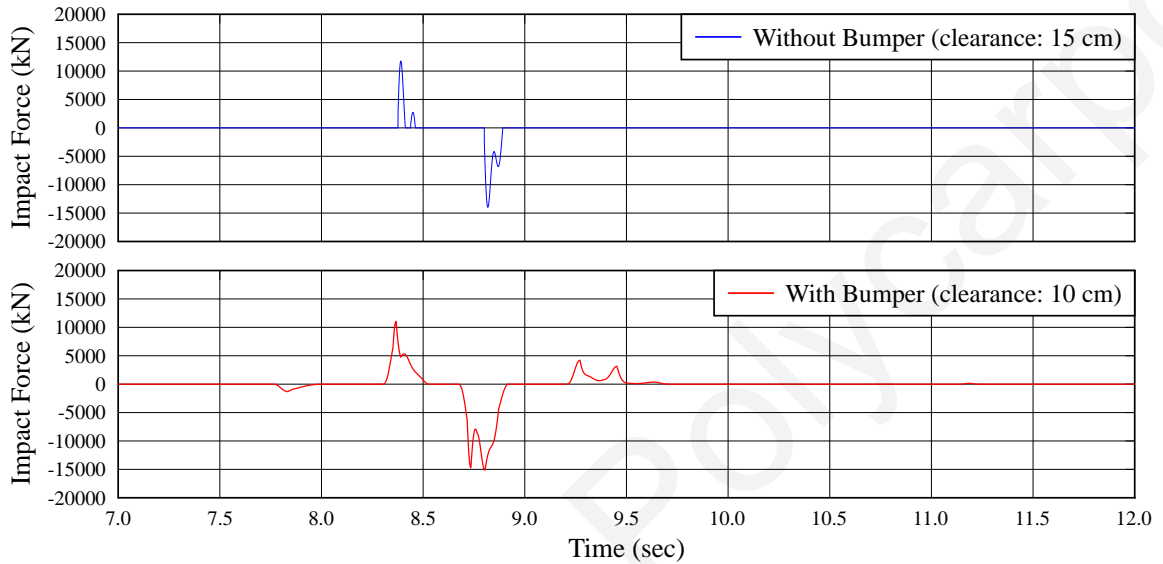


Figure 6.12 Impact force time-histories for the two cases of without and with rubber bumpers attached at the base of the seismically isolated building, considering the Kobe Earthquake.

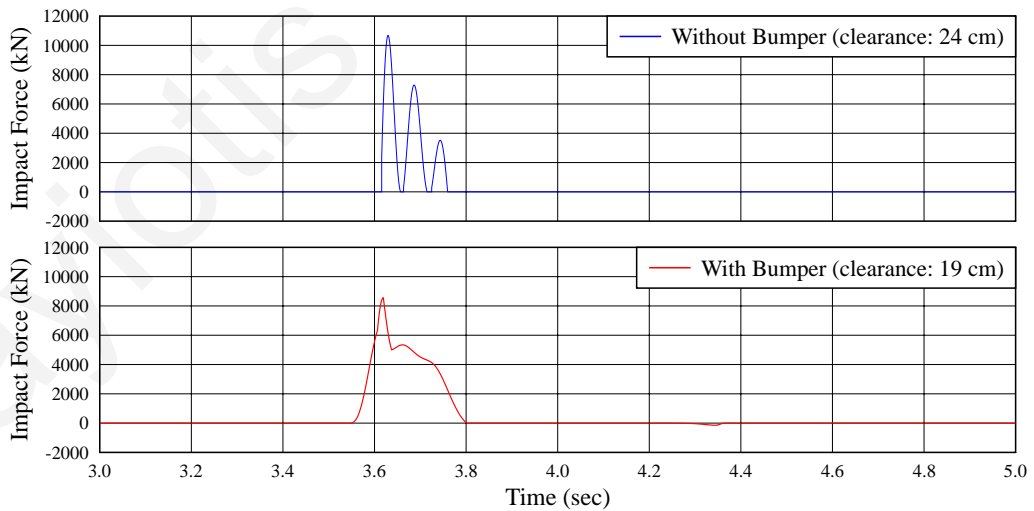


Figure 6.13 Impact force time-histories for the two cases of without and with rubber bumpers attached at the base of the seismically isolated building, considering the San Fernando Earthquake.

The reason of having such relatively high values of impact forces, when using the rubber bumpers, only in the case of the Kobe Earthquake, is because the substantial exceeding of the maximum compressive capacity of the 5 cm thick bumpers, in contrast to the case of the San Fernando Earthquake, where a very small exceedance occurs. This can be seen in Figure 6.14 where the impact forces are plotted in terms of the indentation. It is observed that after the exceedance of the maximum compressive capacity, which in the current case is equal to 4 cm (80 % of the bumper's thickness), the impact forces increase rapidly due to the increased impact stiffness. This sudden change, affects the acceleration response at the corresponding level, which increases drastically. This is mainly the reason for the ineffectiveness of the rubber bumpers as a mitigation measure for poundings under the Kobe Earthquake.

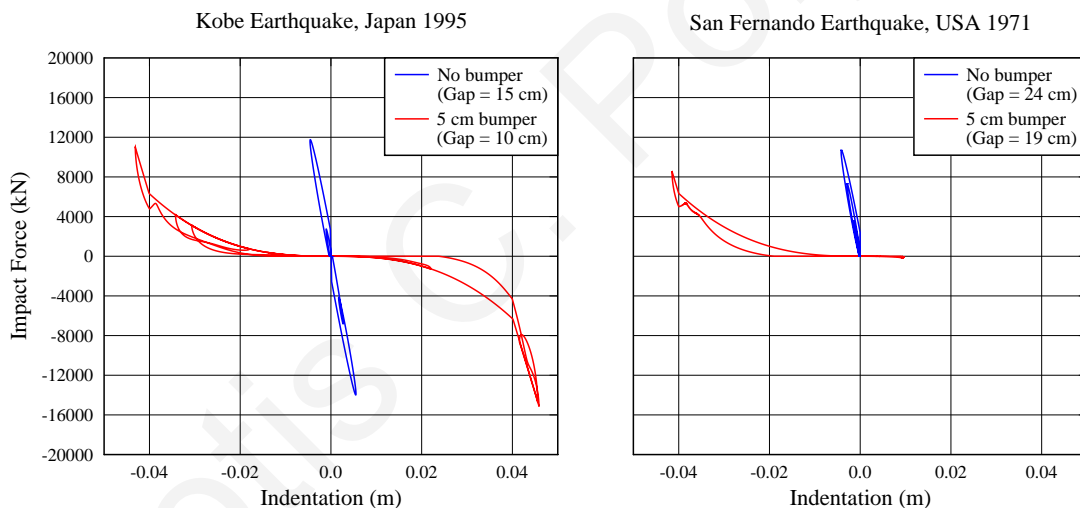


Figure 6.14 Impact force in terms of the resulting indentation for the two cases of without and with bumpers.

The overall response of the seismically isolated building under the Kobe earthquake is demonstrated in Figure 6.15, where the maximum responses at all floors of the seismically isolated building for the two configurations examined, i.e. with and without rubber bumpers, as well as for the case without poundings, are provided. A significant amplification of the interstory deflection is observed in the case of using the rubber bumpers, while the peak floor accelerations remain almost in the same levels as in the case without using the bumpers.

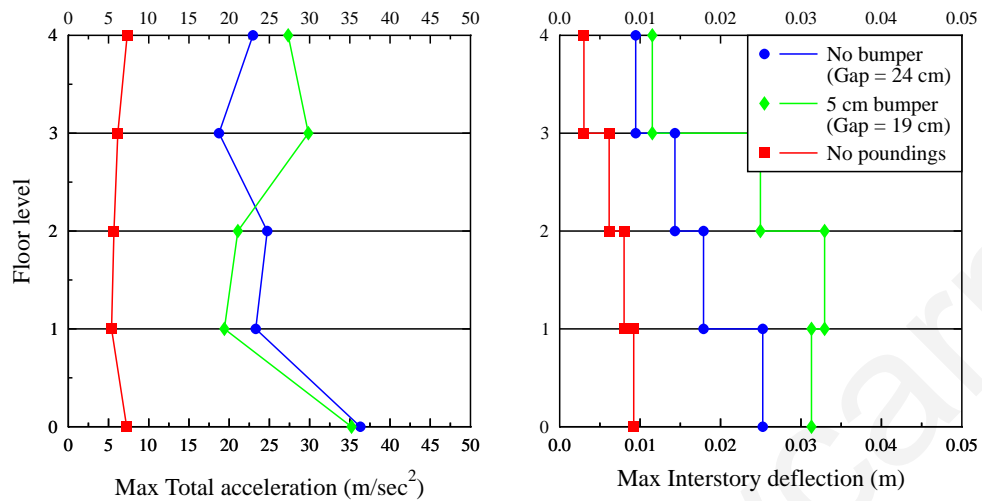


Figure 6.15 Differences on the maximum responses of the seismically isolated building, under the Kobe Earthquake, due to the attachment of 5 cm thick rubber shock-absorbers at the potential impact locations.

The corresponding results are plotted in Figure 6.16 for the San Fernando Earthquake and it is observed that the response is quite different, compared to the case of the Kobe Earthquake. In particular, no significant increases on the maximum interstory deflections or the maximum floor acceleration at the upper floors are observed due to the decreased gap size, when rubber bumpers are used. On the contrary, the maximum interstory deflection at the first story, which is the largest among all stories, slightly decreases through the incorporation of the rubber bumpers. In addition, the peak absolute acceleration value at the base of the seismically isolated building, where the rubber shock-absorbers are attached, are considerably reduced, while at the upper floors of the superstructure the peak floor accelerations remain almost the same with the case without bumpers.

The presented results suggest that the employment of rubber bumpers can mitigate, but, in some cases, can even amplify the detrimental effects of poundings of a seismically isolated building with the surrounding moat wall. The earthquake characteristics seem to play a significant role on the effectiveness of the rubber bumpers. However, a large set of seismic excitations should be used, considering the effect of more parameters before

extracting any general conclusions. The results from a more extensive investigation, involving large number of simulations, are presented in the next paragraph.

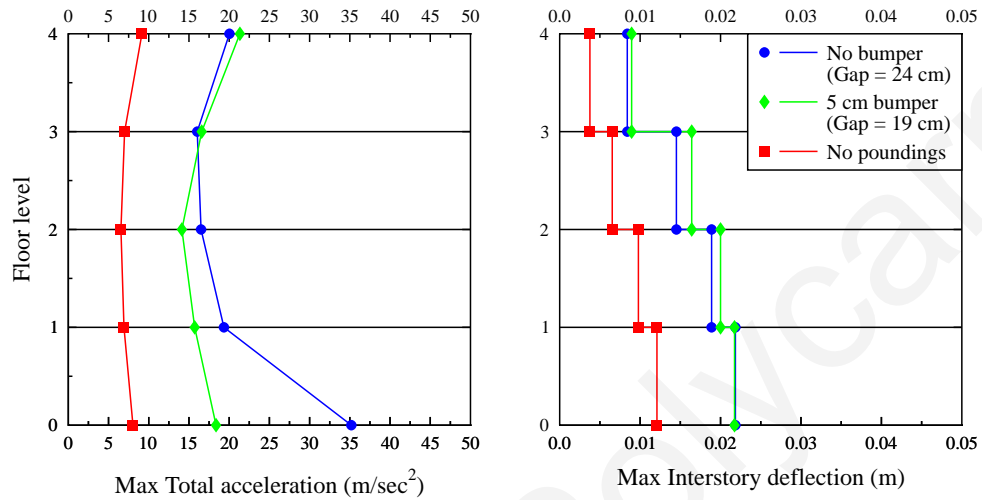


Figure 6.16 Differences on the maximum responses of the seismically isolated building, under the San Fernando Earthquake, due to the attachment of 5 cm thick rubber shock-absorbers at potential impact locations.

6.6 Parametric studies

A large number of numerical simulations has been conducted, considering the 4-story seismically isolated building under different circumstances, in order to assess the overall effectiveness of rubber shock-absorbers, as an impact mitigation measure, for cases of narrow seismic gaps around a seismically isolated building. Poundings are considered to occur only at the isolation level with the surrounding moat wall.

6.6.1 *Effect of the gap size and the earthquake characteristics*

The width of the seismic gap, i.e. the distance of the surrounding moat wall from the base of the seismically isolated building, is varied between the values of 15 to 45 cm. Therefore, in the case where the rubber bumpers are attached, the corresponding gap size on both sides of the seismically isolated building becomes 5 cm smaller. In order to examine the effect of the earthquake characteristics, four different seismic records are considered in the simulations. The Kocaeli Earthquake is excluded from the analyses due to the fact that the

maximum induced displacement of the seismically isolated building, under the specific excitation, is relatively small (11.4 cm).

Figure 6.17 and Figure 6.18 demonstrate the effect of using rubber bumpers on the response of the 4-story seismically isolated building, in terms of the size of the seismic gap. In particular, the plots present the amplification of the peak floor accelerations and peak interstory deflections due to the implementation of four rubber shock-absorbers with the characteristics that have been used in the simulations of the previous section, on each side of the seismically isolated building. Here, the amplification of the response is defined as the ratio of the response obtained after the incorporation of rubber bumpers, which unavoidably reduce the available clearance, to the corresponding response, without the usage of any bumpers.

It is observed that for relatively wide seismic gaps the usage of rubber shock-absorbers increases the response instead of reducing it. In particular, this happens for seismic gaps, where poundings would not occur without the incorporation of the rubber bumpers, which decrease the available clearance from the moat wall. For some seismic actions the response becomes two times greater than the cases of without bumpers. For example, under the Kobe and Northridge Olive Station excitations, the maximum horizontal displacements are 16.74 and 15.63 cm, respectively, and, therefore, the attachment of 5 cm thick bumpers when the available clearance is over 15~16 cm wide is not beneficial for the building, as can be seen from the plots of Figure 6.17. On the other hand, for the cases of the Northridge Converter Station and the San Fernando Earthquake records, where the induced displacements are quite large for the seismically isolated building, the usage of rubber bumpers can be beneficial for relatively narrow gap sizes. Nevertheless, this is not always true, especially concerning the interstory deflections, which are in most of the cases amplified due to the attachment of the rubber bumpers, which reduce the corresponding gap size.

In general, it seems that the use of rubber bumpers is more efficient measure in cases of relatively strong earthquakes where the induced displacements of the seismically isolated building are quite large relatively to the available seismic gap.

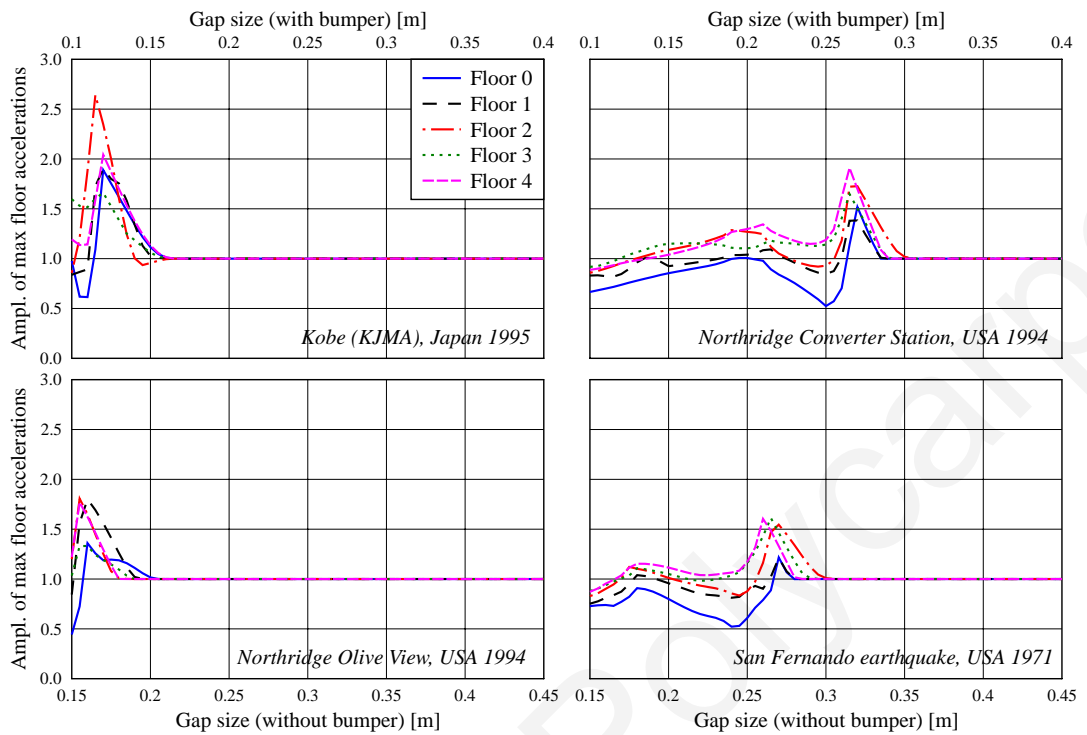


Figure 6.17 Amplification of the peak floor accelerations, due to the usage of rubber shock-absorbers, in terms of the width of the seismic gap.

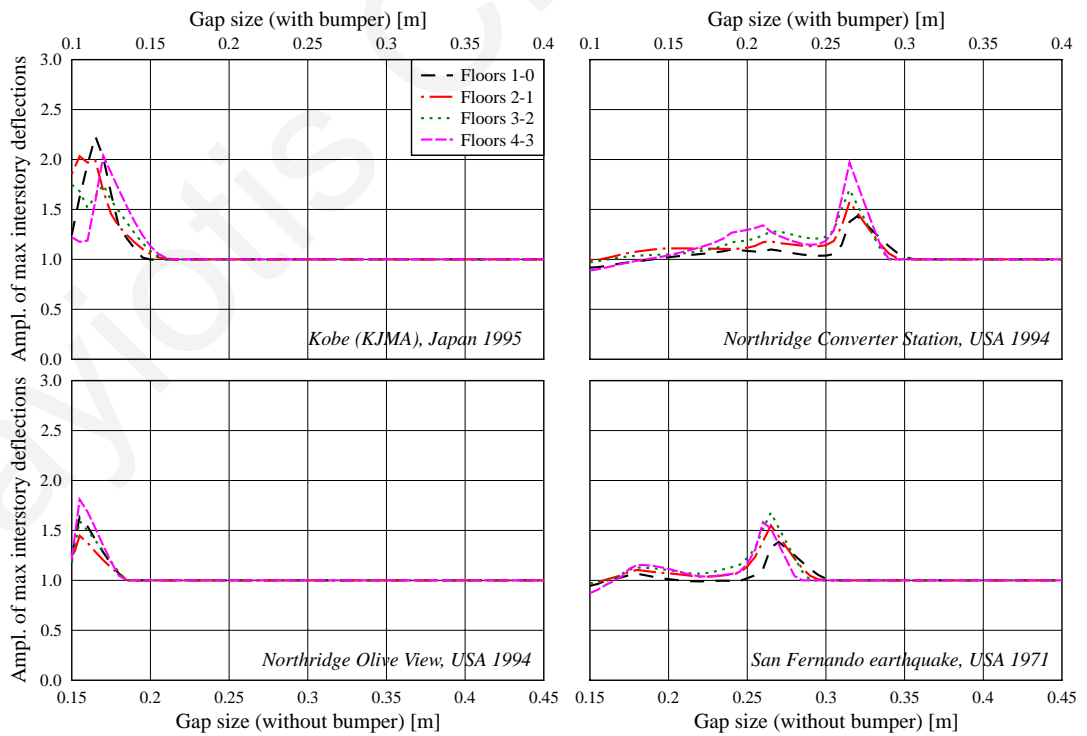


Figure 6.18 Amplification of the peak interstory deflections, due to the usage of rubber shock-absorbers, in terms of the width of the seismic gap.

Moreover, the plots in Figure 6.19 provide useful information about the effect of the peak ground acceleration (PGA) on the potential effectiveness of the rubber bumpers. In particular, the amplifications of the maximum floor acceleration and the maximum interstory deflection, due to the implementation of the rubber bumpers, are plotted in terms of the PGA, for three different initial gap widths and for the San Fernando and the Northridge Converter Station seismic records, which are the two strongest from the selected earthquakes, regarding the maximum induced displacement of the 4-story seismically isolated building. It is observed that, in general, for high values of the PGA, in combination with a relatively narrow seismic gap width, the rubber shock-absorbers benefit the response. However, in other cases the response of the seismically isolated building is worsening when rubber bumpers are used, especially regarding the interstory deflections.

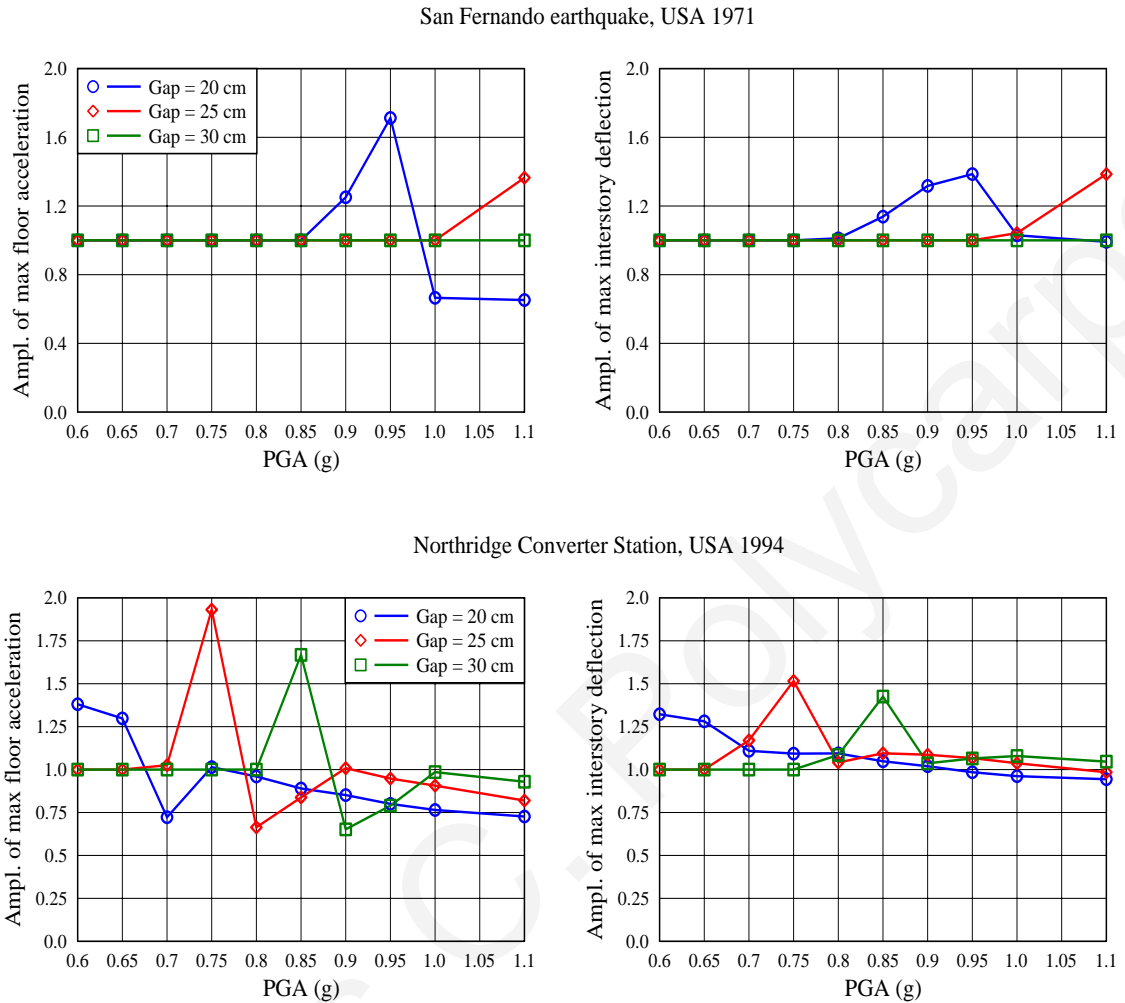


Figure 6.19 Amplification of the maximum responses of the 4-story seismically isolated building due to the usage of rubber shock-absorbers, in terms of the peak ground acceleration of the excitation.

6.6.2 *Effect of the bumper thickness*

Relevant experimental studies [47] have found that the thickness of a viscoelastic material affects the response during impact loading. Specifically, the test results showed that the impact force reduces with the increment of the thickness of the material, while at the same time, the duration of impact is elongated. However, in the current case of using layers of rubber to act as shock-absorbers, along with the increment of their thicknesses, the width of the seismic gap is, unavoidably, reduced. Therefore, conclusions cannot be safely

derived regarding the real effect of the rubber thickness without conducting a parametric investigation.

In order to examine the influence of the thickness of the rubber shock-absorber on the effectiveness of the latter, three cases of different thicknesses are considered. Four rubber bumpers are considered on each side of the seismically isolated building, while a post-yield linear impact stiffness of 1500 kN/mm is assumed. The plots in Figure 6.20 present the maximum responses of the 4-story seismically isolated building in terms of the seismic gap width, considering different thicknesses for the rubber shock-absorbers. The maximum responses for the case without bumpers are also plotted with a dashed line in the figure. The Northridge Converter Station and San Fernando earthquake records are used as representative excitations, which induce the larger relative displacements at the isolation level of the base-isolated building, among the five selected earthquakes.

The results show that an increased thickness of the bumpers reduces the amplification of the maximum floor acceleration values due to poundings, when the seismic gap is very narrow with respect to the maximum induced horizontal displacement. For medium to wide seismic gap sizes, the effect of the bumper thickness on the acceleration response is negligible. On the other hand, the maximum interstory deflections of the seismically isolated building seem to increase with the thickness of rubber shock-absorbers. In general, however, the thickness of the rubber bumpers seems to slightly affect the response. Furthermore, for the specific characteristics assumed in this series of simulations, the attachment of the rubber bumpers is not either beneficial or detrimental, regarding the maximum computed response of the 4-story seismically isolated building.

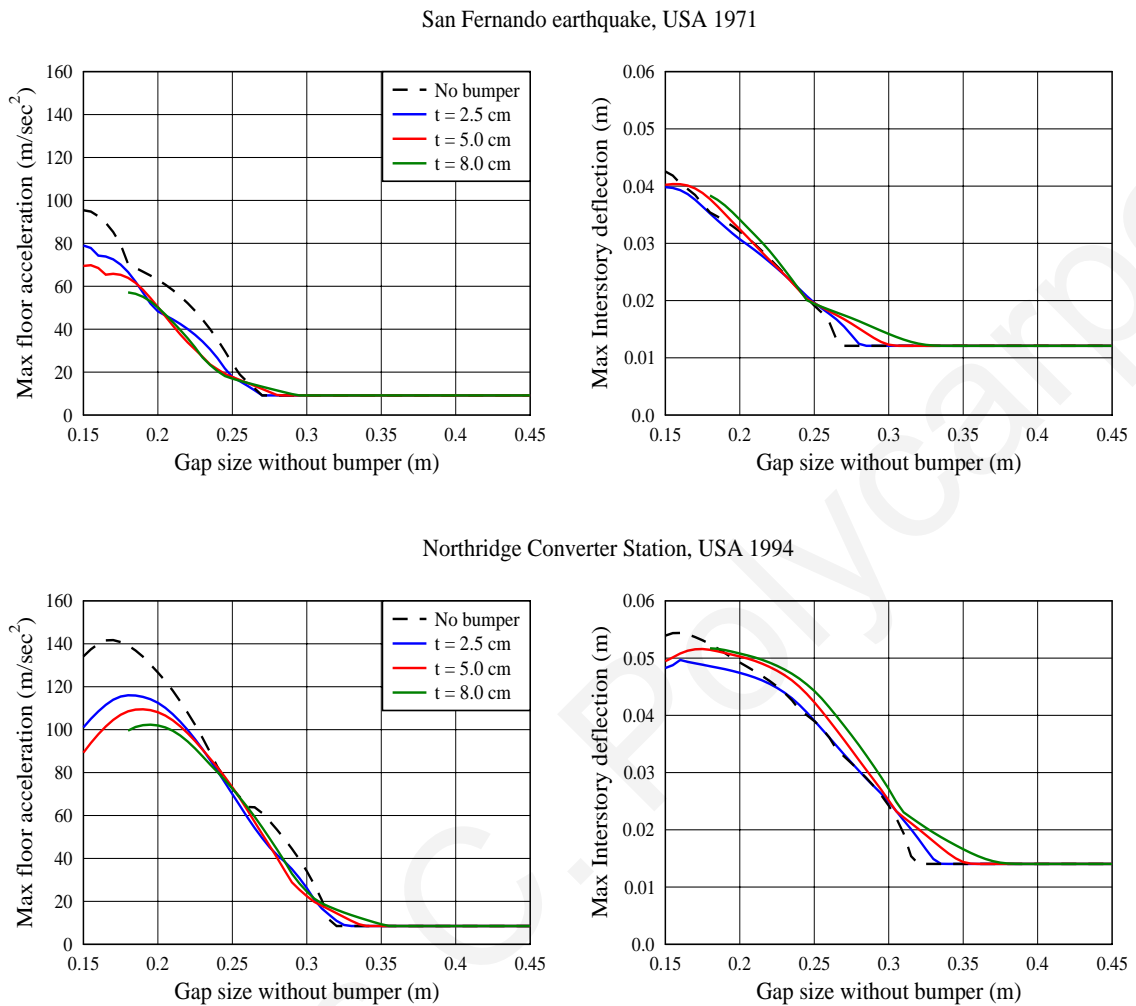


Figure 6.20 Peak responses of the seismically isolated building in terms of the seismic gap width, assuming different thicknesses of the incorporated bumpers.

6.6.3 *Effect of the maximum compressive capacity of the bumpers*

In the previously presented simulations, it is assumed that, after the attachment of rubber bumpers on the side of the seismically isolated building, the reduction of the available clearance from the surrounding moat wall equals to the corresponding thickness of the bumpers. However, there is a possibility of attaching the rubber bumpers in small cavities on the wall, taking advantage only the compressible width of the rubber, as shown in Figure 6.21. For example, if the thickness of a rubber bumper is 5 cm and its maximum compressive strain, ε_u , equals 0.8, then the compressible width of the bumper is 4 cm.

Therefore, if the particular shock-absorber is attached with a cavity of 1 cm deep, then the maximum compressive strain that will be used in the simulations should be equal to 1.0, while its thickness would be 4 cm.

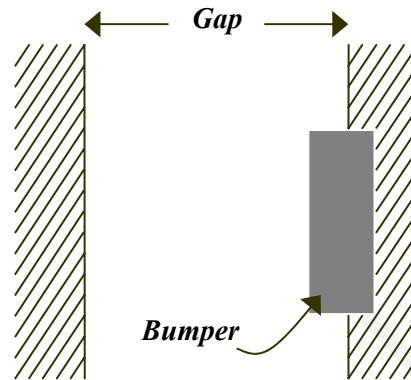


Figure 6.21 Attachment of a rubber shock-absorber in a cavity on the wall.

The plots in Figure 6.22 demonstrate the effect of the value of the maximum compressive strain on the computed response, while the thickness of the rubber bumpers is assumed to be the same, i.e. 5 cm, for all cases. It is observed that both absolute floor accelerations and interstory deflections of the seismically isolated building decrease with the increase of the maximum compressive capacity of the rubber bumpers. Therefore, in order to make the use of rubber shock-absorbers more effective, a good solution would be the attachment of rubber bumpers in cavities, which are deep enough to take full advantage of the whole compressibility of the rubber, achieving a maximum compressive strain equal to 1.0.

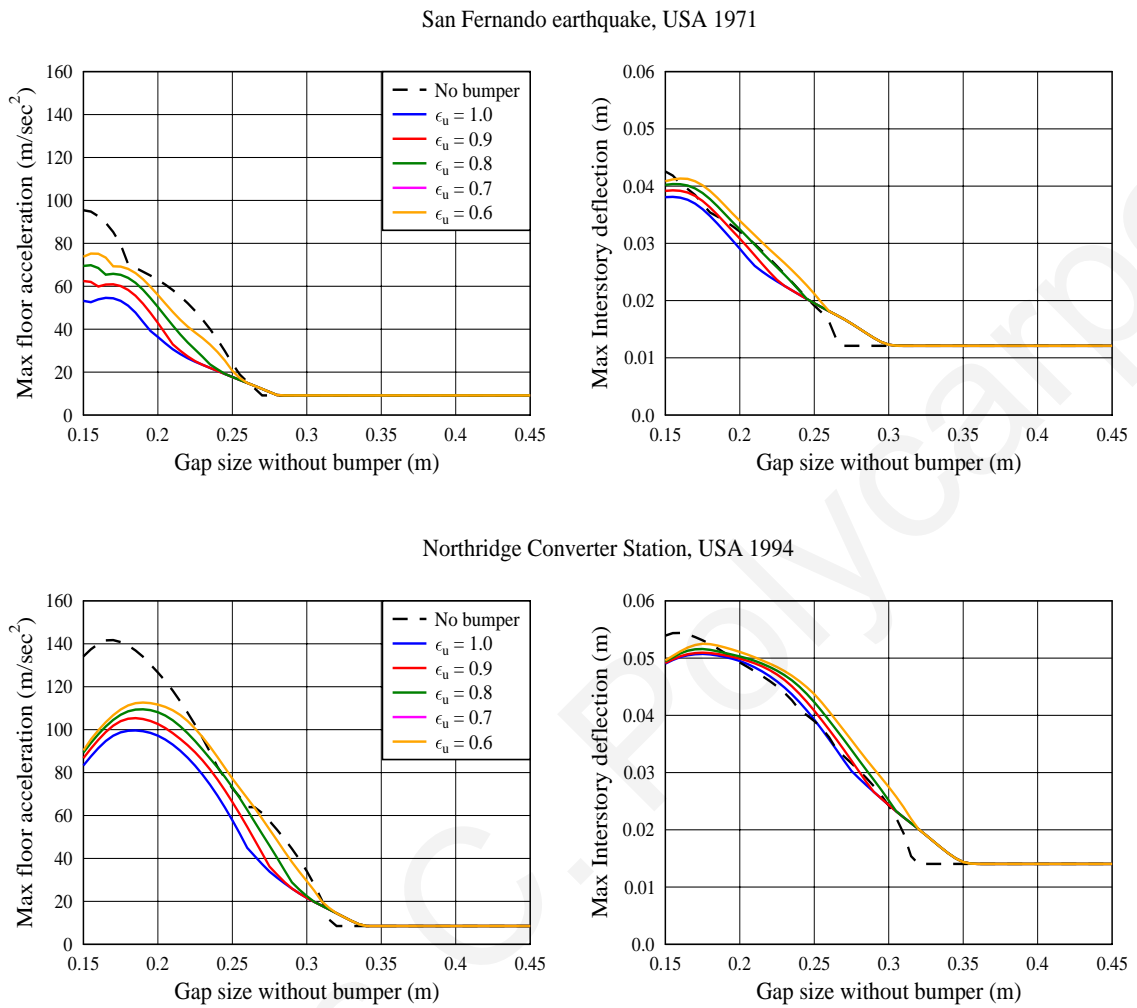


Figure 6.22 Peak responses of the seismically isolated building in terms of the seismic gap width, assuming different values for the maximum compressive strain of the incorporated bumpers.

6.6.4 *Effect of the number of bumpers*

The number of the rubber bumpers, attached on each side of the seismically isolated building is also examined. Specifically, assuming the same characteristics of the bumpers, four different cases are considered with 4, 8, 16 and 32 bumpers with exponential stiffness values of 0.36, 0.71, 1.42 and 2.85 kN/mm^{2.65}, respectively. The post-yield linear impact stiffness is considered to be equal to 1500 kN/mm and remains the same for all four cases, since it is assumed to represent the static stiffness of the moat wall.

The results of the performed parametric analysis are presented in Figure 6.23. It is observed that by increasing the number of bumpers, and, therefore, the exponential impact stiffness, the maximum responses of the seismically isolated building during poundings increase in almost all cases of different seismic gap widths. However, there are some limited cases for very narrow gap sizes, where the maximum responses are lower, when more bumpers are used. This is due to the fact that for the case of very narrow gap sizes, the maximum compressive strain of the bumper is usually exceeded, and the effectiveness of the bumper is reduced. Therefore, the use of more rubber bumpers increases the exponential stiffness, avoiding the exceedance of the ultimate compressive capacity of the rubber.

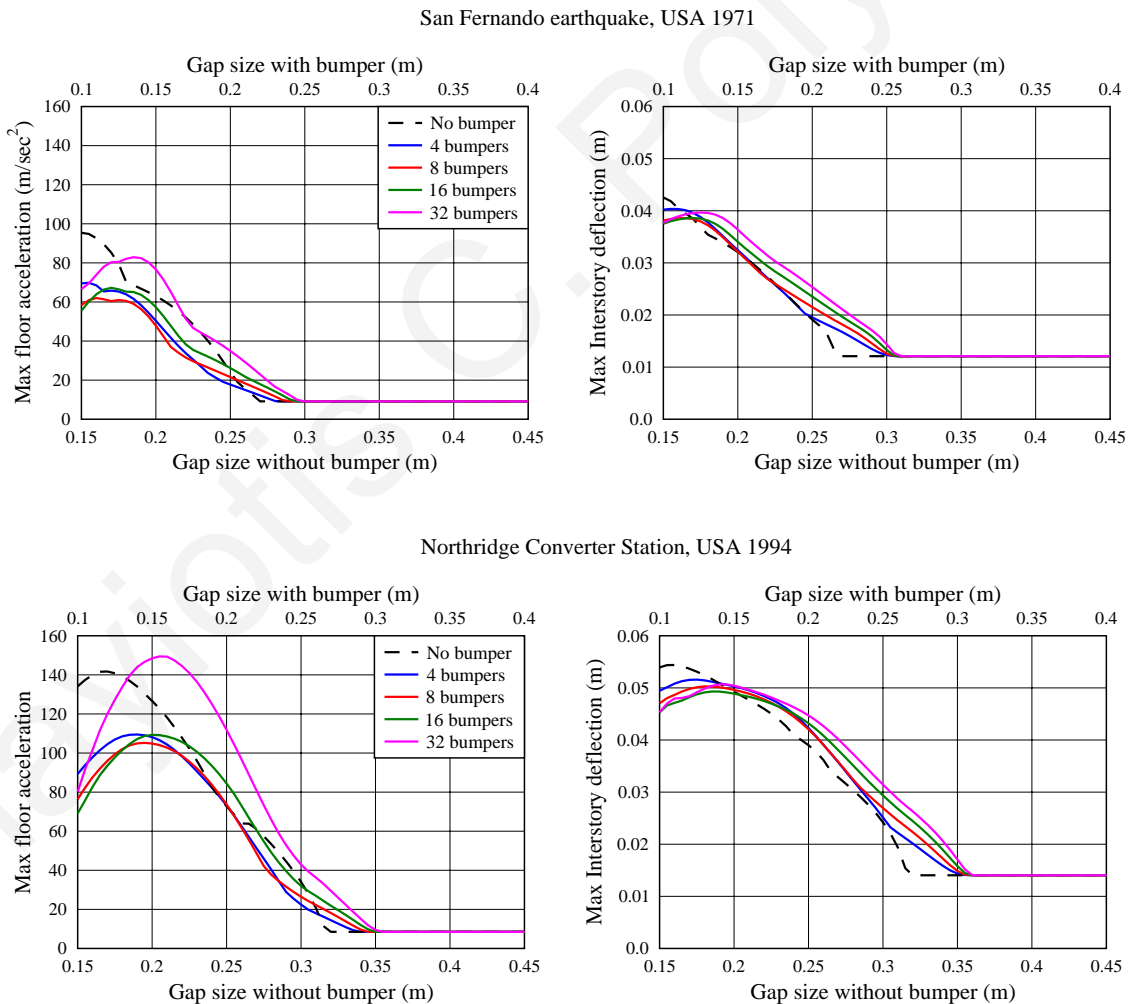


Figure 6.23 Peak responses of the seismically isolated building in terms of the seismic gap width, for various numbers of rubber shock-absorbers.

Figure 6.24 presents the maximum indentation in terms of the seismic gap width, for the four cases regarding the number of bumpers. As mentioned above, the maximum compressive capacity of the bumpers is 80 % of the bumpers' thickness, i.e. 4 cm. It can be seen that by increasing the number of bumpers, the maximum indentation is reduced, while in the case of 32 bumpers the indentation does not exceed the limit of 4 cm for all earthquakes.

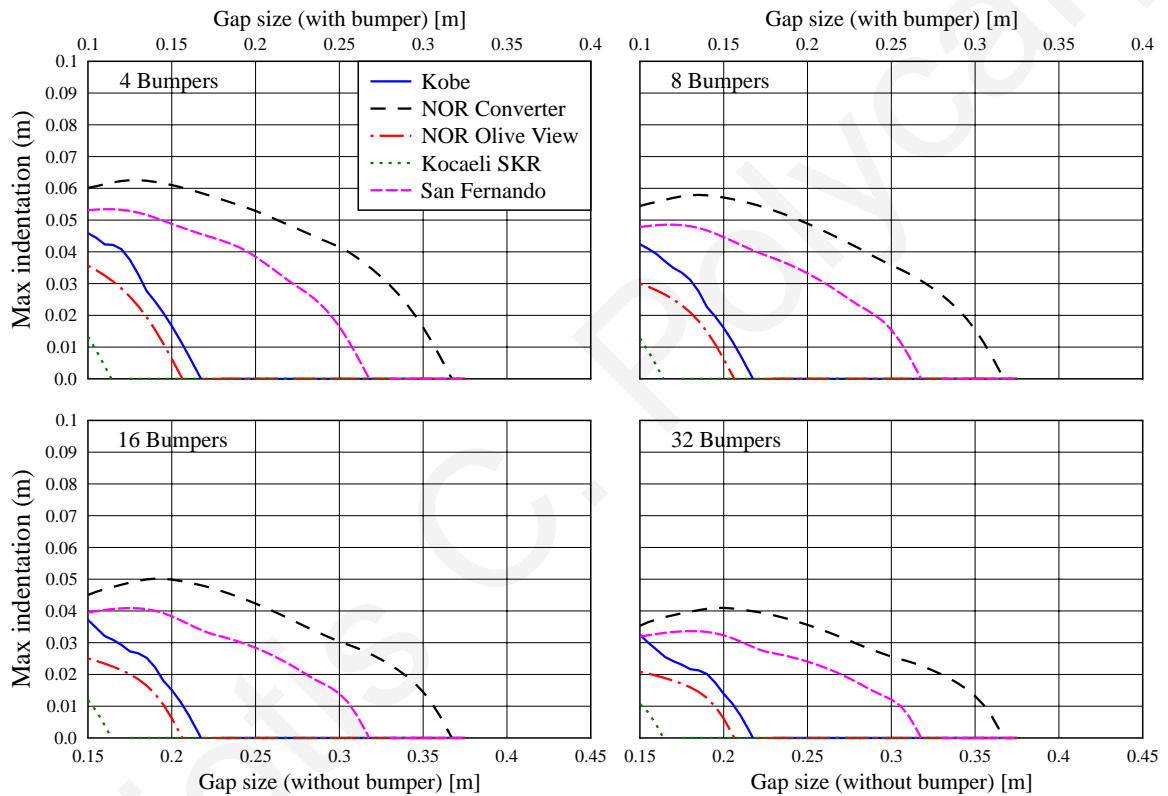


Figure 6.24 Maximum indentation in terms of the seismic gap size, for the various excitations and four cases regarding the number of rubber shock-absorbers.

6.6.5 *Effect of the wall's stiffness*

The influence of the post-yield linear impact stiffness, that, in a way, represents the static stiffness of the surrounding moat wall, is also examined. Three different values are considered: (i) 2500 kN/mm, which is equal to the impact stiffness that is used for the case without bumpers, using the linear viscoelastic impact model; (ii) 1500 kN/mm and (iii) 500 kN/mm, which is lower than the horizontal story stiffness of the superstructure.

The plots in Figure 6.25 indicate that the post-yield impact stiffness of the impact model for the rubber bumpers affects significantly the response during poundings. In particular, the maximum responses, and especially the maximum floor accelerations, of the seismically isolated building are significantly reduced when the linear post-yield stiffness takes relatively low values. The same effect of the stiffness of the surrounding moat wall on the response of a seismically isolated building considering poundings has been observed in the past from other researchers ([57], [76]).

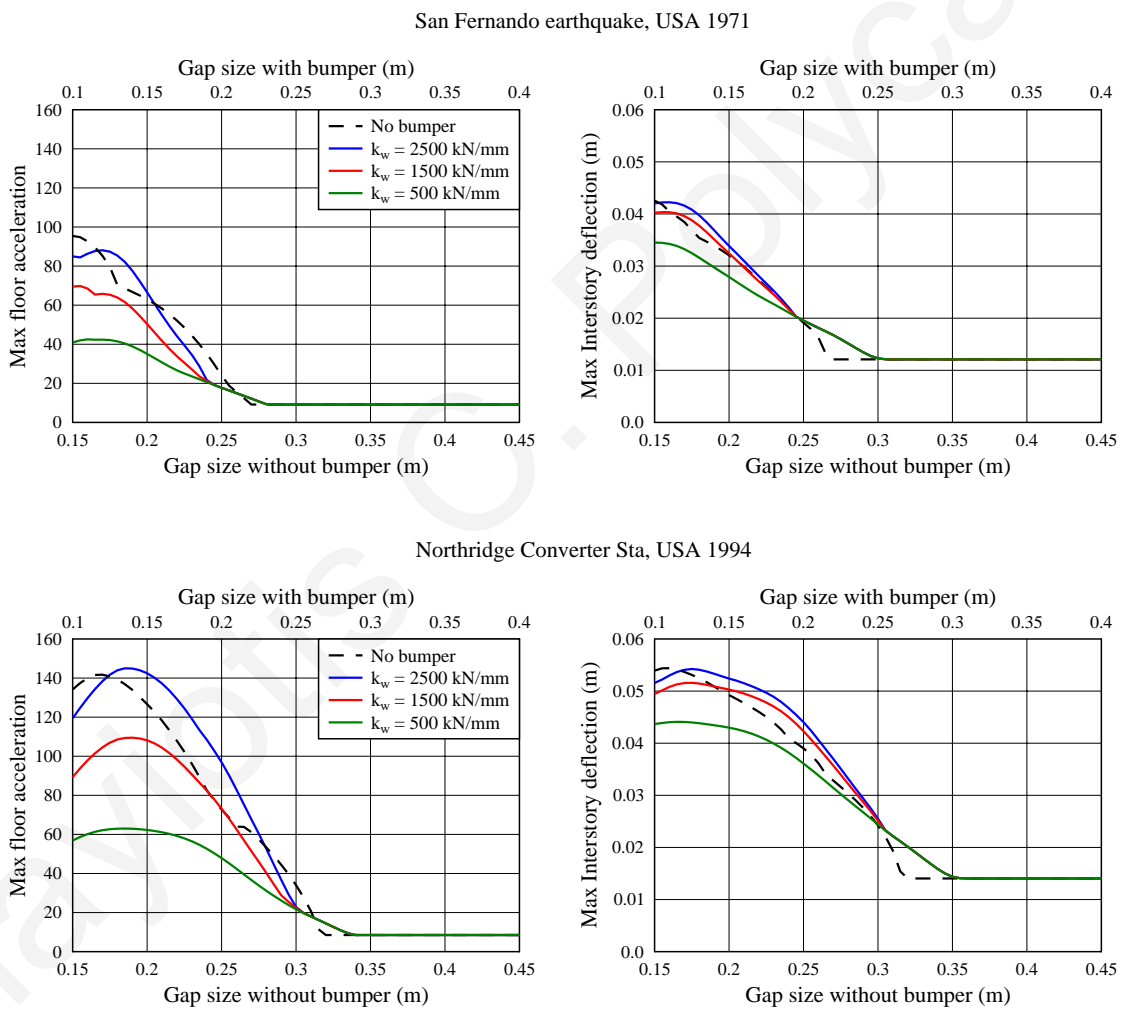


Figure 6.25 Peak responses of the seismically isolated building in terms of the seismic gap width, assuming three different values for the stiffness of the moat wall.

Consequently, the construction of a relatively flexible moat wall around a seismically isolated building that may undergo poundings during a very strong earthquake, in combination with the attachment of rubber shock-absorbers at impact locations can be an effective measure to mitigate the detrimental effects of poundings on the overall structural response.

6.6.6 Effect of the impact damping

Finally, the influence of the impact damping on the computed structural response, when modeling the incorporation of rubber bumpers, by using the proposed non-linear hysteretic impact model, is parametrically investigated. In particular, the coefficient of restitution is varied between the values 0.3 and 1.0, considering the Northridge Converter Station record, a seismic gap size 23.5 cm wide and 5 cm thick rubber bumpers. Without the rubber bumpers, the seismic gap would be equal to 10 % smaller than the maximum horizontal unconstrained displacement at the isolation level under the same earthquake excitation. Two different values of post-yield linear impact stiffness, i.e. 1500 and 2500 kN/mm, are considered.

The plots in Figure 6.26 show that the coefficient of restitution does not affect the peak responses of the seismically isolated building. The main reason for this may be that the approach phase of the non-linear hysteretic impact model and the maximum impact force are not affected by the value of the coefficient of restitution, since the latter is used only during the restitution phase. Similar observations about the insensitivity of the response to the coefficient of restitution have been made also in the previous chapters, where the linear viscoelastic impact model was used to simulate poundings without considering any bumpers.

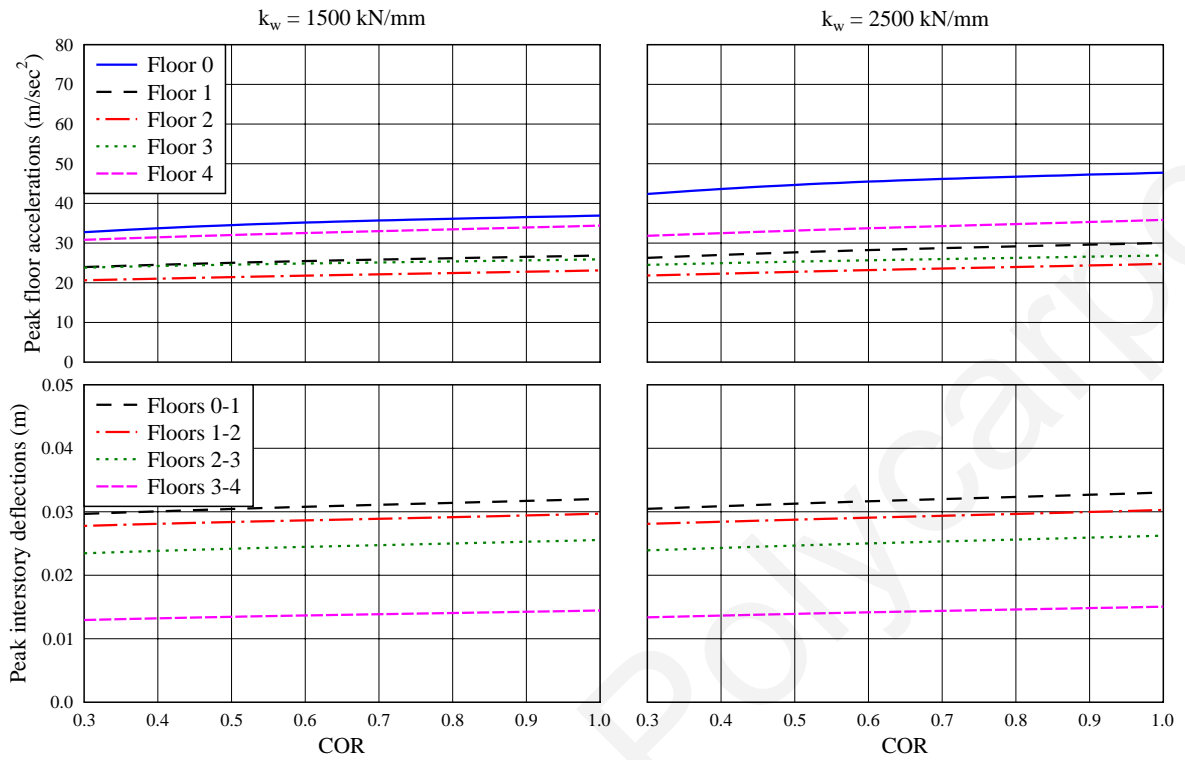


Figure 6.26 Peak responses of the seismically isolated buildings under Northridge Converter Station seismic record, assuming a seismic gap 23.5 cm wide and 5 cm thick rubber bumpers.

CHAPTER 7 CONCLUSIONS

7.1 Research contributions

This research work has focused on the numerical investigation of the effects of earthquake-induced poundings of seismically isolated buildings with their adjacent structures, considering dynamic analyses in two dimensions. Such incidences may occur in cases of limited widths of the seismic gap around a seismically isolated building and in cases of larger than the expected earthquakes that may cause structural impacts of the building against the surrounding moat wall or a fixed-supported building that is in proximity to the seismically isolated building.

A key difference from previous research work on structural poundings of conventionally fixed-supported buildings is that a seismically isolated building behaves essentially on its fundamental mode, with the superstructure moving as an almost rigid body, and the collisions, in most of the cases, take place at the base of the building, instead of the top, where poundings usually occur in the cases of fixed-supported buildings. In addition, compared to previous limited studies on poundings of seismically isolated buildings, this research work seems to provide comprehensive information regarding the consequences of poundings on the effectiveness of seismic isolation, which has been obtained through a large number of simulations and parametric studies. Furthermore, an extensive investigation regarding the type and the characteristics of the structures, adjacent to the seismically isolated building has been performed. Finally, the case of using layers of rubber, which can be attached at the potential impact locations, in order to act as collision bumpers, has been extensively investigated.

For the modeling of structural poundings, the major structural impact models are considered, while two force-based impact models are also proposed in the current study. The first is a linear viscoelastic impact model, which is actually a minor modification of the widely used Kelvin-Voigt impact model, as it has been proposed by Anagnostopoulos [2]. In particular, in the proposed slightly modified impact model, the tensile forces that arise during the restitution phase, due to the damping term, are omitted, introducing a

remaining plastic deformation, which in the case of pounding of buildings increases the available gap size. Simulations showed that the proposed modification improves the accuracy of the linear viscoelastic impact model for cases where impacts occur in sequence. In particular, the results indicate that the tensile forces during the restitution phase reduce the detaching velocity and consequently the impact velocity of the next incident.

The second impact model that is proposed in the current study is the non-linear hysteretic impact model, whereas the impact force increases exponentially with the indentation and the kinetic energy is assumed to be dissipated hysteretically during impact. For the derivation of the appropriate formula for the impact damping coefficient, an iterative procedure has been followed, based on the equilibrium of the kinetic energy loss and the area of the hysteresis loop of the proposed impact model. The non-linear impact model with hysteretic damping has been specifically developed to be used for the modeling of rubber shock-absorbers due to the profile of its force-displacement diagram, which is very similar to corresponding experimental results from the literature. However, it has been found that the proposed non-linear impact model is also appropriate for more general applications, since it has demonstrated a very good accuracy, compared to other force-based impact models.

For the modeling of the usage of rubber bumpers and, specifically, for the consideration of their finite thickness, a modification is made on the proposed non-linear hysteretic impact model. In particular, it is assumed that after a certain value of the indentation, which corresponds to the maximum compressive strain of the rubber, instead of an exponential increase of the impact force, the later increases linearly with the displacement, with a linear post-yield impact stiffness that represents the flexibility of the moat wall. The consideration of the finite thickness of the rubber bumper, along with its non-linear hysteretic behavior, is considered as another innovation of the current study.

In the present study, emphasis has been given in the development of a specialized software application, which is able to efficiently and effectively perform simulations of buildings, either seismically isolated or fixed-supported, subjected to the same ground excitation and possibly interacting with each other through poundings. In addition, the

developed software enables the realization of parametric studies, by performing, automatically, large numbers of simulations, while a certain parameter is varied in order to assess its effectiveness on the computed response.

7.2 Results and discussion

7.2.1 Poundings with the moat wall at the isolation level

When a seismically isolated building is subjected to very strong earthquake ground motions, especially when the latter contain large period impulses due to near fault effects, it may undergo large horizontal relative displacements. If the available seismic gap around the building is smaller than the maximum horizontal relative displacement at the isolation level, poundings occur with the surrounding moat wall. The simulations show that poundings are particularly unfavorable for the structure and its contents, since they increase significantly the absolute floor accelerations and interstory deflections of the building.

In particular, very high accelerations are observed at the times of impacts due to the sudden changes of the velocity. The seismically isolated building may experience maximum floor accelerations at the isolation level, where impacts occur, instead of at the top-floor, which is the most common case without pounding occurrences. These high values of induced floor accelerations can damage sensitive equipment that may be accommodated in the building.

Considering the width of the seismic gap to be 10 % smaller than the maximum unobstructed relative displacement at the isolation level, the peak interstory deflections of a typical 4-story seismically isolated building are amplified up to 3 times due to poundings with the moat wall, compared to the case without poundings. In such a case, almost the same shear forces that act on the corresponding fixed-supported building with the same characteristics, act on particular stories of the superstructure. If not sufficient strength is provided to the structural elements, taking into account these effects of potential poundings during the design of the superstructure of the seismically isolated building, there is a great possibility of considerable structural damages, in such cases.

In cases where, except from the isolation level, the first floor also hits against the surrounding moat wall, i.e. in cases of seismically isolated buildings with a basement, the effects of poundings on the response of the seismically isolated building are more pronounced. Specifically, the peak floor accelerations and the peak interstory deflections at the upper stories become significantly larger than the corresponding responses of the cases when poundings may occur only at the isolation level.

The results of the parametric studies have revealed some interesting information about the influence of certain factors on the response of seismically isolated buildings during poundings:

- When using an equivalent linear elastic model to simulate the behavior of a seismic isolation system, its flexibility determines the fundamental period of the isolated building and, consequently, the maximum value of the displacement and velocity on the response spectra for the equivalent SDOF system. The amplification of the response after impact seems to depend on the combination of these two values. Since the displacements and the velocities in most of the response spectra of typical earthquakes increase with the period, the pounding effects become more pronounced for relatively flexible isolation systems. Therefore, providing excessive flexibility at the isolation system, in order to maximize its effectiveness, may render the building vulnerable to poundings, especially if near-source effects are expected in the ground excitations.
- As the seismic gap at the base of a seismically isolated building increases, in general, both floor accelerations and interstory deflections of the superstructure decrease. However, under very strong excitations and for a range of very narrow widths of the provided seismic gap, compared to the maximum unconstrained relative displacement, the response may increase with the size of the available clearance between the seismically isolated building and the surrounding moat wall.

- The most important characteristic of the earthquake, regarding its effects on the response during poundings, is the range of predominant frequencies and not the peak ground acceleration. In particular, ground motion records that contain long period impulses induce large horizontal displacements for relatively flexible structures, such as the seismically isolated buildings, increasing the possibility of poundings to occur when an inadequate seismic gap is provided around the building. Nevertheless, the results show that the effect of the intensity of the ground motion on the response is not negligible, since for the case where all selected seismic excitations are scaled to have a $PGA = 0.6$ g poundings occur only for very narrow seismic gaps.
- The effect of the values of the impact stiffness and the coefficient of restitution, which are used for the evaluation of the impact forces, using a force-based impact model, is localized, since the only response quantity that seems to be substantially affected by the variation of these two parameters is the peak floor acceleration at the isolation level where impacts occur.

Regarding the impact modeling, the performed simulations have revealed that the effect of using different types of force-based impact models (Section 4.3.3) that are available in the scientific literature, does not significantly affect the overall response of the colliding structures. In addition, the parametric studies have shown that the effect of the values of the impact parameters, eventually, cause negligible effects on the computed responses. Taking into account these observations, as well as the assumptions related to the simplification of such a complicated phenomenon, working on the improvement of the accuracy of an impact model cannot be justified, especially when uncertainties are introduced in the methodology that is employed. Considering that the formula providing the impact damping coefficient for a linear viscoelastic impact model was derived on a methodology with less uncertainties [5] than those in the cases of non-linear viscoelastic impact models ([38], [61], [81]), the use of a simple impact model, such as the linear viscoelastic impact model, seems to be more suitable to simulate structural poundings.

7.2.2 POUNDINGS WITH ADJACENT FIXED-SUPPORTED BUILDINGS

The presence of a fixed-supported building in close proximity with a seismically isolated building may cause unexpected structural impact phenomena at upper floors due to the deformations of the buildings in series. The presented results from the relevant numerical simulations have revealed that:

- The seismically isolated building pounds with an adjacent fixed-supported buildings for wider seismic gaps than for those that are needed to avoid poundings with the surrounding moat wall at its base.
- The number of stories and, consequently, the fundamental period of the adjacent fixed-supported buildings, in combination with the earthquake characteristics, seem to play a significant role in the severity of potential structural impact. In particular, the detrimental effects of poundings are more pronounced when the fundamental period of the adjacent fixed-supported building falls within the predominant periods of the seismic ground motion. Therefore, it is important to take into account the presence and characteristics of the adjacent buildings on the estimation of the required width of the seismic gap around a seismically isolated building, as the design displacement at its base may not be sufficient as a sole criterion for the determination of the required width of the seismic gap.
- The peak interstory deflections during poundings for the case of buildings in series are most of the times smaller than those for the case of having impacts only with the moat wall, especially for relatively narrow seismic gaps. This indicates that in the former case, the adjacent buildings act as constrainers, preventing the large horizontal displacements that may take place when the seismically isolated building hits only against the moat wall at the isolation level
- The SRSS method for the estimation of the required separation distance between a seismically isolated building and its adjacent fixed-supported buildings is found to be insufficient for half of the configurations and earthquake excitations that have been considered in the performed simulations.

- The response of a seismically isolated building during poundings differentiates, depending on whether there is an adjacent structure on the left, on the right side or on both sides of the building. Nevertheless, the case of having the same structure on both sides of a seismically isolated building, envelopes the response of the two former individual cases. Some variations on the results are observed for relatively narrow gap sizes.
- The values of the impact parameters that are used for the estimation of the impact forces, have insignificant effects on the response of the seismically isolated building during poundings, except for the cases of very severe impacts.

7.2.3 *Mitigation measures*

The effectiveness of attaching layers of rubber at potential impact locations, to act as collision bumpers, in order to mitigate the detrimental effects of poundings on the overall response of a seismically isolated building, has been examined. The computed results from the numerical simulation and parametric studies reveal the following remarks:

The presence of rubber shock-absorbers at impact locations may reduce the maximum impact force, as it elongates the duration of the impact. Through this mechanism, the high spikes in the acceleration response may significantly reduce. However this seems to depend from various parameters, such as the width of the seismic gap in combination with the excitation's characteristics, the thickness of the bumper as well as the flexibility of the moat wall.

In particular, parametric studies have shown that:

- For relatively wide seismic gap sizes the usage of rubber shock-absorbers increases the response instead of reducing it. In particular, this happens for seismic gap sizes where poundings would not occur without the incorporation of rubber bumpers, which unavoidably reduce the available clearance. Rubber bumpers seem to be a more effective mitigation measure for relatively narrow

seismic gaps, compared to the maximum induced displacement of the seismically isolated building under a very strong earthquake excitation.

- In most of the considered cases, the interstory deflections of the superstructure are amplified with the usage of rubber bumpers, compared to the case without using the bumpers, due to the reduction of the available width of the seismic gap.
- The thickness of the rubber bumpers does not seem to affect significantly the response under the considered circumstances.
- Both floor accelerations and interstory deflections are reduced when the value of the maximum compressive strain of the rubber bumpers increases. This observation indicates that the use of rubber bumpers can be more efficient when they are attached with a cavity on the wall, taking full advantage of the whole compressible width of the rubber.
- With the increment of the number of bumpers that are attached on each side of the building, the maximum responses of the seismically isolated building during poundings increase for almost all values of the seismic gap width.
- The flexibility of the moat wall, i.e. the value of the post-yield linear impact stiffness, affects significantly the effectiveness of the bumpers. In particular, when a relatively low value of the wall stiffness is considered, both floor accelerations and interstory deflections reduce, compared to the case without rubber bumpers. Therefore, the construction of a relatively flexible moat wall around a seismically isolated building, in combination with the attachment of rubber shock-absorbers at impact locations, may be an efficient measure to mitigate the detrimental effects of potential poundings during a larger than expected earthquake.

7.3 Future work

Many other aspects of the problem of earthquake-induced poundings of seismically isolated buildings can be considered in future extensions of this research work. Some of these ideas are presented below:

Although the formula that has been derived in Section 2.4 for the evaluation of the impact damping coefficient of the proposed non-linear hysteretic impact model, by using an iterative numerical procedure, has demonstrated negligible errors, it is an approximation, based on the energy equilibrium before and after impact. One of the future aims of this study is to derive an analytical expression for the impact damping term, following a mathematically more rigorous approach.

In the simulations performed in the present thesis, the surrounding moat wall of the seismically isolated building is assumed to be rigid and to move with the ground during seismic excitations. It would also be useful to examine the case of the surrounding moat wall modeled as a SDOF system, considering a relatively high stiffness. According to the results of the last chapter, the stiffness of the moat wall may significantly affect the amplification of the response during poundings.

Furthermore, another configuration of a seismically isolated building that can be examined, considering poundings with the surrounding moat wall, may refer to the case that seismic isolation is implemented at the top of the basement's columns instead of the base. In such case, the structural system of the seismically isolated building is quite different, since the top of each column can move independently, having a cantilever behavior.

In the current study the slabs of neighboring buildings are assumed to be at the same level. The case of impacts occurring between the slabs, i.e. at the structure's columns, is a more dangerous scenario, which may lead even to collapse in some cases. Therefore, it would be intriguing to investigate such case, simulating seismically isolated and fixed-supported buildings under these circumstances. A modification and extension of the

current methodology and software is needed for the accomplishment of such an investigation.

Finally, a major extension of the developed software application in three dimensions would be useful for the investigation of poundings of seismically isolated buildings using 3D dynamic analysis and 3D impact modeling. In such a case, more parameters can be taken into account and investigated, such as the structural characteristics and irregularities in plan of the seismically isolated buildings as well as the adjacent fixed-supported buildings, the effect of the friction forces during impacts, the direction of the seismic excitation and so on. Potential torsional effects and their interactions with structural pounding incidences could be considered and studied.

REFERENCES

- [1] Agarwal V.K., Niedzwecki J.M. and van de Lindt J.W. (2007) Earthquake induced pounding in friction varying base isolated buildings. *Engineering Structures*, 29(11), 2825-2832.
- [2] Anagnostopoulos S.A. (1988) Pounding of buildings in series during earthquakes. *Earthquake Engineering and Structural Dynamics*; 16, 443-456.
- [3] Anagnostopoulos S.A. (1995) Earthquake induced poundings: State of the art. *10th European Conference on Earthquake Engineering*, Duma (Ed.), Balkema, Rotterdam.
- [4] Anagnostopoulos S.A. (1996) Building pounding re-examined: How serious problem is it? *11th World Conference on Earthquake Engineering*, Paper No: 2108, 23-28 June 1996, Acapulco, Mexico.
- [5] Anagnostopoulos S.A. (2004) Equivalent viscous damping for modelling inelastic impacts in earthquake pounding problems. *Earthquake Engineering and Structural Dynamics*; 33, 897-902.
- [6] Anagnostopoulos S.A and Karamaneas C.E. (2008) Use of collision shear walls to minimize seismic separation and to protect adjacent buildings from collapse due to earthquake-induced pounding. *Journal of Earthquake Engineering and Structural Dynamics*, 37, 1371-1388.
- [7] Anagnostopoulos S.A and Spiliopoulos K.V. (1992) An investigation of earthquake induced pounding between adjacent buildings. *Earthquake Engineering and Structural Dynamics*; 21, 289-302.
- [8] Athanasiadou C.J, Penelis G.G and Kappos A.J. (1994) Seismic response of adjacent buildings with similar or different dynamic characteristics. *Earthquake Spectra*, 10, 293-317.

REFERENCES

- [9] Bathe K.J. (1996) *Finite Element Procedures*, Prentice-Hall Inc. Englewood Cliffs, New Jersey.
- [10] Bertero V.V. (1986) Observations on Structural Pounding. *Proceedings International Conference on Mexico Earthquakes*, ASCE, 264-287.
- [11] Butcher E.A. and Segalman D.J. (2000) Characterizing Damping and Restitution in Compliant Impacts via Modified K-V and Higher-Order Linear Viscoelastic Models. *Journal of Applied Mechanics (ASME)*, 67, 831- 834.
- [12] Chau K.T. and Wei X.X. (2001) Poundings of structures modeled as non-linear impacts of two oscillators. *Earthquake Engineering and Structural Dynamics*; 30, 633-651.
- [13] Chau K.T., Wei X.X., Guo X. and Shen C.Y. (2003) Experimental and theoretical simulations of seismic poundings between two adjacent structures. *Earthquake Engineering and Structural Dynamics*; 32, 537-554.
- [14] Chau K.T., Wang L.X. and Wei X.X. (2006) Torsional poundings between two adjacent asymmetric structures. *4th International Conference on Earthquake Engineering*, Taipei, Taiwan, October 12-13, Paper NO.: 105.
- [15] Chopra A.K. (2006) *Dynamics of Structures: Theory and Applications to Earthquake Engineering*. (3rd Ed.) Prentice-Hall, Upper Saddle River, NJ, U.S.A.
- [16] Davis R.O. (1992) Pounding of buildings modelled by an impact oscillator. *Earthquake Engineering and Structural Dynamics*; 21, 253-274.
- [17] DesRoches R and Muthukumar S. (2002) Effect of pounding and restrainers on seismic response of multiple-frame bridges. *Journal of Structural Engineering (ASCE)*; 128, 860–869.
- [18] Dimitrakopoulos E., Makris N. and Kappos A. (2008) Dimensional analysis of the earthquake-induced pounding between adjacent structures. *Journal of Earthquake Engineering and Structural Dynamics*, (published online) DOI: 10.1002/eqe.872

REFERENCES

- [19] Dimova S.L. (2000) Numerical problems in modelling of collision in sliding systems subjected to seismic excitations. *Advances in Engineering Software*; 31, 467-471.
- [20] Earthquake Engineering Research Institute (EERI) (1990) "Loma Prieta Earthquake Reconnaissance Report," Rep. No. 90-01, Benuska, L., ed., EERI, Oakland, CA.
- [21] Earthquake Engineering Research Institute (EERI) (1995a) "Northridge Earthquake of January 17, 1994 - Reconnaissance Report, Vol. 1," Rep. No. 95-03, J.F.Hall, ed., EERI, Oakland, CA.
- [22] Earthquake Engineering Research Institute (EERI) (1995b) "The Hyogo-Ken Nanbu Earthquake Reconnaissance Report," Rep. No. 95-04, C.D.Comartin, M.Greene, and S.K.Tubbesing, eds., EERI, Oakland, CA.
- [23] Earthquake Engineering Research Institute (EERI) (2000) "Kocaeli, Turkey, Earthquake of August 17, 1999 Reconnaissance Report," Publ. No. 00-03, Youd, T. L., Bardet, J-P., Bray, J. D., ed., EERI, Oakland, CA.
- [24] Earthquake Engineering Research Institute (EERI) (2001a) "Chi-Chi, Taiwan, Earthquake of September 21, 1999 - Reconnaissance Report," Publ. No. 01-02, J. Uzarski, C. Arnold, eds., EERI, Oakland, CA.
- [25] Earthquake Engineering Research Institute (EERI) (2001b) "The Nisqually, Washington, Earthquake of February 28, 2001- Preliminary Reconnaissance Report," EERI, Oakland, CA.
- [26] Earthquake Engineering Research Institute (EERI) (2002) "Bhuj, India Earthquake of January 26, 2001 Reconnaissance Report." Publ. No 02-01, Jain, S.K., Lettis, W.R., Murty, C.V.R., and Bardet, J.P. (Eds), EERI, Oakland, CA.
- [27] EAK2000 (2001) Greek Antiseismic Code, Athens: Greek earthquake planning and protection organization (<http://www.oasp.gr>).
- [28] Eurocode 8 (2003) "Design of structures for earthquake resistance", prEN 1998-1.

REFERENCES

- [29] Filiatrault A., Wagner P. and Cherry S. (1995) Analytical prediction of experimental building pounding. *Earthquake Engineering and Structural Dynamics*; 24, 1131-1154.
- [30] Geary D.M. (1999) *Graphic Java 2, Volumes 2: Swing*. 3rd Edition, Prentice Hall PTR Upper Saddle River, NJ, USA.
- [31] Goldsmith W. (1960) *Impact: the theory and physical behaviour of colliding solids*, E. Arnold, London, UK.
- [32] Guo A., Li Z., Li H. and Ou J. (2009) Experimental and analytical study on pounding reduction of base-isolated highway bridges using MR dampers. *Earthquake Engineering & Structural Dynamics*, (published online) DOI: 10.1002/eqe.903
- [33] Hall J.F., Heaton T.H., Halling M.W., and Wald D.J. (1995) Near-source ground motion and its effect on flexible buildings. *Earthquake Spectra*, 11, 569–605.
- [34] International Conference of Building Officials (1997) *Uniform Building Code (UBC)*. Whittier, California, USA.
- [35] Ishikawa N., Nishimoto Y. and Ukishima T. (2006) Development Of New Bridge Restrainer Using Laminated Fiber Reinforced Rubber. *Solid Mechanics and Its Applications, Advances in Engineering Structures, Mechanics & Construction*. M. Pandey et al (eds), 140, 809–821.
- [36] Jangid R.S. and Kelly J.M. (2001) Base isolation for near-fault motions. *Earthquake Engineering & Structural Dynamics*, 30, 691-707.
- [37] Jankowski R. (2005) Non-linear viscoelastic modelling of earthquake-induced structural pounding. *Earthquake Engineering and Structural Dynamics*; 34, 595 – 611.
- [38] Jankowski R. (2006) Analytical expression between the impact damping ratio and the coefficient of restitution in the non-linear viscoelastic model of structural pounding. *Earthquake Engineering and Structural Dynamics*; 35, 517 – 524.

REFERENCES

- [39] Jankowski R. (2006) Pounding force response spectrum under earthquake excitation. *Engineering Structures*, 28, 1149–1161.
- [40] Jankowski R. (2008) Earthquake-induced pounding between equal height buildings with substantially different dynamic properties. *Engineering Structures*, 30, 2818–2829.
- [41] Jankowski R., Wilde K., and Fujino Y. (1998) Pounding of superstructure segments in isolated elevated bridge during earthquakes *Earthquake Engineering & Structural Dynamics*, 27, 487-502.
- [42] Jankowski R., Wilde K. and Fujino Y. (2000) Reduction of pounding effects in elevated bridges during earthquakes. *Earthquake Engineering and Structural Dynamics*, 29, 195-212.
- [43] Kajita Y., Kitahara T., Nishimoto Y. and Otsuka H. (2006) Estimation of maximum impact force on natural rubber during collision of two steel bars. *First European Conference on Earthquake Engineering and Seismology (1st ECEES)*, Geneva, Switzerland, September 3-8.
- [44] Kajita Y., Nishimoto Y., Ishikawa N. and Watanabe E. (2001) Energy Absorption Capacity of the Laminated Fiber Reinforced Rubber Installed at Girder Ends. *High Performance Materials in Bridges, International Conference on High Performance Materials in Bridges*, 122, 17, DOI:10.1061/40691(2003)17, Kona, Hawaii, USA.
- [45] Kawashima K., Shoji G., Koshitoge M. and Shimanoe S. (2002) Design of an Earthquake-resistant Expansion Joint with Unseating Prevention System, *FIB Congress*, E-282 (CD-ROM), Osaka, Japan.
- [46] Kelly J.M. (1997) *Earthquake Resistant Design with Rubber*; 2nd edn, Springer-Verlag.
- [47] Kim H.S. and Shafiq R.M. (2001) Model for Thickness Effect with Impact Testing of Viscoelastic Materials. *Journal of Applied Polymer Science*, 81, 1762–1767.

REFERENCES

- [48] Kim S.H. and Shinozuka M. (2003) Effects of Seismically Induced Pounding at Expansion Joints of Concrete Bridges. *Journal of Engineering Mechanics*, 129 (11), 1225-1234.
- [49] Komodromos P. (2000) Seismic Isolation for Earthquake-Resistant Structures, *WIT Press*: Southampton.
- [50] Komodromos P. and Williams J.R. (2002) On the Simulation of Deformable Bodies Using Combined Discrete and Finite Element Methods. *3rd International Conference on Discrete Element Methods*, Santa Fe, New Mexico, USA.
- [51] Lankarani H.M. and Nikravesh P.E. (1994) Continuous Contact Force Models for Impact Analysis in Multibody Systems. *Nonlinear Dynamics*, 5, 193-207.
- [52] Liolios A.A. (2000) A Linear Complementarity approach for the non-convex seismic frictional interaction between adjacent structures under instabilizing effects. *Journal of Global Optimization*, 17, 259–266.
- [53] Mahmoud S., Chen X. and Jankowski, R. (2008) Structural pounding models with Hertz spring and nonlinear damper. *Journal of Applied Sciences*, 8(10), 1850-1858.
- [54] Maison B.F. and Kasai K. (1990) Analysis for Type of Structural Pounding. *Journal of Structural Engineering*; 116, 957-977.
- [55] Maison B.F. and Kasai K. (1992) Dynamics of pounding when two buildings collide. *Journal of Earthquake Engineering and Structural Dynamics*, 21, 771-786.
- [56] Makris N. and Chang Sh.-P. (2000) Effect of viscous, viscoplastic and friction damping on the response of seismic isolated structures. *Earthquake Engineering and Structural Dynamics*; 29, 85-107.
- [57] Malhotra, P.K. (1997) Dynamics of seismic impacts in base-isolated buildings. *Earthquake Engineering and Structural Dynamics*; 26, 797-813.

REFERENCES

- [58] Matsagar V.A. and Jangid R.S. (2003) Seismic response of base-isolated structures during impact with adjacent structures. *Engineering Structures*; 25, 1311-1323.
- [59] Matsagar V.A. and Jangid R.S. (2005) Viscoelastic damper connected to adjacent structures involving seismic isolation. *Journal of Civil Engineering and Management*, Vol. XI, No 4, 309-322.
- [60] Mavronicola E., Polycarpou P., Papaloizou L., Phocas M.C. and Komodromos P. (2008), On the linearization of the seismic behavior of seismic isolation systems, *Proceedings of the 14th World Conference on Earthquake Engineering (14WCEE)*, Beijing, China.
- [61] Muthukumar S. and DesRoches R. (2006) A Hertz contact model with non-linear damping for pounding simulation. *Earthquake Engineering and Structural Dynamics*; 35, 811 – 828.
- [62] Naeim F. and Kelly J.M. (1999) *Design of Seismic Isolated Structures*, John Wiley & Sons Inc.
- [63] Nagarajaiah, S. and Sun, X. (2001) Base-Isolated FCC Building: Impact Response In Northridge Earthquake. *Journal of Structural Engineering*, 127(9), 1063-1075.
- [64] Pantelides C.P. and Ma X. (1997) Linear and non-linear pounding of structural systems. *Computers and Structures*; 66, 79-92.
- [65] Papadrakakis M., Apostolopoulou C., Zacharopoulos A. and Bitzarakis S. (1996) Three-dimensional simulation of structural pounding during earthquakes. *Journal of Engineering Mechanics*; 122, 423-431.
- [66] Papadrakakis M. and Mouzakis H. (1995) Earthquake simulator testing of pounding between adjacent buildings. *Earthquake Engineering and Structural Dynamics*, 24, 811–834.

REFERENCES

- [67] Papadrakakis M., Mouzakis, H., Plevris, N. and Bitzarakis, S. (1991) A Lagrange multiplier solution method for pounding of buildings during earthquakes. *Earthquake Engineering and Structural Dynamics*; 20, 981-998.
- [68] Penzien J. (1997) Evaluation of building separation distance required to prevent pounding during strong earthquakes. *Earthquake Engineering and Structural Dynamics*; 26, 849-858.
- [69] Pacific Earthquake Engineering Research Center (2000) Strong Motion Database, University of California. (<http://peer.berkeley.edu/smcat/>).
- [70] Rosenblueth E. and Meli R. (1986) The 1985 earthquake: causes and effects in Mexico City. *Concrete International (ACI)*, 8, 23–36.
- [71] Ruangrassamee A. and Kawashima K. (2003) Control of nonlinear bridge response with pounding effect by variable dampers. *Engineering Structures*, 25, 593-606.
- [72] Shim V.P. W., Yang L.M., Lim C.T. and Law P.H. (2004) A Visco-Hyperelastic Constitutive Model to Characterize Both Tensile and Compressive Behavior of Rubber. *Journal of Applied Polymer Science*, 92, 523–531.
- [73] Skinner R.I., Robinson W.H. and McVerry G.H. (1993) An Introduction to Seismic Isolation, DSIR Physical Sciences, John Wiley & Sons: Wellington, New Zealand.
- [74] Stavroulakis G.E. and Abdalla K.M. (1991) Contact between adjacent structures. *Journal of Structural Engineering*; 117, 2838-2850.
- [75] Taylor A.W. and Igusa T. (2004) Primer on Seismic Isolation. *ASCE Task Committee on Seismic Isolation*.
- [76] Tsai H.C. (1997) Dynamic analysis of base-isolated shear beams bumping against stops. *Journal of Earthquake Engineering and Structural Dynamics*; 26, 515-528.

REFERENCES

- [77] Van Mier J.G.M., Pruijssers A.F., Reinhardt H.W. and Monnier T. (1991) Load-Time Response of Colliding Concrete Bodies. *Journal of Structural Engineering*; 117, 354-374.
- [78] Warnotte V., Stoica D., Majewski S. and Voiculescu M. (2007) State of the art in the pounding mitigation techniques. *Intersections/Intersectii*, 4 (3), 102-117. ISSN: 1582-3024.
- [79] Watanabe G. and Kawashima K. (2004) Numerical Simulation of Pounding of Bridge Decks. *13th World Conference on Earthquake Engineering*, August 1-6, Paper No.884.
- [80] Won J.H., Mha H.S., Cho K.I. and Kim S.H. (2008) Effects of the restrainer upon bridge motions under seismic excitations. *Engineering Structures*, DOI:10.1016/j.engstruct.2008.05.021
- [81] Ye K., Li L. and Zhu H. (2008) A note on the Hertz contact model with nonlinear damping for pounding simulation. *Earthquake Engineering & Structural Dynamics*, (published online) DOI: 10.1002/eqe.883.
- [82] Zhang W.S. and Xu Y.L. (1999) Dynamic characteristics and seismic response of adjacent buildings linked by discrete dampers. *Earthquake Engineering & Structural Dynamics*, 28, 1163–1185.
- [83] Zhu P., Abe M. and Fujino Y. (2002) Modelling three-dimensional non-linear seismic performance of elevated bridges with emphasis on pounding of girders. *Earthquake Engineering & Structural Dynamics*, 31, 1891–1913.